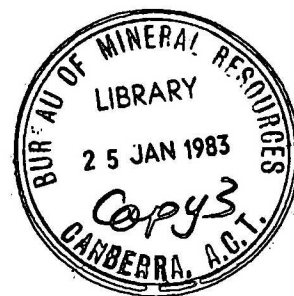


1981/61

03

BMR PUBLICATIONS COMPACTUS
(LENDING SECTION)



BUREAU OF MINERAL RESOURCES, GEOLOGY AND GEOPHYSICS

102802

RECORD

Record 1981/61

HYDROGEOLOGICAL INVESTIGATIONS OF TWO BASINS

AT LANYON, ACT, 1974-1976

by

J.R. Kellett

The information contained in this report has been obtained by the Bureau of Mineral Resources, Geology and Geophysics as part of the policy of the Australian Government to assist in the exploration and development of mineral resources. It may not be published in any form or used in a company prospectus or statement without the permission in writing of the Director.

Record 1981/61

HYDROGEOLOGICAL INVESTIGATIONS OF TWO BASINS

AT LANYON, ACT, 1974-1976

by

J.R. Kellett

CONTENTS

ABSTRACT

INTRODUCTION

History of investigation

Location

GEOLOGY

JOINTING IN THE SILURIAN VOLCANIC ROCKS

Joints in drillcores

Joints in outcrop

Inferred stress history from joints survey and its hydrogeological significance.

GEOMORPHOLOGY

General geomorphic setting

Correlation of landsurfaces of the Lanyon basin catchments with regional models.

Discussion on the evolution of the Lanyon landsurfaces

Geomorphic surfaces of the Lanyon basins

SURFICIAL GEOLOGY

STRATIGRAPHY

Rob Roy pedoderm

Murrumbidgee pedoderm

Murrumbidgee pedoderm - basal fanglomerate facies

Murrumbidgee pedoderm - upper fine-grained facies

Depositional environment of the Murrumbidgee pedoderm

Tuggeranong pedoderm

Tuggeranong pedoderm - basal fanglomerate facies

Tuggeranong pedoderm - upper fine-grained facies

Mineralogy and pedogenesis of the Tuggeranong clay

Depositional and pedogenetic environment of the Tuggeranong pedoderm

Lanyon pedoderm

Lanyon pedoderm - basal clastics facies

Lanyon pedoderm - upper fine-grained facies

Mineralogy and pedogenesis of soils of the Lanyon pedoderm

Depositional and pedogenetic environment of the Lanyon pedoderm

Big Monk pedoderm

Field criteria to distinguish hydromorphic variants of the Big Monk and Lanyon pedoderms

- (14) Groundwater balances
- (15) Remedial drainage for urban development

RECOMMENDATIONS

ACKNOWLEDGEMENTS

REFERENCES

APPENDIXES

1. Palynological examination of drillcore specimens by M.D. Muir
2. Porosity and permeability measurements on drillcore specimens by BMR Petroleum Technology Laboratory
3. Geological logs of diamond drillcores
4. Logs of auger holes drilled during preliminary investigation, 1974
5. Bore hydrographs
6. Fluctuations in potentiometric surfaces, November 1974 to December 1976.

TABLES

1. Hand-specimen descriptions of rock types
2. Significant joint sets
3. Probable principal stress directions inferred from joint classification and geometry
4. Geomorphic surface/soil association
5. Sedimentary parameters of arenites of the Rob Roy pedoderm
6. Field criteria to distinguish between Lanyon and Murrumbidgee subsola
7. Summary of field criteria of hydromorphic variants of Big Monk and Lanyon pedoderms
8. Correlation coefficients, south basin
9. Correlation coefficients, north basin
10. One-dimensional infiltration capacities of Lanyon soils
11. Effective porosities of Lanyon soils
12. Transmissivities and hydraulic conductivities of aquifers
13. Approximate partitioning of E_T^1 into evaporation and transpiration components.

FIGURES

1. Location of investigated area
2. Topographic map of Lanyon basins
3. Joints in the densely welded zone of the blue-grey rhyolite
4. Younger and older basin surfaces - Lanyon north basin
5. Geomorphic map, Lanyon north basin
6. Geomorphic map, Lanyon south basin
7. Outlet of the perched basin
8. Break of slope at 650 m across the north basin
9. Surficial stratigraphy of the Lanyon pediplain basins

Depositional and pedogenetic environment of the Big Monk
pedoderm

Gigerline pedoderm

Depositional and pedogenetic environment of the
Gigerline pedoderm

Riverside pedoderm

Surficial geology of the perched basin

Summary and discussion of the surficial geology

HYDROLOGY

Groundwater hydrology - method of field investigation

Surface drainage

The hydrogeological system

Groundwater discharge zones

Hydraulic continuity of the aquifers and hydrogeological
populations

Infiltration

Effective porosities

Recharge to the surficial aquifers from rainfall infiltration

Hydraulic conductivities

Bore hydrographs and fluctuations in groundwater potentials

Flow nets.

DRAINAGE OF THE BASINS FOR URBAN DEVELOPMENT

Analytical solution for calculation of drain spacing

Comparison of predicted groundwater potentials with
observed piezometer readings

Recommended drain spacings and locations

Groundwater monitoring after urban development

CONCLUSIONS

- (1) Geology
- (2) Jointing
- (3) Geomorphology
- (4) Surficial geology
- (5) The perched basin
- (6) The hydrogeological system
- (7) Surface water-groundwater interaction**
- (8) Hydraulic continuity of the aquifers
- (9) Infiltration
- (10) Effective porosities
- (11) Recharge from rainfall
- (12) Hydraulic conductivities
- (13) Fluctuations in groundwater potentials

10. Surficial geology of the Lanyon north basin
11. Surficial geology of the Lanyon south basin
12. Schematic cross-sectional relationships of pedoderms in the Lanyon basins
13. Cross-stratification and graded bedding in pebbly sand lenses near the top of the basal fanglomerate facies, Murrumbidgee pedoderm.
14. Relict complex cutans, fine grained facies, Murrumbidgee pedoderm.
15. Joint planes and channels in upper facies of the Murrumbidgee pedoderm.
16. Alluvial component of the Tuggeranong fanglomerate
17. Imbrication of platy cobbles in lower Tuggeranong fanglomerate.
18. Textural characteristics of the Tuggeranong fanglomerate
19. Upper catena variant (soloth) of the Tuggeranong clay
20. Lower B horizon of Tuggeranong clay, lower catenary variant
21. Mottling pattern in Tuggeranong clay subsolum, lower catenary position.
22. Hydromorphic variant of the Tuggeranong clay
23. Lanyon pedoderm, basal clastics facies, colluvial-alluvial variant
24. Massive and porous indurated sands of the slopewash variant of the Lanyon pedoderm
25. Type section of the Lanyon clay
26. Strong blocky and prismatic peds in the upper B horizon of the Lanyon clay grading to coarse prismatic aggregates in the lower B and B2 horizons.
27. Type section of the solum of the mid-to-lower catena variant of the Lanyon pedoderm
28. Latosol variant of the Lanyon pedoderm
29. Colluvial component of the Big Monk pedoderm
30. Yellow podzolic variant of the Big Monk pedoderm
31. Grey solodic (hydromorphic) variant of the Big Monk pedoderm
32. Superposition of the layered hydromorphic variant of the Big Monk pedoderm on hydromorphic Tuggeranong clay.
33. Boulder trains within the truncated subsolum of the Gigerline pedoderm on southerly lower slopes of Tuggeranong Hill
34. Type section of the Riverside pedoderm
35. Surficial geology of the perched basin
36. Immature cryoplanation terraces in the northern part of the perched basin.
37. Geomorphology and distribution of pedoderms on lower bajada above the Lanyon north basin
38. Geomorphology and distribution of pedoderms on lower bajada above the Lanyon south basin

39. Southern drainage channel, lower planation surface of south basin
40. Southern drainage channel, lowest planation surface of south basin
41. Lanyon south basin looking south from terminus of central stream in flood
42. Lanyon south basin looking west from terminus of central stream in flood
43. Generalised hydrogeological system - Lanyon pediplain basins
44. Groundwater populations, Lanyon south basin
45. Groundwater populations, Lanyon north basin
46. Infiltration capacities, clover and phalaris grass on prairie soil of the Riverside pedoderm
47. Infiltration capacities, Gigerline pedoderm (grey earth)
48. Infiltration capacities, Lanyon clay-upper B horizon
49. Infiltration capacities, Lanyon clay-lower B horizon
50. Stratified slab model for recharge from infiltration
51. Contours of maximum fluctuation of potentiometric surface over period 12.11.75 to 14.9.76. Surficial aquifers - north basin
52. Contours of maximum fluctuations of potentiometric surface over period 12.11.75 to 14.9.76. Surficial aquifers - south basin
53. Flow net - fractured rock aquifer 12.11.76. Lanyon north basin
54. Flow net - surficial aquifers 12.11.76. Lanyon north basin
55. Flow net - fractured rock aquifer 12.11.76. Lanyon south basin
56. Flow net - surficial aquifers 12.11.76. Lanyon south basin
57. Boundary conditions of flow to a shallow, partly penetrating open drain with Hooghoudt's transformation for parallel streamlines
58. Superposition of solutions for $h(x,t)$ in response to intermittent recharge
59. Comparison between predicted and observed values of hydraulic head, 1.9.76-31.10.76, bore 29 - Lanyon south basin.
60. Comparison between predicted and observed values of hydraulic head, 1.9.76-31.10.76, bore 30 - Lanyon south basin.
61. Comparison between predicted and observed values of hydraulic head, 1.9.76 - 31.10.76, bore 28 - Lanyon south basin.
62. Comparison between predicted and observed values of hydraulic head, 1.9.76-31.10.76, bore 35 - Lanyon south basin.
63. Comparison between predicted and observed values of hydraulic head, 1.9.76-31.10.76, bore 113 - Lanyon south basin
64. Comparison between predicted and observed values of hydraulic head, 1.9.76-31.10.76, bore 106 - Lanyon north basin.
65. Comparison between predicted and observed values of hydraulic head, 1.9.76-31.10.76, bore 107 - Lanyon north basin
66. Rainfall intensity frequency duration diagram, 24-240 hours

67. Predicted maximum heights of the phreatic surface for various drain spacings. Groundwater populations S2, N1. Design rainfall 0.63 mm/hour for 120 hours
68. Predicted maximum heights of the phreatic surface for various drain spacings. Groundwater population S1. Design rainfall 0.63 mm/hour for 120 hours
69. Predicted maximum heights of the phreatic surface for various drain spacings. Groundwater population N2. Design rainfall 0.63 mm/hour for 120 hours
70. Periods of exceedance of given maximum values of the phreatic surface over 30 days for a rainfall of 0.63 mm/hour over the first 120 hours of the month for various drain spacings
71. Constraints on locations and spacings of drains. Lanyon north basin
72. Constraints on locations and spacings of drains. Lanyon south basin.

PLATES

1. Geological map of central Lanyon
2. Joint analysis, central Lanyon
3. Location of bores, piezometers and groundwater discharge zones, Lanyon north basin
4. Location of bores, piezometers and groundwater discharge zones, Lanyon south basin.

ABSTRACT

Hydrogeological investigations in two pediplain basins at Lanyon, in the southern Tuggeranong valley of the ACT, have identified areas which require remedial drainage for urban development.

The rocks of the central Lanyon area consist of faulted Silurian decitic to rhyolitic ash-flow tuffs and interbedded sediments. Significant storage and transmission of groundwater occurs in well-developed sets of open tensile fractures which formed in response to at least two reversals in regional principal stress directions during epeirogenic uplift and erosional unloading.

A thick disconformable sequence of surficial deposits has accumulated in the basins since the Tertiary. Seven stages of instability and remobilisation of the regolith have alternated with quiescent periods of pedogenesis. In general, hillslope denudation and redeposition of the regolith was greatest in the initial unstable phases associated with the oldest pedoderms, and progressively declined in magnitude and intensity with succeeding pedoderms. There is evidence to suggest that unstable periods in the youngest pedoderms coincided with periglacial maxima.

Within each pedoderm the trend from basal clastics to an upper sandy facies records a steady diminution in supply of sediment into the basins as hillslope vegetation adjusted to the new equilibrium conditions, culminating in a stable period of pedogenesis. Unique pedological characteristics of individual pedoderms, in particular the subsolum features, are described in detail.

An understanding of the depositional environments that control the spatial distribution of the surficial units is fundamental to the analysis of the hydrodynamics of the surficial aquifers. Fluvial gravels of the basal facies of the younger pedoderms are the most efficient aquifers because intergranular voids have been only partly restricted by secondary filling; however, their distribution is irregular and they are not hydraulically continuous. The major soaks of the lower basin surfaces are derived from upwards flow of groundwater from buried palaeochannels of prior braided streams, and are found where these open gravels lens out into lower permeability material. Wherever the gravels are confined aquifers, recharge occurs by lateral piping of bed-underflow water from the basin streams and by upwards leakage from the underlying fractured rock.

Statistical analysis of correlations in hydraulic head measurements in the fractured rock and surficial aquifers over a two-year period has identified populations of direct hydraulic connection between the two aquifer systems, populations of impeded hydraulic connection, and populations in which the surficial aquifers and the fractured rock are essentially discrete systems.

Potentiometric contour maps clearly show the locations of permanent groundwater mounds around discontinuities in influent streams and at point sources in the surficial aquifers. Fluctuations in groundwater potentials during the two-year period 1974-1976 ranged from over 3 m in the recharge zones of the basins to zero around the major soaks and some effluent streams. Calculations of groundwater balances show that significant intrabasin losses are incurred in the saturated zone by phreatophyte transpiration.

Hydrogeological parameters measured in the field and laboratory included infiltration capacities, effective porosities, and hydraulic conductivities. From these data a predictive model for drain spacings is developed for all hydrogeological populations and for any given rainfall event. Constraints on locations of drains are also identified. It is recommended that a sufficient number of bores and piezometers be preserved after urban development to adequately assess changes to the groundwater regime.

INTRODUCTION

History of investigation

In July 1972 the National Capital Development Commission (NCDC), requested the Bureau of Mineral Resources (BMR), to carry out geological investigations relevant to the urban development of Lanyon station (Fig 1).

After preliminary investigations, drainage was recognised as a major problem in two pediplain basins at Lanyon, referred to as the north and south basins (Fig. 2). Investigation of the drainage problem areas commenced in June 1974; fieldwork was completed in September of that year, and copies of a preliminary report were given to NCDC and their consultants, Gutteridge, Haskins and Davey Pty Ltd (GHD) in November 1974.

The report summarised what was known of the geology and hydrogeology of the basins, and established the hydraulic conductivities of the components of the saturated zone determined by pump-testing in the field. It was recommended that additional shallow holes be drilled in each basin to delineate high transmissivity aquifers more accurately, thus enabling drainage works to be designed for maximum effectiveness. Where appropriate, these holes were to be equipped with piezometers, and BMR undertook to record water-levels at regular intervals at least up until the end of 1976. It was also recommended that several deep bores be sunk into the rock underlying the basins in order to clarify the role of the fractured rock aquifer in the groundwater regime.

The recommendation for shallow augering and piezometer installation was implemented early in 1975. Groundwater-levels from the expanded piezometer network and other relevant hydrogeological data were recorded at least once a fortnight for the next 21 months.

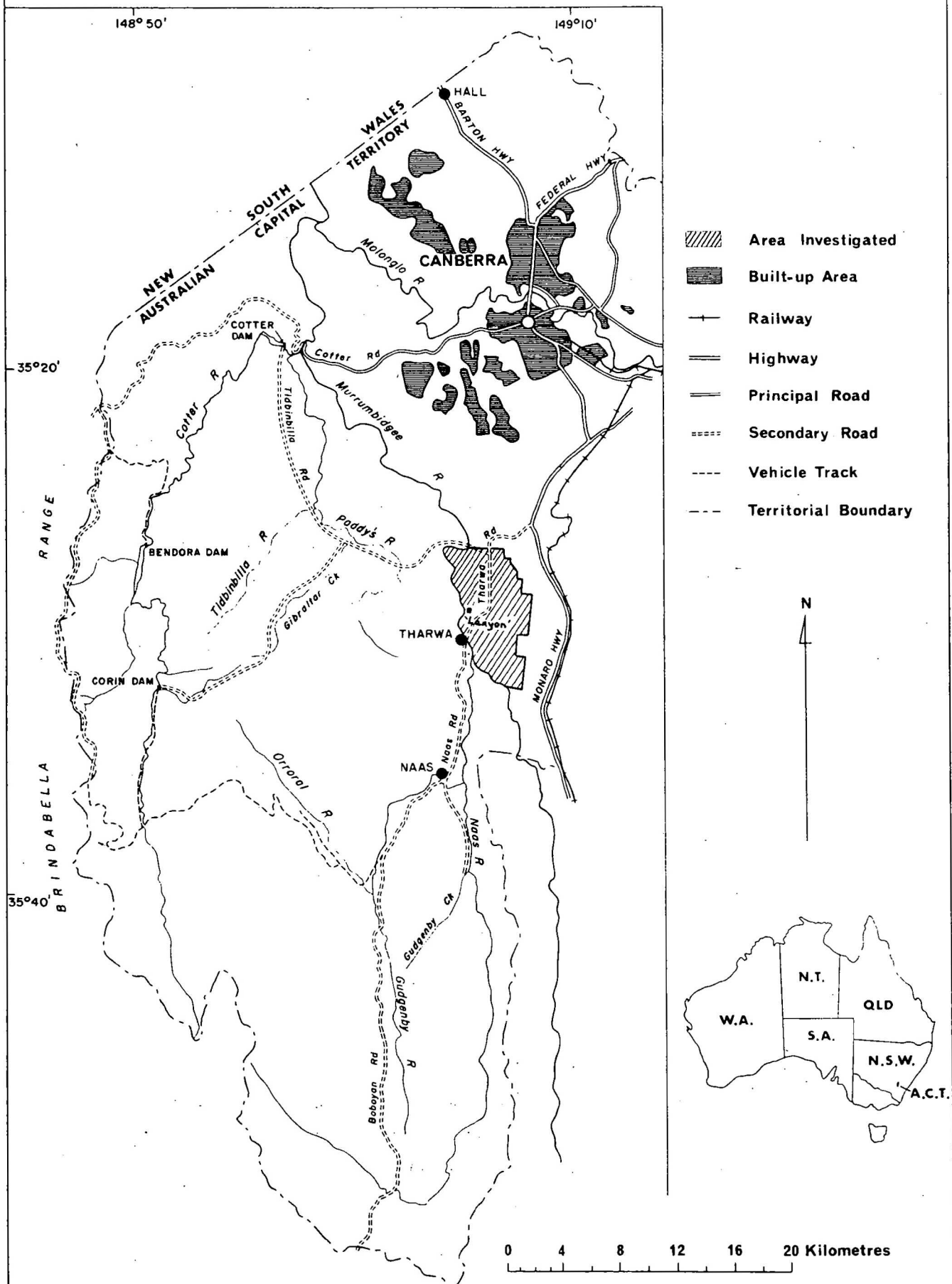
The recommendation for deep bores was met by five diamond-drillholes that were drilled and cased during the latter half of 1976.

Location

The Lanyon north basin is located 18 km due south of Canberra in the southern Tuggeranong valley and can be reached via the Monaro Highway and Tharwa Road (Fig. 1). Its surface-water catchment occupies an area of about 1500 ha of which about 400 ha comprises an undulating wedge-shaped plain and footslopes bisected by the Tharwa Road. About 25 ha of the plain was waterlogged for at least 90 percent of the duration of the investigation,

Fig.1

LOCATION OF INVESTIGATED AREA



and a further 30 ha was intermittently waterlogged (Fig. 2).

The south basin (Fig. 2) lies 4 km farther south along the Tharwa Road. Its surface-water catchment is about 1350 ha, which includes a plain and footslopes of 130 ha, of which about 20 ha is a permanent swamp and a further 50 ha becomes intermittently waterlogged, depending on seasonal conditions.

GEOLOGY

The geology of the central Lanyon area is shown in the outcrop map (Plate 1), and hand-specimen descriptions of the lithological units are given in Table 1.

A gently warped sequence of upper Silurian acid volcanic rocks and thin interbedded volcanoclastics unconformably overlies steeply dipping tuffaceous sediments which crop out to the north-west of the Lanyon north basin (Goldsmith 1975 and 1976), and to the south-east of Tharwa village (Mendum 1975). The western sections of the basins are developed on a down-thrown block bounded by the Murrumbidgee Fault to the west and by a high-angle north-trending fault (Plate 1) to the east. The higher basin surfaces and escarpments up to Mount Rob Roy are developed on the upthrown block east of the north-south fault. Minor block faulting has occurred between parallel south-east cross-faults, but otherwise the rocks are structurally undeformed.

The volcanics range in composition from dacitic to rhyolitic. The dominant units are massive welded ash-flow tuffs with well-developed joints; the rocks are foliated near the tops of flows and also towards the northern part of the mapping area where the units thin out. Massive rhyolite dykes have intruded adjacent to cross-faults on the watershed between the north and south basins; they probably formed as vents for the cream rhyolite which occupies the slopes of Mount Rob Roy.

Subdivision of the upper Silurian sequence on the upthrown eastern block (Plate 1) was based on the various interbeds of sandstone and shale deposited in shallow marine to terrigenous environments during pauses in volcanism. Elsewhere contacts are defined by ash-fall tuffs and agglomerates.

In the absence of sedimentary marker beds in the western part of the mapping area, the subdivision of units and their correlation with units in the east was on the basis of zonal variations within the ash-flow tuffs.

TOPOGRAPHIC MAP OF LANYON BASINS

Fig. 2

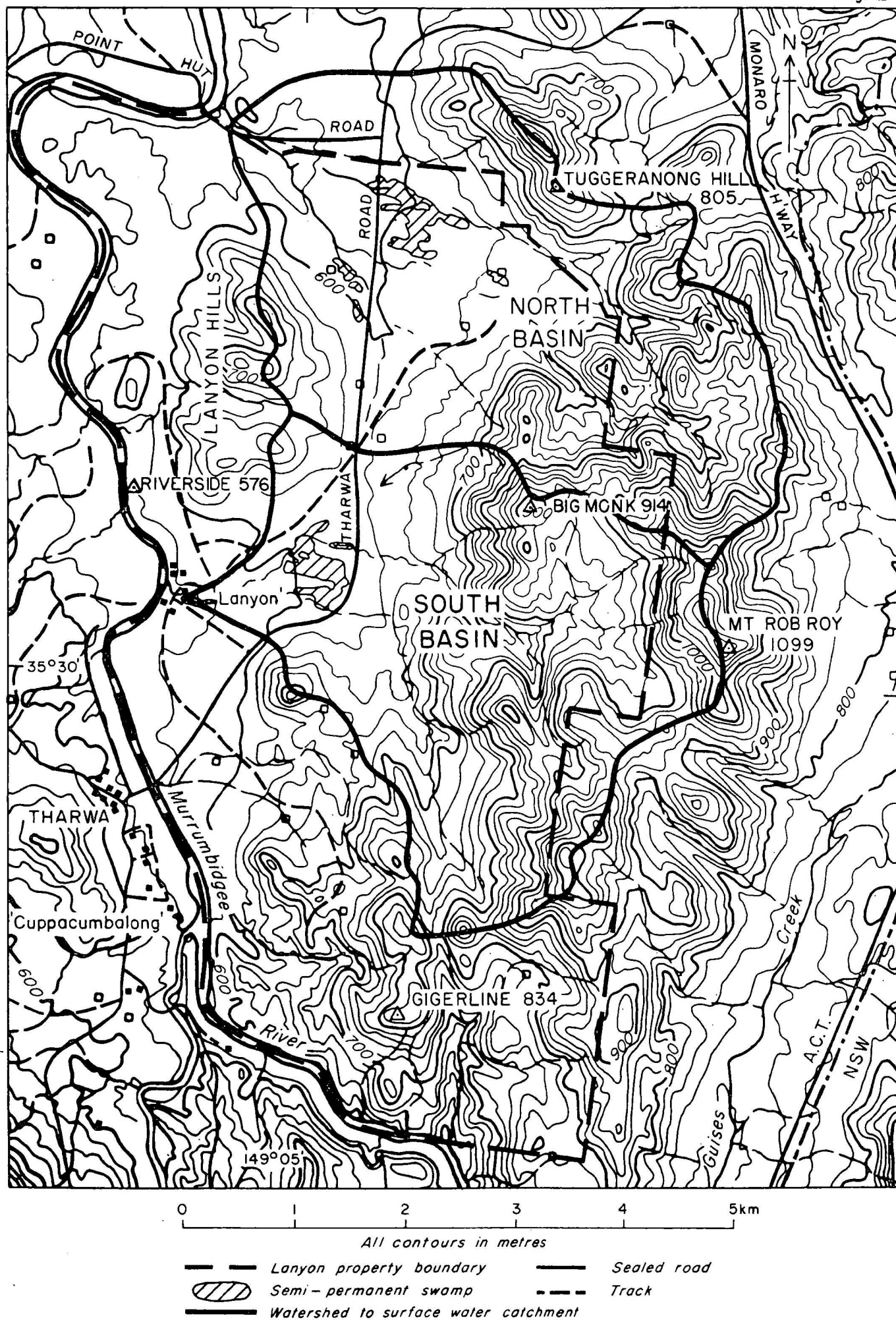


Table 1. Hand-specimen descriptions of Upper Silurian acid volcanics - central Lanyon area

Map unit	Lithology	Comments
Blue-grey porphyritic rhyodacite, dacite (Sul)	<p><u>Mid-zone:</u> Subhedral quartz (to 8 mm) and plagioclase (to 2 mm) phenocrysts in dark blue-grey to green-grey groundmass. Phenocrysts make up to 30% of rock. Minor biotite and chalcedony inclusions.</p> <p><u>Basal zone:</u> Minor broken quartz and plagioclase phenocrysts (to 3 mm) in blue-grey groundmass. Phenocrysts comprise less than 10% of rock. Some rock fragments in places.</p>	<p>Massive. Top of flow not observed.</p> <p>Probably unconformable on the underlying upper Silurian sequence.</p>
Purple-blue porphyritic rhyodacite (Sud 10b)	Subhedral phenocrysts of quartz and zoned plagioclase (2-5 mm) in purple-blue groundmass. Minor pink potash feldspar. Phenocrysts comprises up to 30% of rock.	Massive and homogeneous. May represent the upper part of a multiple ash-flow unit including the underlying rhyolite.
Cream to pale purple porphyritic rhyolite (Sud 10a)	<p><u>Upper zone:</u> Euhedral quartz (to 5 mm) and feldspar (to 3 mm) with noticeable increase in biotite in pinkish to purple-grey groundmass.</p> <p><u>Basal and mid zones:</u> Phenocrysts dominantly broken quartz (to 3 mm) and feldspar (to 2 mm) with accessory biotite and rock fragments in pale green to cream groundmass. Phenocrysts comprise up to 50% of the rock.</p>	Eutaxitic structure consisting of bands of recrystallized quartz and feldspar, particularly in northern areas. Very hard and massive above the perched basin but the unit thins rapidly towards the north near Tuggeranong Hill and becomes strongly banded. Composite extrusive-shallow intrusive with remnants of a chilled margin exposed adjacent to quartz blows on the Lanyon Hills, due west of the tourist entrance gates.
Red Sandstone	Very poorly sorted medium-grained arkosic sandstone with equal proportions of quartz and feldspar; accessory rock fragments and biotite.	Discontinuous. Observed on only one ridge above the north basin. Maximum thickness 30 cm.
Massive rhyolite dykes (Sp4)	Euhedral phenocrysts of pink potash feldspar (5-10 mm) and quartz (2-5 mm) in olive green to pale buff groundmass. Phenocrysts make up to 50% of the rock.	Generally intruded parallel to south-east cross faults. Massive dykes on the basin watershed probably represent vents for the overlying cream rhyolite.

Map unit	Lithology	Comments
Purple porphyritic rhyodacite (Sud 6)	Phenocrysts of quartz (to 10 mm) and euhedral zoned plagioclase (to 5 mm) with accessory potash feldspar, biotite and rock fragments in purple micro-crystalline groundmass. Phenocrysts comprise up to 50% of the rock in the middle of the unit.	Foliated at the top of the unit. Forms eastern planation surface of the perched basin.
Brown ash-fall tuff (Sud6)	Greenish brown, micaceous tuff. Rhythmic bands are 1 cm thick consisting of (i) quartz and feldspar (1 mm) and (ii) greenish grey silicified silt-clay with broken feldspar phenocrysts (3 mm) and minor rock fragments.	Maximum thickness 3 m.
Blue rhyolite	Dark blueish grey fine rhyolite with sparse phenocrysts (1 mm) of quartz and euhedral feldspar. Trace of biotite.	Massive and homogeneous. Top and bottom contacts not exposed.
Purple-blue porphyritic rhyodacite	Euhedral quartz and plagioclase phenocrysts (to 10 mm) with accessory biotite and subrounded rock fragments (to 5 cm) in dark purple-blue groundmass. Phenocrysts and inclusions comprise about 30% of the rock. Increase in biotite towards the top of the unit. Phenocrysts progressively finer-grained (2 mm broken quartz and feldspar) but more abundant (up to 50% of the rock) near the top of the flow.	Upper zone of blue-grey rhyolite. Rock foliated and more easily eroded than underlying densely welded zone which forms escarpments. Western planation surface of the perched basin is developed on this unit.
Blue-grey fine to medium rhyolite (Sud 5e)	<u>Mid zone:</u> Coarse mostly euhedral phenocrysts of beta quartz (10 mm) and subdominant plagioclase laths (3 mm) in dark greenish grey to dark bluish grey groundmass. <u>Basal zone:</u> Broken quartz phenocrysts (to 3 mm) in dark bluish grey glassy groundmass. Phenocrysts comprise less than 10% of the rock. Accessory phyllosilicates, chlorite blebs.	Massive, densely welded. Forms prominent escarpment to the east of the lower basins. Massive, extremely hard when fresh. Conchoidal fracture.
Black shale	Black fossiliferous (shallow marine) laminated shale.	Maximum thickness 10 m
Quartz sandstone (Sud 5d)	Moderately well sorted quartzose sandstone. Framework grains are sub-rounded and bipyramidal quartz (mode 2 mm). Thin lenses of calcareous mudstone inter-	Maximum thickness 15 m. rock heavily quartz-veined.

Map Unit	Lithology	Comments
	calated between sandstone and shale beds in some places.	
Green-grey porphyritic rhyodacite (Sud 5c)	<p><u>Upper zone:</u> Euhedral quartz and feldspar (2/3 plagioclase, 1/3 potash feldspar) phenocrysts to 10 mm in purple groundmass. Phenocrysts less than 20% of rock, becoming very sparse in top 5 m of the unit. Noticeable increase in porosity with opaque oxide void infills; phyllosilicates, chert fragments and veins.</p> <p><u>Mid zone:</u> Euhedral phenocrysts of quartz and pale green plagioclase laths (to 5 mm) in greenish grey to purple grey groundmass. Accessory biotite and pink potash feldspar. Phenocrysts comprise up to 40% of the rock.</p> <p><u>Basal zone:</u> Sparse broken and subhedral phenocrysts of quartz and potash feldspar (to 5 mm) in dark grey groundmass.</p>	<p>Top 5 m of flow characterized by multidirectional wispy chert veining. No definite foliation.</p> <p>Massive.</p> <p>Massive. Basal zone generally less than 10 m thick.</p>
Shale. Tuffaceous sandstone	Dark greenish grey laminated shale. Poorly sorted arkosic sandstone; framework grains are subrounded feldspar, quartz (to 1 mm), and minor rock fragments.	
Ash-fall tuff	Greenish brown, silicified and strongly laminated with rhythmic bands (<10 mm) of fine to medium quartzofeldspathic sand and silt-clay	Maximum thickness of sequence 50 m. Agglomerate dominates in the north, shales and sandstones in the south.
Agglomerate (Sud 5b)	Very pale brown, laminated, containing abundant subrounded dacitic rock fragments up to 5 cm, which are strongly resorbed in places.	
Green-grey tuff	Phenocrysts of quartz and plagioclase (to 3 mm) with accessory rock fragments in pale greenish grey groundmass. Grades to very poorly sorted ash-fall tuff at the top of the unit.	Some reworking evident at the top of the unit.

Map Unit	Lithology	Comments
Tuffaceous Sandstone, ashstone (Sud 5a)	Thin interbeds of greenish grey silicified siltstone, sandstone and ashstones. Sandstones are poorly sorted with framework grains of quartz and feldspar (modal size 2 mm) with accessory biotite and rock fragments. Siltstones are laminated brown-grey, cherty and micaceous. Ashstone is greenish grey with abraded rock fragments in some places.	Only one exposure of this sequence (creek bed in north basin). Thickness at this site 15 m.
Blue-grey, green-grey and purple porphyritic rhyodacite (Sud 4)	<p><u>Upper zone:</u> Subhedral phenocrysts of quartz (7 mm) with buff and pale green zoned plagioclase (5 mm) in blue-grey to purple groundmass. Mica content increases towards top of flow. Some bands of recrystallised quartz and feldspar.</p> <p><u>Mid zone:</u> Scattered large (to 10 mm) broken quartz in mosaic of subhedral quartz and plagioclase (to 3 mm) phenocrysts in green-grey to blue-grey groundmass. Phenocrysts comprise up to 20% of rock.</p> <p><u>Basal zone:</u> Euhedral quartz and plagioclase (to 5 mm) phenocrysts with accessory phyllosilicates in dark bluish grey groundmass. Phenocrysts comprise up to 50% of the rock.</p>	<p>Prominent eutaxitic foliation towards the top of the unit.</p> <p>Massive.</p> <p>Diffuse and discontinuous foliation due to phyllosilicate intercalations.</p>
Sandstone	Pale brown to purple silicified poorly sorted sandstone. Framework grains are subrounded quartz (60%) and feldspar (40%). Modal grain size 1 mm.	Maximum thickness 1.5 m (Southwest face of Tuggeranong Hill).
Mudstone, shale chert, sandstone (Sud 3)	Massive blue-grey to brown silicified mudstone/ashstone grading to purple with prominent partings when weathered. Micaceous and strongly laminated with abraded rock fragments at top of sequence. Cleavage development in some places. Thin chert and tuffaceous sandstone interbeds. Interfingers with 1 to 2-m-thick rhyolite flows in western end of north basin.	No outcrop in mapping area; only observed in north basin drillcore.

JOINTING IN THE SILURIAN VOLCANIC ROCKS

The Silurian volcanics are an important aquifer at Lanyon because joints provide a system of open fractures in which groundwater is stored and transmitted. The hydrogeological properties of joints were analysed by the study of joints in drillcores and joints in outcrops.

Joints in drillcores

Joint frequencies and intercept angles were measured in unoriented cores from 5 diamond-drillholes (L10-L14) in which specific fracture zones had been pumped by airlift during drilling. Frequency logs and steady-state airlift pumping rates are shown in Appendix 3.

Four fracture categories of joints were recognised in the drillcores:

- (i) open, rough-faced extension joints with fractures mainly within the groundmass and no displacement parallel to the joint faces. Protruding phenocrysts provide rough surfaces that are generally limonite-stained. These joints in moderately weathered to fresh-stained rock are the best groundwater producers. Steady airlift recovery rates range from $2 \text{ m}^3/\text{day/m}$ to $10 \text{ m}^3/\text{day/m}$ in 150 mm diameter holes in intervals where these joints comprised at least 50% of fractures.
- (ii) smooth shear joints with planar fractures through both phenocrysts and groundmass and with displacement parallel to the joint face. These joints are generally clay-lined or clay-filled, commonly slickensided, and produce negligible groundwater.
- (iii) open, slightly rough to smooth oblique shear joints. This type of joint was the most frequent in the cores. Faces are generally limonite-stained and/or spotted with a clay film or lining. Protruding phenocrysts, where present, have been partly smoothed by the component of displacement parallel to the joint face. Many fractures appear to result from the rock having been subjected to compressional stress and later to tensile stress, or vice versa. These joints give lower yields

but are significant producers of groundwater. Steady airlift recovery rates range from $0.2 \text{ m}^3/\text{day/m}$ to $1 \text{ m}^3/\text{day/m}$ in 150 mm diameter holes in intervals where these joints comprised at least 70% of fractures.

- (iv) healed joints, generally filled with calcite. Joints with both rough and smooth surfaces have been healed; they are tight and do not yield groundwater.

Joints in outcrop

Joints in rock outcrops in and around the basins were studied to relate them to the four categories of fractures derived from the analysis of drillcore fractures. In particular, the study attempted to identify the youngest continuous joint sets of types (i) and (iii) fractures listed above.

There have been at least 3 distinct phases of joint development in the volcanics:

- (a) cooling (extension) joints. Most of these fractures are probably type (iv) joints given their antiquity. Nevertheless, these joints provided primary planes of weakness which, depending upon their orientation, were susceptible to reactivation during subsequent deformation and to the formation of open joints of type (i) by removal of calcite.
- (b) structurally controlled joints, formed by uplift and faulting are a combination of shear, oblique shear and extension joints. Fracturing from subsequent deformational phases has overprinted pre-existing joints.
- (c) erosional unloading has produced mainly subhorizontal extension joints.

A summary of the joint analysis from major outcrops is shown in Plate 2. Measurements were taken in homogeneous structural and lithological domains (Plate 2), and the aim was to record the following data:

- (i) orientation
- (ii) length
- (iii) spacing

- (iv) relative age of sets
- (v) joint faces

Recordings were taken only if joints were repeated within the outcrop and if they were continuous throughout the outcrop. Sets were recorded only once per outcrop despite their frequency, hence statistical inferences concerning joint distributions should not be made from the contoured stereograms. If absolute joint frequencies were to be plotted it is likely that contours for some percentages of poles would be so increased that the overall fracture history may be less evident.

Recording of joint lengths was discontinued early in the survey because unbiased measurements could not be attained.

Mean joint spacings were obtained and are shown in Table 3 but standard deviations are large.

The determination of the relative age of joints in an outcrop was only partly successful. Consistent age relationships based solely on offsets throughout each domain could not be readily established. However, it was possible to ascertain some obvious upper and lower bounds. For example all unhealed joints in the oldest rhyodacite unit were formed after intrusion of the youngest rhyolite dykes, and all but the low-angle joints were developed before, or at the same time as, cross-faulting. A relationship which appears to be consistent throughout is that high-angle joint sets predate all unhealed fractures of dip up to 20° .

Joint faces which were accessible in outcrop were nearly always weathered but it was generally possible to determine whether the fracture was essentially in the groundmass or cut across both groundmass and phenocrysts by running the palm of the hand over the joint face. Characteristics such as clay minerals and slickensides were also noted.

Results of the survey are shown in Table 2.

Table 2. Significant joint sets

DOMAIN	LITHOLOGY	SET NO. (see Plate 2)	ORIENTATION (dip/dip direction)	MEAN SPACING (m)	PROBABLE FRACTURE TYPE
A	Porphyritic rhyodacite, east of main N-S fault and south of main southern cross-fault. All measurements at least 100 m from faults. (Sud 5c)	1	80/086	1.9)conjugate shears, ^o
		2	78/020	> 2)dihedral angle 65 ^o
		3	77/042	> 2	extension, related to 1&2
		4	58/225	1.7)conjugate shears, ^o
		5	68/082	> 2)dihedral angle 65 ^o
		6	67/241	1.3)conjugate shears, ^o
		7	73/123	1.7)dihedral angle 73 ^o .
		8	31/129	0.5	extension, related to either sets 4 & 5 or 6 & 7.
L	Porphyritic Rhyodacite on main southern cross-fault. All measurements were taken in the deeply incised valley which follows the fault zone. (Part Sud 5c, part Sud 5e)	1	90/130	< 0.1	shear, parallel to fault
		2	90/098	0.4	extension, related to 1.
		3	58/085	1.4	oblique shear.
		4	57/325	1.0)conjugate shears, ^o
		5	68/192	1.1)dihedral angle 70 ^o .
		6	12/292	0.6	extension.
		7	20/005	0.7	extension
C	Blue-grey rhyolite. E-W traverses along the densely welded zone of the scarp and on the partly welded zone above. All measurements at least 100 m from faults. (Sud 5e)	1	90/065	0.8)conjugate shears, ^o
		2	90/175	0.8)dihedral angle 70 ^o .
		3	90/154	0.6	extension, related to 4 & 5
		4	56/076	1.7)conjugate shears, ^o
		5	60/224	1.7)dihedral angle 70 ^o .

Table 2 Con't

DOMAIN	LITHOLOGY	SET NO. (see Plate 2)	ORIENTATION (dip/dip direction)	MEAN SPACING (m)	PROBABLE FRACTURE TYPE
G	Blue-grey rhyolite, bounded to the north and south by cross-faults (Sud 5e)	1	90/055	0.8)conjugate shears,
		2	90/172	0.6)dihedral angle 63°.
		3	90/151	0.7	extension, related to 4 & 5.
		4	58/080	1.9)conjugate shears,
		5	70/230	> 2)dihedral angle 59°
		6	53/126	1.7)orthogonal set of
		7	41/275	1.4)oblique shear or extension.
		8	71/202	1.1)orthogonal set of
		9	28/006	1.5)oblique shear or extension.
N	Pale purple rhyolite north of inferred cross-fault, southeast of Tuggeranong Hill. (part Sud 10a, part Sud 10b)	1	83/342	0.2)conjugate shears,
		2	88/221	0.1)dihedral angle 61°.
		3	90/102	0.3	extension, related to 1 & 2.
		4	69/078	0.6)conjugate shears,
		5	55/224	0.3)dihedral angle 64°.
		6	19/139	0.2	extension.
		7	50/046	0.7	Oblique shear
		8	30/169	0.5	oblique shear
H	Blue to green-grey porphyritic rhyodac- ite. Measurements taken along the south- western face of Tuggeranong Hill (Sud 4)	1	90/119	0.7)conjugate shears,
		2	90/188	1.4)dihedral angle 69°.
		3	66/277	1.3)conjugate shears,
		4	69/050	1.7)dihedral angle 65°.
		5	25/194	0.9	extension
		6	14/100	0.6	extension
E	Blue-grey porph- yritic dacite, west of main N-S fault.	1	86/179	1.9)conjugate shears,
		2	74/071	1.6)dihedral angle 74°.
		3	80/036	> 2	extension, related to 1 & 2

Table 2 Con't

DOMAIN	LITHOLOGY	SET NO. (see Plate 2)	ORIENTATION (dip/dip direction)	MEAN SPACING (m)	PROBABLE FRACTURE TYPE
	(Sul)	4	42/050	1.7)conjugate shears, ^o
		5	71/264	> 2)dihedral angle 73°.
		6	65/132	1.9	orthogonal set
		7	59/025	1.5	oblique shear or ext.
		8	23/300	0.7	extension, related to 4 & 5
F	Blue-grey porphy- ritic rhyodacite, west of main N-S fault All measurements taken in creek exposures on western and southern sides of south basin (Sud 4)	1	90/121	1.1	extension
		2	90/152	0.7	shear, related to 1.
		3	80/137	1.0	extension, related to 1.
		4	58/092	0.7)conjugate shears, ^o
		5	56/306	0.6)dihedral angle 73°.
		6	08/245	0.2	extension.

Inferred stress history from joints survey and its hydrogeological significance

Stereographic plots of centroids of joint set concentrations are shown adjacent to the contoured stereograms of poles to joints in Plate 2. Probable former principal stress orientations shown on the stereonets are derived purely from experimentally established geometrical relationships between brittle fractures and stresses in classical rock mechanics, and must therefore be regarded as idealistic. The most suspect part of the analysis is its dependence on the correctness of field identification of conjugate pairs of shear joints.

The subscripts outside the parentheses of the principal stresses denote the probable stage of joint development. Thus (σ_1^2) reads as the maximum principal stress orientation during the second recognisable major stage of joint formation. Results are summarised in Table 3.

Table 3
Probable principal stress direction inferred from joint classification and geometry

Domain	FIRST MAJOR DEFORMATIONAL PHASE			SECOND MAJOR DEFORMATIONAL PHASE		
	(σ_1^1)	(σ_2^1)	(σ_3^1)	(σ_1^2)	(σ_2^2)	(σ_3^2)
A	02/142	77/045	12/234	(59/326 35/001)	32/157 55/188	05/064 03/093
L	00/098	90	00/008	52/074	37/264	05/170
C	00/030	90	00/120	66/334	24/149	05/240
G	00/023	90	00/113	62/345	27/151	07/243
N	(12/023 10/101)	20/117 81/289	66/263 01/190	60/319	28/155	07/061
H	00/152	90	00/062	46/165	44/342	02/074
E	16/308	72/101	08/217	62/129	21/346	15/250
F	00/121	90	00/031	67/198	24/018	00/108

A common feature in all domains is the apparent stress reversals in successive stages of joint development, indicated for example by initial high-angle intermediate principal stress directions changing to low to intermediate angles in the next stage of fracturing. These gross differences in successive principal stress directions are believed to define former regional compressive and tensile fields, and smaller-scale rotation of sets from one domain to the next is attributed

to subsequent movement (perhaps several times) along the major fault zones.

The regional deformational history is probably most simply illustrated in domain C. From field observations the three dominant vertical joint sets (1, 2, and 3) definitely predate all intersecting joints of dip up to 30° , and in most outcrops they appear to either predate sets 4 and 5 or to have been developed at the same time. Typical outcrop from domain C is shown in Figure 3. Sets 1 and 2 are classified as the earliest recognisable conjugate shear fractures. Sets 4 and 5 appear to be a younger set of conjugate shears, and set 3 represents extension fractures formed during compression in the later deformational stage.

Local modification due to faulting is best shown in domain L. Joint set 1 has been rotated parallel to the main cross-fault, and joint faces of this set are generally slickensided and in places mylonitized. In this domain only one shear joint developed in response to compression. Related extension fractures which in this domain are in places filled with epidote or calcite are represented by set 2.

Price (1966) described interchanging of regional principal stress directions as a consequence of uplift and erosional unloading for rock which contains residual tectonic stresses. Price proposed an initial condition at burial of horizontal σ_1 and σ_2 with vertical σ_3 as residual stress following thrusting. At Lanyon this stress geometry would have existed during initiation of the Murrumbidgee Fault, and it is reasonable to expect the adjacent massive volcanic units to maintain a high residual stress component as opposed to say, a thinly bedded sedimentary sequence which would more readily deform by folding under similar conditions. In Price's model, σ_2 interchanges with σ_3 as uplift proceeds, thus creating the necessary condition for the development of vertical conjugate shear fractures. The release of residual stress by slip along the shear planes, combined with additional uplift, results in the interchanging of σ_1 with σ_2 . At the surface the rock is under a tensile stress field from erosional unloading and lateral extension, although the latter is probably of less significance in this example because the rocks at Lanyon have been tilted.

The joint analysis and the downhole pumping results imply that the youngest tensile fractures, which at Lanyon generally dip at less than 25° , are the most important joints hydrologically.

Significant recharge to these fractures occurs via intersections with older high-angle extension joints and oblique shear joints. Groundwater storages and transmission rates of the fractured rock can therefore be estimated by using

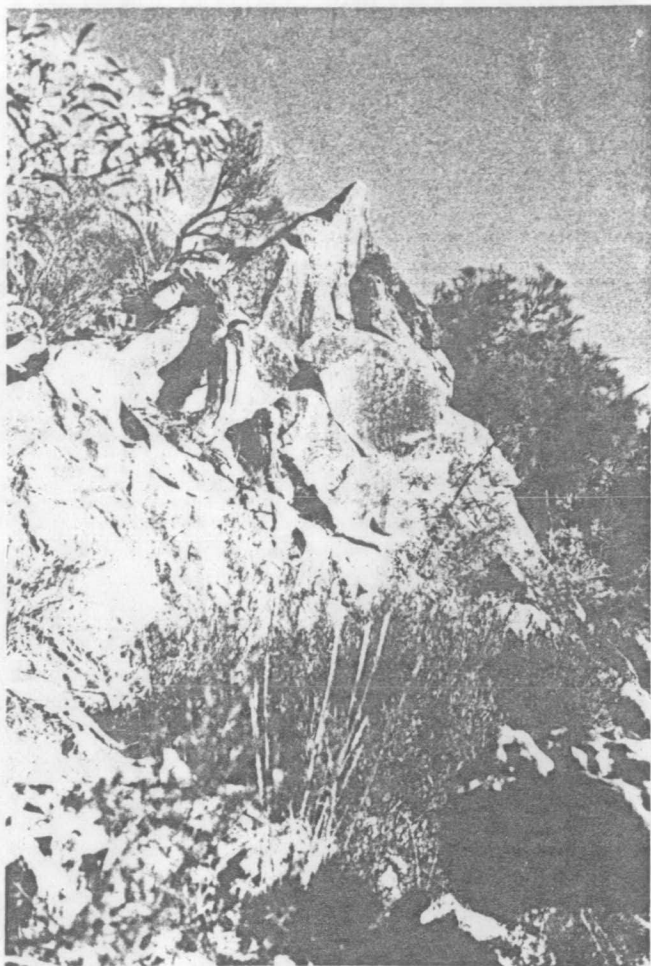


Fig. 3. Typical joints in the densely welded zone of the blue-grey rhyolite (Domain C). The two major vertical smooth-faced sets are slightly offset by the set dipping at 55° (20865E 58084N). BMR Neg. GB/2907-5A.

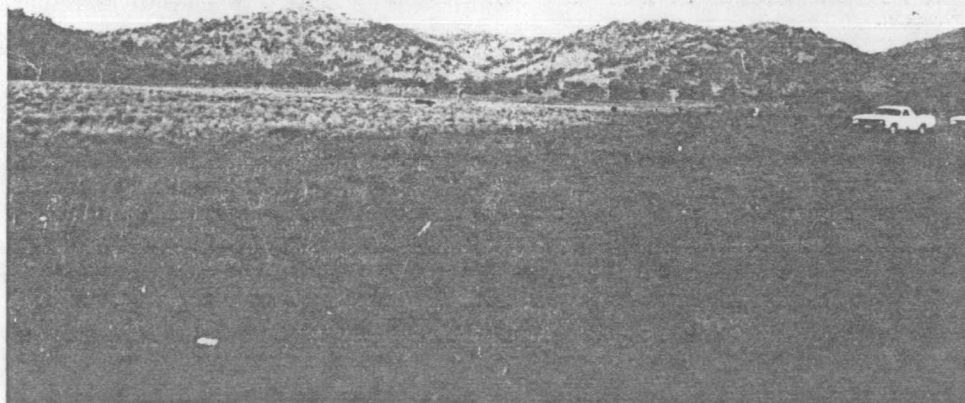


Fig. 4. Looking northeast across the Lanyon north basin. The high terrace on which the cars are parked is the surface of the oldest basin fill represented by the Tuggeranong and Murrumbidgee pedoderms. The lower basin surface to the left is underlain by the Lanyon pedoderm which is inset into the older pedoderms. Up to 4 m of material was eroded from the Tuggeranong and Murrumbidgee pedoderms by headward erosion and lateral development of the basin drainage, and contemporaneous deposition elsewhere in the basin was the first in a sequence of events leading to formation of the Lanyon pedoderm. BMR Neg. GB/2907-15A.

mean frequencies of extension joints from Table 2, provided that joint apertures are known. The estimates are given elsewhere in the report in the section on hydraulic conductivity of the aquifers.

GEOMORPHOLOGY

General geomorphic setting

The geomorphology of the Lanyon north and south basins is shown in Figures 5 and 6. The basins are described as pediplain basins after van Dijk (1959). The landforms are relatively young geomorphic modifications of a much older landscape on which a series of erosional planar surfaces step up, via joint-controlled escarpments, from the Murrumbidgee River at 560 m in the west to the summit of Mount Rob Roy (1099 m) at the eastern boundary of the surface-water catchment.

A similar sequence of stepped landsurfaces was reported by van Dijk (1959) in his study of the Molonglo River valley to the east of the Lanyon area. He regarded the planar surface as pediplains and referred to them as follows:

Monaro landsurface	920 m
Molonglo landsurface	790-850 m
Yass-Canberra tablelands	650-670 m
Yarralumla landsurface	580-610 m

Earlier, Craft (1931, 1932, 1933) had described a sequence of high plains in the southern highlands and in the Shoalhaven River valley of New South Wales. Craft envisaged that the highest plains, the Monaro landsurface, evolved after the Kanimblan Orogeny (Middle Carboniferous), and that planation was completed by the Permian. The lowest plains, which Craft referred to as the Lower Shoalhaven Plain, is at about the same level of the Yarralumla landsurface of van Dijk. According to Craft (1931, 1932) this youngest plain was initiated after deposition of Triassic sediments of the Sydney Basin and attained maturity before it was buried beneath basalts of the Nerriga and Mittagong Provinces. The basalts have been isotopically dated as late Eocene to middle Oligocene (Wellman & McDougall, 1974).

The process responsible for the formation and preservation of these ancient surfaces in the Molonglo and Shoalhaven River valleys has been described as multiple pediplanation (van Dijk, 1959) in response to base-level changes brought about by intermittent periods of epeirogenic uplift (Craft, 1933). The cross-sections (Figs. 5 and 6) may also be interpreted as showing multiple pediplain surfaces in Lanyon with their parallel scarps and pediments, or remnants of them.

Fig. 5

GEOMORPHIC MAP, LANYON NORTH BASIN

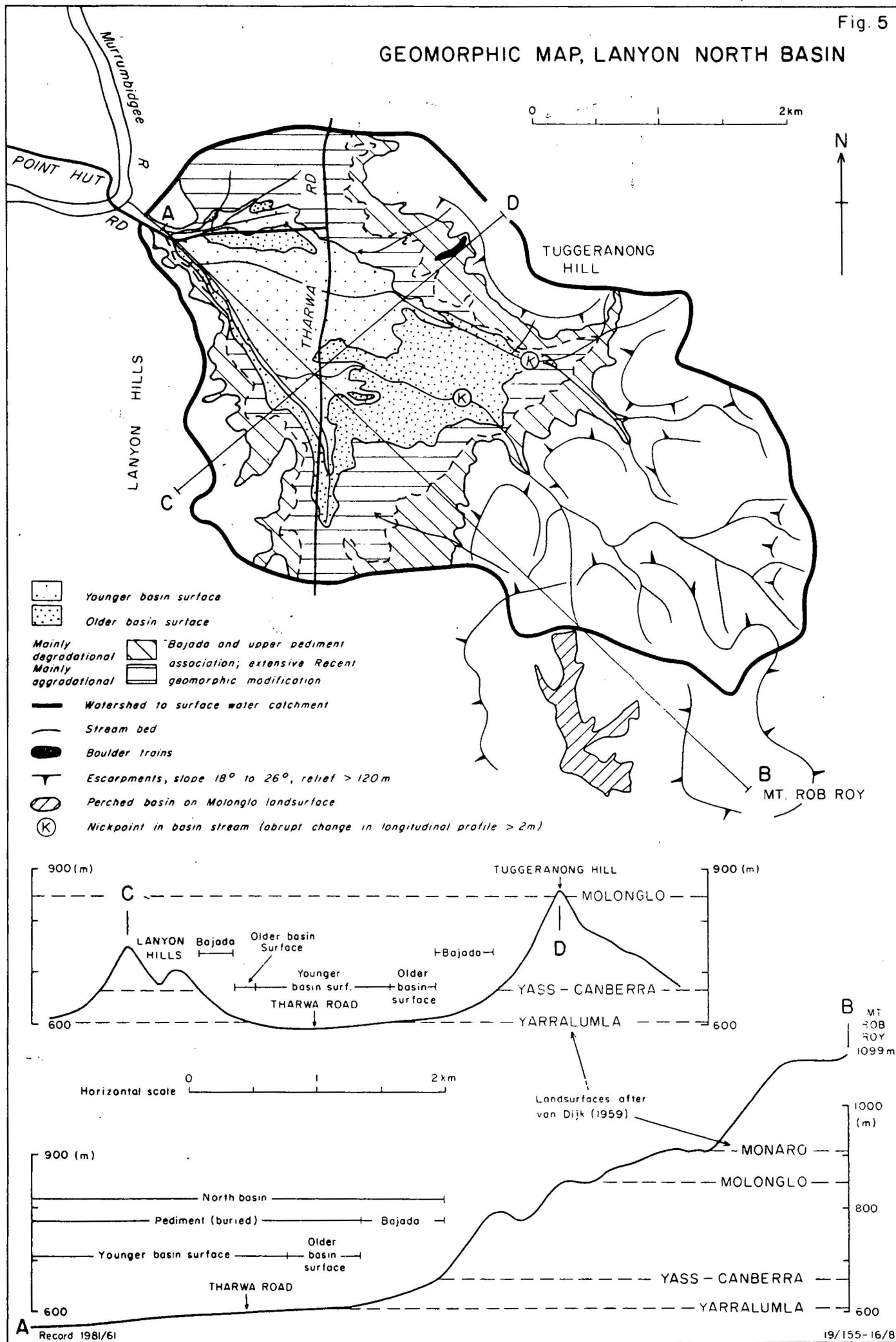
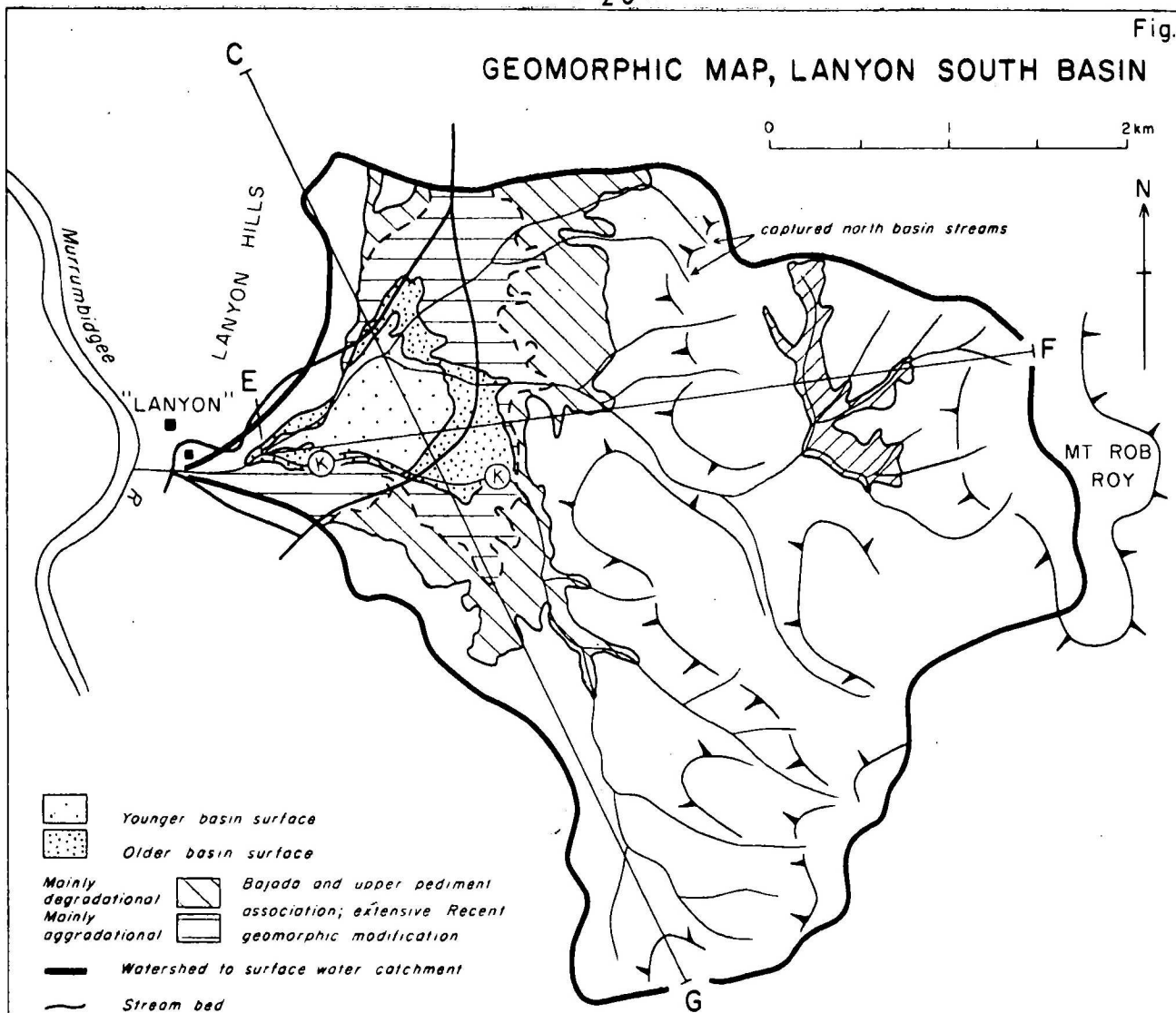
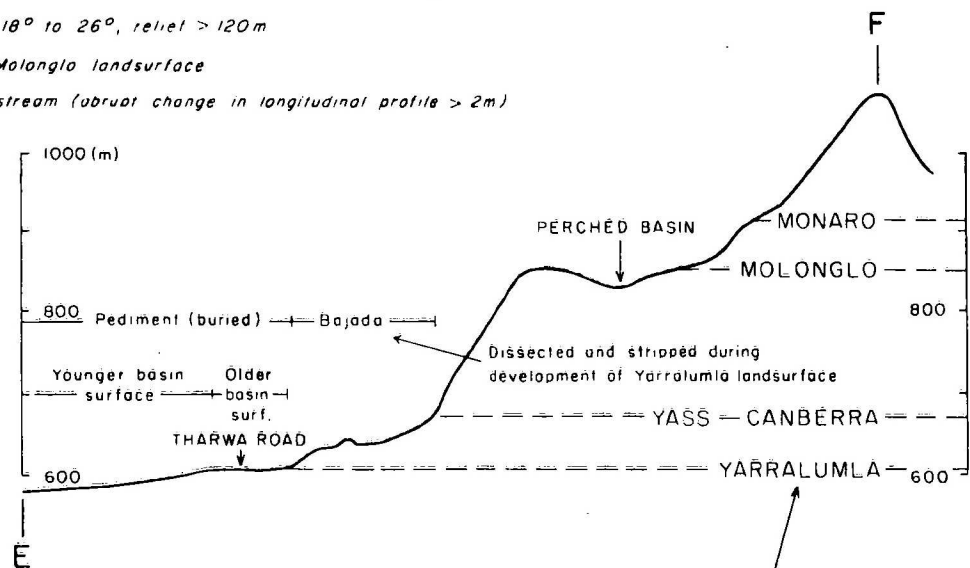


Fig. 6

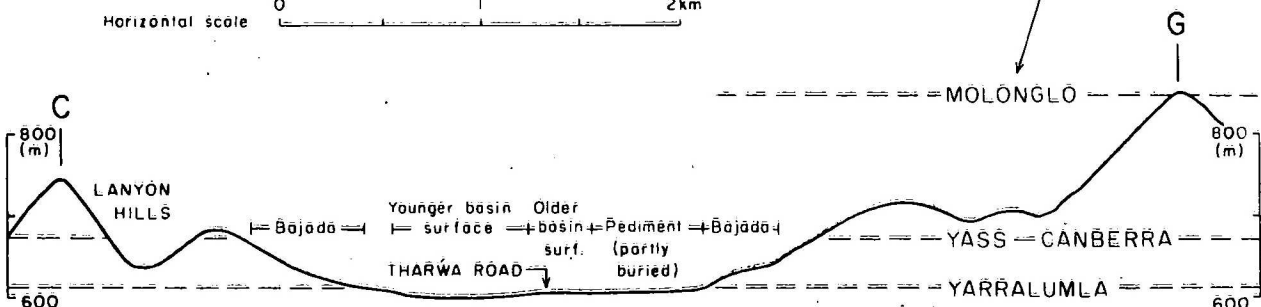
GEOMORPHIC MAP, LANYON SOUTH BASIN



- Younger basin surface
- Older basin surface
- Mainly degradational Bajada and upper pediment association; extensive Recent geomorphic modification
- Mainly aggradational Bajada and upper pediment association; extensive Recent geomorphic modification
- Watershed to surface water catchment
- Stream bed
- Escarpments, slope 18° to 26°, relief > 120m
- Perched basin on Molonglo landsurface
- Nickpoint in basin stream (abrupt change in longitudinal profile > 2m)



Horizontal scale 0 1 2km



Correlation of landsurfaces of the Lanyon basin catchments with regional models.

A prominent change of slope is evident at about 920 m at the foot of the 25° western slopes of Mount Rob Roy and other unnamed peaks in the hills to the east of the Lanyon basins. It marks the upper level of a bench that could be tentatively described as a remnant of the Monaro landsurface which has survived stream dissection and encroachment by the upper pediment of the Molonglo landsurface. Other possible indications of a former high plain at this level are flat-topped hills at 900 m in the central eastern sector, and spurs at 900 to 920 m in the southeast.

Remnants of the Molonglo landsurface may be present to the north, east, and southeast of Lanyon as flat-topped hills and spurs at 800 m to 850 m and as saddles of the higher slopes. In the eastern part of the catchments the Molonglo pediment (slope 2° to 3°) is well preserved, but it has been modified by Quaternary periglacial processes. A perched basin is preserved on the Molonglo landsurface above the south basin (Figs. 6 and 7).

A prominent break of slope at 650 m with embayments to 670 m may define the upper limit of the former Yass-Canberra tablelands level. The nick separates hillslopes of 18° to 26°, which rise up to the Molonglo landsurface some 150 m above, from a concealed pediment of slope 2° to 3°, which extends down to a plain at a similar elevation to the Yarralumla landsurface at about 600 m. The break of slope at 650 m to 670 m is a pronounced, consistent topographic feature within the Lanyon basins (Fig. 8) and throughout the Tuggeranong valley.

Possible remnants of the Yass-Canberra tablelands are also present as saddles at about the same elevation. The rock in these saddles is extremely weathered to about 10 m, and highly weathered to an unknown depth. There are no landscape elements at the 650-670 m elevation that could be considered comparable to the remnants of partial pediplains associated with the Monaro and Molonglo landsurfaces; both of these surfaces appear to have been arrested in the youthful to late-youthful stages of development by uplift that considerably increased the gradient in the Murrumbidgee River and induced vigorous incision. Chemical weathering would have been less advanced before uplift, after which landform modification would have been controlled by physical weathering.

However, the Yass-Canberra tablelands appear to have developed to a mature stage during which chemical etching produced a deeply weathered regolith that offered little resistance to its almost complete removal during the subsequent Yarralumla erosive phase. Craft (1932) noted the tendency of the Intermediate



Fig. 7. Looking northeast across the perched basin with its incised outlet in the foreground. Mount Rob Roy is behind the wooded slopes in the background. The tree line roughly follows the strike of the cream rhyolite. BMR Neg. GB/2907-3A



Fig. 8. Looking south along the Tharwa Road across the north basin. The break of slope at 650 m a.s.l. is clearly shown at the foot of the lightly timbered hills. The perched basin lies on the high ground between the first range of lightly timbered hills and the forested foot-slopes of Mount Rob Roy on the left. BMR Neg. GB/2907-17A.

Shoalhaven Plain (Yass-Canberra tablelands) to progress from discrete plains at Tallong, Nerriga, and Tarago to a condition of almost complete reduction to the Lower Shoalhaven Plain (Yarralumla landsurface) farther upstream in the Braidwood district.

The Lanyon equivalent to van Dijk's Yarralumla landsurface is a buried pediplain of westwards declivity 1° to $1\frac{1}{2}^{\circ}$ on which the north and south basins are superimposed. Headward encroachment into the north basin by the northern pediment of the south basin has brought about the capture of several ancestral north basin streams (Fig. 6).

Discussion on the evolution of the Lanyon landsurfaces

Direct correlation based on similar levels of landsurfaces of the western sector of the Molonglo River valley with those of the Lanyon catchments can be made on the following grounds:

- (i) both valleys are drained by rivers which coalesce 25 km to the northwest, and therefore the base-level of erosion would be common to both valleys
- (ii) there is no significant difference in the lithology across the divide between the two valleys.
- (iii) there are no known faults along the divide between the two valleys on which post Siluro-Devonian movement could have changed the levels of contemporary landsurfaces relative to one another.

However if the Lanyon basins are examined without recourse to the regional models of van Dijk and Craft, it can be shown that considerable control of the landforms can be attributed to geology.

The eastern escarpment and the Lanyon Hills follow the strike of the volcanics (Plate 1), with the exception of Tuggeranong Hill, which is oblique to the strike. The first escarpment to the east starts at the base of the easterly dipping blue-grey rhyolite (Sud 5e) and continues throughout the densely welded zone. The landsurface flattens out where this rock is only partly welded or non-welded, and the perched basin is located on this less-resistant zone and on the overlying non-welded purple rhyodacite (Sud 6) farther east. The escarpment above the perched basin is composed of massive, resistant cream rhyolite (Sud 10a) and becomes subdued farther north where the rhyolite is foliated. Massive cream rhyolite (Sud 10a) also comprises the steepest slopes of the eastern side of the Lanyon Hills. Hence it

may be argued that the levels of the planar surfaces are controlled by the thickness and degree of welding in the volcanic units.

To satisfy the multiple pediplanation hypothesis, several phases of uplift should be interspersed with long intervening periods of relatively constant base-level; yet the rocks at Lanyon are only slightly deformed, testifying to only epeirogenic uplift. However, development of the landscape at Lanyon could equally well be explained by continuous readjustment of the bed of the Murrumbidgee River in response to epeirogenic uplift.

The processes of pediplanation are favoured by the parting and weathering along high-angle joints in the acid volcanic rocks of Lanyon, and wedge and planar failure would have been common on steep slopes. Parallel scarp retreat has been the major process of landscape development and would have persisted throughout the wide range of climatic conditions that existed through the late Palaeozoic and Mesozoic. The northern escarpment (Tuggeranong Hill) of the north basin is still undergoing this form of scarp retreat and the association of jointing, toppling blocks, and potential slope instability has been reported (Macias, in prep.).

Geomorphic surfaces of the Lanyon basins

The basins are divided into five easily recognisable geomorphic surfaces - pediment, bajada and 3 basin surfaces (Table 4). The younger basin surface is one to two metres lower than the older basin surface (Fig. 4), and is inset into it. The youngest basin surface is likewise inset into the younger basin surface, but its lateral extent is restricted to areas adjacent to drainage lines and it is too small to be shown in Figures 5 and 6. As noted earlier, these geomorphic surfaces are erosional and depositional modifications superimposed onto the Yarralumla and Yass-Canberra landsurfaces, probably since the Early Tertiary. Each geomorphic surface possesses a unique soil association, or sequence of pedoderms, indicating that the landscape modifications were contemporaneous with, and are a surface expression of, Cainozoic soil development. The pedoderms are described in the following section on surficial geology.

Table 4
Geomorphic surface/soil association, Lanyon

Geomorphic Surface	Elevation (m)		Dominant Pedoderm Sequence
	North Basin	South Basin	
Youngest basin surface	570-600	570-590	Big Monk/truncated Tuggeranong/ truncated Murrumbidgee
Younger basin surface	570-610	570-590	Lanyon/truncated Tuggeranong/ truncated Murrumbidgee*
Older basin surface	610-625	600-610	Tuggeranong/truncated Murrumbidgee*
Pediment	565-625	575-610	Lanyon-modified Tuggeranong/ truncated Murrumbidgee
Bajada	625-670	610-660	Gigerline/truncated Big Monk/ truncated Murrumbidgee

* In the north basin the sequence is underlain by the Rob Roy pedoderm.

SURFICIAL GEOLOGY

STRATIGRAPHY

Soil stratigraphic units are mapped as pedoderms according to the nomenclature of Brewer, Crook & Speight (1970). Some continuous prominent horizons within individual pedoderms have been named as distinct sedimentary units for convenience of later reference. The soil stratigraphic column is shown in Figure 9. Spatial distribution of the pedoderms is shown in Figure 10 and 11, and cross-sectional field relationships are shown schematically in Figure 12.








Original colour photographs of the black and white copies illustrated in this report are available for inspection at BMR.

Rob Roy pedoderm

The Rob Roy pedoderm is composed of purple to red-brown arenites which were cored in drillholes L10, L13, and L14 (Appendix 3) in the north basin. There is no outcrop. Known thicknesses range from 15 m in L10 and L13 to 4 m in L14.

The arenites are weakly indurated and porous. Primary liquid porosity values from 6% to 11% were measured on core samples in the BMR Petroleum Technology Laboratory and these results, with directional permeability tests, are included in Appendix 2.

SURFICIAL STRATIGRAPHY OF THE LANYON PEDIPLAIN BASINS.

	RIVERSIDE PEDODERM	Minimal <u>prairie soils</u> in terraces, unconsolidated <u>slopewash</u> on perched basin and escarpments.
	GIGERLINE PEDODERM	Brown <u>earths</u> on <u>colluvium</u> grading to grey earths in lower basins. Red <u>earths</u> on <u>aeolian sands</u> on southern slopes of the south basin.
	<i>fine-grained facies</i> BIG MONK PEDODERM <i>basal slopewash/alluvial facies</i>	Yellow <u>podzolics</u> on upper basin surfaces; dark grey <u>solodics</u> in lower planation surfaces. Weak <u>subsolum</u> patterns. <u>Open colluvium</u> at foot of escarpments.
	<i>fine-grained facies</i> LANYON PEDODERM <i>basal clastics facies</i>	Red <u>podzolics</u> on upper catena. Minimal <u>lateritic podzolics</u> on mid-to-lower catena. <u>Latosols</u> on lower catena. Dark grey <u>solodics</u> in lower basin. Slopewash sheets on footslopes and higher basin surfaces. <u>Open gravels</u> in buried prior braided stream channels.
	<i>fine-grained facies</i> TUGGERANONG PEDODERM <i>basal fanglomerate facies</i>	Yellow <u>soloths</u> on elevated sites. Grey-yellow <u>podzolics solodics</u> on lower catena and in basin. Strong <u>subsolum</u> patterns of vertical veining and mottling. <u>Closed fanglomerate</u> ; very poorly sorted.
	<i>fine-grained facies</i> MURRUMBIDGEE PEDODERM <i>basal fanglomerate facies</i>	Distinct <u>pseudogley</u> patterns of multi-directional veining and joint planes; very strong Fe oxide segregation. <u>Closed fanglomerate</u> with relict complex cutans.
	ROB ROY PEDODERM	Lithic and feldspathic quartz <u>arenites</u> of ancient alluvial fan deposits.

The rocks represent prior braided stream deposits; the feldspathic quartz arenites cored in L13 are texturally and mineralogically more mature than the lithic-feldspathic arenites of L10 and L14. Framework grains range from 0.4 mm to 5 mm with a mode of 0.8 mm in cores from the three drillholes. Sedimentary structures include small-scale irregular low-angle cross-stratification in L10, L13, and L14 and imbrication of fine gravels in L10. Faint herringbone cross-stratification is apparent in a fine micaceous sandstone at the base of the sequence in L10 (21.6-23.7 m).

Sedimentary parameters are shown in Table 5; mineralogy was determined petrographically and sorting was ascertained by sieving.

Table 5. Sedimentary parameters of arenites of the Rob Roy pedoderm

Drillhole No.	Framework Grains			Plasma (%)	Cement	Sorting
	Quartz (%)	Feldspar (%)	Volcanic Rock fragments (%)			
L10	35	20	25	20	Phyllos-	v. poor
L13	60	15	5	20	ilicates,	moderate
L14	45	25	10	20	hydrates iron oxides	poor

The basal fine sandstone in L10 contains carbonaceous fragments which have been identified as wood, probably coniferous (M.D. Muir, in Appendix 1), which indicates a maximum age of Devonian; a more probable maximum age would be Late Permian.

In hand specimen the arenites of the Rob Roy pedoderm are difficult to distinguish from Silurian volcanigenic arenites. A comparison of eight thin sections of the upper arenites in three drillholes (L10, L13, L14) with one thin section of the Silurian arenite interbedded with rhyolites in L14 shows the following petrographic distinctions:

- (1) Strained quartz grains. In the Rob Roy arenites, quartz grains strongly reflect their volcanic provenance: they are almost all monocrystalline, generally bipyramidal with embayments, and have straight extinction. In the Silurian arenite about 25% of the quartz grains are polycrystalline and most of the monocrystalline grains exhibit undulose extinction.

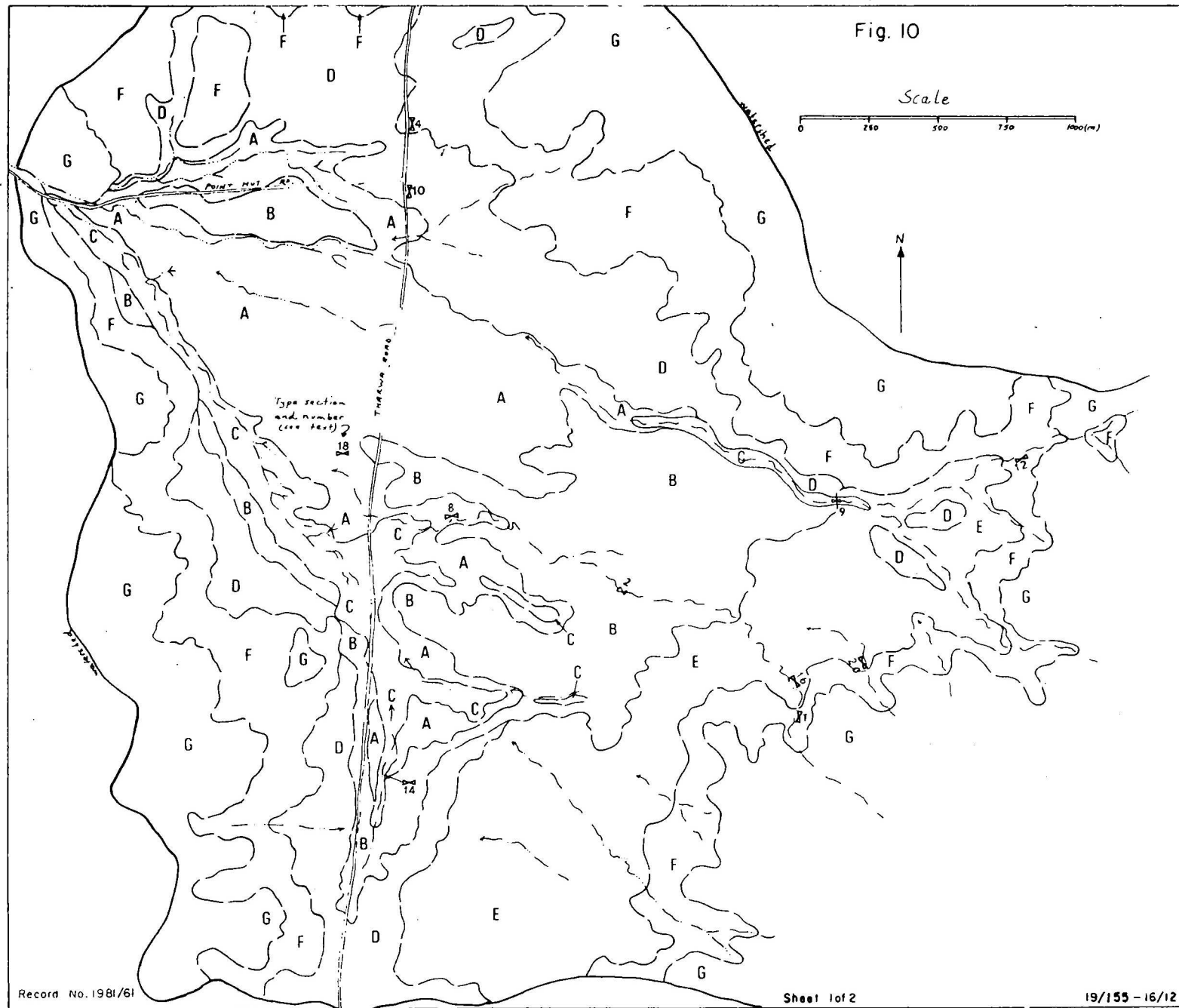
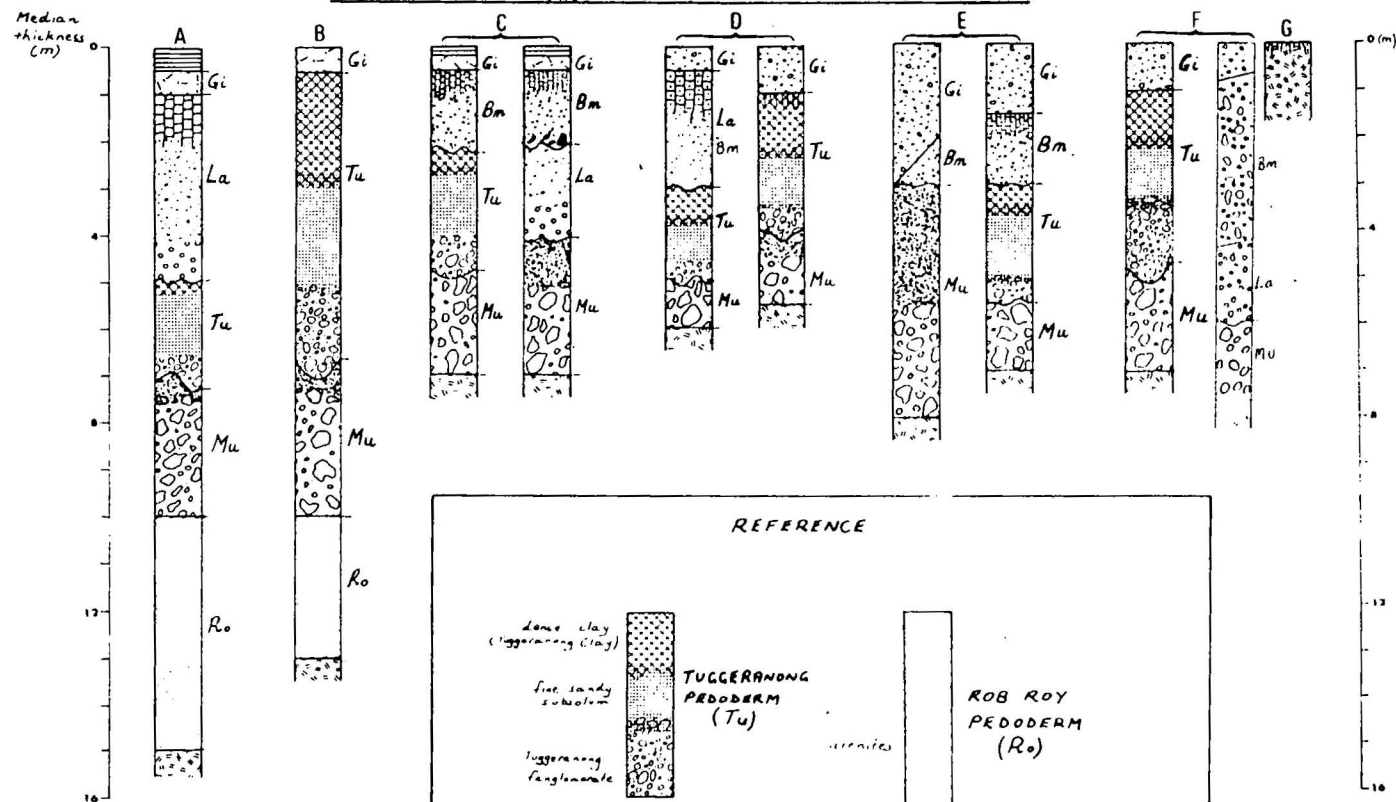


FIG. 10

**SURFICIAL GEOLOGY OF THE
LANYON NORTH BASIN (minor
terrace deposits omitted)**

MODAL SEQUENCE OF PEDODERMS IN THE SURFICIAL MAPPING UNITS



REFERENCE

dense clay
(tuggeranong clay)

fine, sandy
subsoilum

tuggeranong
fanglomerate

**TUGGERANONG
PEDODERM
(Tu)**

**ROB ROY
PEDODERM
(Ro)**

grey earth
(hydromorphic)

colluvium,
slopewash

clay
subsoilum

**GIGERLINE
PEDODERM
(Gi)**

**BIG MONK
PEDODERM
(Bm)**

podzols,
latosols
subsoilum

solodic
(Lanyon clay)

sandy
subsoilum

**LANYON
PEDODERM
(La)**

Lanyon granules

sands
with strong
pseudogley
patterns

Murrumbidgee
fanglomerate

**MURRUMBIDGEE
PEDODERM
(Mu)**

lithosols,
rock

stratified
alluvium

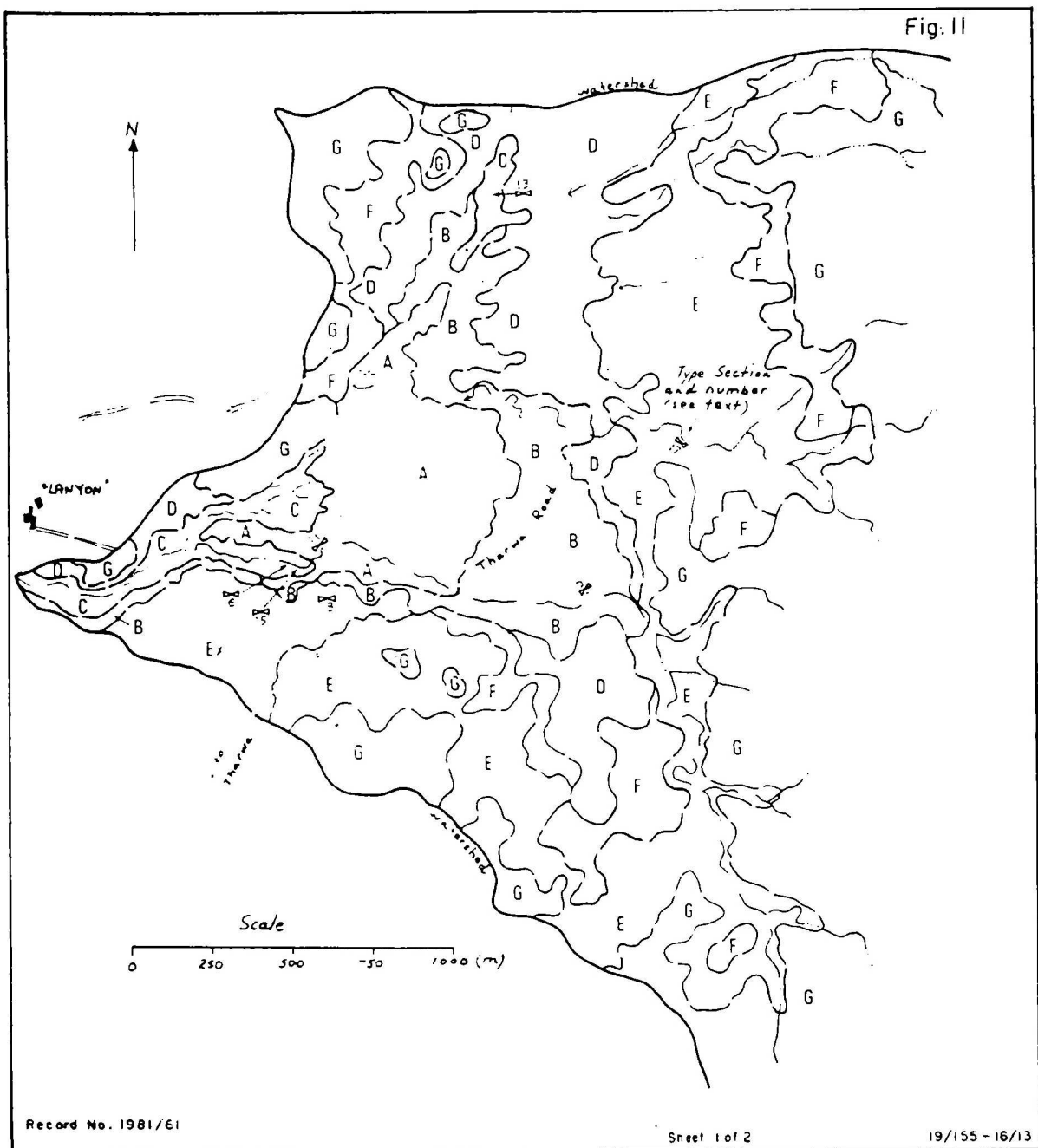


FIG. 11

SURFICIAL GEOLOGY OF THE
LANYON SOUTH BASIN

(minor terrace deposits omitted)

MODAL SEQUENCE OF PEDODERMS IN THE SURFICIAL MAPPING UNITS

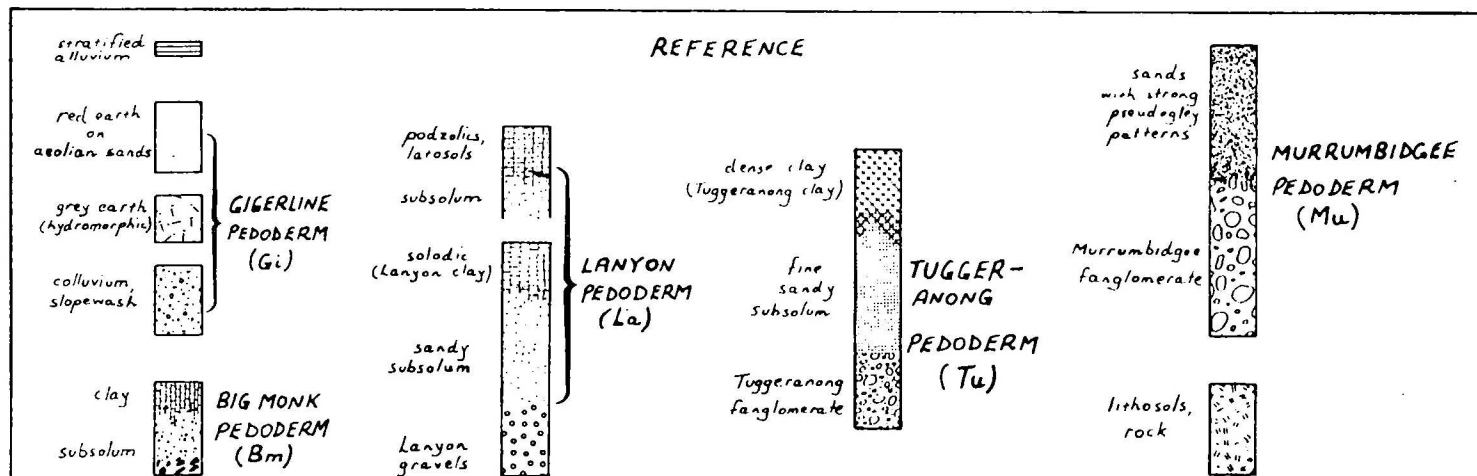
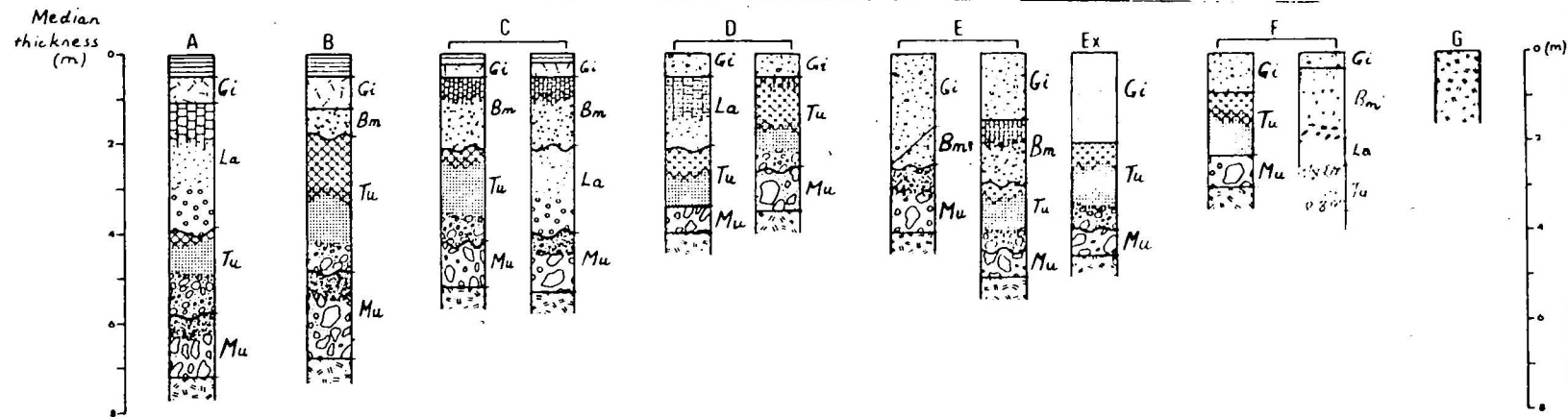
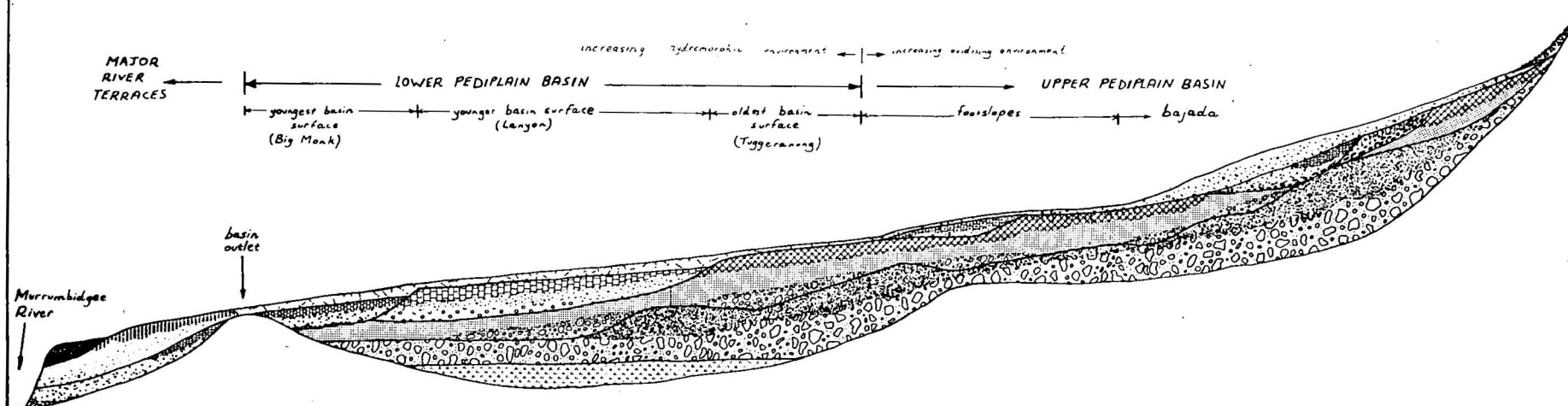
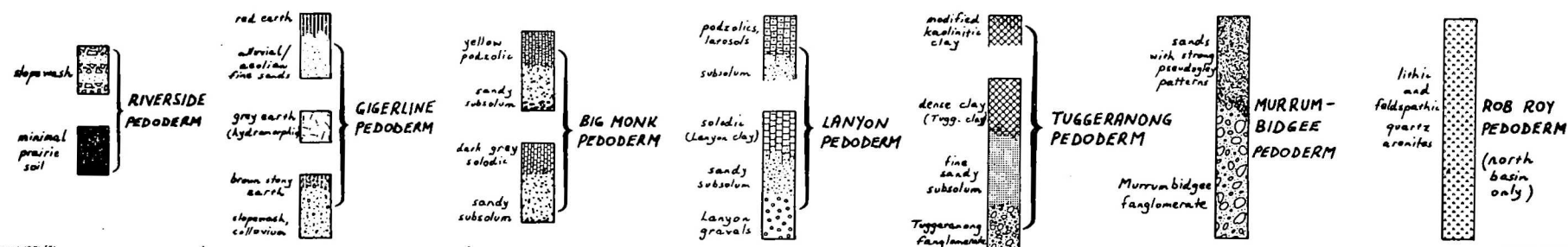


FIG. 12

**SCHEMATIC CROSS-SECTIONAL RELATIONSHIPS
OF PEDODERMS IN THE LANYON BASINS**



REFERENCE



- (2) Deformed rock fragments. In the Rob Roy arenites most rock fragments are subangular to subrounded discrete framework grains in which relict lithic textures are preserved. In the Silurian arenite about half of the lithic material is present as discrete grains and the remainder as an aphanitic paste filling large voids between quartz grains. Many of the discrete fragments between mineral grains are cusped, and have a deformed lithic fabric.
- (3) Plasmic fabric. Packing in the Silurian arenite is denser than in the Rob Roy arenites. Nearly all grains in the Rob Roy arenites have diffuse, poorly oriented sesquans, whereas less than one-third of the framework grains in the Silurian rock have coatings of any form. Void cutans and neosquans are present in the Rob Roy arenites, but are not evident in the Silurian arenite.

If a late Mesozoic-Early Tertiary age is tentatively assigned to the Rob Roy arenites on the basis of the wood fragments described above, then the landsurface on which the Lanyon north basin is developed is of considerable antiquity, an inference which is consistent with Craft's pre-Oligocene Lower Shoalhaven Plain.

The projected base-level of the Rob Roy pedoderm is only 6 m above the present level of the Murrumbidgee River at Point Hut. This implies that either the river has only incised itself by this amount over the past 70 million years or so, or that this section of the eastern block of the Murrumbidgee Fault has been downthrown after deposition of the arenites. The latter appears to be a more likely explanation, as Vanderbroek (1974) has reported Tertiary? fluvial gravels up to 25 m above the river near Pine Island, 3.5 km to the north.

Murrumbidgee pedoderm

The Murrumbidgee pedoderm consists of a basal facies of lithic cobbles and gravels with a maximum thickness of 8 m overlain disconformably by massive indurated silty sands; the contact ranges from clear to gradational. The basal facies is variably truncated by younger sediments but it is continuous throughout the north and south basins with little diminution of grain size away from the escarpments. The overlying fine-grained silty sand attains a maximum thickness of 2.5 m across the pediments and bajada, but thin remnants are exposed intermittently in all gullied stream-beds above the basin outlets.

A complete unmodified type section of the Murrumbidgee pedoderm is not exposed in the basins. Sections of the upper facies are exposed in stream-beds incised into the pediments and bajada; the type section for the upper facies is 20889E, 58295N, ACT Standard Grid (site 1, Fig. 10).

Murrumbidgee pedoderm - basal fanglomerate facies

It is proposed to use the name Murrumbidgee fanglomerate to define the basal facies of the Murrumbidgee pedoderm.

Sorting of the lithic clasts in the Murrumbidgee fanglomerate is very poor to moderate and particle shape ranges from subangular to rounded with subrounded mode. Sedimentary structures are difficult to detect, owing partly to limited exposure of the fanglomerate in the basins and partly to their overprinting by subsequent pedologic modifications. However, poorly preserved bedding, cross-stratification, graded bedding (Fig. 13), and imbrication of pebbles is evident in sandy and pebbly lenses towards the top of the basal facies. The rounding, sorting, and stratification of these deposits, together with the gentle palaeoslope, indicate a dominantly fluvial environment, short transport distances, and reworking of deposits that is typical of braided streams traversing alluvial fans.

Cobbles in the Murrumbidgee fanglomerate have thick complex cutans with an unusual, diagnostic macrostructure. At the base of the type section these fossil cutans protrude out of the matrix at the diffuse boundary between the top of the Murrumbidgee fanglomerate and the bottom of the fine-grained facies of the Murrumbidgee pedoderm (Fig. 14). The middle of the cutan commonly has a calcite medial suture, or alternatively a cavity containing calcite crystallaria may separate clay laminae with mangans that comprise the cutan.

Murrumbidgee pedoderm - upper fine-grained facies

The upper facies of the Murrumbidgee pedoderm is reddish brown to buff, intensely indurated silty sand with pebble lenses in some places. The sequence is very poorly sorted, massive and moderately porous with no sedimentary structures.

Porosity is visually estimated to be as high as 10% but very few of the voids are interconnected. All voids and channels which are discernable under a 10X hand lens have mineral coatings.

In hand-specimen the diagnostic pedologic patterns of the upper facies are the intense iron oxide segregation, calcite veining, and conspicuous joint planes

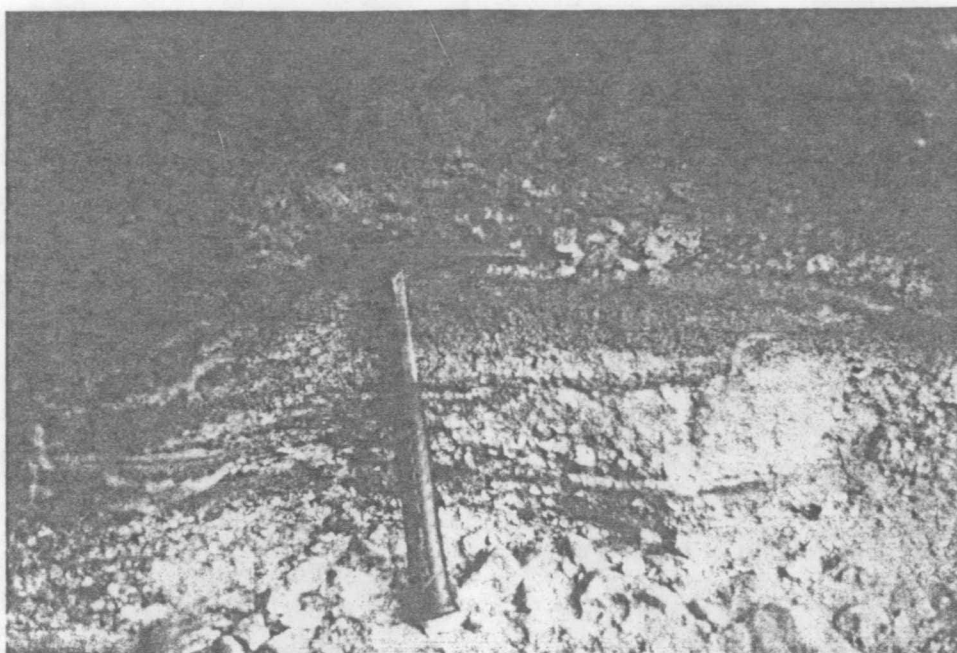


Fig. 13. Cross-stratification and graded bedding, accentuated by iron staining, in pebbly sand lenses near the top of the basal fanglomerate facies of the Murrumbidgee pedoderm. (20730E 58029N). BMR Neg. GB/2907-29A.



Fig. 14. Relict complex cutans at the base of the upper fine-grained facies, Murrumbidgee pedoderm. (20889E 58295N). BMR Neg. GB/2907-11A.

and infilled channels (Fig. 15), which in places extend for several metres vertically and horizontally. Complex cutans as described in the previous section are characteristic of the base of this facies.

Depositional environment of the Murrumbidgee pedoderm

The palaeoslope near the apex of the bajada, adjusted for Quaternary modifications, is estimated as originally $3\frac{1}{2}^{\circ}$, and the maximum thickness of surficial deposits comprising the Murrumbidgee pedoderm is estimated as 11 m. Blissenbach (1954) considered that bajadas and their composite alluvial fans are best developed under semi-arid climates in conditions of high relief, and that alluvial fans with maximum dips between 2° and 5° indicate dominantly fluvial conditions (Hooke, 1967). However, French (1976) described similar fanglomerates from periglacial environments that were also deposited under fluvial conditions. Therefore the depositional environment of the Murrumbidgee pedoderm may well have been both periglacial and semi-arid, since these two conditions are not mutually exclusive.

The upper fine-grained facies of the Murrumbidgee pedoderm may represent sheet-flood deposits associated with the attainment of maturity of the alluvial fan (cf. Davis, 1938).

Tuggeranong pedoderm

The Tuggeranong pedoderm consists of a basal fanglomerate unit overlain by cemented clayey fine sands on which a dense plastic clay is developed.

The name Tuggeranong fanglomerate is proposed for the basal fanglomerate, which is extensive but discontinuous beneath the older basin surface and the lower pediments. Remnants and sheets of the overlying cemented fine sands occupy all geomorphic surfaces right up to the top of the bajada at 670 m, and indicate that this facies of the Tuggeranong pedoderm was once areally extensive.

The older basin surface (Fig. 4) is generally occupied by the upper clay facies of the Tuggeranong pedoderm. Where the Tuggeranong pedoderm is present beneath the younger basin-fill sediments, the clay facies is generally thin or absent, having been stripped from the pedoderm before sedimentation recommenced.

It is proposed to use the name Tuggeranong clay for the dense plastic clay, the subsolum of which is the clayey fine sand facies of the Tuggeranong pedoderm.

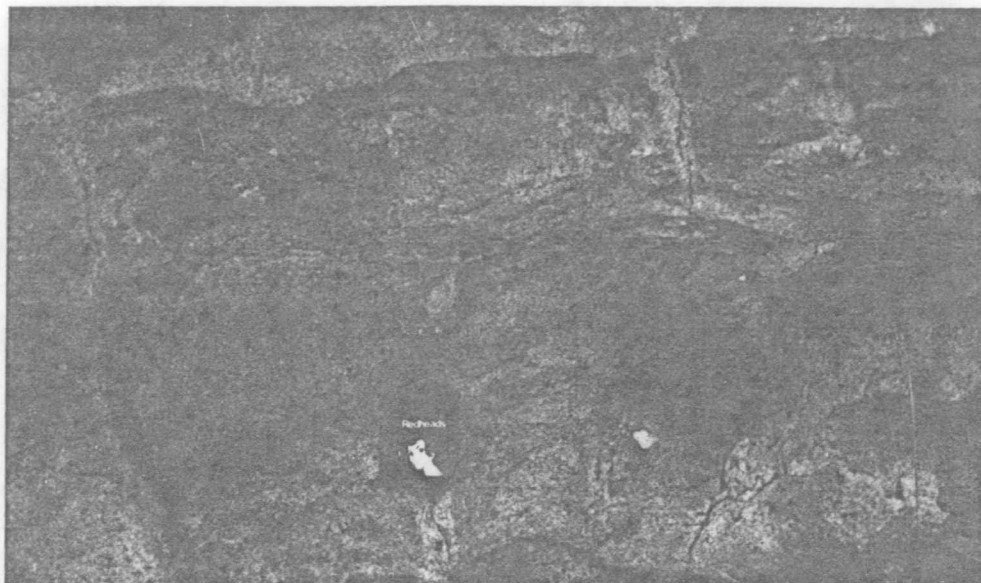


Fig. 15. Infilled joint planes and channels with intense iron oxide segregation - characteristic subsolum features in the upper facies of the Murrumbidgee pedoderm. (20838E 58327N). BMR Neg. GB/2907-20A.

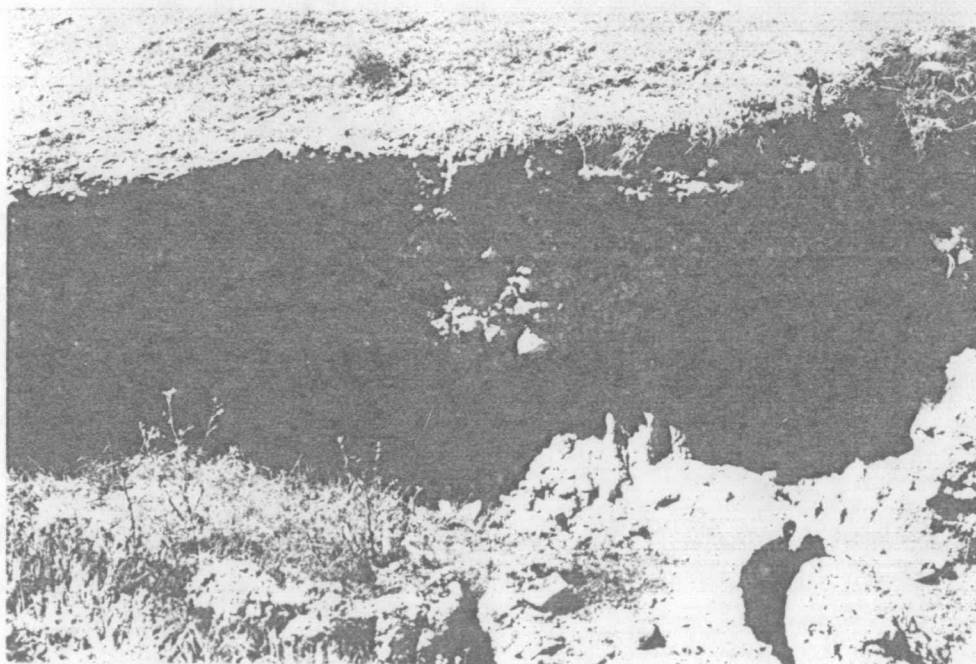


Fig. 16. Alluvial component of the Tuggeranong fanglomerate filling a palaeochannel scoured into the Murrumbidgee pedoderm, from which much of the fine-grained upper facies has been eroded. (20838E 58327N). BMR Neg. GB/2907-9A.

A complete section of the Tuggeranong pedoderm is not exposed because the streams have not incised completely through the older basin surfaces where the entire sequence exists. Type sections of the individual facies are exposed at the following sites:

- (2) 20838E 58327N Tuggeranong fanglomerate, alluvial component.
- (3) 20903E 58560N Tuggeranong clay and subsolum, upper catenary variant.
- (4) 20745E 58503N Tuggeranong clay and subsolum, lower catenary variant.
- (5) 20739E 58031N Tuggeranong clay and subsolum, hydromorphic variant.

Tuggeranong pedoderm - basal fanglomerate facies

The Tuggeranong fanglomerate is composed of very poorly sorted pebbles, cobbles, and boulders in a sandy matrix. Thickness ranges from up to 3 m across the change of slope above the older basin geomorphic surface to an average of about 2 m in the basins. Particle shape of the large clasts is generally subrounded because most of the material was plucked from the Murrumbidgee fanglomerate.

The Tuggeranong fanglomerate occupies extensive depressions and channels which have been cut into the upper surface of the Murrumbidgee pedoderm (Fig. 16). Although bedding is poorly developed, imbricated platy cobbles (Fig. 17) indicate fluvial deposition, but lack the degree of reworking of sediments that is a feature of the Murrumbidgee fanglomerate.

The bottom contact varies from sharp to gradational. It is not yet known whether the time lapse between deposition of the Murrumbidgee pedoderm and the Tuggeranong fanglomerate represents a pause in fan-building, or a period of stability during which soil development on the Murrumbidgee pedoderm was followed by truncation of the soil profiles and burial by the Tuggeranong fanglomerate; a paleosol that would indicate a hiatus before deposition of the Tuggeranong fanglomerate has not yet been found.

Many pebbles and cobbles of the Tuggeranong fanglomerate have grey argillans discernable in hand-specimen. The plasma is pale, mottled yellow and grey, and incipient vertical veining and joint planes are developed in places. Porosity of the matrix is about 5% higher than the Murrumbidgee fanglomerate because there has been less secondary pore filling (Fig. 18).

Tuggeranong pedoderm - upper fine-grained facies

The upper facies of the Tuggeranong pedoderm is generally intensely mottled

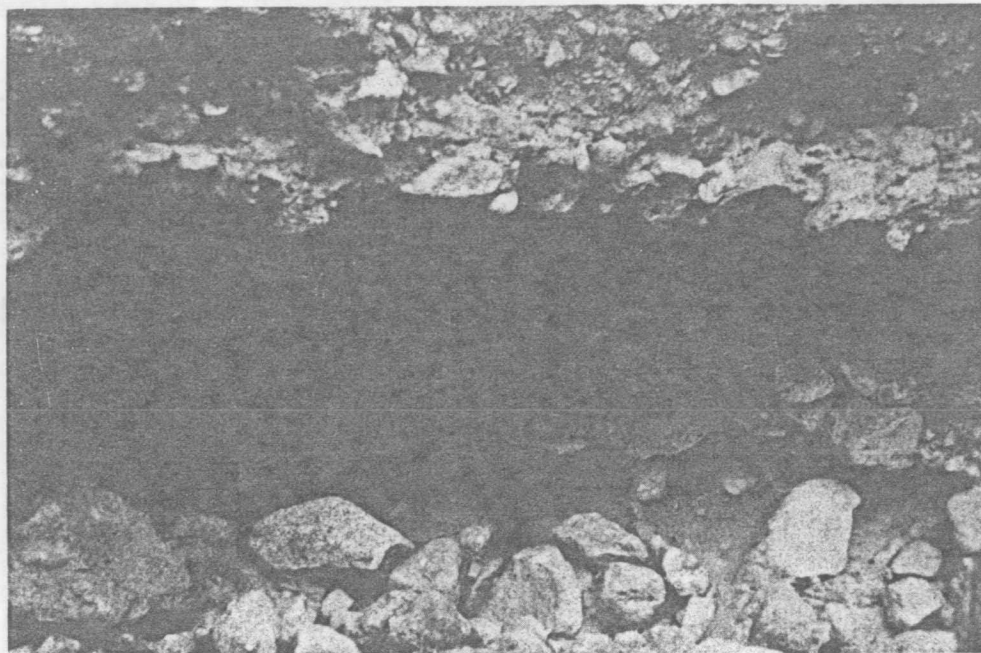


Fig. 17. Imbrication of platy cobbles (top half of photo) in lower Tuggeranong fanglomerate. The palaeochannel flowed from left to right. The hammer rests on material from the upper facies of the Murrumbidgee fanglomerate with its characteristic infilled joint planes. The protruding joint plane infill to the right of the hammer is a feature which commonly occurs on the downstream side of crests at contacts. The joint plane appears to have undergone plastic deformation from the increase in effective stress following drainage and consolidation of the Tuggeranong fanglomerate. Infilling of the curved void occurred later because there is no cleavage development and the clay layer continues along the disconformity. (20831E 58328N). BMR Neg. GB/2907-20A.

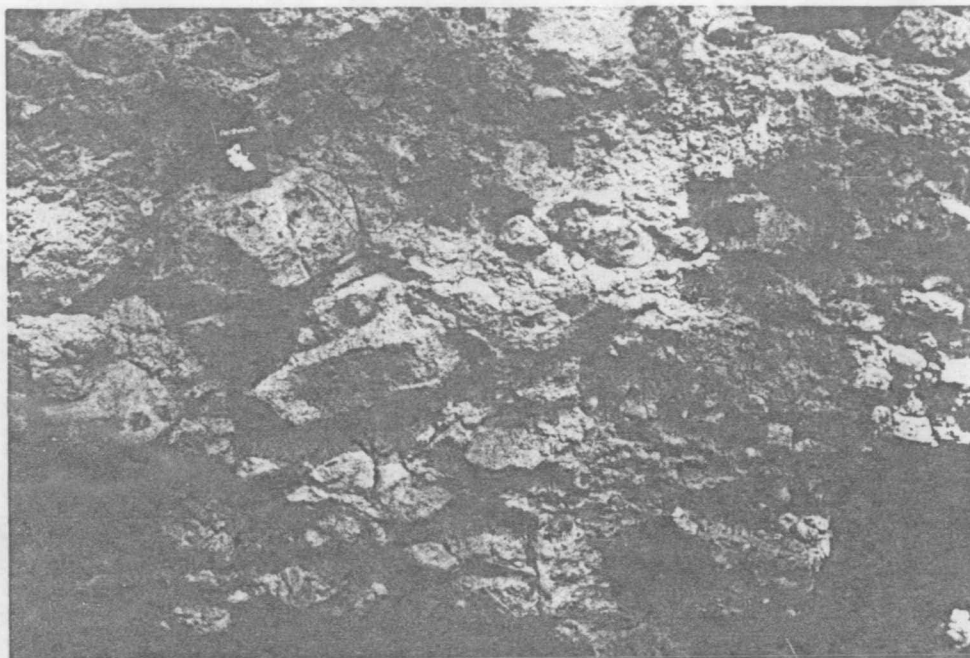


Fig. 18. Textural characteristics of the Tuggeranong fanglomerate. Typical bimodal size distribution; primary mode is about coarse gravel-size and secondary mode 0.7 mm. Matrix porosity is up to 15%. (20834E 58327N). BMR Neg. GB/2907-19A.



Fig. 19. Type section 3 - Upper catena variant (soloth) of the Tuggeranong clay. Dense, highly plastic clay with a calcareous B2 horizon and subsolum (the pale zone in the photograph) overlies thin lag gravels on deeply weathered rhyodacite. The pedoderm is disconformable with the contemporary geomorphic surface. (20903E 58560N). BMR Neg. GB/2907-3A.

yellowish brown and pale grey calcareous-cemented clayey fine sand on which the Tuggeranong clay is developed. Maximum thickness of the clay and subsolum is about 3 m.

The Tuggeranong clay grades from a soloth (Fig. 19) in elevated positions in the landscape to a solodic soil on the mid-to-lower catena and in the hydromorphic environment. The soloth comprises dense, highly plastic yellowish grey clay (pH 4.9-5.3) intensely weathered throughout the solum, generally about 1.5 m thick. Carbonate nodules are sparsely distributed through the B2 horizon and subsolum.

The lower catenary variant (Fig. 20) is pale olive grey, highly plastic clay which is neutral to slightly alkaline throughout. The upper B horizon is composed of smooth manganese-flecked, polyhedral peds grading to larger blocky peds (10 cm) in the lower B horizon, where mangans, slickensides and carbonate pedodes are prominent. Some carbonate pedodes are partly coated with mangans.

Subsolum patterns are best developed in the lower catenary position (Van Dijk, Riddler, & Rowe, 1968); the most prominent are grey vertical veins and intense yellow-grey mottling (Fig. 21), which are enhanced by conspicuous dark grey void cutans and infills.

The hydromorphic variant (Fig. 22) is alkaline, dark grey, dense plastic clay with large prismatic peds (c axis up to 40 cm), which are generally crazed, slickensided, and sporadically bleached. Precipitated carbonate is non-detectable in hand-specimen. The hydromorphic Tuggeranong clay occurs beneath the older basin geomorphic surface; the alluvial origin of the parent material within the basin fill is indicated by sedimentary layering in the subsolum and by fining-upwards textural variations in the B horizon.

Mineralogy and pedogenesis of the Tuggeranong clay

Mineralogical determinations were made by x-ray diffraction on oriented samples of the $-2\ \mu\text{m}$ fraction and on samples that were also glycolated and heated.

The clay mineral assemblage in all unmodified catenary and hydromorphic samples, in order of dominance, is montmorillonite, illite, and kaolinite. In many places the montmorillonite and illite are randomly interstratified; the kaolinite is poorly crystalline and/or very fine-grained in all samples and probably includes halloysite. Vermiculite is accessory in the hydromorphic variant, but nothing above a trace was detected in the catenary samples. There is always a sharp mineralogical break between the base of the Tuggeranong pedoderm and the



Fig. 20. Lower B horizon of Tuggeranong clay, lower catenary variant. Peds are large, irregular, and blocky (e.g., to the left of the mid-point of the hammer stock), and have abundant mangans. Carbonate nodules are disseminated throughout. (20745E 58503N). BMR Neg. GB/2908-5A.



Fig. 21. Intense mottling pattern in Tuggeranong clay subsolum, lower catenary position. The dark grey nuclei in the pale mottles are void cutans and infills. In many places the grey clay veining above the hammer transects the entire subsolum. (20750E 58032N). BMR Neg. GB/2908-30A.

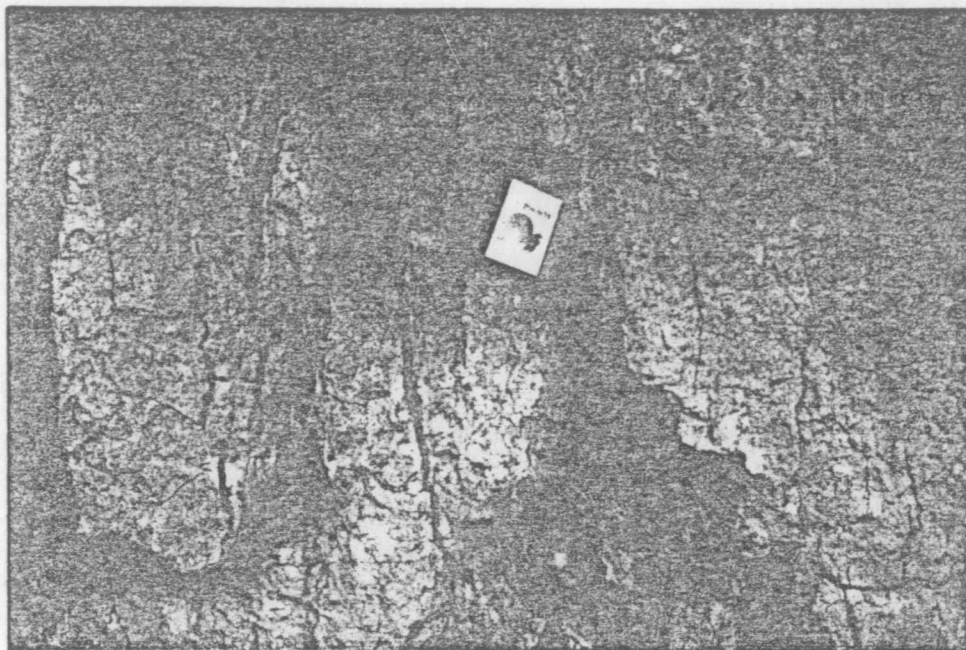


Fig. 22. Hydromorphic variant of the Tuggeranong clay.
Large prismatic peds are crazed, slickensided, and
sporadically bleached. (20739E 58031N).
BMR Neg. GB/2908-27A.



Fig. 23. Lanyon pedoderm, basal clastics facies, colluvial-
alluvial variant. Note lower matrix content, better
sorting of cobbles, and lack of pedologic patterns
cf. Tuggeranong & Murrumbidgee fanglomerates.
(20647E 58041N). BMR Neg. GB/2908-12A.

underlying weathered rock or Murrumbidgee pedoderm. The plasma of the weathered rock is dominantly muscovite-illite and the Murrumbidgee pedoderm contains about equal proportions of kaolinite and degraded illite; the matrix of both of these units contains negligible smectite, except in some planar voids where it has been illuviated in from the overlying Tuggeranong pedoderm.

In high benches and on hillslopes the Tuggeranong clay shows advanced and prolonged pedogenesis; although the solum is intensely weathered it shows minimal textural variation, and pedologic features extending throughout the subsolum completely obscure the depositional fabric. Pedogenesis of soloths is imperfectly understood. Stace & others (1968) suggested that some soloths may have developed under conditions of continuing salt accession and intermittent mild leaching. Leaching must have been very mild during pedogenesis of the Tuggeranong clay because the clay has not progressed past the illite-montmorillonite stages in the weathering sequence (Jackson & Sherman, 1953), and carbonates have accumulated in the lower B horizon. Calcitans in the underlying Murrumbidgee pedoderm appear to have been illuviated down from the Tuggeranong clay subsolum.

Butler (1967) suggested that the calcareous nature of some of the older Canberra subsoils may be due to pedogenesis on an aeolian parent material of fine dust, or parna. He correlated soils developed on parna from Deniliquin and Griffith through to the western slopes of New South Wales, and pointed out that there is no valid reason why dust accession should suddenly terminate at the divide.

The parna hypothesis could be a reasonable explanation for the origin of the Tuggeranong clay parent material. It is unlikely, but not impossible, that the acid volcanic rocks were capable of releasing sufficient divalent cations, particularly Ca and Mg, to develop these thick deposits of montmorillonitic clays in high positions in the landscape. The relative textural homogeneity throughout the upper catena clays and their subsola, and the source of salt, are readily explained by the parna parent material. Thin stonelines at the base of the subsola could then be interpreted as lag gravels on a former sparsely vegetated pavement.

Depositional and pedogenetic environment of the Tuggeranong pedoderm

The fanglomerate facies of the Tuggeranong pedoderm indicates fluvial deposition, but without the degree of reworking and sorting that occurred in the Murrumbidgee fanglomerate.

The Tuggeranong clay may well have been derived from aeolian material that

was deposited on deflated lag gravels on the hillslopes, and from alluvium derived from these slopes and redeposited in the basins where it overlies the fanglomerates and has infiltrated packing voids. Indicators of an aeolian origin are thick deposits at high elevations, minimal textural differentiation down profiles, high montmorillonite content of the clays, and an abundance of calcareous material in the subsola. The alluvial origin of the hydromorphic variant is indicated by marked textural variations down profile and by sedimentary layering in the subsola.

A prolonged hiatus is indicated by the degree of organisation of the Tuggeranong clay. The environment of pedogenesis must have been moderately arid because the clays are mineralogically immature despite the intensely weathered B horizon. Slickensides in the lower B horizon indicate that the Tuggeranong clay was subjected to alternating periods of wetting and drying during advanced pedogenesis.

Lanyon pedoderm

The Lanyon pedoderm consists of a basal clastics facies overlain by interbedded sand, silt, and clay, the upper part of which has undergone pedogenesis.

The basal facies is subdivided into:

- (1) a colluvial-alluvial component of restricted distribution;
- and
- (2) shoestring gravel deposits which are distributed beneath the younger basin surface.

The name Lanyon gravels is proposed for the latter component. The type section for the colluvial-alluvial component is (6) 20647E 58041N. The Lanyon gravels are not exposed; their distribution and description is derived from drillcores.

The overlying fine-grained alluvial facies of sand, silt, and clay forms a continuous sheet under the whole of the unmodified younger basin surface. Equivalent slopewash sheets are present on the lower footslopes and in some places on the higher basin surfaces. The top half of this unit has undergone pedogenesis, generally under hydromorphic conditions, and the name Lanyon clay is proposed for the soil. Type sections of the basin alluvial facies and the catenary variants on the slopes are as follows:

- (7) 20794E 58574N Lanyon pedoderm, fine-grained facies, upper catena colluvial variant.

- (8) 20762E 58355N Lanyon pedoderm, fine-grained facies, mid to lower catenary variant.
- (9) 20865E 58379N Lanyon pedoderm, fine-grained facies, slopewash variant.
- (10) 20745E 58469N Lanyon pedoderm, fine-grained facies, lower catenary hardpan variant.
- (11) 20659E 58045N Lanyon pedoderm, fine-grained facies, hydromorphic variant (Lanyon clay).

Lanyon pedoderm - basal clastics facies

The colluvial-alluvial component is of very minor areal extent, restricted to a few relict terraces inset into the Tuggeranong pedoderm on the older basin surface and in small colluvial splays at the foot of the bajada. Maximum thickness is 2.5 m. The unit is composed of poorly sorted pebbles, cobbles, and boulders (Fig. 23) some of which have a long axis of around 90 cm, indicating that deep ephemeral flows occurred during deposition. The sand matrix comprises about 20% of the unit. There are very few cutans, and pedological patterns consist entirely of sesquioxide coatings and concretions.

The Lanyon gravels constitute the majority of the basal clastics facies. Poorly sorted and rounded sandy gravels, about 1 m thick, occupy rectilinear but discontinuous buried palaeochannels trending subparallel to the present streams. The gravels are bed-load deposits of prior braided streams, and they lie within palaeochannels cut into the Tuggeranong pedoderm that are only a few metres wide and no longer than 150 m. Core recovery of the Lanyon gravels was poor because the gravels were always saturated and lacked cohesion; however, it is assumed that secondary pore filling has been minimal.

Lanyon pedoderm - upper fine-grained facies

Paleosols developed on slopewash sheets up to 1.5 m thick on the footslopes and higher basin surfaces have mostly been stripped from the subsolum during subsequent erosive events. In such instances, field recognition of this unit depends upon diagnostic subsolum features.

The subsolum is very poorly sorted, has no sedimentary structures, and is highly porous (Fig. 24). Liquid porosity generally exceeds 20%, as determined from cored specimens of the matrix by the BMR Petroleum Technology Laboratory (Appendix 2). Colour varies from pinkish grey for dacite-rhyodacite provenances to a very pale yellow for rhyolitic detritus; the latter also tends to have a smaller median grainsize for

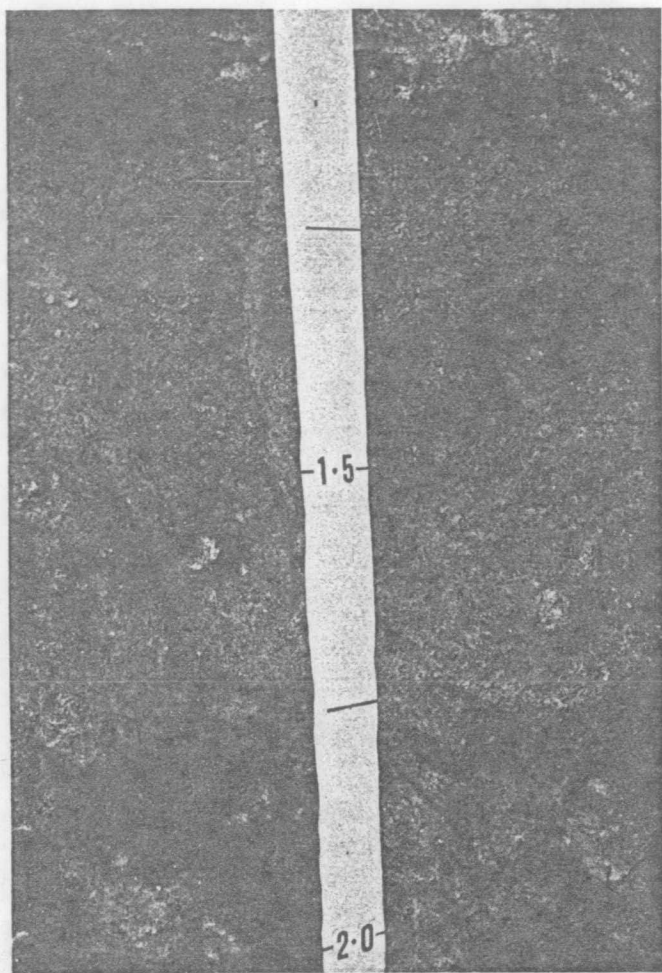


Fig. 24. Massive and porous indurated sands of the slopewash variant of the Lanyon pedoderm. Divisions on tape are 25 cm. (20925E 58363N). BMR Neg. GB/2908-25A.

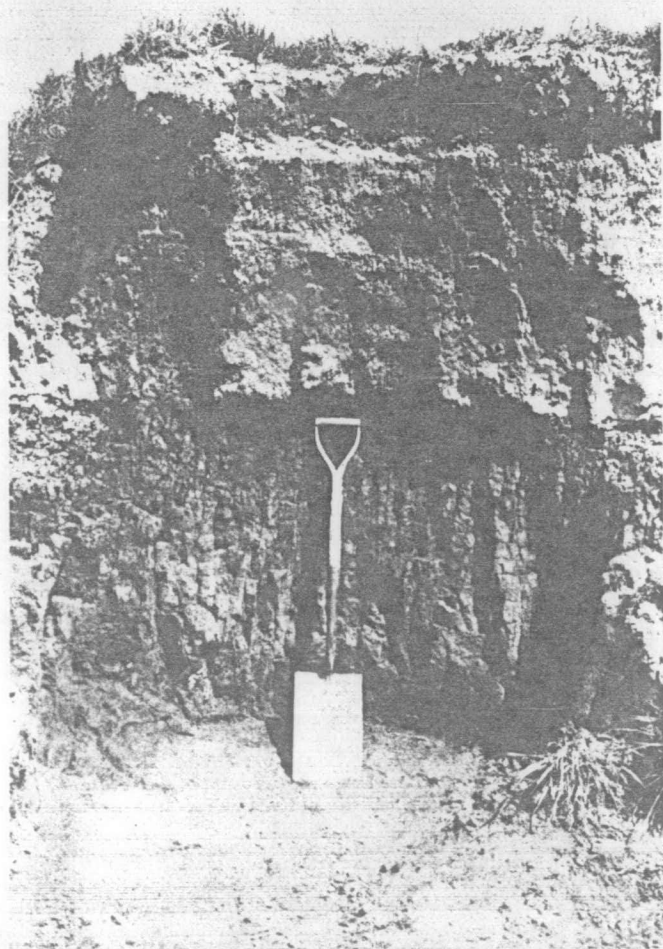


Fig. 25. Type section (11) of the Lanyon clay buried beneath a grey earth (Gigerline pedoderm, hydromorphic variant) overlain by stratified alluvium. Lanyon clay is a strongly structured solodic soil which occurs beneath the younger basin surfaces where pedogenesis has always been under hydromorphic conditions. The overlying Gigerline pedoderm resembles a buried A horizon but the unit can be traced laterally without breaks over disconformable contacts between hydromorphic Tuggeranong and Lanyon clays, which it therefore postdates. The pseudo-A2 horizon development is from past and present lateral throughflow of groundwater perched on top of the Lanyon clay. (20659E 58045N). BMR Neg. GB/2908-20A.

any given distance from escarpments. In fact, provenance becomes increasingly important in the hillslope variants of the Lanyon and younger pedoderms, as pedogenetic modification becomes progressively less intense, and less readily identified.

The Lanyon subsolum exhibits a high to moderate degree of both pedologic organisation, and iron oxide segregation in which macroscopic ferruginous halos surround lithic clasts. Vertical veining and incipient joint-plane development are optimised in the lower catenary position but are nowhere near as well-developed as in say, the Murrumbidgee pedoderm. The slopewash variant of the Lanyon pedoderm and the upper facies of the Murrumbidgee pedoderm may be distinguished in the field by the criteria listed in Table 6.

Table 6. Field criteria to distinguish between subsola of the slopewash variant, Lanyon pedoderm and upper facies of the Murrumbidgee pedoderm.

	Murrumbidgee pedoderm	Lanyon pedoderm
Porosity	10%	20%
Nature of voids	Essentially discrete spherical and ellipsoidal voids. Most voids have clay infills or linings. No chambers.	Spherical and ellipsoidal voids, both discrete and interconnected. Many open voids. Chambers up to 10 cm with mangans.
Organisation	Well organized a continuous network of multidirectional infilled joint planes and channels extend throughout the unit. Polygonal pattern of relict complex cutans.	Random pattern of vertical cracks, many with grey and yellow clay infills. Planar voids rarely continue throughout the entire subsolum.

In the lower basins the fine-grained alluvial facies, including the Lanyon clay, has an average thickness of about 2.5 m, and blankets the Lanyon gravels, where they exist, and the truncated Tuggeranong pedoderm elsewhere. The sequence becomes finer-grained nearer the surface, reflecting progressive stabilisation of hillslope vegetation.

Depositional fabric is well-preserved in coarse sand and fine gravel layers in the bottom 30 cm where it has not been reorganised by pedogenesis. The subsolum is organised into coarse incipient prismatic aggregates which leave distinctive columns protruding on weathered sections. Colour is coarsely segregated

pale grey and yellow-brown interspersed with concretions of black oxides, mostly around chambers. Argillans are rare, but many quartz and feldspar sand-size grains have Fe/Mn coatings which are particularly prominent on weathered surfaces. The Lanyon pedoderm is the oldest surficial unit in which relatively unaltered mica has been observed.

The Lanyon clay (Fig. 25) is neutral to slightly alkaline throughout. Its upper B horizon is strongly structured with irregular blocky (5 cm) and prismatic (8 x 4 cm) peds. The peds are defined by thick, dark grey to black organo-argillans enclosing sandy clay cores. The lower B horizon (Fig. 26) is composed of coarse prismatic peds (20 x 8 cm) with organo-argillans, 1 to 2 mm thick, enclosing porous fine sands which have distinctive internal fabric patterns of intense iron oxide segregation around voids and a fine vermiform type of veining.

The well-drained equivalent soils of the Lanyon clay grade from minimal red podzolic soils developed on colluvium in the upper catenary position to differentiated brown podzolics on the mid-to-lower catenary positions. In some areas on the lower catena the soil is an immature lateritic podzolic. The soils of the slopes are neutral to slightly acid throughout the solum and in most places they overlie Tuggeranong clay.

The upper catena colluvial variant is about 50 cm thick, consisting of a reddish brown weakly pedal to earthy solum developed on unstratified colluvium with sesquioxide concretions and faint red and yellow mottling in the B2 horizon and subsolum. In places where this unit overlies the Tuggeranong clay, a siliceous hardpan up to 5 cm thick is developed at the interface.

The solum of the mid-to-lower catena variant is about 1 m thick with a highly organised upper B horizon of reddish brown friable clay of low to medium plasticity. Primary peds are about 5 mm. The lower B horizon is a yellow-brown clay of medium to high plasticity with pale grey mottling and clay veining. Primary peds are blocky (2 cm), and many have grey argillans. Sesquioxide nodules are disseminated throughout the solum and are generally most abundant in the B2 horizon.

In many places the B2 horizon of the podzolics grades down into Tuggeranong clay. The B horizons of these profiles have the best-developed pedality, and the clays are the most friable with the characteristic floc appearance throughout. There is also minimal textural variation throughout the sola. In the absence of clear depositional breaks, these soils are interpreted as having developed from in-situ weathering of Tuggeranong clay.

The type section (Fig. 27) has a sharp contact between the sandy clay subsolum and the Tuggeranong clay and grades from clay size in the upper B horizon to sandy ped centres in the lower B horizon. These soils are not as intensely pedal and the clays are not as friable as those formed by secondary pedogenesis of the Tuggeranong clay.

The most mature pedologic development of the Lanyon pedoderm is an aggregated sesquioxide hardpan (Fig. 28) of lateritised sand-size alluvium which occurs in the lowest catenary positions above the zone of contemporary intermittent waterlogging on the footslopes around the basin. The reddish brown aggregates (Fig. 28) contain black spherical nodules segregated towards the outer surfaces of the blocks. Internally the large aggregates consist of concretionary ellipsoids of cemented mineral grains as well as discrete sand-size framework grains of quartz and feldspar with cutans all set in a reddish brown clayey groundmass. The pale yellow material has been subsequently illuviated into megavoids.

Mineralogy and pedogenesis of soils of the Lanyon pedoderm

The clays of the Lanyon pedoderm on the slopes contain no montmorillonite, which accounts for their friable consistence; the dominant clay minerals are kaolinite and illite. The ratio of kaolinite to illite in the upper B horizons averages about 2:1; in the lower B horizons the proportions are about equal. Goethite is present in the plasma and as discrete nodules in percentages ranging from less than 5% in the colluvial variant, but increasing downslope to 20% in the lower catena podzolics.

On the slopes the Tuggeranong clay which was not buried during the depositional phase of the Lanyon pedoderm has been completely kaolinized in the top 50 cm of the B horizon. For the next 30 to 50 cm there is a steeply rising diffraction background at low angles which could not be defined by the standard diagnostic tests of glycolating and heating. It probably represents the residue from desilication of montmorillonite to kaolinite because there is an increase in intensity with expansion on glycolation as the unmodified Tuggeranong clay is approached deeper in the profile.

The black spherical nodules in the sesquioxide hardpan are hematite-geothite. The red plasma in the aggregates, in order of abundance is, kaolinite, goethite, gibbsite, hematite, and possibly allophanes.

The clay mineralogy and soil morphology indicates that pedogenesis of hillslope soils of the Lanyon pedoderm and the second phase of pedogenesis of

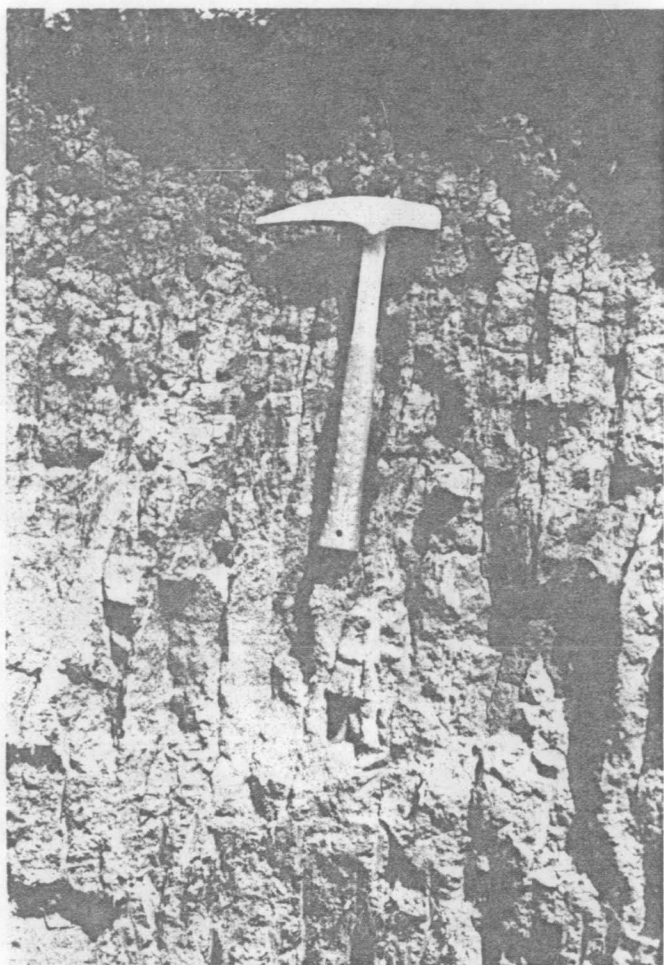


Fig. 26. Strong, blocky, and prismatic peds with thick organo-argillans in the upper B horizon of the Lanyon clay grading to coarse prismatic aggregates in the lower B and B₂ horizons. Rainfall after prolonged dry periods produces substantial B-horizon interflow in the Lanyon clay. The infiltration capacity is very high in the upper B horizon when the antecedent soil moisture content is low, but admittance is very much slower through the lower B and B₂ horizons because of the weaker pedologic structure. Subsoil seepage out of the Lanyon clay was particularly noticeable in the western part of the south basin throughout the spring of 1976 after winter drought conditions in which large-scale cracking developed in the upper B horizon. (20659E 58045N). BMR Neg. GB/2908-21A.

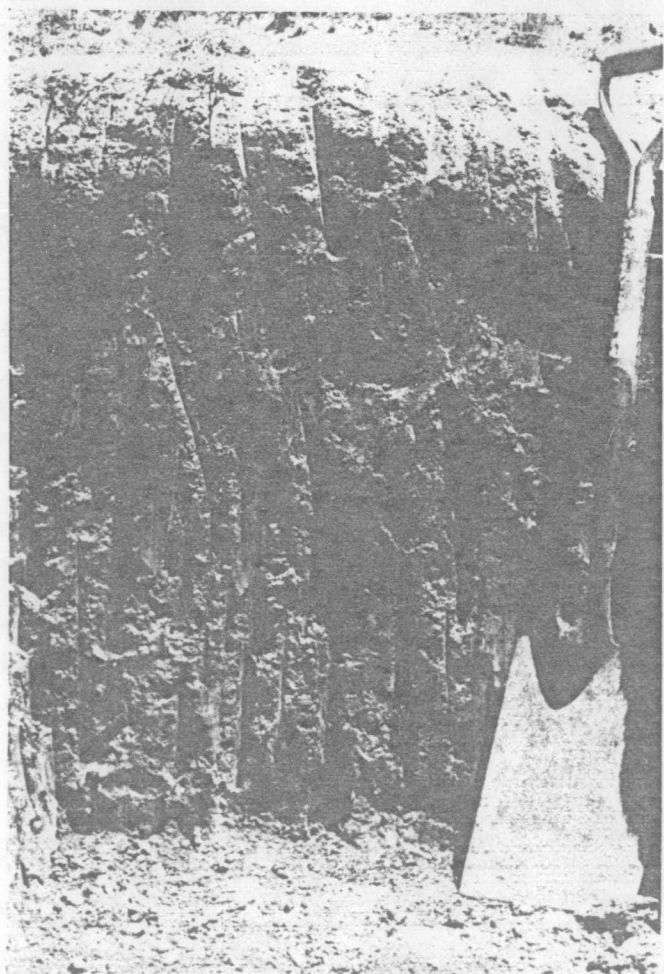


Fig. 27. Type section (8) of the solum of the mid-to-lower catena variant of the Lanyon pedoderm.

This soil is the well-drained equivalent of the Lanyon clay in the basins. The B horizon is 90cm thick and comprises an upper zone of reddish brown friable kaolinitic clay grading to a lower zone of yellow-brown clay of increased plasticity. Pedality is highly developed throughout. Grey clay veining and mottling reaches optimum development in the B₂ horizon (at bottom of photograph) and extends well into the subsolum. Sesquioxide nodules are disseminated throughout the solum. At this location the subsolum is 1.2 m thick and is underlain by truncated Tuggeranong clay. (20762E 58355N). BMR Neg. GB/2908-16A.

exposed Tuggeranong clay occurred by intensive leaching in a strongly oxidising environment. The increase in mineralogical maturity from the kaolinite stage in elevated positions to the hematite-goethite stage downslope is an expression of the greater degree of weathering due to the historically higher water content in the lower catena soils. In these sites the modified Tuggeranong clay surface is adjacent to the sesquioxide hardpans, which are further advanced in the weathering stage. An explanation to account for the mineralogical differences of soils in identical geomorphic sites probably lies in the different rates at which water would have been admitted into the profiles, and at which dissolved silica and bases in soil water could be drained from the profiles. In the sesquioxide hardpan, the permeability of the alluvium was high enough to permit rapid drainage and lateral throughflow of percolating groundwater, whereas in the Tuggeranong clay the permeability was too low to allow the second phase of weathering to proceed beyond the illite-kaolinite stage.

In the hydromorphic environment of the basins, pedogenesis proceeded under gleization conditions; mineralogy of the Lanyon clay is dominantly randomly interstratified montmorillonite-illite, in which discrete illite and kaolinite each constituting about 20%, and quartz is accessory. Seepage water into the basins would have always been rich in bases and silica leached from the hillslope soils, a condition which has continued through to the present day, particularly after burial of the Lanyon clay.

Depositional and pedogenetic environment of the Lanyon pedoderm

Up to 4 m of surficial material from the Murrumbidgee and Tuggeranong pedoderms was excavated in the western sectors of the basins during the initial erosive phase associated with the Lanyon pedoderm. Erosion of the pre-existing soil surfaces on the hillslopes was on a smaller scale and there was no deposition of fanglomerates as with the older pedoderms but extensive slopewash sheets were laid down. The sequence of slopewash deposition is well exposed in the incised channel of the northernmost stream of the north basin, where pinkish grey sheets derived from the rhyodacites of the northern escarpment (Tuggeranong Hill) consistently wedge-out and overlie the pale yellow sheets of rhyolitic slopewash from the eastern escarpments.

The vigorous erosion in the basins appears to be directly related to rejuvenation of the Murrumbidgee River, resulting in a local increase in gradient and deep incision of the tributary streams into the older pedoderms of the western

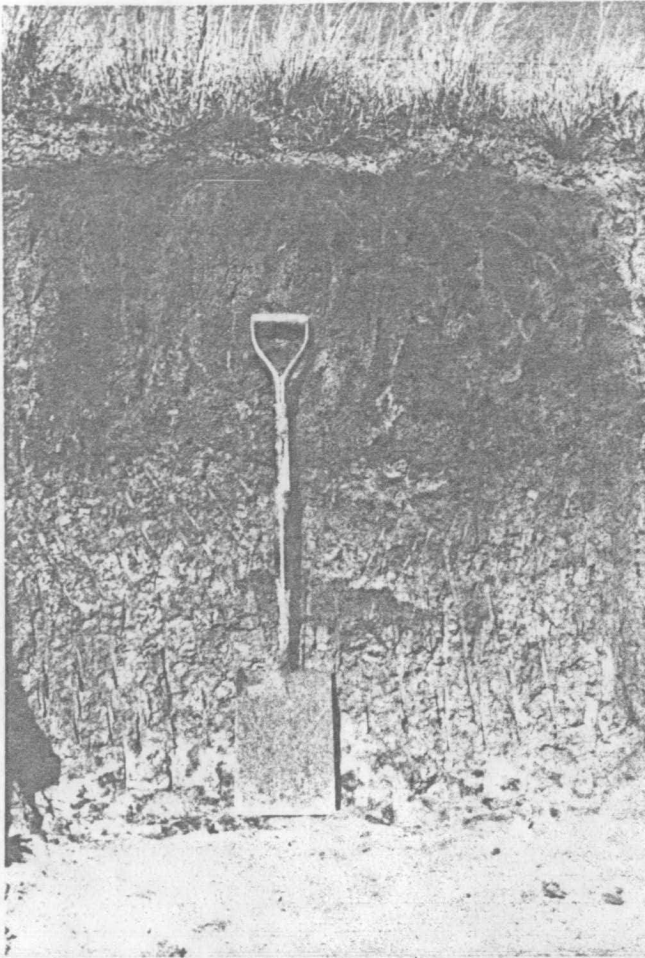


Fig. 28. Type section (10): latosol variant of the Lanyon pedoderm. Aggregated sesquioxide hardpans of lateritised alluvium occur extensively on the lower catena on the footslopes around the Lanyon basins. The reddish brown aggregates are composed of hematite-goethite nodules in a kaolinite-goethite-gibbsite groundmass and represent the most mineralogically mature development of the Lanyon pedoderm. The underlying soil is Tuggeranong clay with its characteristic carbonate-rich zone at the bottom of the photograph. (20745E 58469N). BMR Neg. GB/2908-6A.

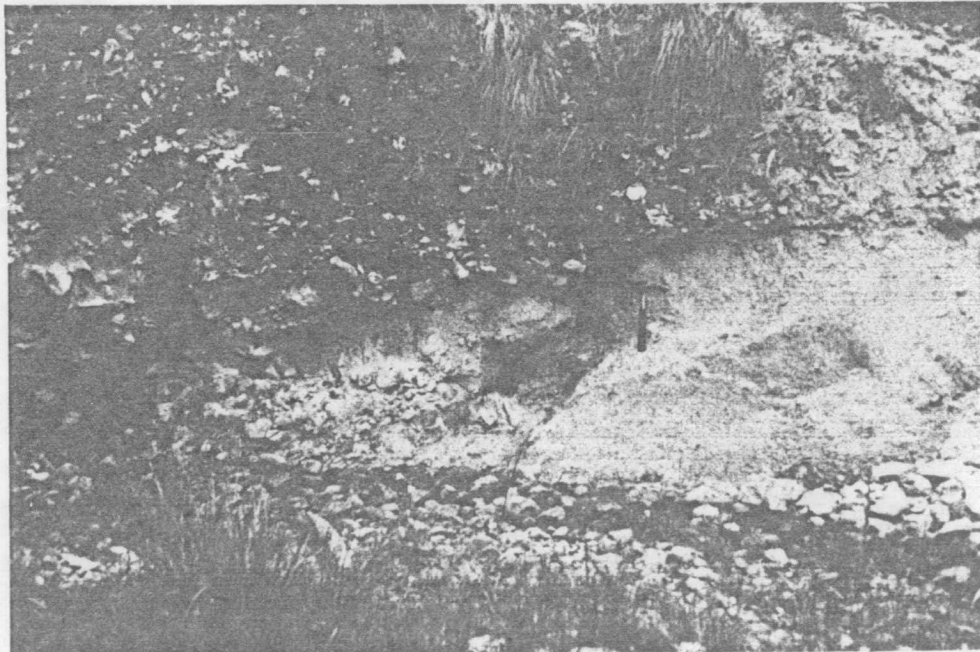


Fig. 29. Type section (12): colluvial component of the Big Monk pedoderm infilling a depression cut into the slopewash variant of the Lanyon pedoderm on the bajada. The hammer points downstream and is resting on the Lanyon slopewash. Note the random orientation of boulders and lack of subsolum features in the Big Monk colluvium. (20970E 58384N). BMR Neg. GB/2907-24A.

parts of the basins. Headward erosion in the basins caused by entrenchment of the Murrumbidgee River would have commenced with lowering of the basin outlets and radiated headward into the basin sediments. Secondary planation occurred after the tributary streams attained grade and commenced lateral erosion. Parting and collapse of large blocks of the Tuggeranong clay from bank undercutting is facilitated by its dispersive clays and its coarse structural organisation in the lower B horizon.

A concurrent climatic change towards greater net humid conditions is indicated by the increased leaching capacity during pedogenesis of the Lanyon pedoderm compared with that of the Tuggeranong pedoderm. An increase in humidity in this context need not imply an increase in rainfall; it could have been accomplished by a reduction in evapotranspiration associated with a decrease in temperature with virtually no change in rainfall. Also the latosols around the basin boundaries may indicate highly seasonal rainfalls.

During the ensuing hiatus, pedogenesis was by podzolisation on the upper slopes grading to latosolisation on well-drained lower slopes and to gleization in the basins.

Big Monk pedoderm

The Big Monk pedoderm consists of a basal clastics facies of colluvium on the bajada, grading downslope into outwash sands and fine gravels, on which a yellow podzolic soil is developed in moderately to well-drained positions and a dark grey solodic soil is formed in the hydromorphic environment.

Type sections are:

- (12) 20970E 58384N Big Monk pedoderm, colluvial component
- (13) 20713E 58152N Big Monk pedoderm, yellow podzolic variant
- (14) 20737E 58260N Big Monk pedoderm, hydromorphic variant, type (i)
- (15) 20650E 58042N Big Monk pedoderm, hydromorphic variant, type (ii).

The basal colluvial component is restricted to secondary fans and splays on the bajada where it overlies the Lanyon slopewash and onlaps onto the Murrumbidgee and Tuggeranong fanglomerates. The deposits are of limited lateral extent and thin rapidly downslope, but thicknesses of up to 8 m are exposed in streams which dissect the bajada. The colluvium is very poorly sorted, comprising randomly oriented cobbles and boulders in a slightly indurated sand matrix (Fig. 29). Secondary pore-filling has been minimal and pedologic patterns are only poorly developed. They consist of diffuse yellowish brown vertical veins,

generally less than 20 cm long, in a pale grey earthy groundmass.

The yellow podzolic variant of the upper facies of the Big Monk pedoderm covers a broad gentle depression on the northern pediment of the south basin and the gently undulating slopes around the southwest boundary of the north basin. Remnants of it also occur extensively on the lower bajada and in minor depressions on the upper basin surfaces where it disconformably overlies truncated Lanyon, Tuggeranong, and Murrumbidgee pedoderms.

In the north basin the hydromorphic variant is inset into the southwestern sector of the Lanyon pedoderm, and in the south basin, where it planes across both the Lanyon and Tuggeranong pedoderms, it occupies a wedge extending from the basin outlet to the nick points 250 m upstream.

Thickness of the Big Monk pedoderm on the higher basin surfaces ranges from 80 cm to 1.2 m (Fig. 30). The A horizon is 20 cm thick, and is characterised by pronounced bleaching in the A2 horizon. The B horizon is 30 cm thick and composed of irregular, rough blocky to columnar peds (7 x 2 cm). The peds are constructed of mottled grey and yellow-brown clayey coarse sands coated by grey cutans. In the dry state the soil is tough, and shrinkage cracks up to 5 mm wide transect the entire B horizon. The B2 horizon is generally 30 cm thick. Colour is yellow-brown with grey clay-filled vertical joint planes spaced about 10 cm apart. In the best-drained sites the B2 horizon is mottled yellow and reddish brown with sparse sesquioxide nodules. The solum is acid throughout (pH 5.5-6.7).

The subsolum is generally alkaline (pH 8.3-8.6) with patches of carbonate. It is a drab grey-brown with yellow patches, intensely indurated, silty coarse sand. Framework grains are subrounded to subangular quartz, feldspar, and rock fragments. There is no sedimentary layering apart from pockets of basal cobbles, and no distinctive pedologic patterns. About half of the megascopic voids have pale grey cutans.

On the higher basin surfaces the subsolum becomes more gravelly where slopewash sheets merge with stonelines radiating out from the colluvial deposits of the lower bajada. The subsolum patterns of the Big Monk pedoderm reach their maximum development in these areas, where they are characterised by an intensely mottled yellowish brown and grey earthy matrix with thick (1 cm) grey cutans around large clasts. There is very little carbonate, and veining is absent. The subsolum is not as intensely indurated as the equivalent units in the lower basins. On the perched basin angular rock fragments account for about half of the framework

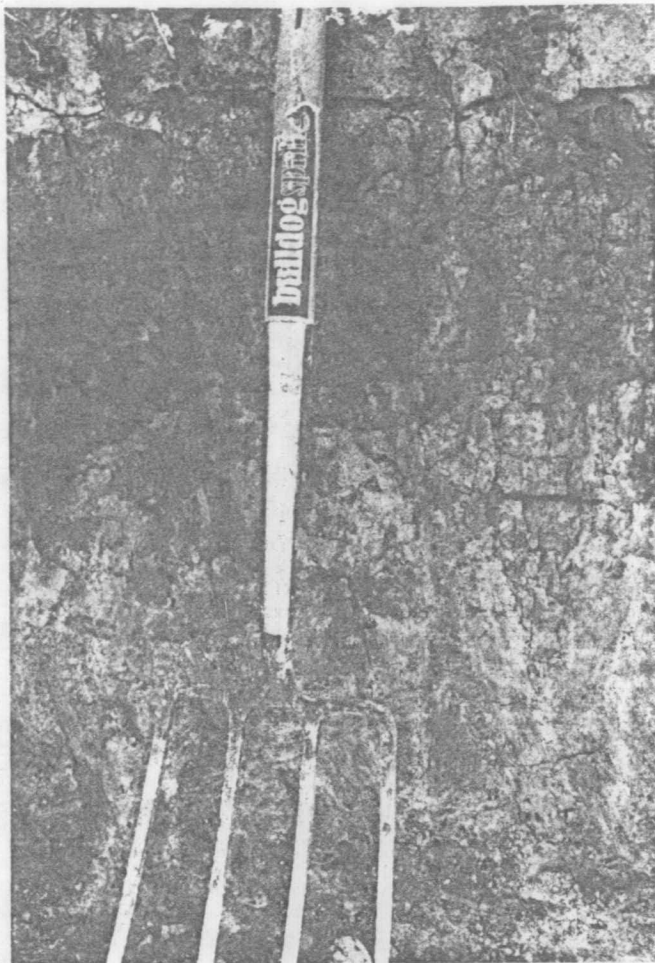


Fig. 30. Type section (13) - yellow podzolic variant of the Big Monk pedoderm. Characteristic features include pronounced bleaching in the A2 horizon and tough cracking clays in the thin B horizon. Peds are rough blocky to columnar with grey cutans. (20713E 58152N). BMR Neg. GB/2908-19A.

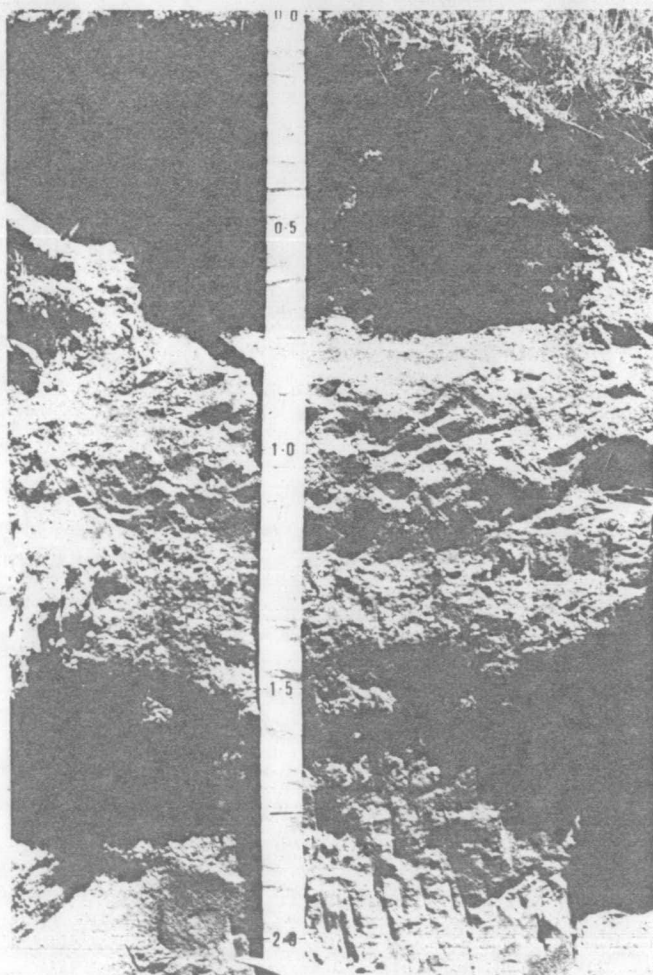


Fig. 31. Type section (14) - grey solodic (hydromorphic) variant of the Big Monk pedoderm. The subsolom has no distinct patterns and extends to the clear wavy boundary which intersects the tape at 1.69 m. The unit below with the grey clay veins and mottling is the subsolum of the Lanyon pedoderm from which the upper clay layer was removed during the initial erosive phase of the Big Monk pedoderm. (20737E 58260N). BMR Neg. GB/2908-17.

grains in the subsolum and are also disseminated throughout the B horizon.

The hydromorphic variant (Fig. 31) is slightly acid in the A horizon (pH 6.5), neutral to alkaline throughout the B horizon (pH 7.2-8.8), and alkaline in the subsolum (pH 8.7-9.4). Total average thickness of the pedoderm is 1.8 m. Fabric and texture of the B horizon are similar to those of the yellow podzolics, except that the peds are smaller and blockier (3 cm) and they are coated by dark grey organo-argillans. Where a B2 horizon exists, it is mottled yellow and dark grey. The subsolum is weakly cemented silty coarse sand and fine gravel; it has no distinct pedologic patterns, apart from occasional clusters of sesquioxide nodules (which may be reworked from the Lanyon pedoderm) and black oxide stains around megavoids.

There are two divisions in the hydromorphic variant of the Big Monk pedoderm. In topographically higher insets into the Lanyon pedoderm, the solum grades via the B2 horizon into the subsolum (Fig. 31); in depressions cut into the Lanyon and Tuggeranong pedoderms towards the basin outlets, the sequence is layered: the contact between the B horizon and subsolum is sharp because the B2 horizon is lacking (Fig. 32).

Field criteria to distinguish hydromorphic variants of the Big Monk and Lanyon pedoderms

In the hydromorphic environment, the Big Monk pedoderm may be difficult to distinguish from the Lanyon pedoderm. Criteria which have proved useful in the field are summarised in Table 7.

Table 7. Summary of field criteria of hydromorphic variants of Big Monk and Lanyon pedoderms

	Lanyon pedoderm	Big Monk pedoderm
Geomorphic setting	Younger basin surface	Inset into younger basin surface
B Horizon	(Thickness Pedality Weathering)	(Thickness Pedality Weathering)
	≤ 1 m Strong prismatic peds Interior of peds intensely weathered in upper B horizon to mostly clay-silt/clay	≤ 30 cm Weak blocky columnar peds Interior of peds slightly to moderately weathered to mostly coarse sand-size
Subsolum patterns	Well organised into prismatic aggregates to depths of 2.5 m. Pronounced colour segregation into coarse pattern of yellow-brown and grey	None, apart from tubules in the top 20 cm

Table 7 con't

Sedimentary characteristics	Gradual fining upwards sequence; basal gravels rounded	Subangular gravels disseminated throughout or sharp break between B and C horizons (no B2).
Framework grains in subsolum	Mainly quartz and feldspar	Mainly rock fragments

Depositional and pedogenetic environment of the Big Monk pedoderm

The colluvial and slopewash sheet deposits which comprise the Big Monk pedoderm indicate an initial period of instability and mass movement on the hillslopes, particularly on the lower bajada, and a period of incision around drainage lines on pediments, especially on those with a mainly southerly aspect. Headward erosion of streams in the lower basin sectors initiated lateral planation adjacent to the streams by erosion of the Lanyon pedoderm.

Hillslope instability appears to have been initiated during a periglacial maximum which destroyed much of the frost-sensitive slope vegetation; evidence for this hypothesis is described in the section on the surficial geology of the perched basin. Sporadic storms of high intensity or spring rains of long duration promoted vigorous stream incision and induced mass movement on the slopes. Lateral widening of the basin streams was apparently terminated by a steady decrease in stream discharge, culminating in partial infilling of the depressions. Early pedogenesis of the Big Monk pedoderm appears to have been under conditions of mild leaching during the following interstadial.

No mineralogical analysis was done on the clays of the Big Monk pedoderm. From the high plasticity of the clay and its demonstrated shrinkage and swelling characteristics, it is expected to have a significant expandable clay content. The high plasticity and yellow-grey colours are probably inherited from the source materials of the Tuggeranong and Lanyon clays.

Gigerline pedoderm

The Gigerline pedoderm consists of brown and grey earths and minimal podzolics developed on outwash sediments, alluvial terraces, and aeolian sand deposits.

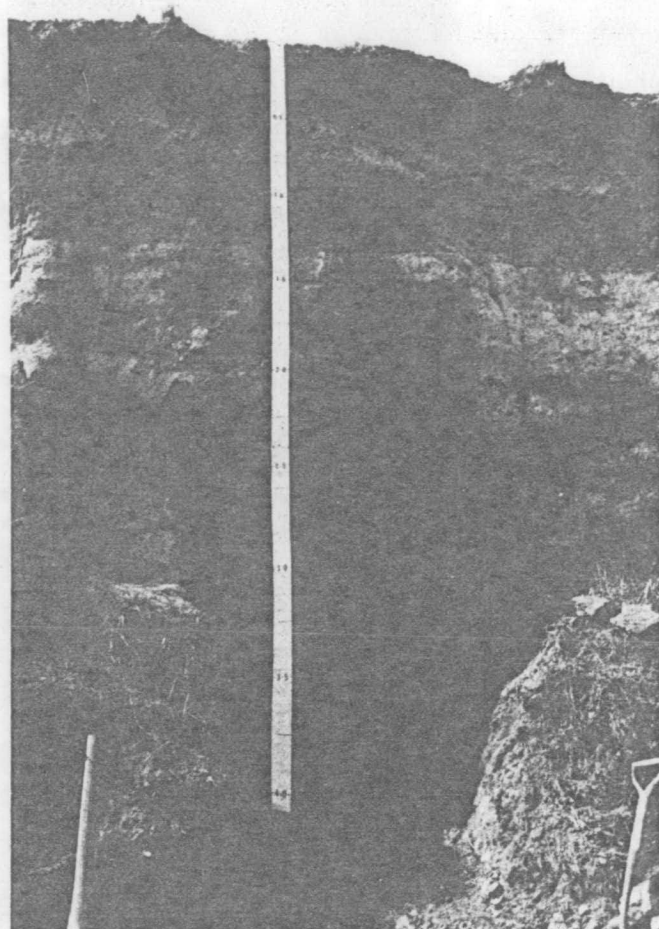


Fig. 32. Superposition of the layered hydromorphic variant of the Big Monk pedoderm (0.77-2.35 m) on hydromorphic Tuggeranong clay. The B horizon (0.77-1.30 m), which is weakly pedal with organo-argillans and tubules, is distinguished from the Lanyon clay by its lower degree of clay weathering, its poorer organisation, and lack of B₂ horizon. The subsolum has no patterns, and depositional fabric is clearly evident. The Big Monk pedoderm is overlain by stratified alluvium (0-0.33 m) on the grey earth of the hydromorphic Gigerline pedoderm (0.33-0.77 m). (20650E 58042N). BMR Neg. GB/2909-24.

Type sections are:

- (16) 20890E 58287N Gigerline pedoderm red-brown earth, colluvial variant
- (17) 20772E 58076N Gigerline pedoderm, minimal red poszolic alluvial terrace variant.
- (18) 20715E 58381N Gigerline pedoderm, grey earth, hydromorphic variant
- (19) 29660E 58032N Gigerline pedoderm, red-brown earth, aeolian variant

On the bajada, the colluvial variant generally disconformably overlies, or is inset into, truncated Tuggeranong, Murrumbidgee or Big Monk pedoderms. Maximum thickness of the pedoderm on the lower bajada is 3.5 m, and average thickness is 2 m, of which the top 80 cm has been modified by pedogenesis. The soil is apedal red-brown earths grading to minimal podzolics developed on unstratified, weakly cemented greyish brown silty coarse sands with no distinctive subsolum patterns. Subangular lithic gravels are disseminated throughout the sola and subsola.

The alluvial variant is a minimal red podzolic soil which in the study area is confined to high terraces in re-entrants on the lower bajada. A brown A horizon 10 cm thick overlies a weakly pedal to earthy reddish brown sandy clay loam 30 cm thick on about 1.2 m of very poorly sorted silty gravels. This variant is of limited areal extent within the basin catchments, but its finer-grained equivalent unit is widely distributed to the north and south of the south basin outlet on the highest sand terraces of the Murrumbidgee River.

The hydromorphic variant is a grey earth up to 50 cm thick which covers the Big Monk and Lanyon pedoderms on the younger basin surfaces, and covers about half of the Tuggeranong pedoderm on the older basin surfaces, where it grades upslope into brown earths with gravelly subsola. The top 20 cm is black to dark grey organic silty loam which grades into pale grey coarse sandy clay loam. The soil is highly porous, partly from negligible secondary filling of packing voids and partly from bioturbation. In the lower basins the Gigerline pedoderm may be mistaken for the A horizon of some of the older solodic soils, but the unit can be traced laterally over hydromorphic Tuggeranong and Lanyon clays without discontinuities. The pseudo-A2 horizon development (e.g. Fig. 25) is attributed to past and present lateral throughflow on top of the older clays. On the older basin surface and on the lower slopes, clasts larger than coarse sand-size account for up to 30% of the volume. Where these coarse-grained soils overlie clays with no stone content in their B horizons, it is considered that this is sufficient justification for the soil-layering interpretation.

Older fanglomerates on the undulating windward slopes near the southern watershed of the south basin are covered by up to 3 m of aeolian sand sheets on

which a red earth has developed on the top 40 to 50 cm. These soils show the least organisation of any of the earths and minimal podzolics of the Gigerline pedoderm because of their dominantly quartzose sand provenance, unlike the source of the other variants, which contain a variable proportion of reworked older soils in their parent material.

All variants of the Gigerline pedoderm are acid to neutral throughout (pH 5.3-7.2).

Depositional and pedogenetic environment of the Gigerline pedoderm

The initial erosional-depositional environment of the Gigerline pedoderm appears to have been a return to cold conditions, which permitted mass movement of the regolith on the hillslopes but resulted in little renewed planation on the basin surfaces.

Boulder trains (Fig. 5) on the lower slopes of Tuggeranong Hill indicate the degree of instability of southerly facing slopes during this period. An excavation into one of the boulder trains shows that the boulders are bedded within the truncated subsolum of the colluvial variant of the Gigerline pedoderm, which on the southern slopes of Tuggeranong Hill (Fig. 33) contains about 20% angular cobbles. The underlying soil which provided the slip plane is Tuggeranong clay with no rock fragments. The surface boulders were initially loosened by ice-wedging in joints at the free face, and were deposited up to 500 m downslope in mudflows during ensuing heavy rains.

A dry environment with strong westerly winds is indicated for a part of the unstable phase by the sand dunes blown up from the Murrumbidgee River bed to a level of 600 m a.s.l. Therefore the period of instability probably occurred during a periglacial maximum with dry windy winters and substantial spring rains.

Pedogenesis during the interstadial occurred during a relatively humid climate, but was apparently of short duration. The soils of the Gigerline pedoderm are young enough to show the dependance of soil morphology on provenance of parent material. The hillslope catenary variations from brown earths in upslope sites to yellow and grey earths in poorer-drained localities are about the same as those that could be expected for soils developing under the present climate in the same geomorphic setting.

Riverside pedoderm

The Riverside pedoderm is a minimal prairie soil which occurs in the

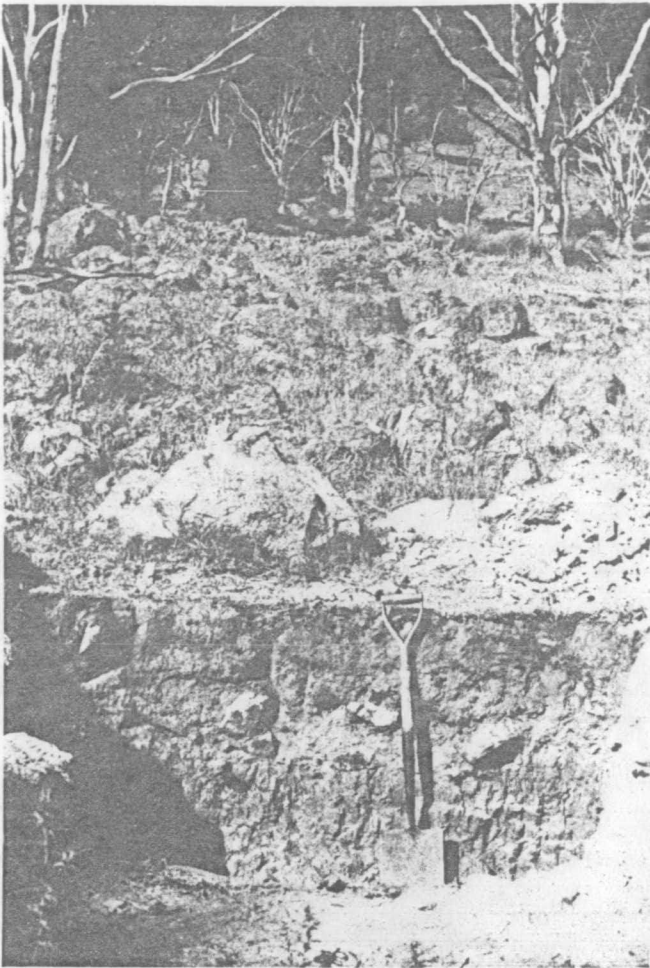


Fig. 33. Boulder trains and substrate on southerly lower slopes of Tuggeranong Hill. The exhumed boulders are bedded within the truncated subsolum of the colluvial variant of the Gigerline pedoderm. The underlying stone-free soil is Tuggeranong clay. The boulders indicate hillslope instability and mass wastage during the most recent periglacial maximum, when the Gigerline pedoderm was initiated. (20835E 58438N). BMR Neg. GB/2909-28.

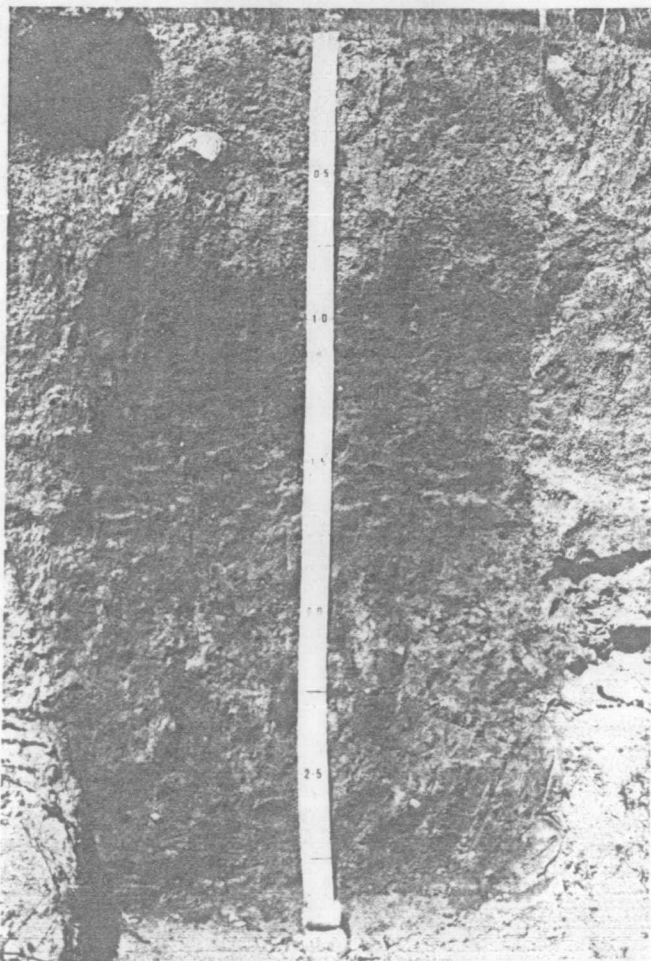


Fig. 34. Type section (20) of the Riverside pedoderm overlying the subsolum of the colluvial variant of the Gigerline pedoderm. The diffuse boundary between the two units is at 1.7 m. Minimal prairie soils of the Riverside pedoderm lack any profile differentiation, but are bioturbated enough to destroy depositional fabric and to obscure soil contacts. (20912E 58307N). BMR Neg. GB/2909-12.

youngest alluvial terraces in re-entrants on the bajada and in low terraces of streams which transect the older basin geomorphic surfaces. Its average thickness is 1.5 m in the bajada and about 70 cm in the upper basins. At the westerly ends of the basins it is probably incorporated in the top sections of the cumulic Tuggeranong pedoderm.

The soil is dark grey organic silty sand, unstratified with negligible textural variation throughout the profile; it is highly porous, intensely bioturbated, and slightly acid throughout (pH 6.6-6.9). The type section (20) is at 209 12E 58307N (Fig. 34).

The Riverside pedoderm covers the least area of any of the surficial units in the basin catchments and has therefore hardly modified the geomorphic surfaces. However, it is equivalent to the black organic silty loams which occupy the extensive intermediate terrace of the Murrumbidgee River to the north and south of the south basin outlet, and also appears to be equivalent to unconsolidated slopewash deposits of the perched basin.

Surficial geology of the perched basin (Fig. 35)

The significant differences in the geomorphic settings of the perched basin and the pediplain basins of the Murrumbidgee River are:

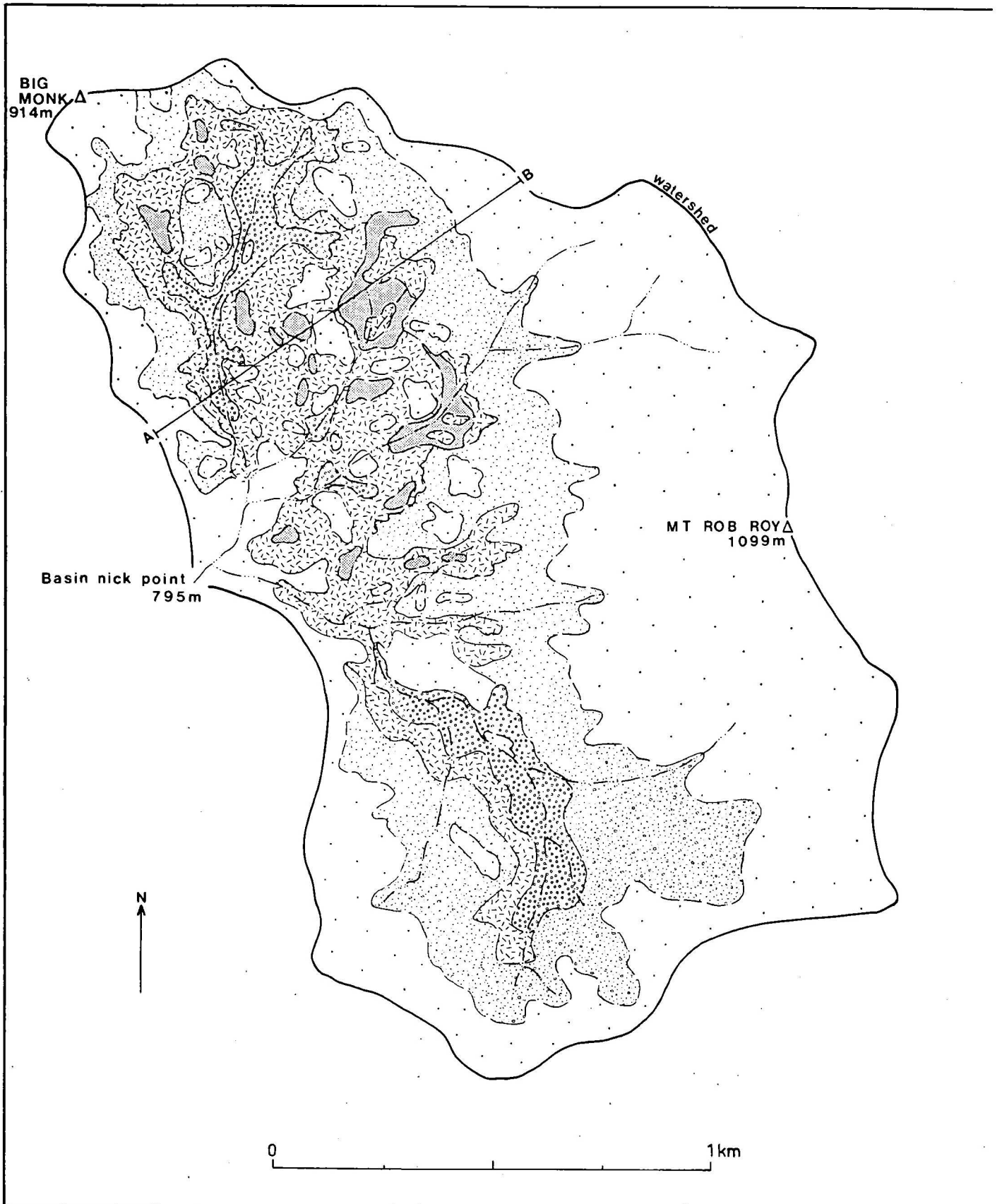
- (1) an increase in average elevation from 600 m on the plains to 820 m on the perched basin,

and

- (2) the southerly aspect of most of the perched basin surface, in contrast to the dominantly westerly aspect of the north and south basins.











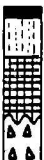



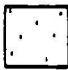
The combined effects of (1) and (2) was that mass wastage during periods of landscape instability was more severe in the perched basin, resulting in almost complete stripping of the regolith older than the Big Monk pedoderm and a very thin soil cover generally. The oldest surficial unit recognized is the Tuggeranong fanglomerate which occurs in stumps underneath the Big Monk pedoderm, usually in the higher valley sections and down near the basin outlet. The Tuggeranong clay and the entire Lanyon pedoderm appear to have been completely removed; however it should be noted that no drillholes were put down in the perched basin, so there may be buried remnants of these materials in some interfluves.

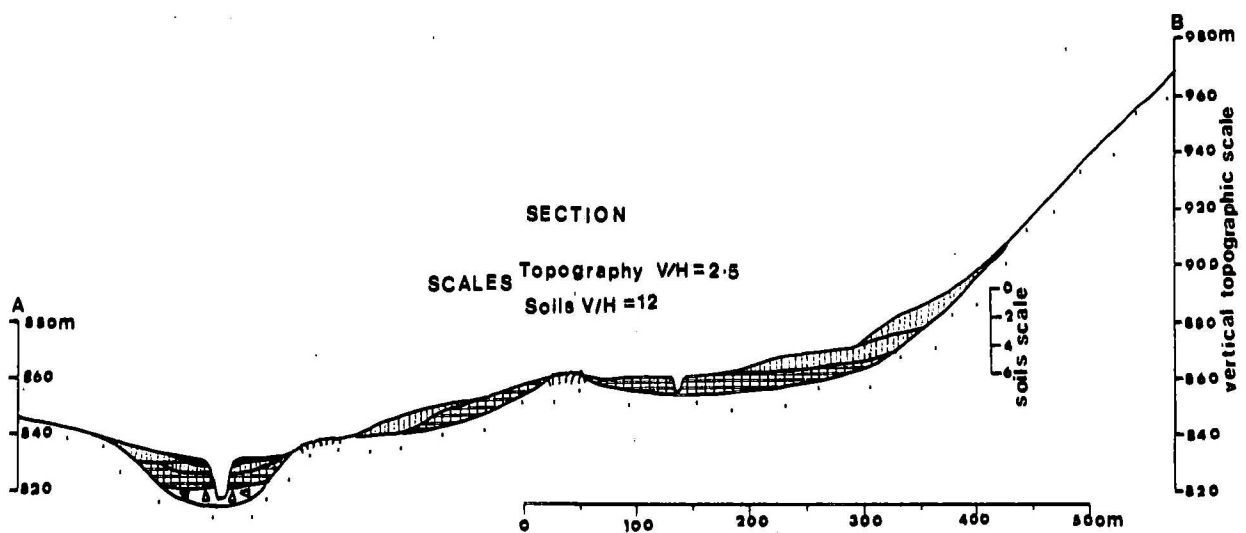
The morphology of the perched basin is quite different from that of the lower basins. In the northern half of the perched basin, stepped surfaces (Fig. 35)



**SURFICIAL GEOLOGY
OF THE PERCHED BASIN**

Fig 35

SURFICIAL MAPPING UNIT	SOIL ASSOCIATION
	 Riverside Pedoderm (pale grey slopewash)  Gigerline Pedoderm (yellow earths)
	 Gigerline Pedoderm (yellow & grey earths)  Big Monk Pedoderm (yellow podzolics)
	 Big Monk Pedoderm (yellow podzolics)  Big Monk Pedoderm (yellow podzolics)
	 Stratified alluvium  Gigerline Pedoderm (grey earths)  Big Monk Pedoderm (grey podzolics)  Fanglomerate (Tuggeranong?)
	Lithosols, rock rubble & outcrop



between rocky knolls are covered by thin lobes of the Gigerline pedoderm overlying the Big Monk pedoderm. Talus and slope wash sheets, probably equivalent to the Riverside pedoderm, cover the steep colluvial slopes to the south and east and onlap onto the Gigerline pedoderm. The central valley sections contain the Gigerline and Big Monk pedoderms disconformably overlying fanglomerate stumps.

The stepped profile (Fig. 36) resembles immature cryoplanation terraces and appears to have evolved contemporaneously with the Big Monk pedoderm. French (1976) described cryoplanation terraces as a periglacial slope form which is best developed in semi-arid continental areas; the process depends on intensive frost wedging with efficient sheetwashing and does not necessarily require permafrost conditions. The underlying rock should be resistant to erosion and have negligible intergranular porosity, but at the same time the rock must be sufficiently fractured to allow entry of water and effective frost-shattering. The acid volcanic rocks of the perched basin are resistant, closely-jointed rocks and therefore conform to this condition. French also specified that the winter snow cover showed not to be thick enough to insulate the substrate from changes in air temperature.

The most obvious differences between the pedoderms of the perched basin and their equivalent units in the lower basins is the stone content and shape; the soils of the perched basin are more gravelly and the gravels are more angular.

The fanglomerate exposed in the creeks is composed of subangular to subrounded pebbles and minor cobbles in a porous sandy matrix. Maximum exposed thickness is 1.8 m. On the basis of plasma colour, degree of pedologic differentiation, and subsolum patterns, the unit is tentatively correlated with the Tuggeranong fanglomerate of the lower basins. In addition to the cutanic and veining features of the Tuggeranong pedoderm, the fanglomerate in the lower valley section of the perched basin is impregnated with sesquioxide nodules; this is interpreted as secondary development during the Lanyon pedoderm or later.

The essential difference between the fanglomerate in the perched basin and the Tuggeranong fanglomerate of the lower basins is in the depositional fabric. There is no stratification or imbrication typical of the lower basin fanglomerate but there is a coarse pattern of sieving, in which randomly oriented cobbles and pebbles occur in diffuse clusters. In some places there is a secondary crude sieving of the matrix; irregular patches of sand with low silt content are segregated towards the periphery of matrix clusters. This pattern may have developed by frost sorting.

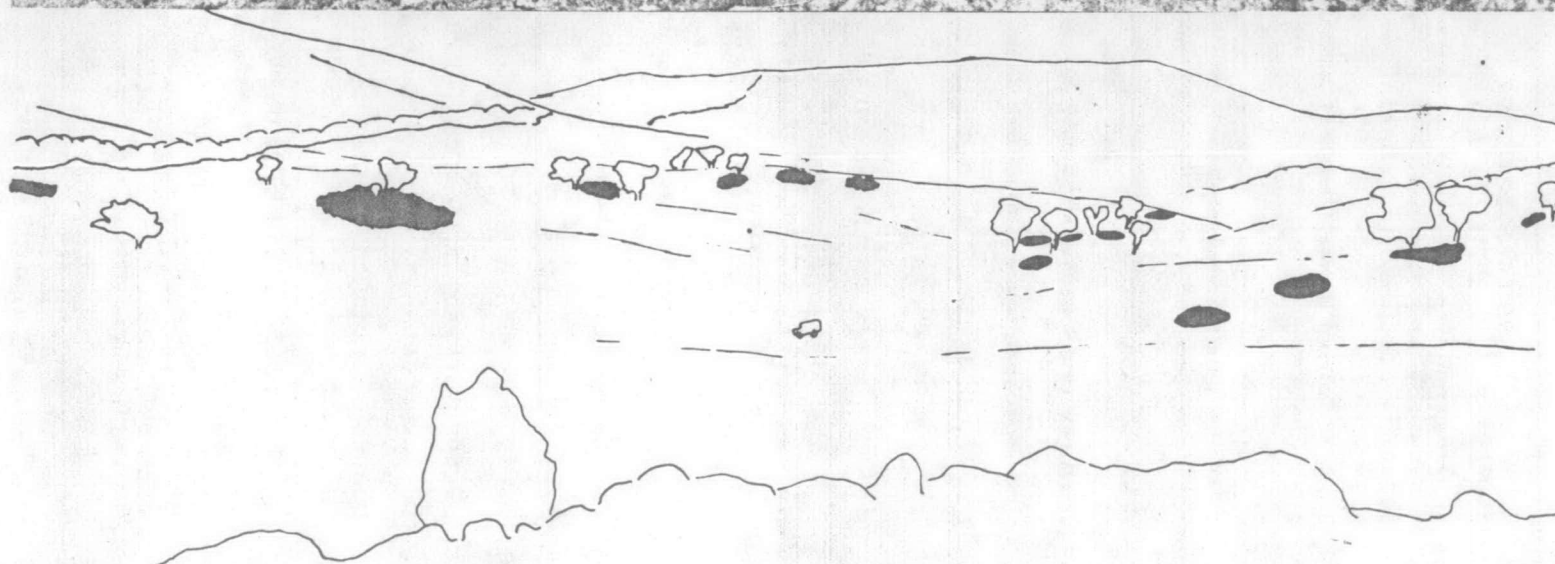
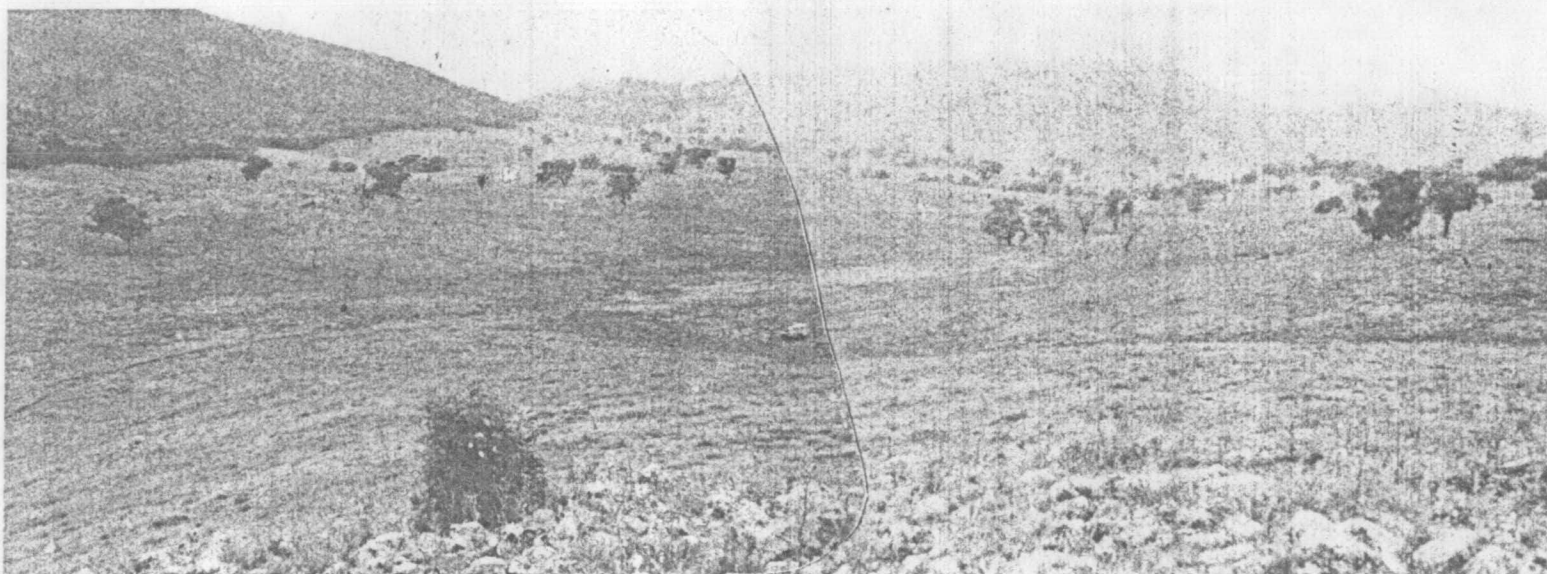


Fig. 36. Looking south across the northern part of the perched basin. The stepped sequence of tors appears to indicate late Quaternary periglacial modifications to the pediment when the regolith was severely stripped, and immature cryoplanation terraces were developed. The process apparently started contemporaneously with the initial unstable phase of the Big Monk pedoderm, but was arrested during subsequent pedogenesis under more equable conditions. Reactivation occurred during a return to active periglaciation in the initial unstable phase of the Gigerline pedoderm. BMR Neg. GB/2909-3 & 4.

The Big Monk Pedoderm has an A horizon about 10 cm thick with conspicuous bleaching in the lower half. The B horizon is 30 cm thick with blocky peds (5 cm) of mottled grey and brown clayey sands coated by grey cutans. The internal fabric of the peds is characterised by prominent subhorizontal partings defined by planar voids about 3 mm apart around which iron oxides have precipitated. The B2 horizon and subsolum are about 35 cm thick and consist of clayey subangular fine gravels with some sesquioxide concretions and minor clay-filled vertical joint planes. Angular rhyolite cobbles with grey cutans are randomly distributed throughout all horizons of the pedoderm.

The Gigerline pedoderm grades from yellow-grey earths developed on slopewash sheets and lobes to grey earths on reworked slopewash sands in the valley. Thickness of the pedoderm ranges from an average of 30 cm on the slopes to 50 cm in the valleys. The material is a sandy silt, weakly arranged into very coarse columnar aggregates with minimal profile differentiation. Angular rhyolite gravels occur throughout the unit on the slopes, but are infrequent in the valley. Low concentrations of sesquioxide nodules are in the lower sola.

The overlying slopewash sheets of uncemented whitish grey silty sand which mantles the upper slopes are tentatively assigned to the Riverside pedoderm. There is no profile differentiation apart from minimal accumulation of organic matter in the top few centimetres and the unit lacks the intense bioturbation that is characteristic of the prairie soils of the lower basins. Average thickness of the slopewash is about 60 cm, but it attains a thickness of up to 2 m in small depressions immediately below the change of slope in the wooded hills to the east of the basin. The highest deposits on interfluvies contain significant bladed rhyolite clasts; the lower deposits are mostly cohesionless silty sands which, upon saturation, are prone to slumping and creep on cleared slopes greater than 8°.

Summary and discussion of the surficial geology

In a hydrogeological study primarily concerned with remedial drainage of surficial aquifers, the three-dimensional distribution and hydrologic characteristics of the surficial units must be defined. For this reason the pedoderms have been investigated in detail.

The hydrogeological significance of the relative ages of the pedoderms is that the subsola of the youngest pedoderms have undergone the least secondary void filling and other pedologic modifications and, therefore, the least diminution in hydraulic conductivity, since deposition. It follows that the sands and gravels of the Riverside, Gigerline, Big Monk, and Lanyon pedoderms are the most permeable aquifers, whereas the older fanglomerates are generally aquitards. From the inferred

depositional environments it is apparent that the basal gravels in the Big Monk and Lanyon pedoderms behave as line sources, but the overlying sand sheets are hydraulically continuous aquifers. Since the clays at the top of these units are of low permeability then confined aquifers are to be expected if a hydraulic head is operative. Conversely, the Riverside (slopewash) and Gigerline pedoderms always overlie lower-permeability substrate; hence, groundwater flow in these units will have a strong interflow component.

It has been shown that the basins accumulated a thick sequence of surficial deposits over a long period of time. Prior braided stream deposits of the Rob Roy pedoderm have been found only in the north basin, and the small elevation difference between the base of the pedoderm and the contemporary Murrumbidgee River suggests early Cainozoic movement on the Murrumbidgee Fault and on some of the major cross-faults. A tectonic origin of the north basin is supported by the probable late rotation of joint sets on Tuggeranong Hill (domain H, Plate 2). Indeed, the downthrown wedge protected against erosion readily explains why the arenites of the Rob Roy pedoderm have been preserved in the Lanyon basin, but have not been reported anywhere else locally, apart from the Canberra Plain (Opik, 1958).

It is significant that the Silurian volcanics beneath the south basin are extremely to highly weathered, but the rocks under the north basin have not undergone the same degree of weathering. The south basin appears to have originated by deep chemical etching, which is proposed as the classical mode of evolution of pediplain basins of the Southern Tablelands (Van Dijk & Woodyer, 1961).

The Murrumbidgee pedoderm represents a period of fan-building on the bajada and fluviatile deposition from braided streams in the basins. The failure to locate a paleosol related to pedogenesis at the top of the Murrumbidgee pedoderm has been noted earlier, but the pseudogley patterns unique to this pedoderm are considered to be sufficient proof that the unit was subjected to prolonged subaerial weathering and pedologic aggregation before it was buried by the Tuggeranong fanglomerate. In this context it is important to note that - although there has been much material illuviated into the Murrumbidgee pedoderm - the infilled cracks and planar voids were pre-existing structures which in general do not extend up into the Tuggeranong pedoderm.

The Tuggeranong fanglomerate indicates a secondary phase of fan-building, and fluvial deposition in depressions scoured out of the Murrumbidgee pedoderm in the basins. On mineralogical evidence and on textural and fabric characteristics

of the Tuggeranong clay, an aeolian parent material is a plausible explanation for the upper facies of the Tuggeranong pedoderm. The blanket of Tuggeranong clay infiltrated voids in underlying fanglomerates and lag gravels, and much of it was redeposited in the basins. Pedogenesis of the Tuggeranong clay was characterised by very mild leaching under a moderately arid climate during initial organisation, but it was subjected to prolonged alternating periods of deep wetting and drying during advanced pedogenesis.

The Lanyon pedoderm was deposited during a period of vigorous planation in the basins, and hillslope denudation on a smaller scale, probably initiated by rejuvenation of the Murrumbidgee River. Red podzolic soils developed on the upper slopes, and latosols formed on the lower slopes above the zone of intermittent saturation. A strongly structured solodic soil, the Lanyon clay, developed under hydromorphic conditions in the basins. The pedogenetic environment was characterised by a greatly increased leaching capacity, which also desilicated exposed hillslope sections of Tuggeranong clay. Rainfall was probably seasonal and may have promoted the development of slickensides and the deposition of mangans in the lower B horizon and subsolum of the Tuggeranong clay.

The yellow podzolic soils of the Big Monk pedoderm developed on high terraces, slopewash sheets, and colluvial fans, which appear to have locally modified the bajada to a greater degree than the preceeding Lanyon pedoderm. Development of the hydromorphic equivalent soil in the basins followed a short period of planation of the Lanyon pedoderm. On the perched basin, erosion of the regolith and redeposition of detritus to form the Big Monk pedoderm occurred mainly by slopewash and to a lesser degree by solifluction. The western pediment was modified into incipient cryoplanation terraces; the dominant processes were severe frost-shattering and sheetwash erosion. The inferred depositional environment of the Big Monk pedoderm is that the onset of periglacial conditions destroyed frost-sensitive vegetation on the hillslopes and on the perched basin, and thereby induced mass wastage during heavy spring rains. Winter snowfalls were apparently sparse because classical nivation processes did not operate. Early pedogenesis was apparently under conditions of mild leaching and increased temperature.

The Gigerline pedoderm was probably initiated by another climatic perturbation towards periglacial conditions, accompanied in part by strong westerly winds. Boulder trains on the southern slopes of Tuggeranong Hill

indicate dry winters with effective frost-wedging at the free face followed by spring or summer rains of high enough intensity to promote large mudflows. Duration of pedogenesis was comparatively short, but leaching produced earths with low soluble salts. The podzolics of the Big Monk pedoderm may well have undergone secondary partial saturation in the B horizon and significant A horizon interflow to evolve to their present morphology during the stable phase of the Gigerline pedoderm.

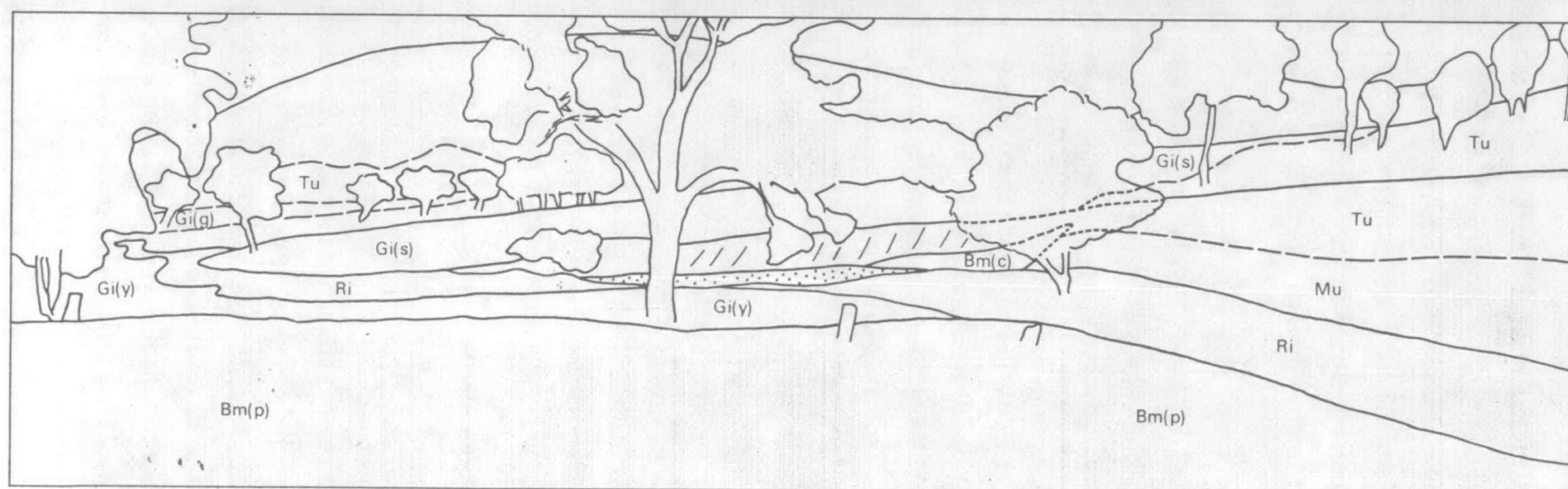
The Riverside pedoderm, a minimal prairie soil restricted to low alluvial terraces, hardly affected the basin surfaces, but extensive slopewash sheets were deposited in the perched basin.

The youngest pedoderms may be correlated with the K-cycle soils (Van Dijk, 1959; Butler, 1959) of the Molonglo River valley at Canberra. Equivalence is based on the degree of organisation of the soils and the relative positions in the terrace sequences of the Murrumbidgee and Molonglo Rivers:

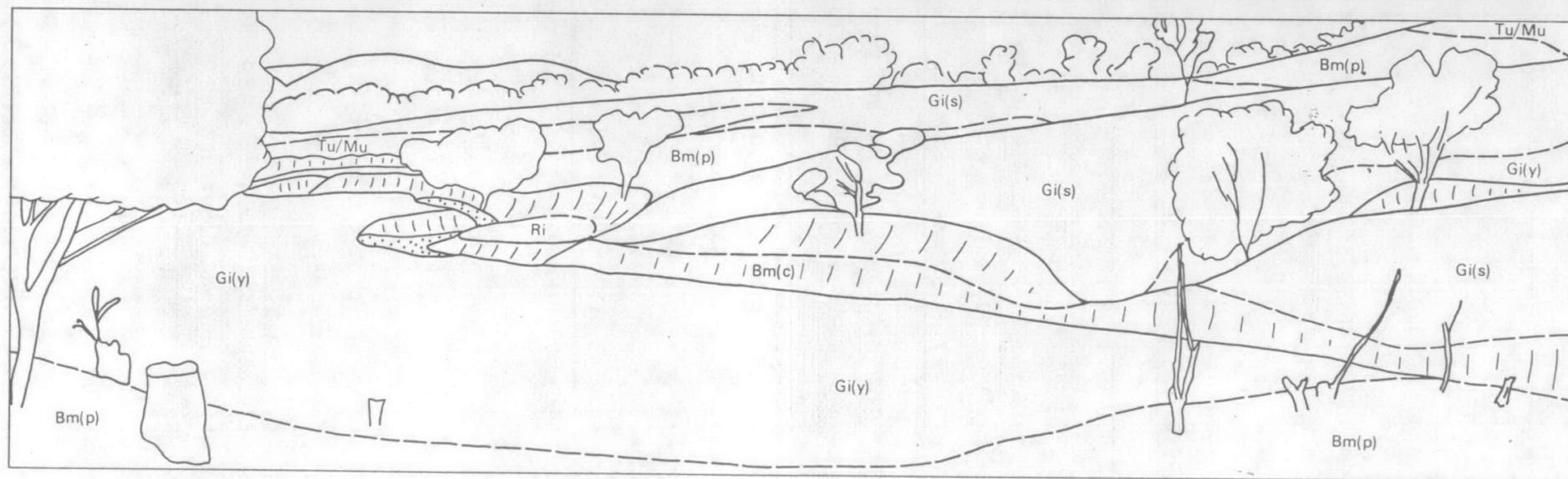
- K1 - Riverside pedoderm
- K2 - Gigerline pedoderm
- K3 - Big Monk pedoderm

Subsolum patterns in the Big Monk pedoderm on the higher basin surfaces appear to be similar to those in the Black Mountain 'Fanglomerate B' (Opik, 1958; Costin & Polach 1973). Costin & Polach attributed a periglacial origin to the Black Mountain fanglomerate, and have established an average age of 27 800 years B.P. by radiocarbon dating.

Mapping of the pedoderms in the basins was straight forward because of the 'layer-cake stratigraphy' and the good exposures in the basin streams; it was aided by core from a large number of drillholes. However, mapping on the bajada was difficult because alternating erosional and depositional processes have operated there, at least since deposition of the Big Monk pedoderm. In this regard, the work of Butler (1959), who has described hillslope soil processes and the nature of soil disconformities, proved to be a most useful guide. The use of subsolum patterns for correlation (Van Dijk & others, 1968; Van Dijk, 1969) proved to be invaluable because in many places the solum had been removed during erosive phases of subsequent pedoderms; it is difficult to envisage how surficial mapping in such a complex environment



Ri	RIVERSIDE PEDODERM	Minimal prairie soils in low terraces.	Gi(y)	GIGERLINE PEDODERM	Yellow earths developed on alluvium.	Bm(p)	Yellow podzolics developed on alluvium-colluvium	Tu	TUGGERANONG PEDODERM	Tuggeranong clay - (multiple pedogenesis) and fine-grained subsolum overlain by thin cover of Gigerline colluvial material
Gi(g)		Grey earths on the older basin surface overlying Tuggeranong pedoderm.	Gi(s)		Brown stony earths developed on slopewash.	Bm(c)	Colluvial subsolum only	Mu	MURRUMBIDGEE PEDODERM	Upper sheetwash facies



Ri	RIVERSIDE PEDODERM	Minimal prairie soils in low terraces.	Gi(y)	GIGERLINE PEDODERM	Yellow earths developed on alluvium.	Bm(p)	BIG MONK PEDODERM	Grey and yellow podzolics developed on alluvium-colluvium	Tu/Mu	TUGGERANONG/ MURRUMBIDGEE PEDODERMS	Tuggeranong clay and fanglomerate overlying Murrumbidgee pedoderm
			Gi(s)		Brown stony earths developed on slopewash.	Bm(c)		Colluvial subsolum only			

could have been achieved without their use.

Typical soil contacts and their surface expression on the bajada above the north and south basins are shown in Figures 37 and 38.

HYDROLOGY

Groundwater hydrology - method of field investigation

In June 1974, 38 holes were augered by Holland and Thomson Pty. Ltd., under contract to NCDC and supervised by BMR. The recovery of undisturbed samples in thin-wall sampling tubes was attempted in all holes. The tubes were pushed hydraulically to refusal and where necessary the hole was deepened by continuous augering. Logs of the holes are included in Appendix 4.

Twenty-nine open-tube piezometers were established in auger holes by first washing down blank HQ steel casing and flushing out. Sixty-millimetre internal-diameter PVC piping, perforated to align with the aquifer, was then inserted inside the HQ casing. When the PVC pipe was set with the perforations at aquifer levels, the outer HQ casing was removed, allowing the aquifer to slump against the perforated PVC pipe. Gravel was tamped down the hole to slightly above the top perforation level and the hole was cleaned by jetting. Local clays were used to seal off the hole above a 20-cm sand filter. After several cycles of alternating pumping and recovery, the technique generally produced a successful pumping well, but its usefulness as a long-term observation bore was limited in areas of low hydraulic conductivity because of the time lag and attenuation of piezometer response (Talsma, 1963). Also the clay seal was found to be ineffective in areas where the groundwater potential rose above ground level. Twenty-seven of the twenty-nine piezometers remained operational throughout the observation period, September 1974 to December 1976.

In January and February 1975, 36 additional holes were augered by the Department of Housing and Construction (DHC) under contract to NCDC and were supervised by GHD. Most of the drilling was by continuous solid-flight augering; the recovery of undisturbed samples was attempted in hollow augers, but the yield was poor. Piezometers were installed in 29 of these holes; 26 of them remained operational as groundwater observation points throughout the observation period March 1975 to December 1976. These piezometers consisted of thin (16 mm) plastic conduit connected to ceramic cylinders in a sand filter.

Bentonite and AM9 grout were used to seal off the hole. Problems of time lag to piezometer response were considerably reduced by the thinner-diameter tube, and the seals were more effective in preventing blow-outs when the groundwater potential rose above ground level. Logs of these holes are given in DHC report No. 144 (McDevitt, 1975).

Five diamond-drillholes were put down by BMR between July and December 1976 to establish the nature of the underlying rock and to assess its hydraulic properties. Continuous HQ cores provided structural information, in particular jointing characteristics. Core photographs in colour are available for inspection at BMR, and detailed fracture logs are included in Appendix 3. All bores were cased to sound rock, and minimum groundwater flow rates from specified fracture zones were estimated by airlifting. Rock bores L1, L2, TU4, and TU5 which had been drilled during the Tuggeranong regional investigations in 1972 and 1973 were also airlifted during this period.

The solid geology and surficial cover was mapped at 1:10 000 scale during June and July 1974 and detailed mapping was undertaken at 1:2 500 scale intermittently through 1975 and 1976.

Other fieldwork was aimed at quantifying hydrogeological parameters of the aquifers, namely conductivities, storages, and recharge rates. Hydraulic conductivities were determined by pump-testing during July and August 1974; infiltration capacities and effective porosities were measured during June and July 1976. Water-levels were recorded on average about once a fortnight from September 1974 through to December 1976, apart from a period of high-frequency monitoring during June, September and October 1976.

Surface drainage

Surface drainage of the north basin is provided by two unnamed ephemeral streams which flow from east to west along the northern and southern margins of the area of low relief (Plate 3). Gullies have been cut into the colluvial fans at the head of the basin to depths of up to 10.m. On entering the basin the gullies range from 2 to 3 metres in depth through the high terrace containing the oldest basin fill sediments. When the gradient decreases to below $1\frac{1}{2}^{\circ}$, the stream beds lose definition and the drainage system assumes a moderately braided character. Swampy areas occur at these discontinuities; ephemeral groundwater mounds are charged by surface outwash during streamflow,

and are sustained for several days after cessation of stream discharge by lateral subsurface piping of bedunderflow water into adjacent shallow aquifers.

To the west of the Tharwa Road the northern stream has reincised the lower basin terrace to depths of 3 to 4 m, but the channel is choked out by levees and outwash at a bog 700 m farther west. The southern portion of the basin to the west of the Tharwa Road is drained to the northwest by a continuous gully 4 to 5 m deep. The two streams comprise the main groundwater drains of the north basin; the southern stream flowed continuously throughout the bore observation period, September 1974 to December 1976, and baseflow was sufficient to maintain flow in the northern stream over the same period, apart from a brief cessation during June and July 1976.

The south basin is drained by three major unnamed streams (Plate 4). Two east-west streams flow through the central section and along the southern boundary of the basin, and the third creek flows towards the southwest near the western boundary of the basin.

The southern stream bed is incised up to 6 m through the oldest and highest basinfill sediments, 3 m through the younger basin sediments, and up to 5 m below the nick point between the younger and youngest basinfill sediments in the western part of the basin. The stream is a continuous line sink for groundwaters in the surficial aquifers and did not cease to flow during the period September 1974 to December 1976.

In contrast, the central stream is a significant line source for the surficial aquifers of the south basin. The stream rises on the western slopes of Mount Rob Roy; it flows through the perched basin, and then follows the trace of a fault through the eastern escarpment down to the south basin, before losing definition near the centre of the basin. The stream is intensely joint and fault-controlled on the eastern slopes, as shown by its rectilinear course, until it meanders across fanglomerates on the bajada (Plate 4). At this point the stream bed becomes filled with sand and boulders. During low stage, streamflow is reduced to less than half over the first 60 m of bed-load deposits, and on reaching the outwash sediments and levees at the end of the channel there is no discernable flow. Recharge to the groundwater store by subsurface piping from bed underflow in this stream occurs in the same manner as that of the influent streams of the north basin.



Fig. 39. Looking northeast from the southern drainage channel across the lower planation surface of the Lanyon south basin. Stream discharge is shown 4 hours after cessation of 34 mm of rainfall on 5.9.74. BMR Neg. GB/2910-A.



Fig. 40. Looking westwards along the southern drainage channel through the lowest terrace of the Lanyon south basin. The rock outcrop is 200 m downstream from the creek crossing in Fig. 39 and marks the nick point between the younger (Lanyon) and youngest (Big Monk) basin terraces. BMR Neg. GB/2910-B.

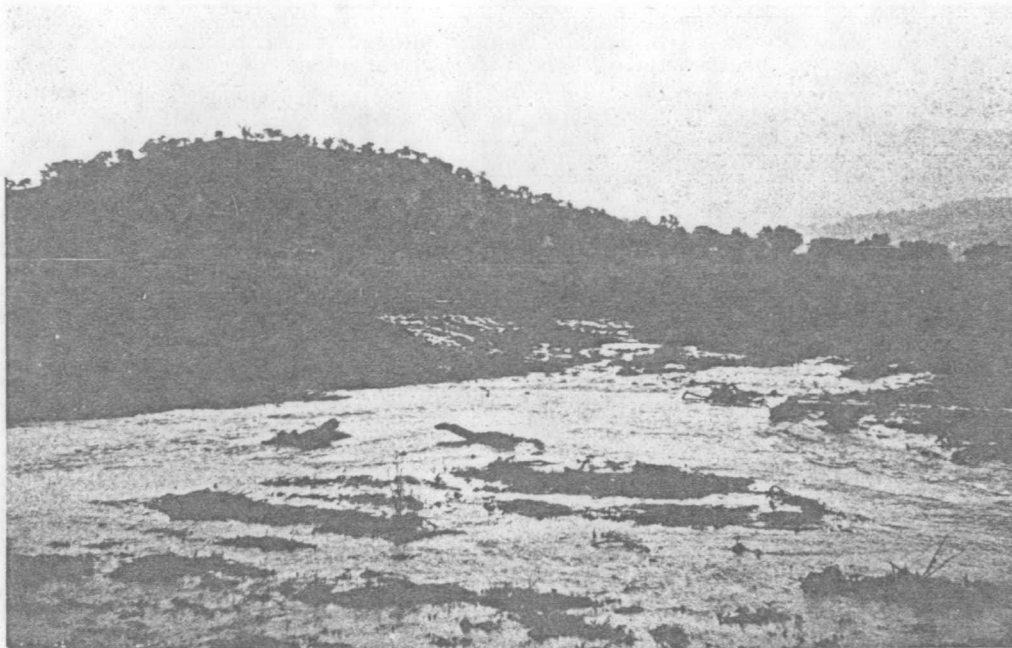


Fig. 41. Looking south from the terminus of the central stream across the lower planation surface of the Lanyon south basin. Piezometers 26, 26B and 26C are in the middle distance. Stream outwash is shown 4 hours after cessation of 34 mm rainfall on 5.9.74. Surface detention in depressions between clumps of sedge grass in the discharge zones of both basins persisted throughout the abnormally wet winter and spring seasons of 1974 and 1975 and the spring of 1976. BMR Neg. GB/2910-C.



Fig. 42. Looking west across the south basin on 5.9.74. The over-topped farm dam on the western boundary of the basin is in the middle distance. Piezometer 25 is to the immediate right of the bottom right-hand corner of the photograph. BMR Neg. GB/2910-D.

The stream near the western boundary of the basin loses definition at about the same elevation as the central stream, and much of its discharge ultimately permeates through the surficial cover into the large dam 250 m farther down gradient (the landholder states that this dam has never been dry during living memory). The creek below the dam is incised into rock, and this section of the stream is a prominent line sink which flowed continuously throughout the period of bore monitoring. The western and southern creeks coalesce at the toe of the south basin and then fall rapidly towards the Murrumbidgee River.

Apart from the southern stream of the south basin, the streams of both basins are discontinuous and are highly inefficient in removing surface runoff from the basin catchments. The photographs shown in Figures 39 to 42 were taken at 11 00 hours on Thursday 5 September 1974, four hours after cessation of 34 mm of rain which fell over 17 hours. This particular storm generated a high component of surface runoff because the soil moisture store was saturated following rainfall of 133 mm which started on 25 August and continued intermittently until 1 September.

The hydrogeological system

The Lanyon north and south basins contain a complex system of leaky surficial aquifers hydraulically connected to the underlying fractured-rock aquifer (Fig. 43).

Recharge to the rock aquifer occurs on the slopes above the head of each basin by seepage through skeletal soils into open joints. The recharge zone of the fractured rock extends down the bajada and onto the upper basin surfaces, where rainfall is admitted into temporary storage in the surficial cover: a proportion of water in the surficial store percolates down into the underlying rock fractures, and ultimately is transmitted westwards towards the basin outlets by deep circulation. The zones of highest recharge appear to be on the lower bajada where open-work colluvium of the Gigerline pedoderm directly overlies fractured bedrock.

The discharge zone of the fractured rock aquifer is along the western margins of the basins, where the groundwater potential of the rock aquifer is generally above that of the surficial aquifers. This potential difference induces upwards transmission of groundwater from the rock fractures into the

surficial aquifers and effluent streams.

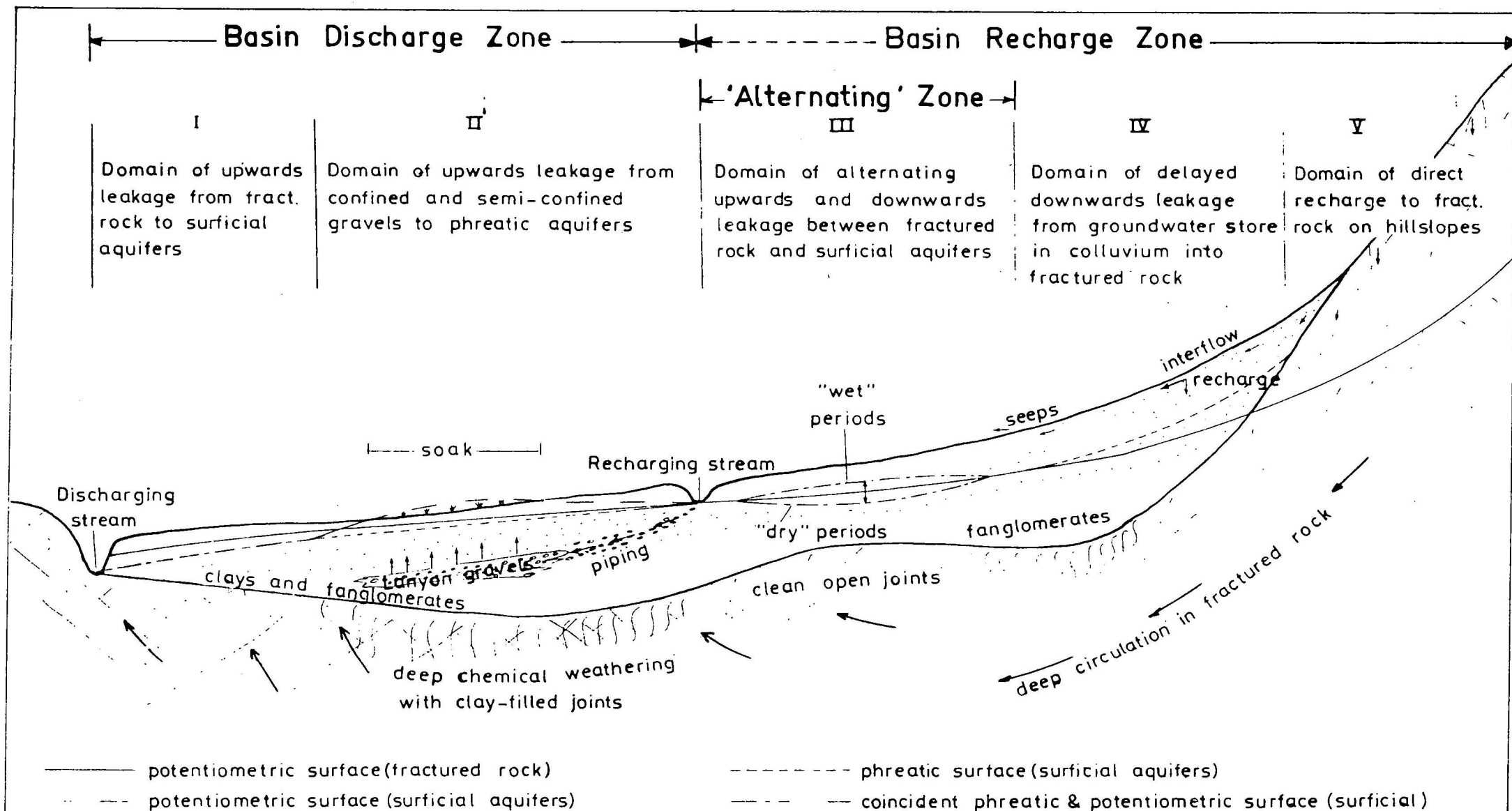
An alternating zone of upwards and downwards leakage occupies the lower basin surfaces between the recharge zone and discharge zone. In most winter and spring periods the leakage is predominantly from the surficial aquifers downwards into the fractured rock; in prolonged dry spells the groundwater potential in the surficial aquifers may fall several metres below that of the fractured rock and thereby induce upwards flow.

The boundaries of the recharge, alternating, and discharge zones vary according to seasonal conditions and therefore the boundaries of the hydrogeological domains shown in Figure 43 should be regarded as a generalisation only.

The fractured rock aquifer thus provides a steady 'baseflow' for the hydrogeological system. Superimposed on it is the more complex surficial aquifer system which undergoes fluctuations in groundwater potential of far greater magnitude. The increased hydrologic complexity of the surficial aquifers arises from:

- (i) the interaction of a major unsaturated flow component in the surficial aquifers vs saturated flow in the fractured rock, and
- (ii) an irregular spatial arrangement of surficial aquifers with gross differences in storages and conductivities, and affected by point and line sources and sinks, vs an (assumed) continuous network of interconnecting fractures in the rock, which undergoes more uniform recharge (plane source) and discharge (plane sink), and in which lateral changes in transmissivity are gradational, being largely dependent upon the degree of chemical weathering.

As noted earlier in the section on surficial geology, the units older than the Lanyon pedoderm have undergone such a high degree of secondary pore-filling that on the regional scale they may be regarded as aquitards, which, together with extremely weathered bedrock surfaces, impede transmission of groundwaters upwards or downwards between higher-permeability surficial aquifers and open rock fractures below. On a smaller scale this generalisation is questionable because it will be demonstrated in the section on hydraulic continuity of the aquifers that, in some parts of the basins, pathways in the



GENERALISED HYDROGEOLOGICAL SYSTEM - LANYON PEDIPLAIN BASINS
(not to scale)

older pedoderms facilitate the mixing of groundwaters from above and below with negligible time lags.

For example, lenses of loosely cemented sand and gravel occur at some places in the upper facies of the Murrumbidgee pedoderm (Fig. 13). These zones are generally limonite-stained, indicating at least significant prior sub-horizontal groundwater transmission. Irregular pathways for rapid vertical groundwater transmission in the Murrumbidgee fanglomerate exist in some areas from which the Tuggeranong pedoderm has been stripped and replaced by a younger unit with low soluble salts. Vein and joint plane infills of calcite in the Murrumbidgee fanglomerate that were originally derived from the Tuggeranong pedoderm have been partly removed during subsequent periods of high dilution with meteoric waters, thereby creating an irregular system of tertiary voids for vertical groundwater transmission. The increase in permeability due to the removal of calcite by reaction with carbonic acid in infiltrated rainwater appears to be optimised on the upper basin surfaces. It has also been observed in a few places in the groundwater discharge zone, but a satisfactory explanation is not readily available.

The aquitard which produces the greatest impedance to groundwater exchange is, in fact, the ancient weathering surface of extremely weathered rock with clay-filled joints in the central areas of the basins.

The most significant aquifers in the surficial cover are the bed-load deposits of Lanyon gravels. The gravels occupy discontinuous channels cut into the Tuggeranong pedoderm and are buried by sheets of floodplain sediments grading up into the Lanyon clay. Laterally the palaeochannels terminate abruptly against lower-permeability material of the upper facies of the Lanyon or Tuggeranong pedoderms. Recharge to the Lanyon gravels occurs by vertical infiltration of rainwater through overlying strata, by infiltration from stream outwash where contemporary streams lose definition, and by subsurface piping from bed underflow of such streams. Since the hydraulic conductivity of the Lanyon gravels is much higher than that of the surrounding media in all directions, then groundwater mounds are generated around the lower ends of the palaeochannels when the gravel reservoir becomes charged, culminating in the creation of bogs and soaks when the groundwater potential rises above ground surface.

All the major soaks in the swampy areas of the lower basin terraces are associated with abrupt terminations of palaeochannels of the Lanyon gravels where they lens out against much lower permeability media; in these situations the aquifers are truly artesian. This does not mean that soaks occur wherever there are Lanyon gravels, because at least 70% of the area underlain by the gravels is moderately well-drained except during very wet periods; the gravels are not hydraulically connected to contemporary streams and generally overlie open fanglomerates or rock with open joints extending to the surficial/rock interface. Recharge is dominantly by vertical downwards infiltration of rainwater through the overlying strata. The aquifer in these situations will be semi-unconfined except during very wet periods when the potentiometric surface rises above the phreatic surface in the upper subsolum or the Lanyon clay.

Groundwater discharge zones

Groundwater discharge zones of the surficial aquifers (Plates 3 and 4) represent areas of upwards leakage where the potentiometric surface was observed to be above ground level for at least 50% of the time during June and July, 1974. As noted earlier, the boundaries of these zones are by no means fixed in time but fluctuate with seasonal conditions.

The most extensive discharge zone of the north basin lies to the east of the Tharwa Road (Plate 3) and is caused by upwards flow from the Lanyon gravels in response to lateral recharge from the northern braided stream and from vertical upwards recharge from the fractured rock below. Lateral throughflow in the surficial material is impeded by the peripheral lower-permeability units, and impedance to throughflow in the fractured rock is caused by the low permeability of clay-filled joints in the more highly weathered rock beneath the swamps. The highest groundwater potentials are generated by northwest trending palaeochannels of buried Lanyon gravels around piezometers 12 and 123, and in the willow plantation 50 m north of piezometer 7.

The small but significant swamp immediately to the east is sustained by springs in rock fractures on the southwest face of Tuggeranong Hill. Recharge is initially into the overlying debris flow deposits of the Gigerline pedoderm, through which it is funnelled downslope into lenses of buried Lanyon gravels on the edge of the floodplain.

The discharge zone which supplies the farm dam near bore TU4 (Plate 3) is unique because it is the only known zone of permanent upwards leakage which is not associated with either the Lanyon or Big Monk pedoderms. It is caused by vertical upwards transmission of groundwater from the fractured rock through the overlying Murrumbidgee and Tuggeranong pedoderms.

Soaks on the lowest basin surface in the north west are caused by impedance to lateral discharge of permeable bodies in the subsolum of the Big Monk pedoderm. The swamp immediately to the west of the Tharwa Road in the southwest is generated by the wedging-out of Lanyon gravels against the less permeable Big Monk pedoderm; surface discharge and subsurface piping from the outwash area of the southern stream is a major contribution to recharge to the gravels.

The large swamp which dominates the south basin (Plate 4) is generated by upwards leakage from the Lanyon gravels. The most important permanent discharge points are in the neighbourhoods of piezometers 117 and 26. In bore 26, free water was intersected during drilling in the subsolum (floodplain sediments) of the Lanyon pedoderm at 1.8 m. The Lanyon gravels were intersected at 1.9 m, whereupon groundwater immediately flowed up the annulus to the surface; water has been flowing over the top of the bore casing ever since. Recharge to the Lanyon gravels in this area is dominantly by subsurface piping of bed underflow water from the central east-west stream. The Lanyon gravels intersected by piezometer 26 are hydraulically connected to the bed-load deposits of this stream.

In the case of piezometer 117, the most significant recharge to the Lanyon gravels occurs by upwards leakage from the fractured rock.

Hydraulic continuity of the aquifers and hydrogeological populations

In order to establish the degree of hydraulic connection between the surficial aquifers and the underlying fractured rock, linear regression was done on each bore, the measured static level in the fractured-rock bore was used as the independent variable, and the simultaneous level in the piezometer set in the surficial aquifer was used as the dependent variable. Correlation coefficients were calculated, resulting in polymodal distributions of coefficients in both basins, with each mode apparently inferring a unique

hydrogeological population.

Each population is defined by its piezometer response in the surficial cover to variations in recharge and discharge compared with the response in the fractured rock. Consistent high linear correlation in a population is assumed to indicate that hydraulic continuity with negligible time lags exists between the surficial aquifers and the fractured rock. A population with low linear correlation does not necessarily imply independence between the two aquifer systems, but more probably indicates that the relation is non-linear, or autocorrelated, especially in areas with a thick surficial cover.

Correlation coefficients for the south basin are shown in Table 8 and for the north basin in Table 9.

Table 8. Correlation coefficients, south basin

X = TU5 for i = 1, 2,23

X = LI for i = 24,28

piezometer (Y)	i	sample correlation coefficient (r_i)	no. of simultaneous observations (n_i)	regression coefficient (b_i)	hydro- geological population
(X = TU5)					
23	1	0.7920	121	0.6350	S1
31	2	0.8802	95	1.8207	
35	3	0.8433	90	1.7244	
111	4	0.8024	69	0.9486	
113	5	0.7902	64	1.5740	
115	6	0.8314	25	1.3655	
116	7	0.7820	69	0.9120	
118	8	0.8619	72	0.8478	
119	9	0.7856	68	1.8648	
120	10	0.8072	61	2.1744	
127	11	0.8755	71	1.1442	
128	12	0.8683	69	0.9975	
24	13	0.6861	127	0.6366	S2
26C	14	0.7212	136	0.5007	
28	15	0.7472	96	1.0518	
29	16	0.6070	95	0.8072	
30	17	0.6635	82	1.1608	

Table 8 (cont.)

112	18	0.6744	64	0.5108	S2
114	19	0.6592	56	2.2107	
117	20	0.5803	43	1.0874	
126	21	0.7420	72	0.8889	
25	22	0.3127	99	1.1208	S3
L1	23	0.0632	88	0.1733	
<hr/>					
(X = L1)					
25	24	0.4018	56	1.2759	S3
29	25	0.8374	89	1.1334	S4
28	26	0.6922	90	0.9950	
113	27	0.6782	69	1.6605	
35	28	0.5316	90	1.0981	

Period of observations:

i = 1, 2, 3, 13, 14, 15, 16, 17, 22, 23, 24, 25, 26, 28 between 3/9/74 and 6/12/76
i = 4, 5, 6, 7, 8, 9, 10, 12, 18, 19, 20, 21, 27 between 14/3/75 and 6/12/76

Sampling theory of correlation is discussed by Graybill (1961) and Haan (1977). Certain inferences may be made about the population correlation coefficients assuming that the random variables (X, Y) are drawn from a bivariate normal distribution.

The test statistic $Z = \text{arctanh } r$ is Fisher's Z transformation and is approximately normally distributed with

$$\left. \begin{array}{l} \text{mean } \mu_Z = \text{arctanh } \rho \\ \text{and variance } \sigma_Z^2 = 1/(n-3) \end{array} \right\} \text{ for } n \geq 25$$

where r = sample correlation coefficient

ρ = population correlation coefficient estimated by r

n = number of simultaneous readings of X and Y.

For k bivariate normal populations with population coefficients $\rho_1, \rho_2, \dots, \rho_k$ and sample correlation coefficients r_1, r_2, \dots, r_k calculated from samples of size n_1, n_2, \dots, n_k , then the null hypothesis, $H_0 : \rho_1 = \rho_2 = \dots = \rho_k$ is tested with the quantity

$$X^2 = \sum_{i=1}^k (n_i - 3) (Z_i - \bar{Z})^2$$

which has a chi-square distribution with $k - 1$ degrees of freedom,

where $Z_i = \text{arctanh } r_i$

$$\text{and } \bar{Z} = \frac{\sum_{i=1}^k (n_i - 3) Z_i}{\sum_{i=1}^k (n_i - 3)}$$

(Graybill, 1961, theorem 10.19).

H_0 is rejected at a level of significance α , if $X^2 \geq \chi^2_{1-\alpha, k-1}$ where $\chi^2_{1-\alpha, k-1}$ is the critical chi-square value for $k - 1$ degrees of freedom and probability $1 - \alpha$.

If H_0 is accepted, then the pooled estimate \bar{r} of the common population coefficient ρ , is given by

$$\bar{r} = \tanh (\bar{Z} - m \rho^*/2)$$

$$\text{where } \rho^* = \frac{1}{k} \sum_{i=1}^k r_i$$

$$\text{and } m = \sum_{i=1}^k \left[(n_i - 3)/(n_i - 1) \right] / \sum_{i=1}^k (n_i - 3)$$

(Graybill, 1961, theorem 10.20).

In the south basin the above theory is used to verify inferred uniqueness of hydrogeological populations by testing the following hypotheses:

- (i) $H_0 : \rho_1 = \rho_2 = \dots = \rho_{12} = \rho_{13} = \dots = \rho_{21}$. (all correlation coefficients in populations S1 and S2 are equal)
against H_1 : at least one equality does not hold.

Since observed $X^2 = 66.80$
and critical $\chi^2_{20} = 31.41$,
then H_0 is rejected at the 5% level of significance.

- (ii) $H_0 : \rho_1 = \rho_2 = \dots = \rho_{12}$ (all correlation coefficients in population S1 are equal).

Since observed $X^2 = 12.82$
and critical $\chi^2_{11} = 19.68$,
then H_0 is accepted for $\alpha = 0.05$.
Furthermore, $\bar{r}_{S1} = 0.829$.

- (iii) $H_0 : \rho_{13} = \rho_{14} = \dots = \rho_{21}$ (all correlation coefficients in population S2 are equal).

Since observed $X^2 = 6.28$
and critical $\chi^2_8 = 15.51$,

then H_0 is accepted for $\alpha = 0.05$,

and $\bar{r}_{S2} = 0.685$.

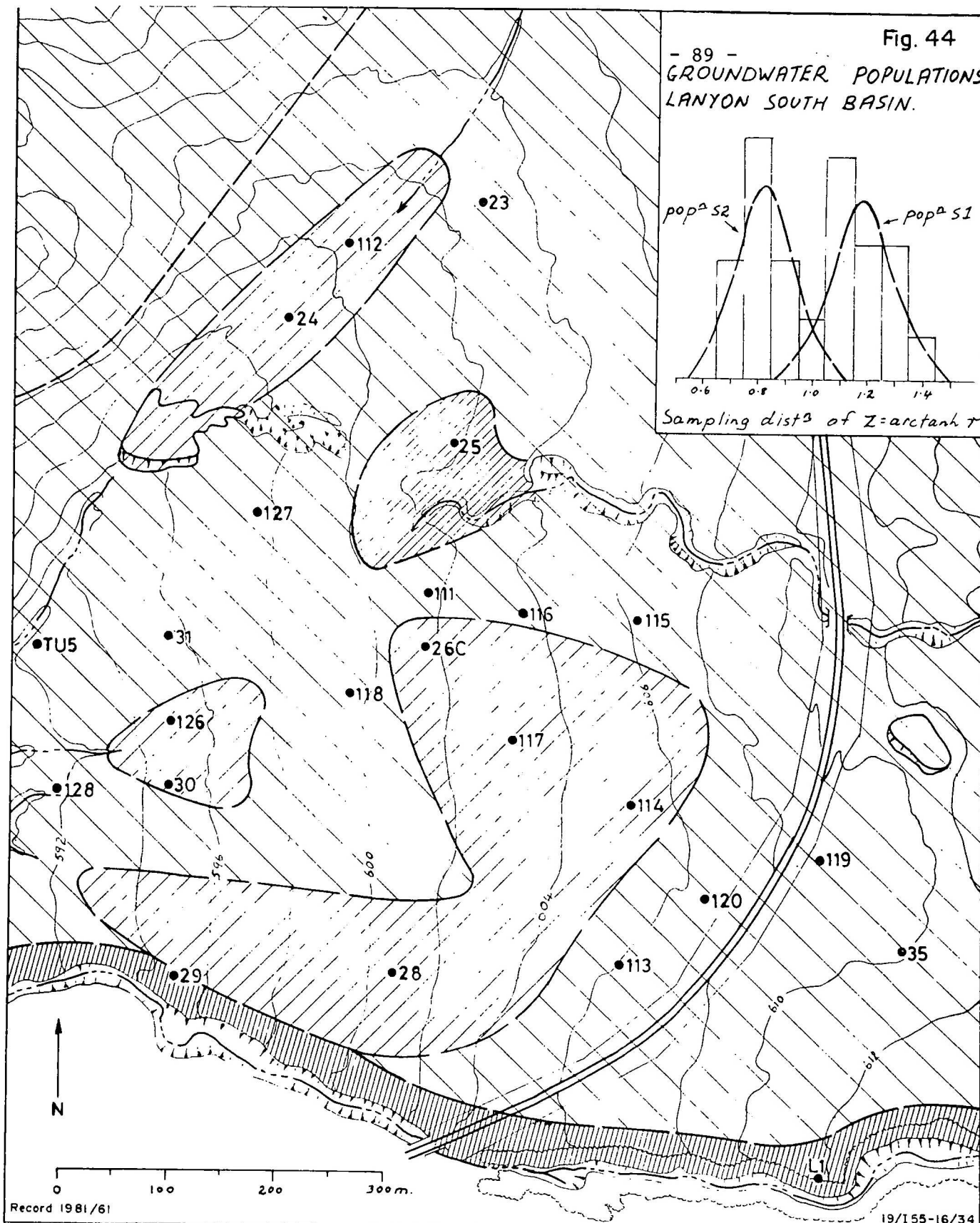
The areal distribution of hydrogeological populations confirmed by the hypotheses testing of correlation coefficients is shown in Figure 44. A close linear relationship exists between water-level fluctuations in fractured-rock bore TU5 in the groundwater discharge zone of the south basin and the piezometers $i = 1, 2, \dots, 12$ in the surficial cover of population S1 ($\bar{r}_{S1} = 0.829$). The stochastic dependence is taken to indicate that hydraulic continuity exists between the two aquifer systems and supports the leaky aquifer theory. Surficial piezometers of population S1 intersect sands and shoestring gravels of the Lanyon pedoderm on truncated Tuggeranong and Murrumbidgee fanglomerates. The underlying rock is moderately to highly weathered with enough open joints to ensure significant leakage.

Water-level fluctuations in the surficial piezometers of population S2 show a weaker linear relationship ($\bar{r}_{S2} = 0.685$) with TU5. Piezometers 26C and 117 are set in the most extensive deposits of Lanyon gravels and occur in permanently saturated zones of the south basin. The other piezometers in population S2 intersect the same sequence in the surficial cover as those of population S1 but the pedoderms in population S2 are underlain by extremely weathered rock with clay-filled joints which is considered to be an aquitard between the two aquifers. Piezometers 24 and 112 of population S2 are additionally influenced by the large dam near the western boundary (Fig. 44); this impedes groundwater throughflow, and in this respect behaves similarly to the underlying aquitard of extremely weathered rock.

Bore L1 is in fractured rock in the recharge zone of the south basin but it also receives substantial intermittent recharge from bed underflow of the adjacent stream (Fig. 44). As expected, there is no linear relationship between rock bore TU5 in the discharge zone of the south basin with bore L1 in the recharge zone ($r = 0.06$).

Population S3 (piezometer 25) has a very weak linear relation with the fractured rock bores L1 and TU5. This is not surprising since population S3 comprises the pronounced zone of surface recharge of the south basin where the central westerly-flowing stream loses definition.

Fig. 44
- 89 -
GROUNDWATER POPULATIONS
LANYON SOUTH BASIN.



Population	Linear Correlation Coefficient (X = Fractured-rock bore)		Hydraulic Continuity Between Surficial Aquifers and Fractured Rock
S1	High	$\bar{r}_{s1} = 0.829$ (X=TU5)	Continuous, with negligible time lag to piezometer response.
S2	Moderate	$\bar{r}_{s2} = 0.685$ (X=TU5)	Impeded by underlying aquitard of extremely weathered rock.
S3	Low	$\bar{r}_{s3} = 0.313$ (X=TU5)	Unknown. Piezometer response dominated by surface recharge.
S4	High	$\bar{r}_{s4} = 0.837$ (X=LI)	Continuous within the radius of influence of the southern creek only.

Population S4 reflects the dominant influence on groundwater drainage in the southern part of the basin by the deeply incised creek adjacent to bore L1. The independent variable for regression analysis is the static water-level in rock bore L1 which shows a close linear correlation with simultaneous levels in piezometer 29 ($r = 0.84$), and a partial correlation with piezometers 28, 113 and 35, decreasing in proportion to distance from the stream bed. Correlation coefficients with L1 as the independent variable are low for all the other surficial piezometers of the south basin. The mean linear coefficient for population S1 is $\bar{r} = 0.29$ and in population S2 the value is $\bar{r} = 0.44$.

Table 9. Correlation coefficients, north basin

X = TU4 for j = 1, 2, 29

piezometer (Y)	j	sample correlation coefficient (r_j)	no. of simultaneous observations (n_j)	regression coefficient (b_j)	hydro- geological population
2	1	0.4987	35	0.6986	N1
5	2	0.6294	72	0.7565	
7	3	0.5611	75	0.3127	
8	4	0.6664	74	0.3896	
9	5	0.6133	70	0.3848	
13	6	0.5668	71	0.3685	
19	7	0.5649	71	0.0785	
100	8	0.6358	55	0.6647	
101	9	0.7248	27	0.9924	
106	10	0.5500	58	0.2190	
121	11	0.5311	29	0.1789	
124	12	0.7393	65	0.3623	
125	13	0.4801	65	0.2022	
3	14	0.2815	19	0.3487	N2
10	15	0.3584	47	0.2079	
11	16	0.2710	38	0.1495	
12	17	0.2332	38	0.1283	
14	18	0.3396	75	0.0397	
20	19	0.3203	45	0.4195	
21	20	0.3524	52	0.2664	
105	21	0.2565	66	0.2004	
107	22	0.2669	61	0.0545	
122	23	0.1215	63	0.0659	
123	24	0.3476	36	0.2263	N3
102	25	-0.2752	66	-0.1167	
103	26	-0.2090	66	-0.0604	
109	27	0.0642	35	0.0151	
129	28	-0.0738	31	-0.0763	
Bore L2	29	0.4659	23	0.5004	

Period of observations:

- j = 1, 2, 3, 4, 5, 6, 7, 14, 15, 16, 17, 18, 19, 20 between 3/9/74 and 6/12/76
j = 8, 9, 10, 11, 12, 13, 21, 22, 23, 24, 25, 26, 27, 28 between 14/3/75 and 6/12/76
j = 29, between 4/3/76 and 6/12/76.

Bore TU4 is set in fractured rock in the recharge zone of the north basin and L2 is in the discharge zone (Fig. 45). Therefore it is to be expected that only partial linear correlation exists between groundwater fluctuations in TU4 and those in the surficial piezometers, most of which are in the discharge zone of the basin. It was not possible to use readings in L2 as the independent variable in linear regression because of the insufficient number of observations after the bore was recommissioned in March 1976; thereafter, groundwater levels in many of the surficial aquifers fell below the level of the piezometers during the dry autumn and winter of 1976. In any case, it is more prudent to observe water-level fluctuations over at least 2 major wet and dry periods, as was done in the south basin, before statistical inferences can be made about population parameters.

Even though TU4 is in the recharge zone of the basin, a trimodal distribution of correlation coefficients is affected when water-level fluctuations in the surficial piezometers of the discharge zone are used as the dependent variables.

Existence and uniqueness of hydrogeological populations in the north basin is confirmed by the following hypothesis testing:

$$(iv) \quad H_0: \rho_1 = \rho_2 \dots = \rho_{13} = \rho_{14} = \dots = \rho_{24}$$

(all correlation coefficients in populations N1 and N2 are equal
note that the test does not include population N3 because of the obvious negative bias)

H1: at least one equality does not hold.

Since observed $X^2 = 62.31$
and critical $\chi^2_{23} = 35.16$,
then H_0 is rejected at the 5% significance level.

(v) Ho: $\rho_1 = \rho_2 = \dots = \rho_{13}$ (all correlation coefficients in population N1 are equal).

Since observed $X^2 = 9.34$

and critical $\chi^2_{12} = 21.03$,

then Ho is accepted for $\alpha = 0.05$,

and $\bar{r}_{N1} = 0.600$

(vi) Ho: $\rho_{14} = \rho_{15} = \dots = \rho_{24}$ (all correlation coefficients in population N2 are equal).

Since observed $X^2 = 3.01$

and critical $\chi^2_{10} = 18.31$,

then Ho is accepted for $\alpha = 0.05$,

and $\bar{r}_{N2} = 0.282$

(vii) Ho: $\rho_{25} = \rho_{26} = \rho_{27} = \rho_{28}$ (population N3)

Since observed $X^2 = 2.92$

and critical $\chi^2_3 = 7.81$

then Ho is accepted for $\alpha = 0.05$,

and $\bar{r}_{N3} = -0.1656$.

The distribution of populations N1, N2, and N3 is shown in Figure 45. Population N1 occupies much of the poorly drained areas of the north basin. Piezometer 121 is set in the Rob Roy pedoderm, numbers 2 and 13 are set in sands with sparse basal gravels of the Lanyon pedoderm, and all the other piezometers are set in fanglomerates. The underlying rock is moderately weathered.

In population N2, piezometers 123, 3, 10, 11, 12 and 14 are set in the Lanyon gravels. The most extensive deposits of Lanyon gravels occur in the vicinity of piezometers 123 and 12, and these are semi-permanent zones of upwards groundwater flow. All other piezometers of population N2 are set in thick fanglomerate sequences in well-drained areas of the basin. The underlying rock is highly to moderately weathered.

Population N2 appears to delineate zones of higher transmissivity than N1 in the discharge zone of the north basin, but the linear analysis using the fractured-rock bore in the recharge zone as the independent variable is not sensitive enough to distinguish the very different lithologies within populations. When sufficient data become available it is likely that the

permanently wet areas of population N2 would be differentiated from the well-drained areas of that population by regression analysis with L2, the fractured-rock bore in the discharge zone.

The small negative correlation coefficients in population N3 arise from significant time lag of piezometer response to perturbations to the system, particularly during initial periods of sustained rises in groundwater levels in TU4, where receding or stationary levels in the piezometers may persist for up to a month. In major dry periods the fall in groundwater-levels in the surficial aquifers of population N3 is roughly proportional to groundwater recession rates in the fractured rock. It appears that population N3 delineates areas of delayed hydraulic correction between the surficial aquifers and the fractured rock.

Infiltration

Infiltration tests were run at two sites in the north basin (Plate 3) and at one site in the south basin (Plate 4) during June 1976, when initial soil moisture contents were very low following 4 months of below-average rainfall. The test sites were chosen on the basis of drill-log information and surficial mapping, which indicated that these areas contain representative sequences of the most areally extensive pedoderms covering the basins through which rainfall is infiltrated before recharging the surficial aquifers. Units tested were the hydromorphic grey earth of the Gigerline pedoderm, the Lanyon clay, and the topsoil/vegetation cover.

Undisturbed soil samples were obtained by excavating a pit down to the top of the required horizon and then levelling the exposed soil surface with a sharp blade; care was taken to minimise closure of macropores by smearing. A steel cylinder of height 15 cm and diameter 30 cm was driven into the soil until the upper edge of the ring was horizontal and about 1.5 cm above the sample surface. The ring containing the soil sample was excavated by extending the depth of the pit to about 20 cm below the cutting edge of the cylinder and then fracturing the protruding soil column below the base of the ring by impact with a steel bar and then leverage. The ring and sample were placed on a porous stand after the base of the soil specimen was carefully trimmed; disturbance to the fabric was kept to a minimum.

One-dimensional infiltration capacities were determined by measuring the rate at which water flowed out of a permeameter secured to the top

of the ring in order to maintain a constant head of about 1.5 cm. These tests were run for several soil antecedent moisture contents and were continued until an approximate steady-state infiltration rate was attained. Duplicate in-situ tests were run at site 2 (Plate 3) where the cylinder of soil was left in the ground throughout infiltration testing. Results of the one-dimensional tests are shown in Figures 46 to 49, and are summarised in Table 10.

Table 10. One-dimensional infiltration capacities of Lanyon soils

Soil	Site (see Plates 3 & 4)	Determinations based on:	Infiltration rate (mm/hr)			Ante- cedent moisture content (%)
			after 1 hour	after 3 hours	after 5 hours	
Clover and phalaris grass on prairie soil	2	mean of 4 samples	375	266	233	4
	2	mean of 3 samples	244	179	154	13
	2	mean of 2 samples	68	56	54	18
	2	single test	17	16	15	20
Native grasses and clover on prairie soil	1	mean of 4 samples	274	197	168	6
	1	mean of 3 samples	89	61	56	13
	1	mean of 2 samples	62	46	44	16
	1	single test	16	16	15	21
Grey earth	1,2,3	mean of 9 samples	25	23	23	9
	1,2,3	mean of 6 samples	18	17	17	19
	1,2,3	mean of 3 samples	13	12	12	22
Upper B horizon of solodic soil	2	mean of 5 samples	61	17	7.2	17
	2	mean of 4 samples	32	5.7	4.6	22
	2	mean of 3 samples	5.5	3.4	2.9	25
	2	mean of 2 samples	0.8	0.6	0.5	29
	2	single test	0.05	0.04	0.04	38
	1	mean of 2 samples	1.4	1.4	1.4	53
	1	single test	0.9	0.8	0.8	57
	3	mean of 4 samples	124	25	16	16
	3	mean of 3 samples	33	9.2	6.8	24
	3	mean of 2 samples	11	5.2	3.8	26
	3	single test	1.2	1.1	1.1	27
Lower B horizon of solodic soil	2	mean of 5 samples	12	3.2	2.9	14
	2	mean of 4 samples	3.5	1.6	0.8	17
	2	mean of 3 samples	1.1	0.6	0.2	21
	2	mean of 2 samples	0.03	0.03	0.03	27
	2	single test	0.03	0.03	0.03	35

The topsoil (Fig. 46) over the basins is well-conditioned as a

Fig. 46 INFILTRATION CAPACITIES
CLOVER AND PHALARIS GRASS
ON PRAIRIE SOIL OF THE RIVERSIDE PEDODERM

Constant head above soil surface 5.5 cm
(grass trimmed to 5 cm)

Final infiltration rates

after 5 hours (mm/hr.)

(i1) 233

(i2) 154

(i3) 55

(i4) 15

Ksat (m/day)

4.74

3.13

1.12

0.31

AMC 0.04

AMC 0.13

AMC = antecedent moisture content

AMC 0.18

AMC 0.20

Time in hours

Infiltration Capacity (i) in mm/hour

Cumulative Infiltration (I) in mm

- 96 -

$i_0 = 1560 \text{ mm/hr}$

i1

i2

i3

i1

i2

i4

i3

i4

Fig. 47 INFILTRATION CAPACITIES
GIGERLINE PEDODERM (GREY EARTH)

Constant head 1.5 cm

Final infiltration rates after 5 hours (mm/hr.)		Ksat (m/day)
(i1)	22.5	0.43
(i2)	17.3	0.33
(i3)	12.4	0.25

AMC = antecedent moisture content

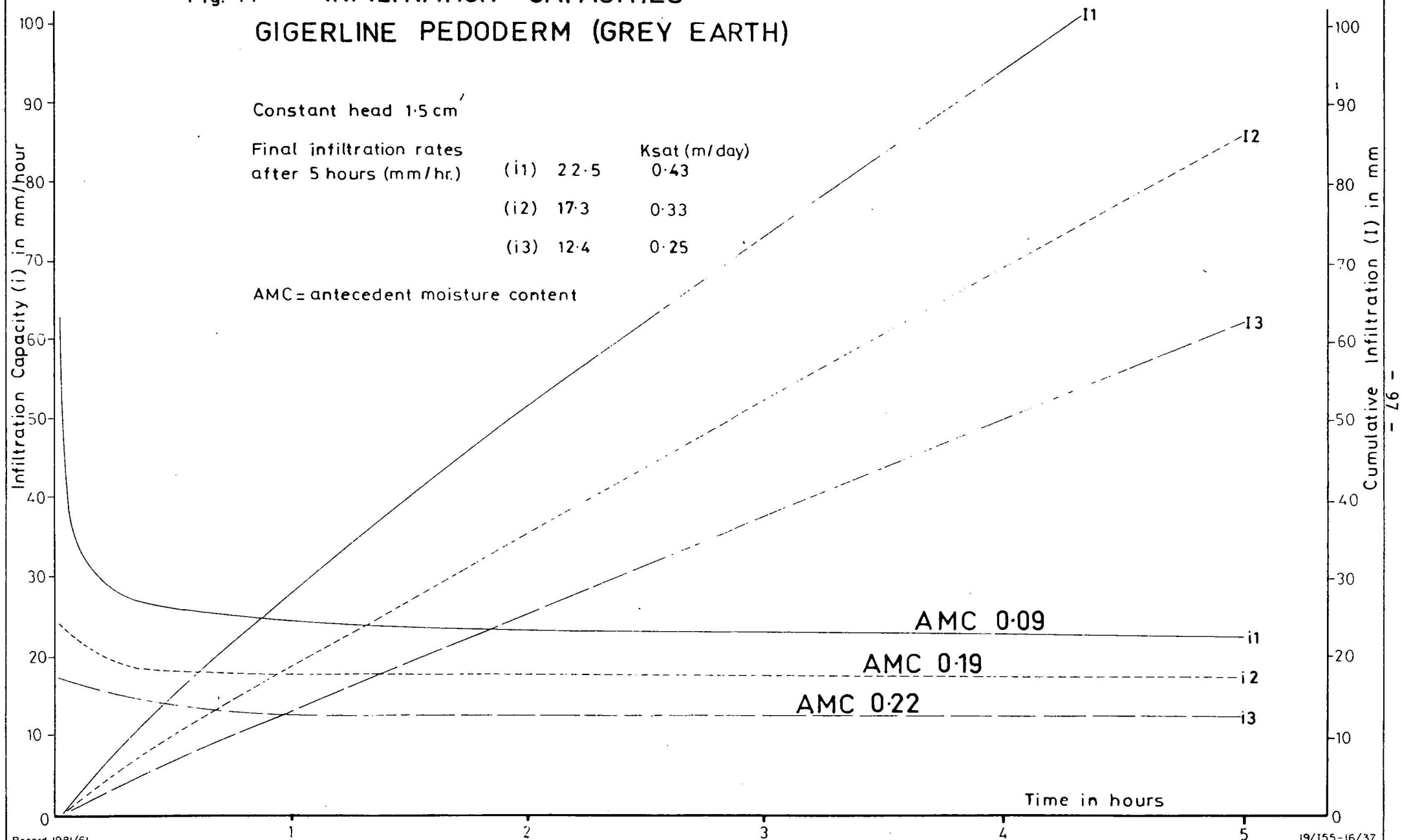


Fig. 48 INFILTRATION CAPACITIES
LANYON CLAY-UPPER B HORIZON

Constant head 1.5 cm

Final infiltration rates
after 5 hours (mm/hr.)

(i1) 7.3
(i2) 4.6
(i3) 2.9

Ksat(m/day)

0.14
0.09
0.06

AMC = antecedent moisture content

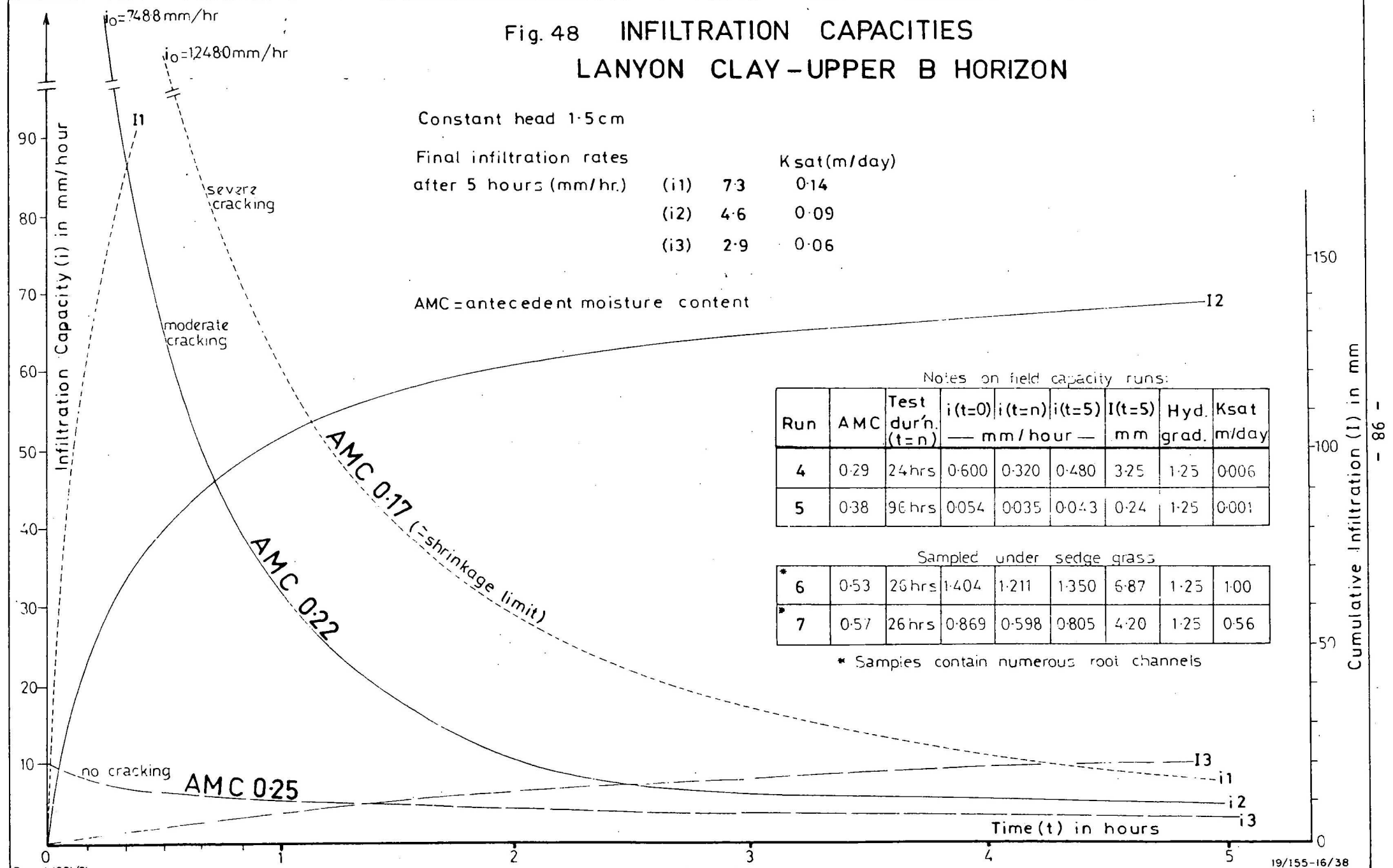
Notes on field capacity runs:

Run	AMC	Test dur'n. (t=n)	i(t=0) — mm/hour —	i(t=n)	i(t=5)	I(t=5) mm	Hyd. grad.	Ksat m/day
4	0.29	24 hrs	0.600	0.320	0.480	3.25	1.25	0.006
5	0.38	96 hrs	0.054	0.035	0.043	0.24	1.25	0.001

Sampled under sedge grass

* 6	0.53	26 hrs	1.404	1.211	1.350	6.87	1.25	1.00
* 7	0.57	26 hrs	0.869	0.598	0.805	4.20	1.25	0.56

* Samples contain numerous root channels



Cumulative Infiltration (I) in mm

Fig. 49 INFILTRATION CAPACITIES
LANYON CLAY—LOWER B HORIZON

Constant head 1.5 cm

Final infiltration rates
after 5 hours (mm/hr.)

(i1) 2.9

Ksat (m/day)

0.056

(i2) 0.8

0.015

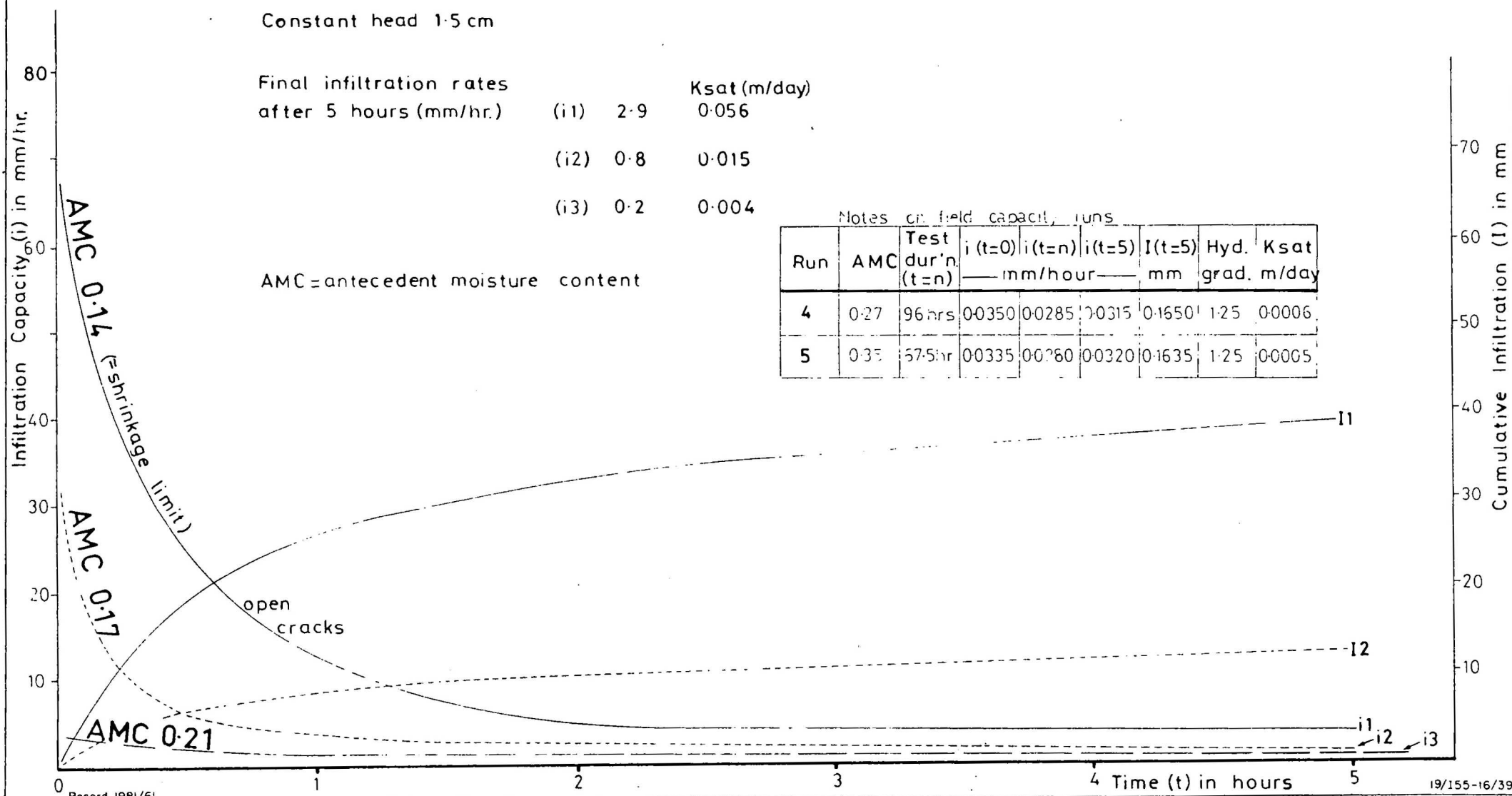
(i3) 0.2

0.004

AMC = antecedent moisture content

Notes on field capacity runs

Run	AMC	Test dur'n (t=n)	i(t=0) mm/hour	i(t=n)	i(t=5)	I(t=5) mm	Hyd. grad. m/day	Ksat
4	0.27	96 hrs	0.0350	0.0285	0.0315	0.1650	1.25	0.0006
5	0.35	57.5 hr	0.0335	0.0260	0.0320	0.1635	1.25	0.0005



consequence of crop rotation, regular applications of superphosphate, and avoidance of overgrazing which has been the long-established soil management practice at Lanyon station. Therefore the topsoil over the Lanyon basins probably has a higher biogenic porosity and a correspondingly higher infiltration capacity than other areas with the same soil type in the Tuggeranong valley.

Infiltration tests on the Gigerline grey earth gave the most consistent results of the units tested; for the three test sites, the curves shown in Figure 47 represent the mean values, which were all within 20% of each other.

Infiltration capacities of the upper B horizon of the Lanyon clay were highly variable for low antecedent moistures, and admittance rates depended considerably on the geometry and continuity of cracks. Results (Fig. 48) are reported only from site 2 because it was considered that the degree of cracking and pedality at this site was the most representative of the unit over both basins.

Infiltration into the cracked upper B horizon of the Lanyon clay is dominated by gravity flow down open cracks and along ped faces for the first hour or so. The ped and plane cutans eventually take up water and swell, but do not close entirely because of entrapped fibrous material and interped propping, which provides partly open tortuous drainage paths for continued reduced admittance. Infiltration into the peds in the form of a subcutanic moist halo, of 2 to 3 mm width, was not observed until the end of the fifth run, which represented a cumulative intermittent soaking time of around 200 hours. It appears that a soaking period of 2 to 3 weeks is required for moisture to become distributed throughout the peds.

Samples at field capacity were obtained from the swampy area adjacent to site 2, but infiltration rates are not directly compatible with earlier results because of the unusually large number of root channels in the swamp samples under sedge grass.

There was no noticeable slaking of peds in the Lanyon clay throughout the tests.

Steady infiltration capacities of the lower B horizon of the Lanyon clay (Fig. 49) are an order of magnitude lower than in the upper B horizon despite the much lower mean grainsize of the latter. The most important factor for admittance through the Lanyon clay is the degree of structural organisation which is optimised in the upper B horizon.

It should be emphasised that infiltration rates determined from ponded tests represent the maximum capacity at which soils can admit water (Dunin, 1976), and the method is generally considered to give a poor field simulation of rainfall infiltration. Ponding in the field during and after rainfall occurs only in the swampy areas of the basins where surface detention in depressions between clumps of sedge grass has been observed to persist for several months through wet winters and springs.

The in-situ tests are not reported in Table 10 because of some misleading anomalous results due to extraneous factors which could not be controlled in the experiments. Final infiltration rates after 5 to 6 hours were about the same as those obtained in the samples removed from the ground at site 2, but the in-situ tests generally showed an initially higher infiltration capacity in response to a lateral potential gradient in dry soil adjacent to the test cylinder. The infiltration rate of most of the in-situ specimens declined at a steeper rate for up to 1 to 3 hours from the start of wetting, and was followed by a temporary increase as impeding effects of subsoil boundaries and delayed expulsion of entrapped compressed air were overcome. Other problems experienced in the in-situ tests were oscillations about the mean recession curve owing to changes in air temperature and pressure throughout the duration of the tests; these variations were not experienced in the one-dimensional tests and in the effective porosity determinations because most samples removed from the ground were tested in the controlled environment of the laboratory.

Effective porosities

Undisturbed soil samples were obtained using the same procedures and equipment described for infiltration testing, except that steel cylinders 30 cm high were used.

The samples in the rings were moistened. A 12.5-mm-diameter hole was bored along the central vertical axis of the cylinder, and a piezometer of perforated PVC conduit was inserted in the hole. The samples were wetted until it was estimated that they were at about field capacity, and the base was sealed. Wetting cycles were continued, and water was pipetted out of the piezometer until it was considered that there had been sufficient seepage to eliminate puddling on the soil surface adjacent to the piezometer.

The initial water-level was recorded after the cylinder had been allowed

to drain overnight and a known volume of water was applied to the soil surface the following morning. The final piezometer level was measured after equilibrium had been attained, and the effective porosity was approximated as the ratio of the height of water added to the soil to the change in height of the column of water in the piezometer. Results are shown in Table 11.

Table 11. Effective porosities of Lanyon soils

Soil type	Site (see Plate 3)	Determinations based on:	Effective porosity (%) at field capacity for rising water-table
Prairie soil	2	mean of 3 samples	8
Grey earth	1	mean of 3 samples	4
Solodic soil (Upper B horizon)	2	*single test	3
Solodic soil (Lower B horizon)	2	mean of 2 samples	1
Subsolum	2	single test	4

* Only one measurement taken from 3 samples because one of the borings belled out and one boring created excessive structural disturbance to the soil.

The values of effective porosities (Table 11) are used subsequently in this report to estimate soil storages, but it should be emphasised that the effective porosity of a soil is not constant; in fact the parameter increases roughly in proportion to depth to the water-table, and approaches a maximum constant value when the capillary zone falls below the level of the soil and, for clay soils, when soil moisture decreases towards the shrinkage limit. Therefore the results in Table 11 represent the minimum effective porosities of the soils, since the samples were tested close to field capacity for a rising water-table. The value for the upper B horizon of the Lanyon clay in particular is likely to be substantially in error when the soil is cracked after a prolonged dry spell.

Ideally, effective porosities should be determined in the field by observing piezometer response to a measured rainfall slug when all other terms of the water balance are known. This was not possible at Lanyon because of the difficulties associated with isolating individual soil units for observation and the fact that subsoil outflows from the system were unknown.

Recharge to the surficial aquifers from rainfall infiltration

Piezometer response to rainfall events indicates that the simplest model describing leakage of infiltrated water from the soil store to recharge the underlying surficial aquifers is an exhaustion process in which the rate of leakage, $\frac{dQ}{dt}$, is proportional to the head of water $h(t)$ in the store at time t :

$$\frac{dQ}{dt} = -\lambda h(t) = -\lambda Q(t) \text{ for a unit cross-sectional area.} \quad (1)$$

The solution to (1) with initial condition $Q(0) = Q_0$ is

$$Q(t) = Q_0 \cdot \exp(-\lambda t)$$

which represents the quantity of water left in a unit cross-sectional area of the soil store at time, t , after the start of leakage. Therefore the amount of water left in the store on the n th day after rainfall is $Q_0 \cdot \exp(-n\lambda)$ and the amount which recharges the aquifer on the n th day is

$$R(t = n) = Q_0 \cdot (\exp(-(n-1)\lambda) - \exp(-n\lambda)).$$

The decay constant λ was determined empirically from observed response of porous pot piezometers in the north and south basins to have a mean value of $\lambda = 0.1$ for all t .

The simplified model for calculating recharge from rainfall (Fig. 50) assumes that the stratified sequence of soil layers is continuous over the lower basin surfaces, and that each layer possesses a constant effective porosity and infiltration rate. The latter simplification was introduced after failure to derive a consistent relationship between antecedent moisture content (AMC) and antecedent precipitation index (API) over the period 1974-76. The constant infiltration rate arbitrarily assigned to each layer is the steady infiltration rate measured on the third run for each layer in the tests described earlier.

The model states that for a rainfall slug (discretised into hourly time units) of intensity I and duration t which infiltrates the stratified slab with layers of infiltration capacities i_j , effective porosities u_j , and thicknesses d_j :

- (i) if $I \leq \text{all } i_j$, then all rainfall is admitted through the slab to recharge the groundwater reservoir.
- (ii) if $I > \text{any } i_j$, then a proportion $i_j t$ of rainfall is admitted through layer j and the excess $I - i_j t$ initially occupies infilled drainable pore space in the overlying layer in which interflow (or surface runoff) commences

STRATIFIED SLAB MODEL FOR RECHARGE FROM INFILTRATION

Fig. 50

RAINFALL 3.7 mm/hour for 24 hours
(Recurrence Interval 5 years)

RAINFALL 2.2 mm/hour for 24 hours
(Recurrence Interval 1 year)

← surface runoff after 18 hrs. →

no surface runoff

interflow
← after 14.6 hrs

$t_1 = 4.4$ hrs

RIVERSIDE PRAIRIE SOIL
($i_1 = 15$ mm/hr., $\mu_1 = 0.08$)

20 cm

GIGERLINE GREY EARTH

($i_2 = 12.4$ mm/hr.)

($\mu_2 = 0.04$)

60 cm

LANYON CLAY "UPPER B"

($i_3 = 2.9$ mm/hr., $\mu_3 = 0.03$)

90 cm

LANYON CLAY "LOWER B"

($i_4 = 0.3$ mm/hr.)

($\mu_4 = 0.01$)

140 cm

SUBSOLUM ($\mu_5 = 0.04$)

LANYON GRAVELS
(μ_6 est. 0.05-0.10)

leakage to
aquifer delayed
until suction → 0

$t_4 = 16.7$ hrs

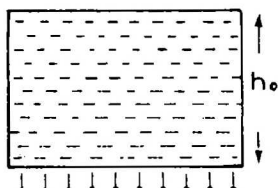
$\Sigma t_i = 28.5$ hrs

leakage to
aquifer delayed
until suction → 0

$t_4 = 16.7$ hrs

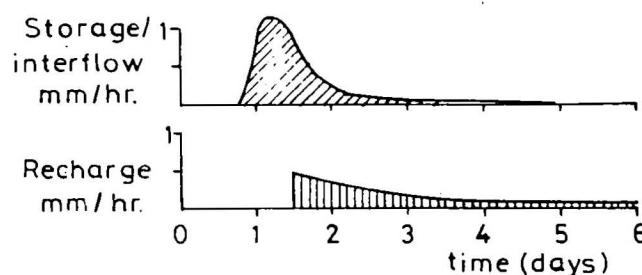
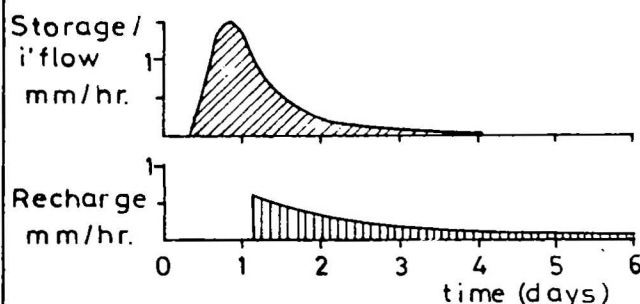
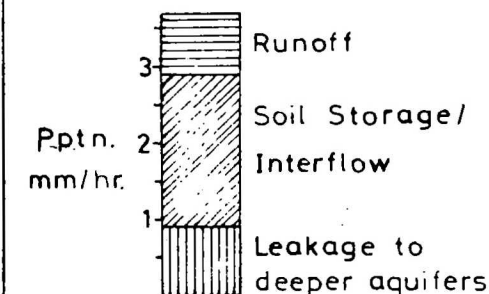
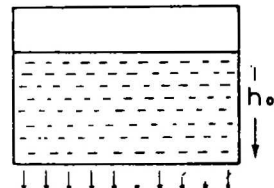
$\Sigma t_i = 35.4$ hrs

Available
store full at
cessation of
infiltration.



RECHARGE TO AQUIFER $R(t=n) = Q_0(\exp(1-n)\lambda - \exp(-n\lambda))$

Available store
70% full at
cessation of
infiltration.



once saturation occurs (cf. Calver, Kirkby & Weyman, 1972).

Wetting-front velocities V_j and travel times t_j through layer j are approximated by $V_j = i_j/\mu_j$ and $t_j = d_j/V_j$; these approximations are considered to be reasonable because of the low effective porosities of each soil layer, but they will be highly inaccurate in the first few hours of infiltration through the upper B horizon of the Lanyon clay when the soil is cracked.

The critical layer for impedance to infiltration through the stratified slab is the lower B horizon of the Lanyon clay, which has the lowest infiltration capacity. If water is being infiltrated at a rate greater than 0.3 mm/hour through the overlying layers, then interflow is induced in the upper B horizon once all drainable pore space in this horizon is filled. The back-up, saturation, and creation of interflow continues through the overlying Gigerline and Riverside pedoderms until the soil store is completely saturated and surface runoff commences. If prolonged rainfall intensity is greater than 2.9 mm/hour, then interflow commences in the Gigerline pedoderm several hours before initiation in the upper B horizon of the Lanyon clay.

Progress of the wetting front through the lower B horizon and upper subsolum of the Lanyon clay to recharge the underlying sand and gravel aquifers is further impeded by up to several hours until the infiltrated water is at sufficiently low tension to permit admittance into the larger voids of the aquifer. The mechanics of delayed entry from fine-grained to coarse-grained strata is discussed by McIntyre & Watson (1975) and illustrated experimentally by Miller & Gardner (1962). The phenomenon was observed in the field when, after excavating the rings following in-situ infiltration tests on the lower B horizon of the Lanyon clay, the underlying sand was found to be irregularly wetted in patches. The wet patches were often, but not always, confined to finer-grained zones; coarse sand and gravel lenses were dry but fine sands around the boundaries of the lenses were wet, indicating that infiltrated water had preferentially flowed around the bodies with larger pore spaces. The same degree of impedance to inflow is apparently not experienced when the wetting front is moving from the Gigerline pedoderm into a cracked upper B horizon of the Lanyon clay possessing a (temporary) higher pore space because of the micropores on the peds and high water affinity of the cutans. Under drought conditions when the clay is severely cracked, the gravitational effect dominates anyway, at least for the first few hours.

Impedance to inflow from coarse-grained layers to fine-grained layers may also occur if downward movement of air into the fine-grained layer is delayed (McIntyre & Watson, 1975). This may and probably does occur as the wetting front moves from the Riverside pedoderm into the Gigerline pedoderm, and to a lesser degree from the upper B horizon of the Lanyon clay into the lower B horizon when antecedent soil moisture contents are high. As noted earlier, impedance to infiltration due to delayed air expulsion was experienced in the in-situ tests.

The above qualifications show that the model (Fig. 50) proposed for infiltration and aquifer recharge from rainfall is indeed highly simplified. The physics of unsaturated flow through stratified soils is exceedingly complex, particularly the interface effects, and is beyond the scope of this study (cf. Talsma, 1974). However, it is known from field observations that the soil cover takes up large amounts of rainfall into temporary storage, and that surface runoff from the typical soil sequence of Figure 50 is generated only from rainfalls of intensity greater than about 3 mm/hour and durations of the order of 24 hours or more. According to the model, interflow far exceeds downwards leakage to groundwater recharge for most rainfall events, which again is verified from field observations. The hypothesis that the soil cover releases stored water to recharge the aquifers at a rate proportional to the amount in the store cannot be argued theoretically, but is based wholly on continuous observations of piezometer response after rainfalls during the spring of 1976.

The model states that recharge to the aquifers will not start to occur until one to two days after the start of rainfall, which is in good agreement with field observations. Exceptions to this are piezometers no. 25 in the south basin and no. 17 in the north basin which show response times of a few hours, but this is attributed to circumventing the surface infiltration process by rapid lateral piping of water through shallow gravel aquifers hydraulically connected to nearby streams.

The smallest recorded discrete rainfall event to produce piezometer response in the model soil sequence was 6.8 mm approximately normally distributed over 4 hours on 27 August 1976. Rainfalls less than 5 to 6 mm are apparently absorbed completely by interception and soil storage, and are never released to recharge the underlying aquifers. Therefore a further constraint on the model is that $I > 5$ mm must be satisfied before groundwater recharge can occur.

Note that interception and evapotranspiration losses are assumed to be negligible for the duration of rainfall and leakage.

Hydraulic conductivities

Eight-hour constant-discharge pumping tests were done on bore 12 (north basin) and bore 26 (south basin). Both bores are set in the Lanyon gravels, and have an array of observation wells in which drawdown in response to pumping can be measured.

Drawdown during the test on bore 12 was recorded in piezometers 10 and 11, and conductivity and storage were calculated in accordance with Theis's curve-fitting method for unsteady-state flow in a confined aquifer. Theoretically, if the aquifer was homogeneous, the cone of depression generated around the pumped well should have continued to spread radially to the adjacent piezometers 7, 8, and 9, but no drawdown was observed in these wells during the test. The reason for this is that bores 7, 8, and 9, are set in the floodplain sediments of the Lanyon pedoderm and are thus not in direct hydraulic continuity with the pumped well.

The drawdown test on bore 26 in the south basin was unsuccessful because of the failure to induce drawdown in the observation well 26C after 8 hours pumping. As in the previous case, these two wells are in poorly connected aquifers where the cone of depression becomes elliptical in time; the major axis of the ellipse is parallel to the trend of the palaeochannel containing the Lanyon gravels before delayed yield is induced from the surrounding floodplain sediments. Drawdown recordings in bore 26B, set in the Lanyon gravels 2 m from the pumped well no. 26, were useless because of a leaking plug in bore 26B.

Thirteen other bores in the north and south basins were pump-tested using Theis's recovery method for unsteady-state flow in confined aquifers (Kruseman & De Ridder, 1970); two others were bailed in accordance with the auger hole method (Van Beers, (1958), for instantaneous recovery in a phreatic aquifer of low to moderate permeability. These methods have the advantage that all measurements are done in the pumped (or bailed) hole and do not require observation piezometers. Duration of pumping for Theis's recovery method was between 2 and 4 hours in each hole.

Results of the aquifer tests are shown in Table 12; the figures were derived after discarding those portions of the recovery curves affected by casing

storage and delayed yield. Apparent increases in transmissivity during the final recovery stages due to delayed yield were most prevalent in the fractured-rock bores TU4 and TU5.

Most of the pump tests in the surficial aquifers were done in the gravels and in the sands of the floodplain sediments of the subsolum of the Lanyon pedoderm. For the sands, measured transmissivities range from $0.2 \text{ m}^2/\text{day}$ ($k = 0.1 \text{ m/day}$) to $2.3 \text{ m}^2/\text{day}$ ($k = 1.9 \text{ m/day}$), giving a mean hydraulic conductivity of 0.5 m/day and variance $0.4 (\text{m/day})^2$. Transmissivities in the Lanyon gravels range from $1 \text{ m}^2/\text{day}$ ($k = 0.9 \text{ m/day}$) to $7.2 \text{ m}^2/\text{day}$ ($k = 3.4 \text{ m/day}$) with a mean hydraulic conductivity of 2.2 m/day and variance $0.7 (\text{m/day})^2$. These surprisingly low conductivities were also indicated by the narrow and steep cones of depression generated during pumping, and are due to the poor sorting of the aquifers, although some are due to pedogenetic pore-filling as well.

Recovery tests in fractured-rock bores TU4 and TU5 gave transmissivities of $6.5 \text{ m}^2/\text{day}$ and $9.8 \text{ m}^2/\text{day}$ respectively, but these results are uncorrected for partial penetration of the aquifer. An estimate for the lumped mean hydraulic conductivity of the fractured rock over the basin catchments may be obtained from empirical tables relating permeability to fracture spacings and apertures (e.g., Hoek & Bray, 1974; Fig. 50). Mean joint apertures could be measured only in drillcore, and even then only in sections where there was 100% recovery, because partings in outcrop open up on exposure to weathering and exfoliation. From the drillcore measurements, the mean joint aperture of open fractures in the Silurian volcanics is $(0.2 \pm 0.1) \text{ mm}$; from the joint analysis described in this report, the mean spacing of extension joints in outcrop in and around the basins is $(0.9 \pm 0.4) \text{ m}$. According to Hoek & Bray (1974) a continuous parallel joint set with these parameters is expected to possess a hydraulic conductivity of $(0.5 \pm 0.3) \text{ m/day}$.

Table 12

Measured transmissivities and hydraulic conductivities of aquifers

Aquifer	Location	Method	T (m^2/day)	K (m/day)
Gravelly sands of Big Monk subsolum	piezometer 35	Theis's recovery	1.3	0.9

Table 12 con't

Aquifer	Location	Method	T (m ² /day)	K (m/day)
Lanyon clay, - 'upper B' horizon	(near piezo. 2 (" " 13 (" " 30	Auger hole method " "	- - -	0.03 0.01 0.01
Lanyon clay-"lower B'	" " 13	"	-	0.002
Stratified sands of floodplain sediments of Lanyon subsolum	(piezometer 13	Theis's recovery	0.2	0.2
	(" 19	Auger hole method	2.3	1.9
	(" 20	Theis's recovery	1.2	1.1
	(" 21	" "	0.3	0.2
	(" 25	" "	0.9	0.7
	(" 26C	" "	0.2	0.1
	(" 27	" "	0.2	0.2
	(" 28	" "	0.2	0.1
Lanyon gravels	(" 31	Auger hole method	0.2	0.2
	(piezos. 10, 11, 12	Theis's curve-fitting	2.2	1.6
	(piezo. 11	Jacob's method	2.5	1.8
	(" 12	Theis's recovery	2.6	1.9
	(" 23	" "	1.4	2.6
	(" 26	" "	6.6	3.1
	(" 26B	" "	7.2	3.4
	(" 27	" "	0.8	2.5
Stratified gravels in loosely cemented sands of Murrumbidgee pedoderm (upper facies)	(" 29	" "	1.0	0.9
	piezometer 23	Theis's recovery	2.9	3.1
Gravel stringers in cemented sands of Murrumbidgee pedoderm (upper facies)	piezometer 28	Theis's recovery	0.7	0.2
Fractured rhyodacite	bore TU4	Theis's recovery	6.5	-
" "	bore TU5	" "	9.8	-

Bore hydrographs and fluctuations in groundwater potentials

Hydrographs for the period September 1974 to December 1976 are shown in Appendix 5. Maps showing contours of the potentiometric surface of the surficial aquifers for various time intervals over the period of bore monitoring are shown in Appendix 6.

Locations of the potentiometric contours in Appendix 6 are considered to be reasonably accurate because of the high density of observation piezometers in each basin. Point controls consist of 30 piezometer readings in the north

basin and 24 in the south basin. When piezometers became dry the groundwater-level below the bottom of the hole was estimated by linear regression using, as the regressor variable, a highly correlating ($r > 0.9$) piezometer in the same hydrogeological population. Semi-quantitative information collected simultaneously with the piezometer recordings-such as estimates of water-levels in certain farm dams, ranking of moisture conditions around seepage zones, and noting the extent of flow in effluent streams-provided upper and lower bounds for fixing the locations of potentiometric surface contours around the perimeters of the basins.

The potentiometric surface contour maps of the north basin show permanent groundwater mounds around the major discharge points near bore TU4, piezometers 12 and 123, and the willow plantation 50 m to the north of piezometer 7. The prominent mound generated around the point of discontinuity of the northern stream 250 m to the northwest of these piezometers indicates the importance of this stream as a recharge source for the surficial aquifers in the northern part of the basin. The southern and southwestern stream channels are permanent line sinks with low radial resistance to drainage from the surficial aquifers, as shown by the low degree of curvature of the depression of the equipotential lines. A groundwater mound sustained by bed underflow is generated in the intervening area between the two streams.

Ephemeral groundwater mounds in the north basin occur around piezometers 2 and 17 during very wet seasonal conditions. The mound around piezometer 17 does not persist for extended periods because of the proximity of the incised channel of the northern stream, which is generally a line sink but in prolonged dry spells it may recharge the surficial aquifers by seepage from bed underflow.

In the south basin, groundwater mounds near piezometers 117, 26, and the terminus of the central stream indicate the locations of the permanent discharge sources of the basin. The depressions in the potentiometric surface contours around the southern stream clearly indicate that it is a constant line sink of moderate radial resistance to drainage from the surficial aquifers. Depressions in the potentiometric surface contours up-gradient from the dam on the western boundary illustrate its role as an important plane sink for groundwaters being transmitted through the surficial material on the northeastern slopes of the basin; down-gradient the dam is a plane source which sustains perennial flow in the downstream section of the western creek.

Variations in the potentiometric surface contours are synthesised into maps showing contours of maximum fluctuations of the potentiometric surface over an eleven-month period in the north basin (Fig. 51) and south basin (Fig. 52). The fluctuation contours were derived by superimposing the two potentiometric surface contour maps for 12 November 1975, the time of maximum storage after the introduction of the porous pot piezometers into the observation bore network in March 1975, and 14 September 1976 the time of minimum groundwater storage in the surficial aquifers over the monitoring period September 1974 to December 1976. Storages were actually at an absolute maximum in September 1974 but at that time there were fewer observation points and therefore less control in drawing contours of the potentiometric surface.

Figure 51 clearly shows the dominant discharge zones of the central northern area of the north basin, where fluctuations in groundwater potentials are small (< 1 m). Fluctuations of the same low order of magnitude around the streams in the western part of the basin explain why these streams were discharging for most of the observation period. The greatest fluctuations occur on the interfluvies in the eastern and western sectors of the basin. These areas coincide with the 'alternating' zone (Fig. 43), and they undergo the largest depletions in storage when the system is stressed during prolonged dry spells - a variation of 5 m in water-table represents an approximate 25% change in storage in the surficial aquifers.

The general trend in the south basin (Fig. 52) is one of maximum water-table fluctuations in the recharge areas on the eastern slopes; potentials are progressively less responsive to changes in recharge from rainfall towards the western part of the basin. Steady-state conditions were attained in the soak around piezometer 26 and within the radius of influence of the westerly stream below the dam.

The area around piezometer 25 experiences the greatest fluctuations in groundwater potentials in the discharge zone of the south basin. This area coincides with groundwater population S3 which shows rapid piezometer response to surface outwash and overland flow from the terminus of the central stream. In fact, the fluctuation map completely defines groundwater flow directions in this rather interesting little segment of the basin. Head variations around the eastern section of the central stream are kept relatively low (≤ 0.5 m)

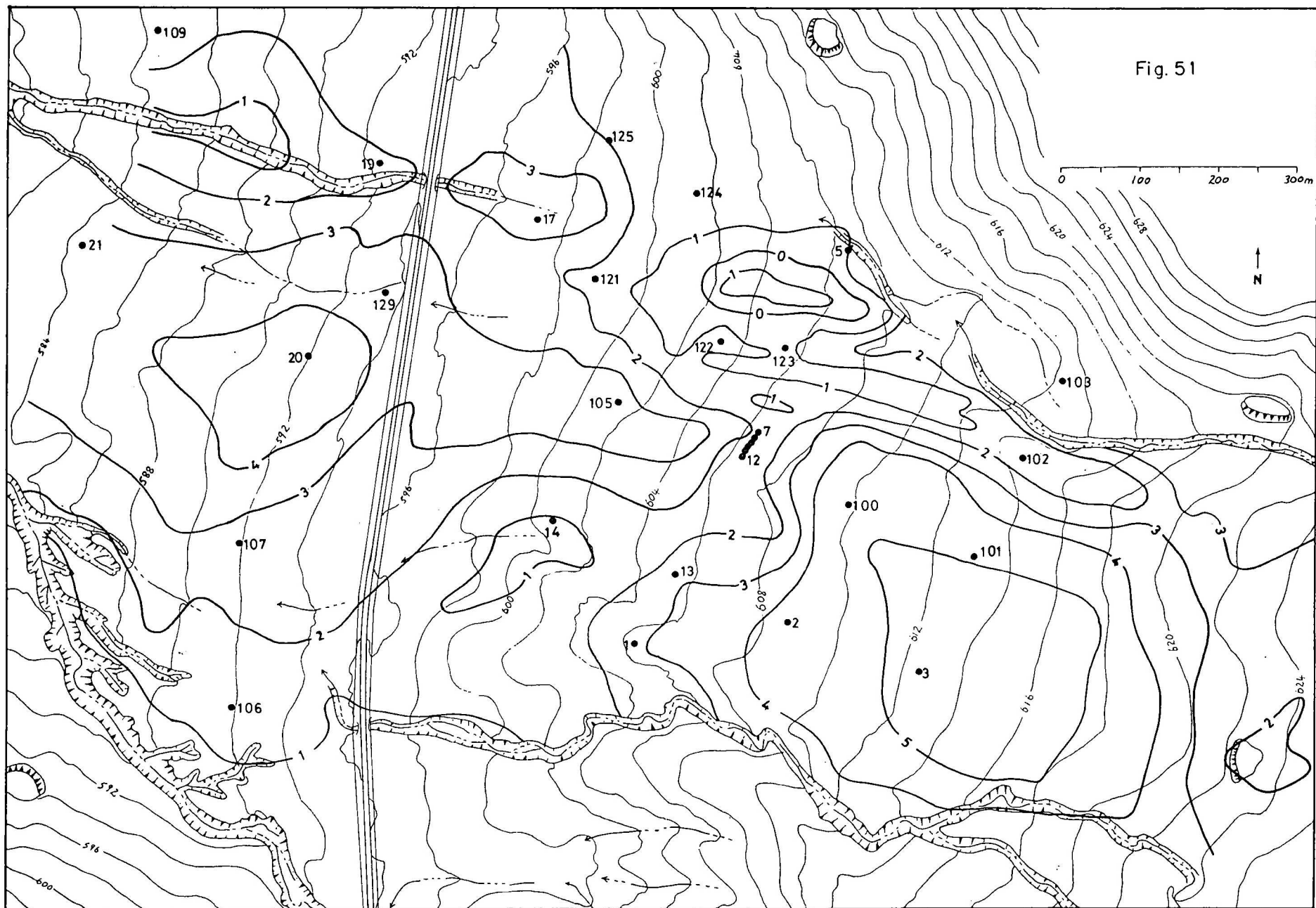
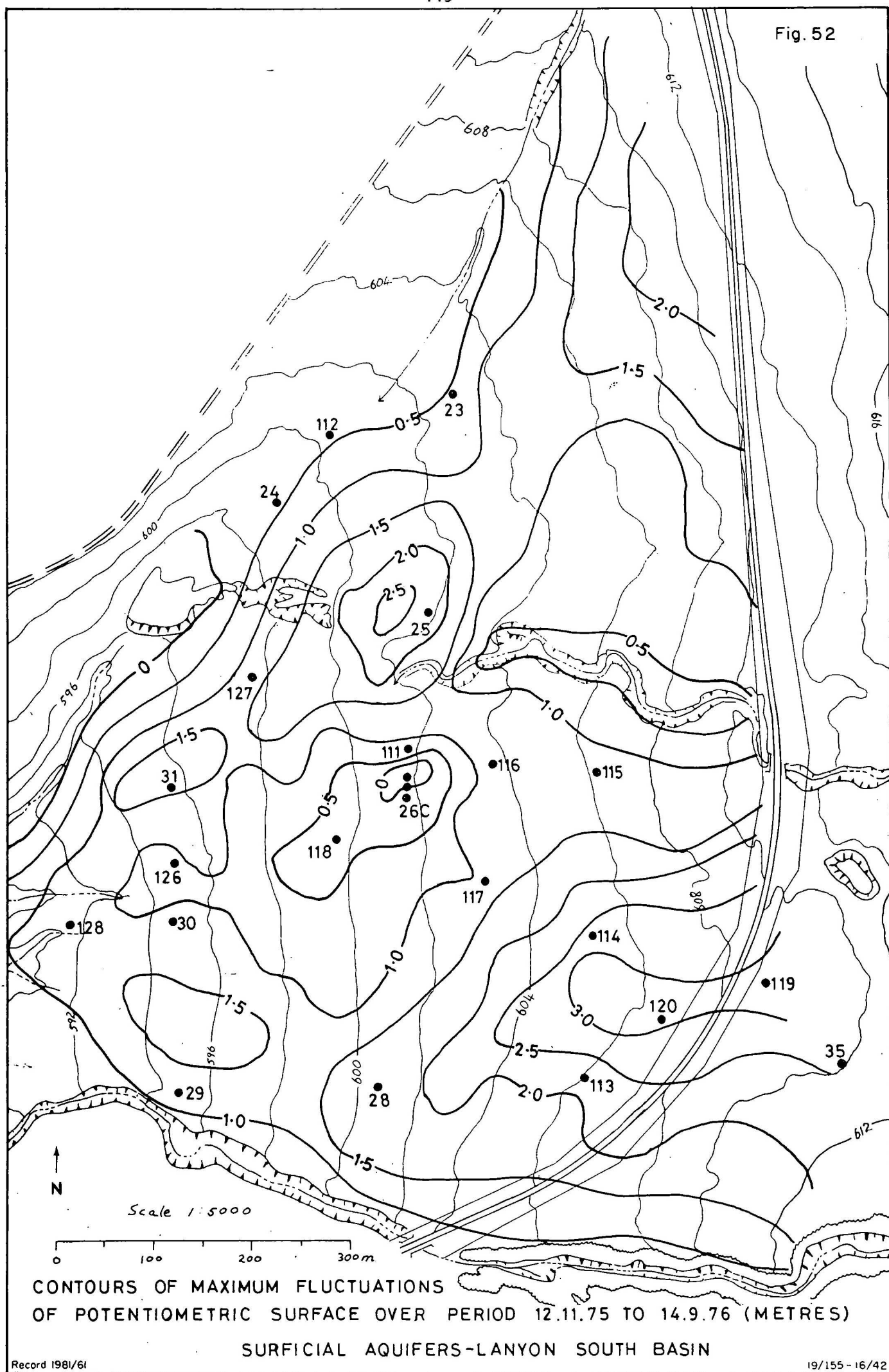


Fig. 51

Contours of maximum fluctuations of potentiometric surface over period 12-11-75 to 14-9-76 (metres). Surficial aquifers — North Basin

19/155-16/41

Fig. 52



by groundwater storage and bed underflow in the debris-filled channel. The dominant direction of subsurface piping of groundwater from the stream terminus must be in the direction of least fluctuations of the potentiometric surface, namely towards the southwest. Therefore the high fluctuations around piezometer 25 can be due only to changes in storage produced by surface recharge from overland flow when the central stream discharges onto the basin surface. Field observations during flooding of this stream verify that the main flow path is to the north of west from the terminus through the neighbourhood of piezometer 25.

Flow nets

The general directions of groundwater flow in the central part of the Lanyon north basin is summarised in flow nets for the fractured rock (Fig. 53) and surficial aquifers (Fig. 54). The major streams of the basin provide convenient boundaries for the flow nets of both aquifer systems since they generally approximate dividing streamlines. The flow nets were constructed from groundwater potentials recorded on 12 November 1976, the first date on which a water-level could be recorded in L14—the final bore drilled for the investigation. At that stage groundwater storage in the basin was quite high after 161 mm of rainfall during the previous month. The last rain to recharge the groundwater store before 12 November 1976 was a fall of 15.8 mm over 21 hours on 2 and 3 November. Antecedent precipitation was light showers on 6 (0.4 mm), 10 (0.6 mm), and 11 (1.2 mm) November, which produced no surface runoff or recharge to groundwater but was all absorbed by plant interception and temporary topsoil storage.

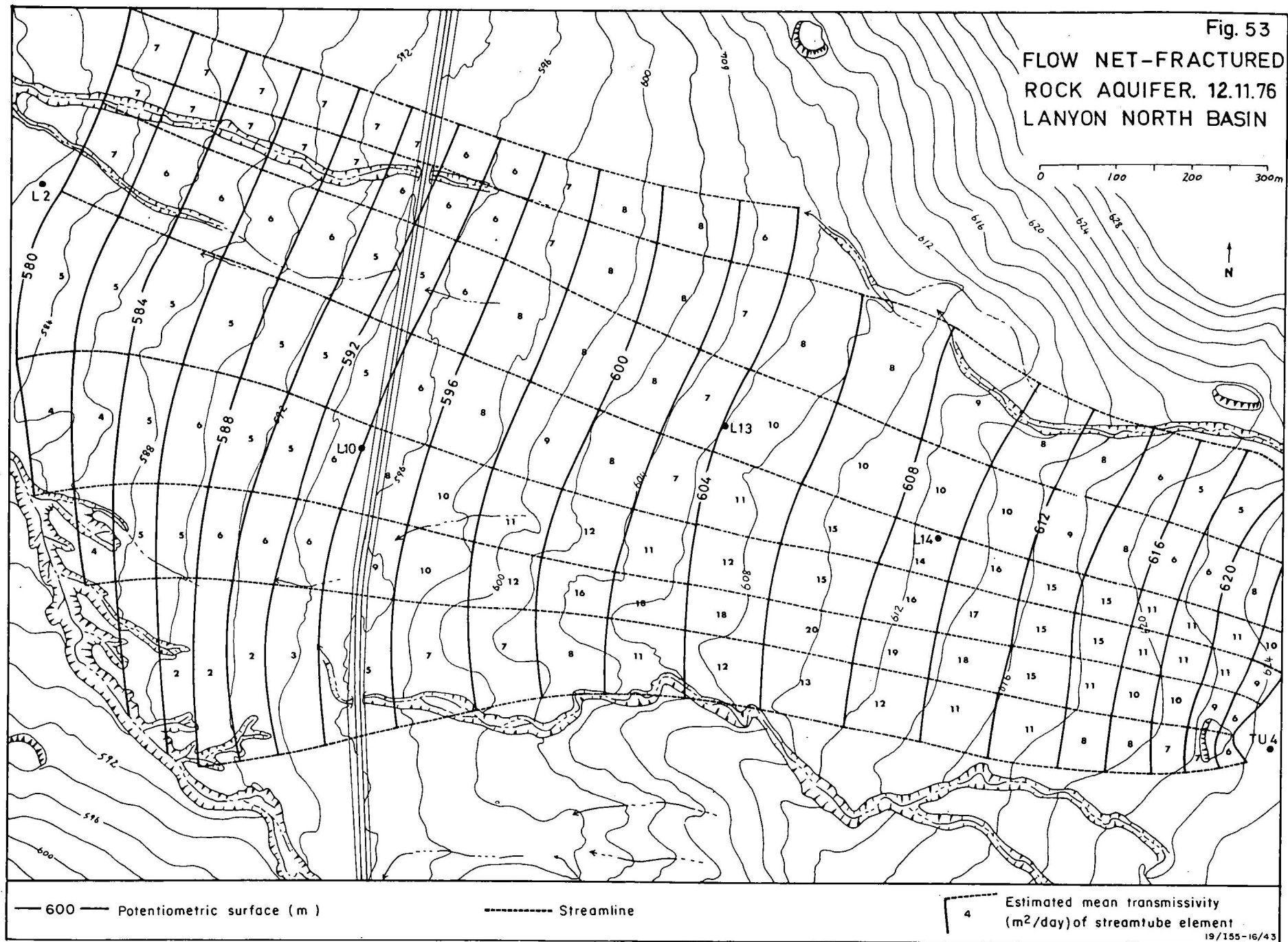
Note that the elements of the flow nets are not squares because the basin never attains dynamic equilibrium. In any case, the occurrence of point sources in the surficial aquifers, and the inhomogeneity of the aquifers in general, causes refraction of streamlines around potentials, making it most unlikely that a net of square elements could ever be constructed.

The groundwater discharge q (m^3/day) through a three-dimensional element of thickness $d(\text{m})$ bounded by streamlines $\Delta x(\text{m})$ apart, orthogonal to potentials $\Delta y(\text{m})$ apart of potential difference $\Delta h(\text{m})$ is given by Darcy's Law as

$$q = K \frac{\Delta h}{\Delta y} d \Delta x$$

where k = hydraulic conductivity (m/day)

Therefore the total discharge Q (m^3/day) between two equipotential lines across



the flow net is

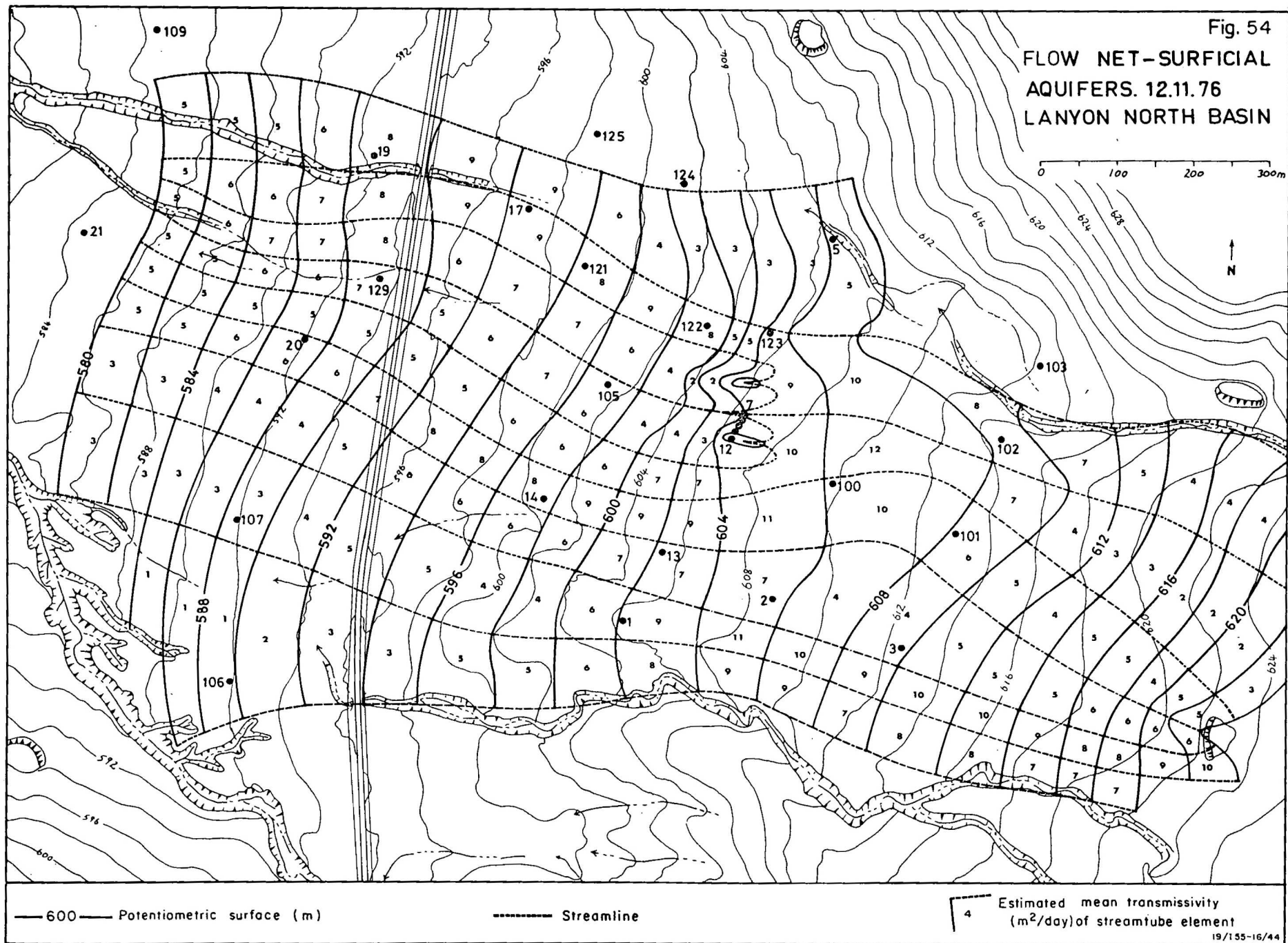
$$Q = \Delta h \sum_{i=1}^N \frac{\Delta X_i}{\Delta Y_i} T_i \quad (2)$$

where $T_i = k_i d_i$ (m^2/day) = transmissivity of i th streamtube element
and N = number of elements bounded by the equipotentials.

Equation 2 may be used for calculating discharge rates across equipotential lines of the flow nets if the transmissivity of the aquifer within each element is known. The values of mean transmissivity of the flow net elements shown in Figure 53 are estimated from correlations of measured transmissivities and bore yields with frequency of open joints and degree of rock weathering. From subsurface investigation and natural exposure these conditions are known for several elements of each stream-tube, which allows the transmissivities of intervening stream-tube elements to be estimated by proportion. The mean transmissivities shown in Figure 54 for the surficial elements are derived by summation of measured transmissivity values from pump testing over the known or estimated saturated thickness of pedoderms.

From Figure 53 the total groundwater flow rate through the fractured rock in the recharge zone of the north basin bounded by the flow net was $140 \text{ m}^3/\text{day}$ on 12 November 1976. Impedance to groundwater transmission through the deeply weathered rock beneath the swampy area of the discharge zone of the basin resulted in an overspill of $15 \text{ m}^3/\text{day}$ into the surficial aquifers between the 604 m and 608 m equipotential lines. The direction of leakage was reversed on the western side of the discharge zone, where the rock is not as severely weathered, such that the $15 \text{ m}^3/\text{day}$ loss from the fractured-rock aquifer had been fully regained by downwards leakage from the surficial aquifers between the 590 m and 604 m equipotentials.

Total discharge through the western end of the net was $135 \text{ m}^3/\text{day}$, of which $55 \text{ m}^3/\text{day}$ flowed into effluent streams and $80 \text{ m}^3/\text{day}$ was transmitted farther westwards by lateral throughflow. The overall deficit of $5 \text{ m}^3/\text{day}$ between inflow and outflow is attributable to upwards leakage into the surficial aquifers between the 580 m and 590 m equipotentials, but it is also possible that such an insignificant loss over 1.7 km could equally well be caused by errors in estimation of the transmissivities.



Total recharge rate for the surficial aquifers of the north basin on 12 November 1976 is estimated from the flow net (Fig. 54) as $145 \text{ m}^3/\text{day}$, and its components are shown below. The recharge components calculated from flow nets drawn for 14 September 1976, a period of groundwater recession, are included for comparison; antecedent precipitation was 33 mm on 1 September and intermittent showers totalling 5.4 mm on 9 and 10 September:

	<u>12.11.76</u>	<u>14.9.76</u>	
(i)	$115 \text{ m}^3/\text{day}$	$80 \text{ m}^3/\text{day}$	total lateral transmission through eastern boundary of net.
(ii)	$25 \text{ m}^3/\text{day}$	$10 \text{ m}^3/\text{day}$	vertical upwards flow from point sources at piezometers 12, 123, and the willow plantation to the north of piezometer 7.
(iii)	$5 \text{ m}^3/\text{day}$	$10 \text{ m}^3/\text{day}$	upwards flow from the fractured rock in the western sector of the basin.
	<hr/>	<hr/>	
	$145 \text{ m}^3/\text{day}$	$100 \text{ m}^3/\text{day}$	

The recharge for (ii) on 12 November 1976 was composed of $15 \text{ m}^3/\text{day}$ from the fractured rock and $10 \text{ m}^3/\text{day}$ from subsurface piping from the discontinuous northern stream.

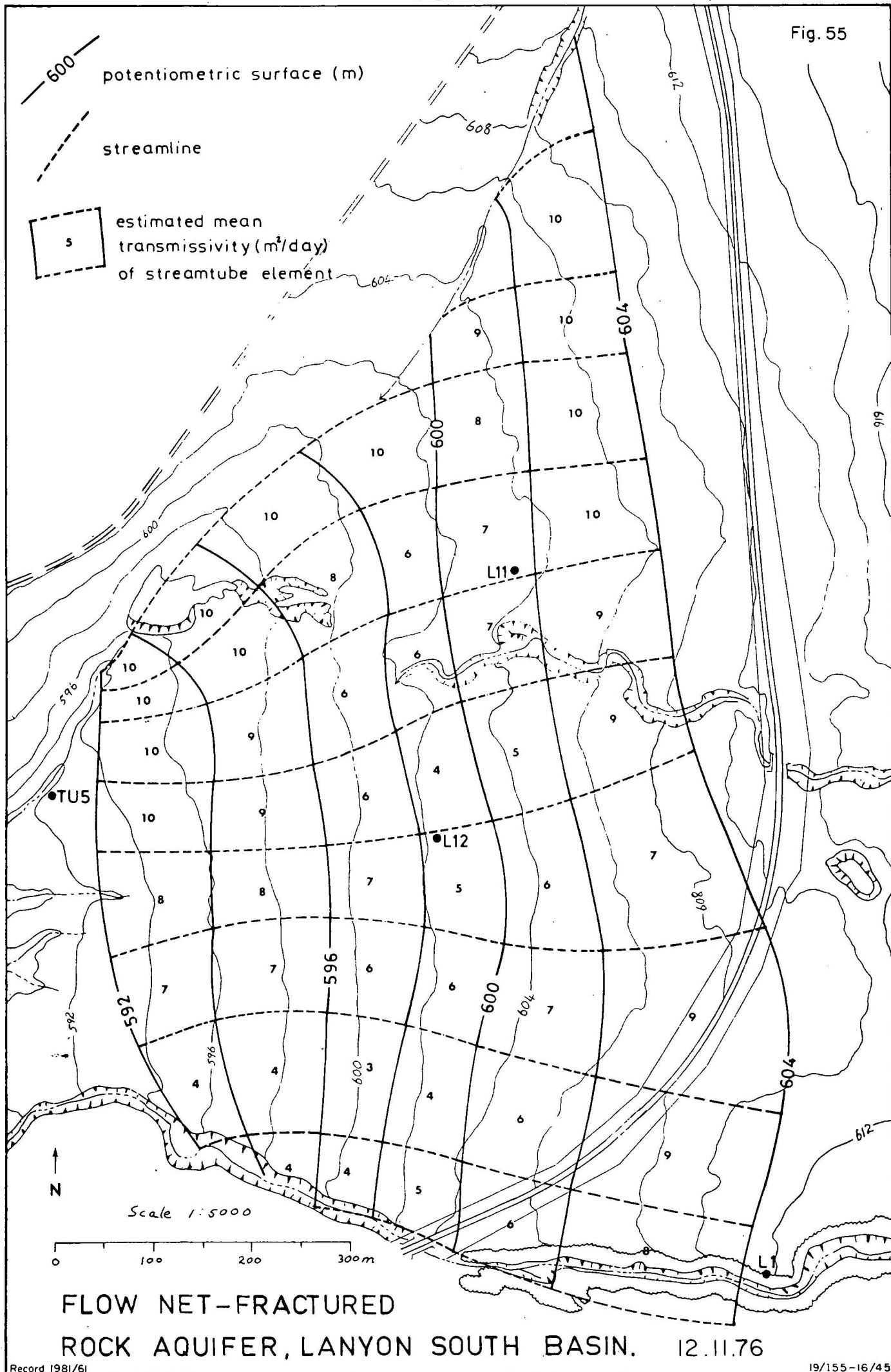
Discharge through the western end of the net is partitioned as follows:

<u>12.11.76</u>	<u>14.9.76</u>	
$35 \text{ m}^3/\text{day}$	$15 \text{ m}^3/\text{day}$	baseflow into effluent streams.
$50 \text{ m}^3/\text{day}$	$45 \text{ m}^3/\text{day}$	lateral throughflow
<hr/>	<hr/>	
$85 \text{ m}^3/\text{day}$	$60 \text{ m}^3/\text{day}$	

Therefore the groundwater deficits from east to west in the surficial cover of the north basin over the area covered by the flow nets were $60 \text{ m}^3/\text{day}$ on 12 November 1976 and $40 \text{ m}^3/\text{day}$ on 14 September 1976.

Flow nets for the south basin on 12 November 1976 are shown in Figure 55 (fractured rock) and 56 (surficial aquifers). Mean transmissivities of the flow net elements were estimated by the same techniques described earlier for

Fig. 55



the north basin.

Fractured-rock recharge through the eastern area of the south basin bounded by the flow net (Fig. 55) was $185 \text{ m}^3/\text{day}$. Discharge through the western end of the net was $165 \text{ m}^3/\text{day}$, comprising $90 \text{ m}^3/\text{day}$ baseflow into effluent streams and the dam on the western boundary, and $75 \text{ m}^3/\text{day}$ lateral transmission through the interfluvial transected by the 592 m potential. This gives an upwards leakage rate into the surficial aquifers in the western half of the basin of $20 \text{ m}^3/\text{day}$.

Total recharge rates for the surficial aquifers of the south basin on 12 November 1976 (Fig. 56) and 14 September 1976 are partitioned as follows:

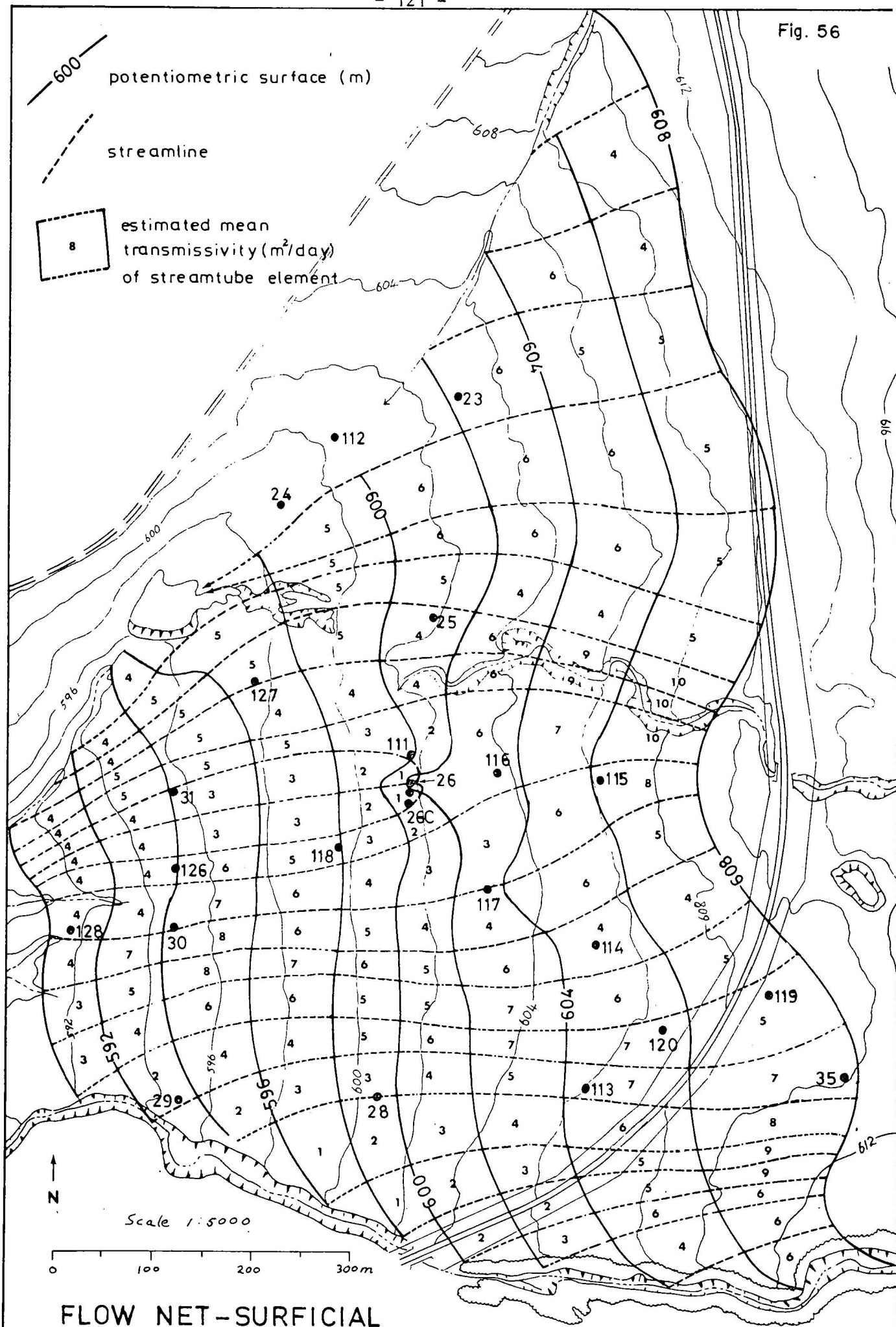
<u>12.11.76</u>	<u>14.9.76</u>	
$130 \text{ m}^3/\text{day}$	$95 \text{ m}^3/\text{day}$	total lateral transmission through eastern boundary of net
$15 \text{ m}^3/\text{day}$	$10 \text{ m}^3/\text{day}$	bed underflow from the central stream
$10 \text{ m}^3/\text{day}$	$5 \text{ m}^3/\text{day}$	vertical upwards flow from point sources at piezometers 26 and 117
$20 \text{ m}^3/\text{day}$	$10 \text{ m}^3/\text{day}$	upwards flow from the fractured rock in the western half of the basin
<hr/> $175 \text{ m}^3/\text{day}$ <hr/>	<hr/> $120 \text{ m}^3/\text{day}$ <hr/>	

Discharge through the western ends of the stream-tubes consisted of:

<u>12.11.76</u>	<u>14.9.76</u>	
$35 \text{ m}^3/\text{day}$	$15 \text{ m}^3/\text{day}$	baseflow into southern stream
$40 \text{ m}^3/\text{day}$	$30 \text{ m}^3/\text{day}$	seepage into farm dam and baseflow into downstream section of western drainage channel
$35 \text{ m}^3/\text{day}$	$30 \text{ m}^3/\text{day}$	lateral transmission through the interfluvial between the southern and western streams across the 590 m equipotential line.
<hr/> $110 \text{ m}^3/\text{day}$ <hr/>	<hr/> $75 \text{ m}^3/\text{day}$ <hr/>	

Total groundwater losses across the area of the south basin covered by the flow nets were therefore $65 \text{ m}^3/\text{day}$ on 12 November 1976 and $45 \text{ m}^3/\text{day}$ on 14 September 1976 which are slightly higher than the equivalent losses incurred in the north basin.

Fig. 56



The nature of these groundwater losses will now be considered.

Firstly, an intrabasin loss from the surficial aquifers is incurred for all nets drawn on the dates shown in Appendix 6 over the period September 1974 to December 1976. There is a tendency for losses to be minimised during colder months and maximised during warmer months, but this is not a conclusive relationship because winters of 1975 and 1976 also coincided with periods of groundwater recession, whereas the warmer months were periods of accession.

Secondly, an interesting problem is posed if the intrabasin loss as a proportion of the surface area covered by the flow nets is taken into account. The lumped mean rate of loss in the south basin is over $1\frac{1}{2}$ times that of the north basin. It will be shown later that this anomaly arises because there is a greater area of free-water surfaces which are groundwater-charged in the south basin than there is in the north basin.

The deficits between groundwater inflows and outflows therefore represent a continuing withdrawal by evapotranspiration (E_T) from the system within the basins. They cannot represent changes in aquifer storage because this would lead to the untenable proposition of an unbounded increase in storage with time, irrespective of whether water-tables were rising or falling.

In conventional hydrologic useage, E_T is defined as the combination of evaporation from moist surface soil and transpiration by vegetation. But the present analysis is concerned only with the component of E_T which is drawn directly from the groundwater store accounted for in the flow nets. The relevant E_T component (E'_T) comprises:

- (i) Evaporation losses from free-water surfaces which are groundwater-charged. These include the farm dam in the south basin and areas of surface detention in swamps which are charged by upwards flow of groundwater in both basins. Evaporation losses from stream channels are not included because baseflow to effluent streams has already been counted in net outflows.
- (ii) Transpiration by phreatophytes. It is important to note that the considerable evapotranspiration which occurs from the unsaturated zone is assumed to be independent of groundwater losses in this analysis. In fact, the dates 12 November 1976

and 14 September 1976 - for which the flow net calculations are reported - were deliberately chosen because the light antecedent precipitations were considered to be sufficient to maintain moisture in the topsoil such that capillary rise from groundwater was minimised, but at the same time were not sufficient to produce an extraneous surface recharge component from influent streams. In both cases the dates are separated from the preceding groundwater recharge event by at least 9 days.

An approximate partitioning of E_T^I into evaporation from free-water surfaces and transpiration by phreatophytes is shown in Table 13. The mean transpiration losses lumped over the entire basin surfaces are in themselves meaningless quantities in the absence of a floral taxonomic study of the basins. They are included to demonstrate that - once the evaporation from freewater surfaces is discounted from the net groundwater loss - the mean phreatophyte transpiration rates in the north and south basins are not significantly different

Table 13
Approximate partitioning of E_T^I into evaporation and transpiration components

		12 November 1976		14 September 1976	
		North basin	South basin	North basin	South basin
Approximate area of free-water surfaces (m^2)	Dam	-	2800	-	2300
	Surface Detention	1800	2700	600	1500
Pan evaporation (mm)		6.1	6.1	3.7	3.7
Estimated potential evaporation (mm)		4.9	4.9	2.6	2.6
Estimated volume of evaporation loss from free-water surfaces (m^3)	Dam	-	14	-	6
	Surface Detention	9	13	2	4
Residual = Estimated volume transpired by phreatophytes (m^3)		51	38	38	35
Maximum available surface area for phreatophyte transpiration = area of flow net ₂ - area of free-water surfaces (m^2)		985 700	631 800	986 900	633 500

Table 13 Con't

	12 November 1976		14 September 1976	
	North basin	South basin	North basin	South basin
Mean transpiration loss from groundwater lumped over available basin surface (mm)	0.052	0.060	0.039	0.055

DRAINAGE OF THE BASINS FOR URBAN DEVELOPMENT

Sustained high groundwater potentials in certain areas of the north and south basins (Appendix 6) show that the existing natural drainage system is inadequate for urban development.

The main objective of the Lanyon hydrogeological investigation was to determine an optimum spacing between parallel sets of drains, such that the water-table is not permitted to rise to less than 1 metre below ground surface. In keeping with drainage practice employed earlier in the Tuggeranong valley, some drains in the form of open channels will serve the dual purposes of floodways and groundwater drains, and others in the form of buried perforated pipes will serve solely as ground-water drains (Gutteridge, Haskins and Davey Pty Ltd, 1975). Efficient drainage design should ensure, on the one hand, that resources are not wasted by placing drains unnecessarily close to each other, and, on the other hand, that the drain spacing is sufficient for most rainfall events to prevent water-logging damage to house foundations and other engineering structures.

The approach which has been adopted in this report to solve the drain-spacing problem is to develop a deterministic model for transient hydrodynamic flow which predicts hydraulic head as a function of time and distance from a drain for variable recharge from rainfall. Methods of determination of hydrogeological parameters used in the model have been described earlier. Model predictions for prior rainfall events are then compared with observed fluctuations in groundwater potentials recorded in piezometers which lie within the radius of influence of existing natural groundwater drains.

After demonstrating that the model adequately describes the hydrogeological system, recommendations are made for drain spacings based on rainfall intensity-frequency-duration curves for Canberra.

Analytical solution for calculation of drain spacing

The equation describing diffusion of groundwater through porous media in one spatial dimension based on the Dupuit-Forchheimer assumptions is:

$$KD \frac{\partial^2 h}{\partial x^2} = \mu \frac{\partial h}{\partial t} - R \quad (3)$$

where h = hydraulic head (m)

K = hydraulic conductivity (m/day)

D = mean saturated thickness of the aquifer (m)

μ = effective porosity (dimensionless, assumed constant)

x = horizontal distance from a boundary or reference point (m)

R = recharge (or discharge) rate per unit surface area (m/day)

t = time (days)

The derivation of (3) with discussions on the Dupuit-Forchheimer assumptions is given by Van Schilfgaarde (1970) and IILRI (1972-74, Vols. 1 and 2). In general, the Dupuit-Forchheimer linearisation (3) of the groundwater diffusion equation is applicable for groundwater motion defined by parallel streamlines in shallow aquifers of low to moderate hydraulic conductivity where the magnitude of both temporal and spatial variations in hydraulic head are small.

The parameters μ , K and D are defined for an unconfined aquifer. Where the aquifer is confined, for example in the neighbourhood of bore 26 in the south basin, the effective porosity μ , is replaced by the storage coefficient S , and the product KD is replaced by T , the transmissivity of the aquifer.

Equation (3) may be solved subject to the boundary conditions:

$$h(0, t) = 0 \quad (3a)$$

$$h(L, t) = 0 \quad (3b)$$

$$\text{and the initial condition, } h(x, 0) = f(x) \quad (3c)$$

Since the Dupuit-Forchheimer assumption of parallel streamlines is not satisfied in the region of radial convergence of streamlines near a drain which does not penetrate the entire aquifer, it is necessary to use Hooghoudt's 'equivalent depth' transformation for D . The transformation for this boundary value problem is:

$$d = \frac{D}{1 + \frac{4D}{\pi L} \ln \frac{D}{u}}$$

where d = Hooghoudt's 'equivalent depth'
 u bottom width of open drain

Hooghoudt's d-transformation and the boundary conditions in a vertical plane perpendicular to the drain at the instant before recharge is shown in Figure 57.

By the method of separation of variables and equating the eigenfunction expansions of the problem with the Fourier sine series, the solution of equations (3) to (3c) is:

$$h(x,t) = \underbrace{\frac{R}{2Kd} \left[\frac{(L^2 R + 2Kd \theta)x}{LR} - x^2 \right]}_{\text{steady-state solution}} + \underbrace{\sum_{n=1}^{\infty} B_n \sin \frac{n\pi x}{L} \exp\left(\frac{-Kdn^2 \pi^2 t}{\mu L^2}\right)}_{\text{transient term}}$$

where

$$B_n = \frac{2}{L} \int_0^L f(x) \sin \frac{n\pi x}{L} dx - \frac{R}{Kd} \left[\frac{2L^2}{n^3 \pi^3} (1 - (-1)^n) - \frac{2Kd \theta}{Rn \pi} (-1)^n \right] \quad (5)$$

Note that D has been replaced by the equivalent depth d , and K refers to the hydraulic conductivity of the aquifer(s) below drain level.

Equation (4) is expressed more usefully as:

$$h(x,t) = R \beta(x,t) + \theta \left[\gamma(x,t) + \delta(x,t) \right] \quad (6)$$

where

$$\beta(x,t) = \frac{x(L-x)}{2Kd} - \frac{4L^2}{\pi^3 Kd} \sum_{n=1}^{\infty} \frac{1}{(2n-1)^3} \sin \frac{(2n-1)\pi x}{L} \exp \frac{(-Kd(2n-1)^2 \pi^2 t)}{\mu L^2}$$

is the solution of the associated homogeneous equation,

$$\gamma(x,t) = \frac{x}{L} + \frac{2}{\pi} \sum_{n=1}^{\infty} \frac{(-1)^n}{n} \sin \frac{n\pi x}{L} \exp \frac{(-Kdn^2 \pi^2 t)}{\mu L^2}$$

is generated by the non-zero boundary condition 3(b),

$$\text{and } \delta(x,t) = \sum_{n=1}^{\infty} \frac{2}{n\pi(16 + n^2 \pi^2)} \left[n^2 \pi^2 (e^{-4} - 1) (-1)^n + 16(1 - (-1)^n) \right] \sin \frac{n\pi x}{L} \exp \frac{(-Kdn^2 \pi^2 t)}{\mu L^2}$$

is generated by the non-zero initial condition 3(c).

The $\delta(x,t)$ term was evaluated after approximating the typical initial configuration of the phreatic surface at $t=0$ with $f(x) = \theta (1-\exp(-4x/L))$ which is preferred over a polynomial approximation because it gives a simple closed form solution to the integral in (5). The function was obtained by empirical curve-fitting using piezometer measurements in vertical planes normal to deeply incised creek beds in both basins.

The great advantage in using the linearised diffusion equation (3) is that the principle of superposition may be used for predictions of hydraulic head under conditions of variable recharge rates from rainfall. The use of the principle of superposition to calculate water-table fluctuations induced by intermittent recharge is discussed by Maasland (1959) and IILRI (1972-4, Vol. 2). The example shown in Figure 58 describes graphically the fluctuations in hydraulic head in response to two recharge events of unequal intensity R_1 and R_2 on days 1 and 2 respectively.

At the end of the first day (Fig. 58) after recharge R_1 , the hydraulic head is

$$h(x,1) = R_1 \beta(x,1) + \theta_0 (\gamma(x,1) + \delta(x,1)).$$

In order to obtain an analytical solution for (3) to (3c) it was implicit that R_1 was constant for all t . Therefore, to satisfy field conditions it is necessary on the second and subsequent days to subtract an equal negative recharge which reduces steady-state recharge to zero. Therefore, at the end of the second day, the component of the hydraulic head due to R_1 is

$$h'(x,2) = R_1 \beta(x,2) + \theta_0 (\gamma(x,2) + \delta(x,2)) - [R_1 \beta(x,1) + \theta_0 (\gamma(x,1) + \delta(x,1))]$$

But to account for the second recharge event R_2 , the value for h at the end of the second day is

$$h(x,2) = R_2 \beta(x,1) + \theta_1 (\gamma(x,1) + \delta(x,1)) + h'(x,2)$$

where the θ_1 value at the start of day 2 is calculated from $h(x,t=1)/f(x)$.

The negative juxtaposition of R_2 values for the third and subsequent days is continued in the same manner as for R_1 until the difference

$$[R_2 \beta(x,i+1) + \theta_1 (\gamma(x,i+1) + \delta(x,i+1))] - [R_2 \beta(x,i) + \theta_1 (\gamma(x,i) + \delta(x,i))]$$

becomes insignificant.

The hydraulic head at the end of the third day on which there is no recharge is

$$h(x,3) = \left[R_1 \beta(x,3) + \theta_0 (\gamma(x,3) + \delta(x,3)) + R_2 \beta(x,2) + \theta_1 (\gamma(x,2) + \delta(x,2)) \right] - \left[R_1 \beta(x,2) + \theta_0 (\gamma(x,2) + \delta(x,2)) + R_2 \beta(x,1) + \theta_1 (\gamma(x,1) + \delta(x,1)) \right]$$

By inspection of Figure 58, the algorithm for the hydraulic head at the end of the nth day after intermittent recharge events R_1, R_2, \dots, R_n is given by the algebraic sum of the ordinates at day n:

$$h(x,t_n) = \sum_{i=1}^n R_{n-i} \left(\beta_{i+1} - \beta_i + \xi \left[R_n \beta_1 + \theta_{n-1} (\gamma_1 + \delta_1) \right] \right) + \sum_{i=2}^n \eta \left(\theta_{n-i} \left[(\gamma_i - \gamma_{i-1}) + (\delta_i - \delta_{i-1}) \right] \right) \quad (7)$$

where the unit step functions ξ and η operate as follows:

$$\xi = \begin{cases} 1 & \text{if } R_n > 0 \\ 0 & \text{if } R_n = 0 \end{cases}, \quad \eta = \begin{cases} 1 & \text{if } R_{n-i+1} > 0 \\ 0 & \text{if } R_{n-i+1} = 0 \end{cases}$$

The algorithm (7) operates on $h(x,t_n)$ and calculates the appropriate θ value by substitution into

$$\theta_n = h(x,t_n) / (1 - \exp(-4x/L)) \text{ which then becomes the initial } \theta \text{ value for day } n + 1.$$

Comparison of predicted groundwater potentials with observed piezometer readings

The boundary conditions to equation (3) were posed in their asymmetric form to enable the validity of the model (7) to be assessed by comparing model predictions and field measurements of the potentiometric surface. In the Lanyon basins, the boundary and initial conditions 3(a)-3(c) are satisfied by seven piezometers within the radius of influence of deeply incised creeks which are natural groundwater drains.

It was originally intended to test the model during June and July 1976 because of the minimal evapotranspiration (unknown) during that part of the year. Piezometer levels were read every second day starting in June, but the intensive monitoring program was terminated after three weeks when it appeared as though groundwater-levels in some of the observation holes

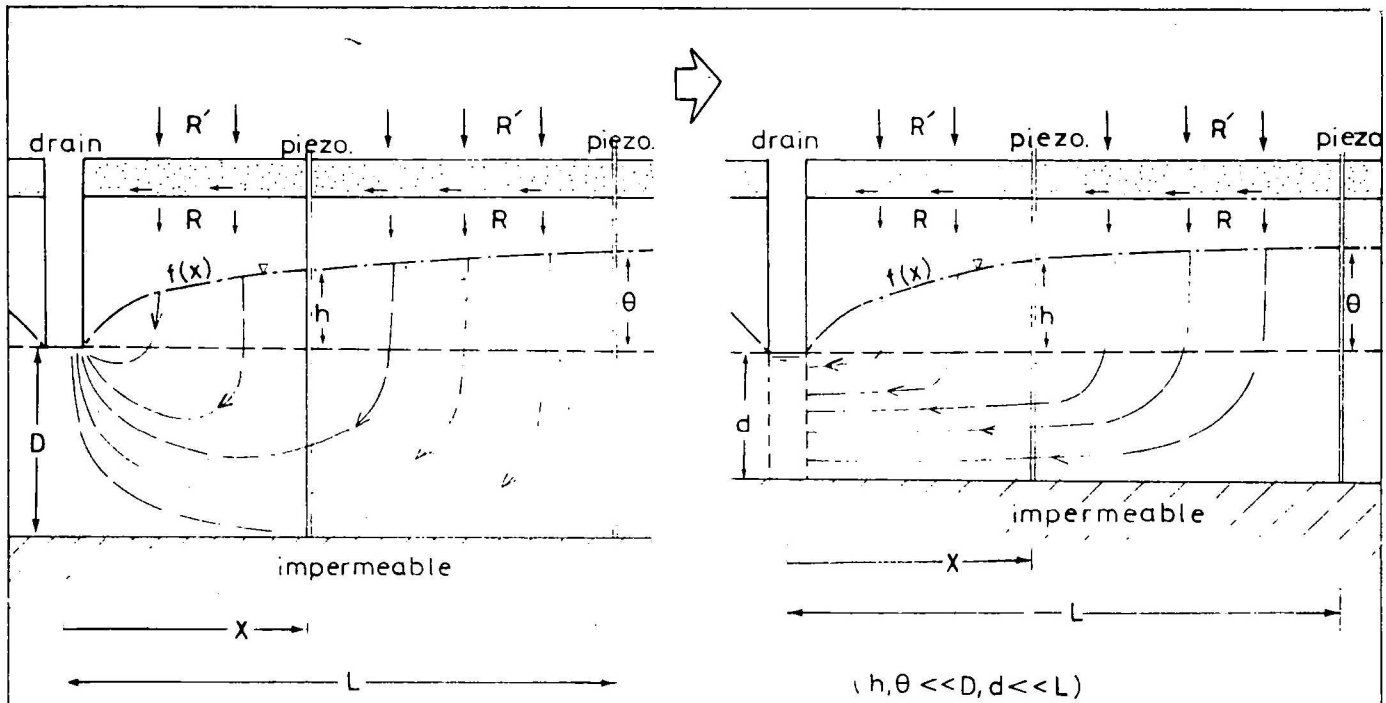


Fig 57. Boundary conditions of flow to a shallow, partly penetrating open drain with Hooghoudt's transformation $D \rightarrow d$ for parallel streamlines.

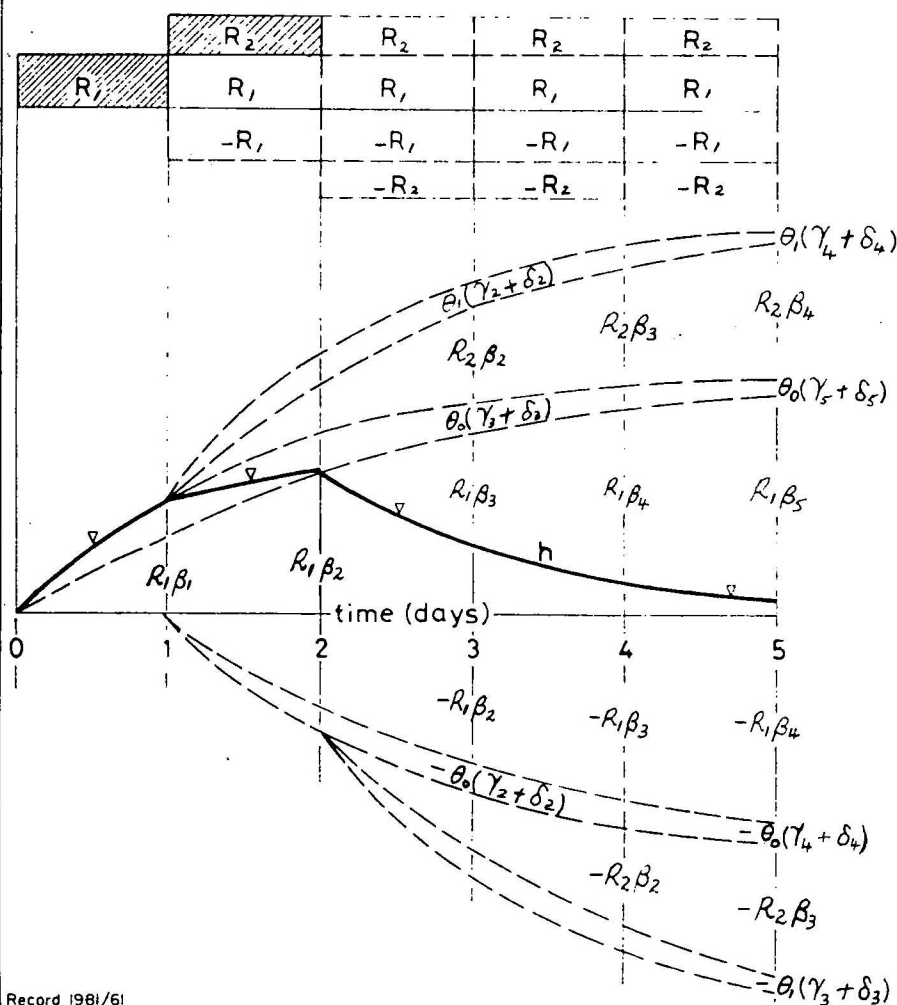


Fig 58. Superposition of solutions for $h(x,t)$ in response to intermittent recharge.

would fall below creek level, thus violating the boundary conditions. Low intensity rains which produced no runoff during late July and August 1976 induced groundwater-levels to rise sufficiently for the two-day measurements to be recommenced during September and to be continued until the end of October 1976. It eventuated that this was the best possible time for frequent monitoring because rainfall for both months was well above average and included some exceptionally heavy prolonged falls during October.

All observation piezometers except for no. 29 in the south basin were simulated at a distance L metres from the natural groundwater drains and dummy values for hydraulic head were generally calculated at a distance x metres such that $L/3 \leq x \leq L/2$. Daily recharge to the groundwater store was calculated in accordance with the stratified slab model (Fig. 50), which partitions rainfall into runoff, interflow, and storage and permits delayed leakage at a rate proportional to the quantity of water in soil storage. It is assumed that the stratified slab forms a continuous sheet of constant thickness over the basin surfaces.

Mean values of K , D (d), and μ obtained from field and laboratory tests were assigned to the groundwater populations depicted in Figures 44 and 45 as follows:

- (a) Populations S2, N1 $\overline{Kd} = 5\text{m}^2/\text{day}$, $\bar{\mu} = 0.04$ ($\sim 100 < L < \sim 200$)
- (b) Population S1 $\overline{Kd} = 10\text{m}^2/\text{day} - 15\text{m}^2/\text{day}$, $\bar{\mu} = 0.05$ ($\sim 200 < L < \sim 400$)
- (c) Population N2 $\overline{Kd} = 20\text{m}^2/\text{day}$, $\bar{\mu} = 0.05$ ($\sim 200 < L < \sim 400$)

Recall that groundwater populations were defined by the correlation between water-level fluctuations in the surficial and underlying fractured-rock aquifers. High linear correlation between both sets of bores in the same hydrogeological domain was interpreted as indicating hydraulic continuity between the two aquifer systems; therefore the D -value in populations S1 and N2 includes the surficial material below drain level, as well as the estimated thickness of fractured rock in which low-angle joints are continuous and open. The mean hydraulic conductivity for these populations has been weighted accordingly - a mean K value of 0.5 m/day was used for the fractured-rock aquifer in the weighting. Conversely, in populations S1 and N2, where the statistical analysis indicates an independent (or non-linear) discrete two-layer aquifer system with impeded hydraulic connection through an intervening aquitard of highly to extremely weathered rock, the D -value is the

thickness of the surficial aquifers below the bottom of the drain, and the K-value is the weighted mean of the surficial aquifers only.

Comparisons between predicted and observed values of hydraulic head over the period September-October 1976 are shown in Figures 59 to 65.

The model predictions are generally within 10% of observed results for $L < \sim 200$ m, which is considered to be reasonable for a deterministic model that uses mean rounded hydrogeological parameters as inputs. For $\sim 200 < L < \sim 400$ m, the model is accurate for small recharge, but seriously underestimates the groundwater wave generated by large recharge events in mid-October 1976 (Figs. 62, 63).

The reasons for the divergence between observed and predicted values of hydraulic head for large R, L include:

- (i) departure from Dupuit-Forchheimer theory for large distances away from the drain where changes in h are not small
- (ii) an extraneous flow component parallel to, and out of the radius of influence of the drain; a model that only describes flow in a vertical plane normal to the drain does not account for this
- (iii) the rise of the water-table into a zone which is progressively influenced upwards by pedogenetic pore-filling, and is therefore of lower effective porosity, which magnifies head differences
- (iv) suspected seepage during rainfall between the soil surface and piezometer wall in bore 30 (Fig. 60).

It is considered that (ii) is the most important of the above factors for the underestimation of h for large R and L. The problem may be resolved by introducing a second spatial co-ordinate axis y orthogonal to x and posing the appropriate boundary conditions to solve numerically for h (x,y,t). But it is argued that such an exercise is unnecessary for confidence in model predictions because the system will more closely approximate the boundary value problem (3)-(3c) after sets of parallel drains are installed in the basins.

Fig.59 COMPARISON BETWEEN PREDICTED AND OBSERVED VALUES OF HYDRAULIC HEAD

SOUTH BASIN — BORE 29

Observation period : 1/9/76 — 31/10/76

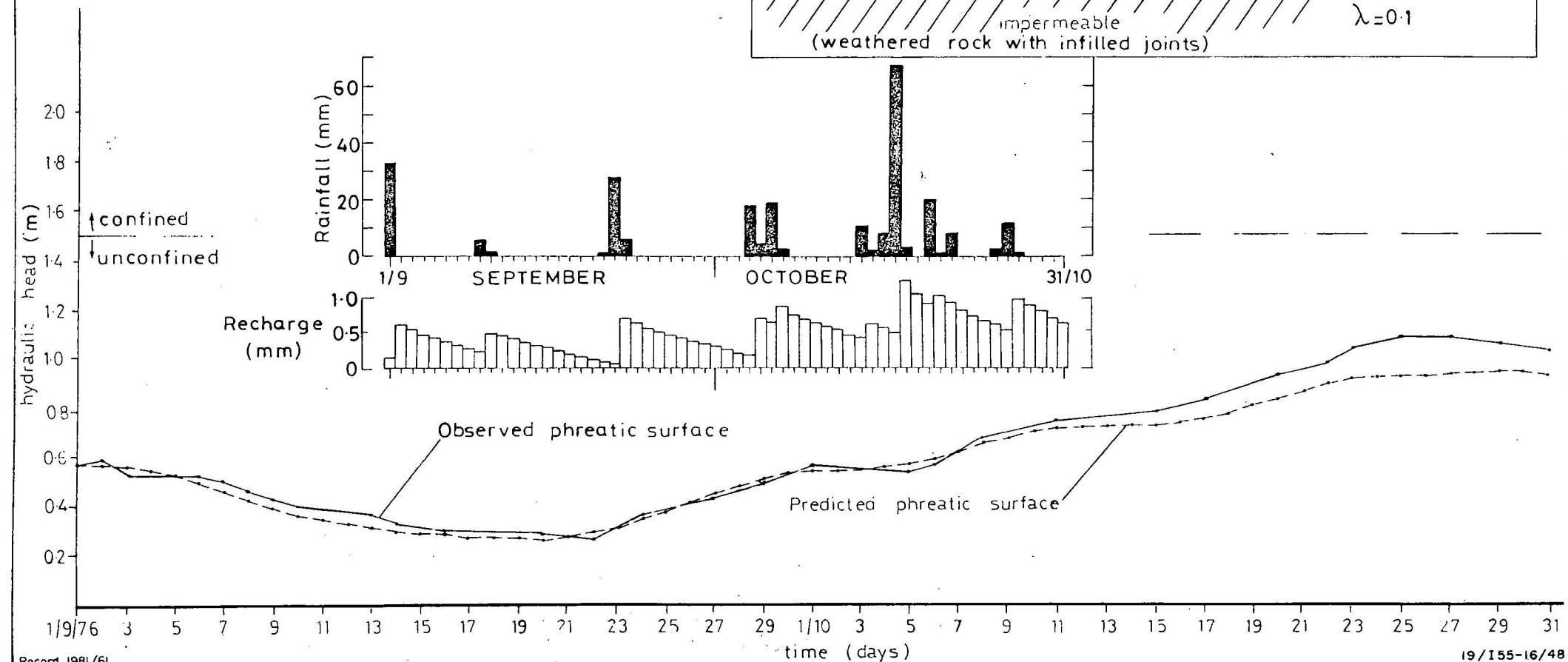
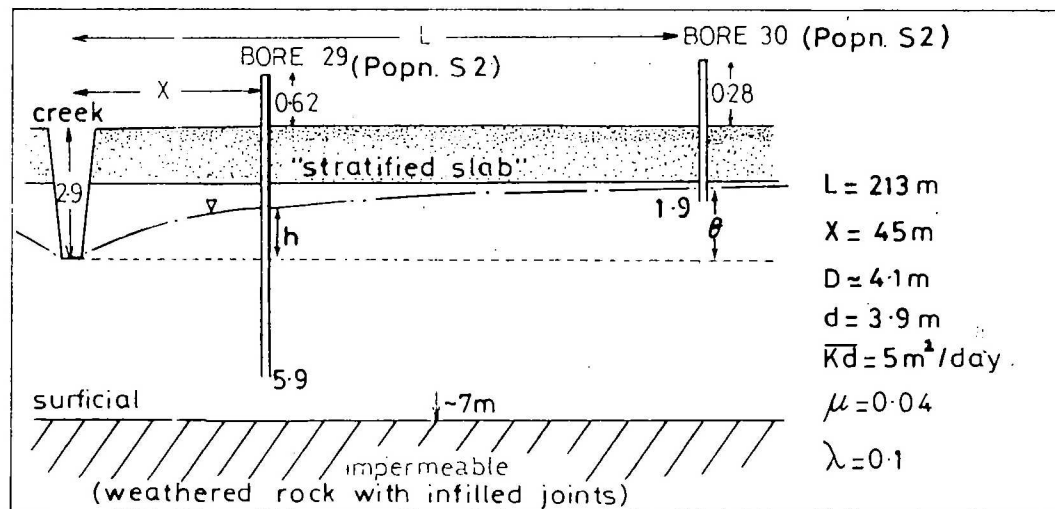


Fig. 60 COMPARISON BETWEEN PREDICTED AND OBSERVED VALUES OF HYDRAULIC HEAD

SOUTH BASIN — BORE 30

Observation period : 1/9/76 — 31/10/76

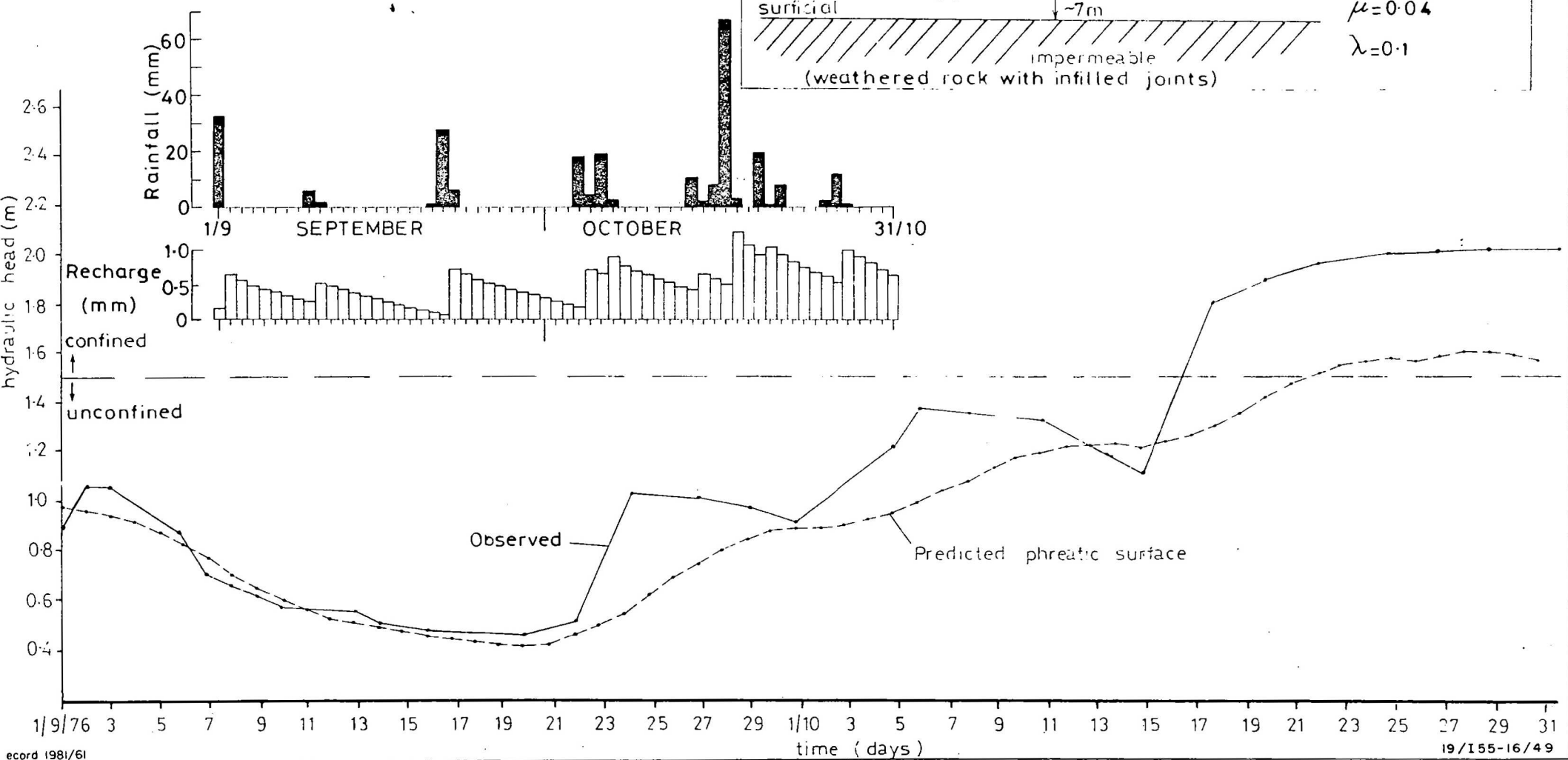


Fig. 61 COMPARISON BETWEEN PREDICTED AND
OBSERVED VALUES OF HYDRAULIC HEAD
SOUTH BASIN — BORE 28
Observation period : 1/9/76 — 31/10/76

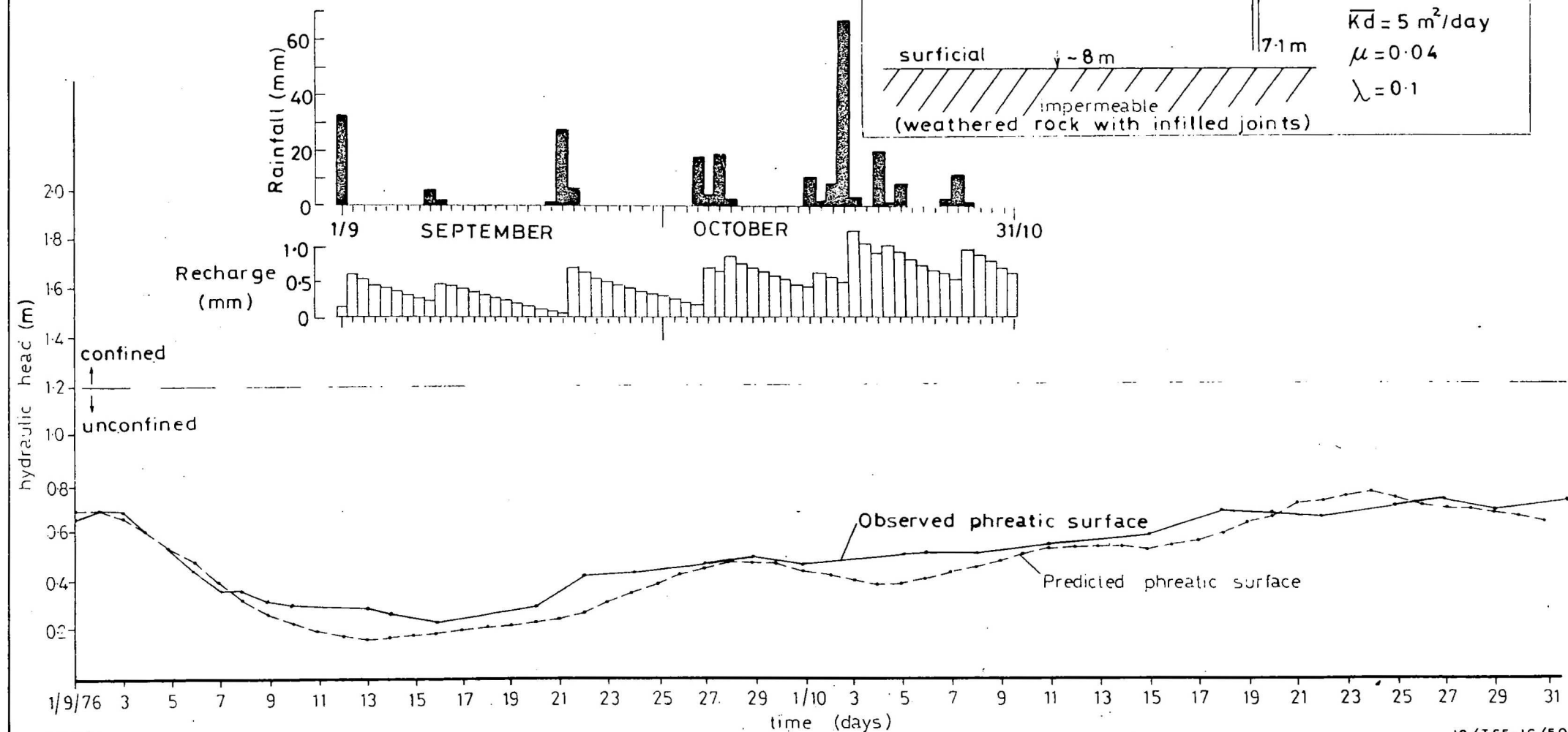


Fig. 62 COMPARISON BETWEEN PREDICTED AND
OBSERVED VALUES OF HYDRAULIC HEAD
SOUTH BASIN BORE 35
Observation period : 1/9/76 - 31/10/76

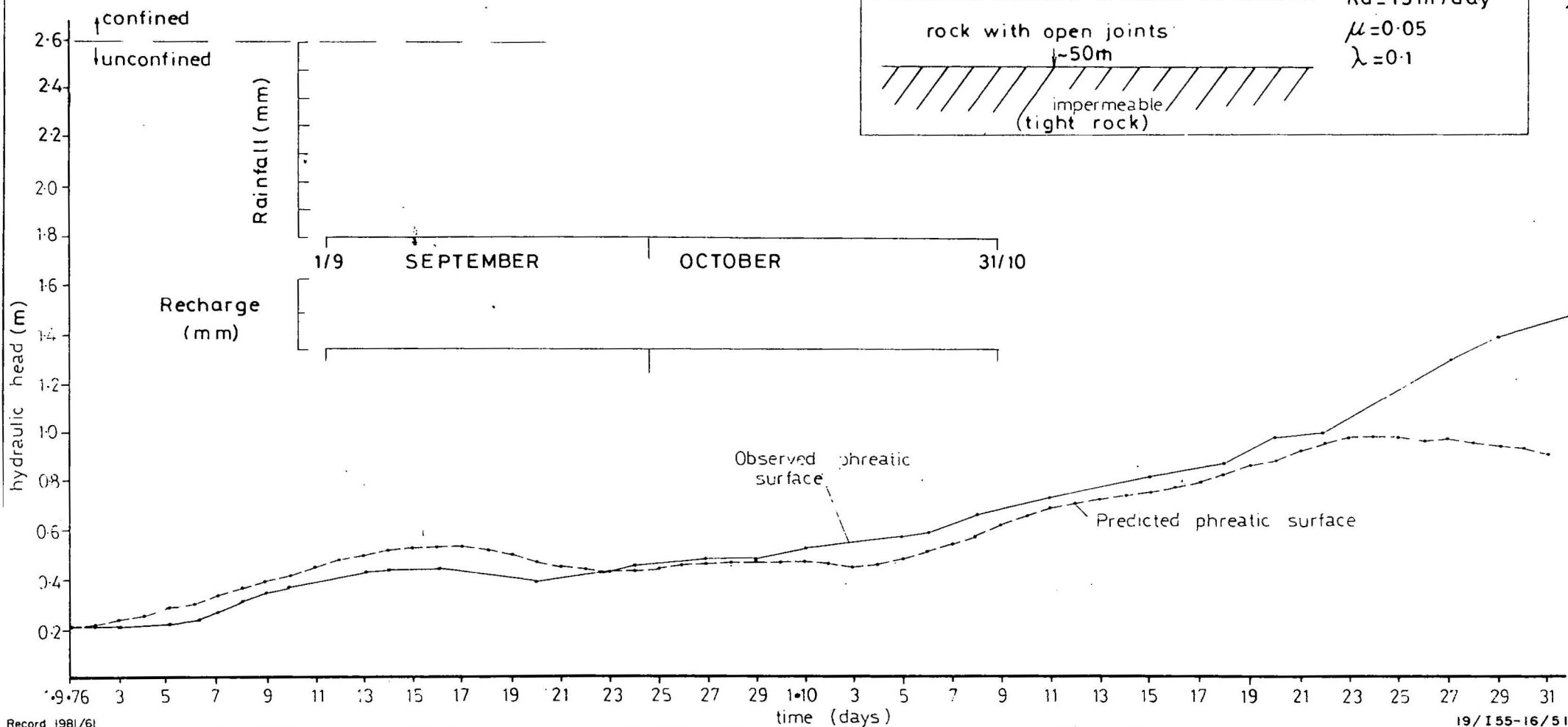


Fig. 63 COMPARISON BETWEEN PREDICTED AND OBSERVED VALUES OF HYDRAULIC HEAD

SOUTH BASIN – BORE 113

Observation period : 1/9/76 – 31/10/76

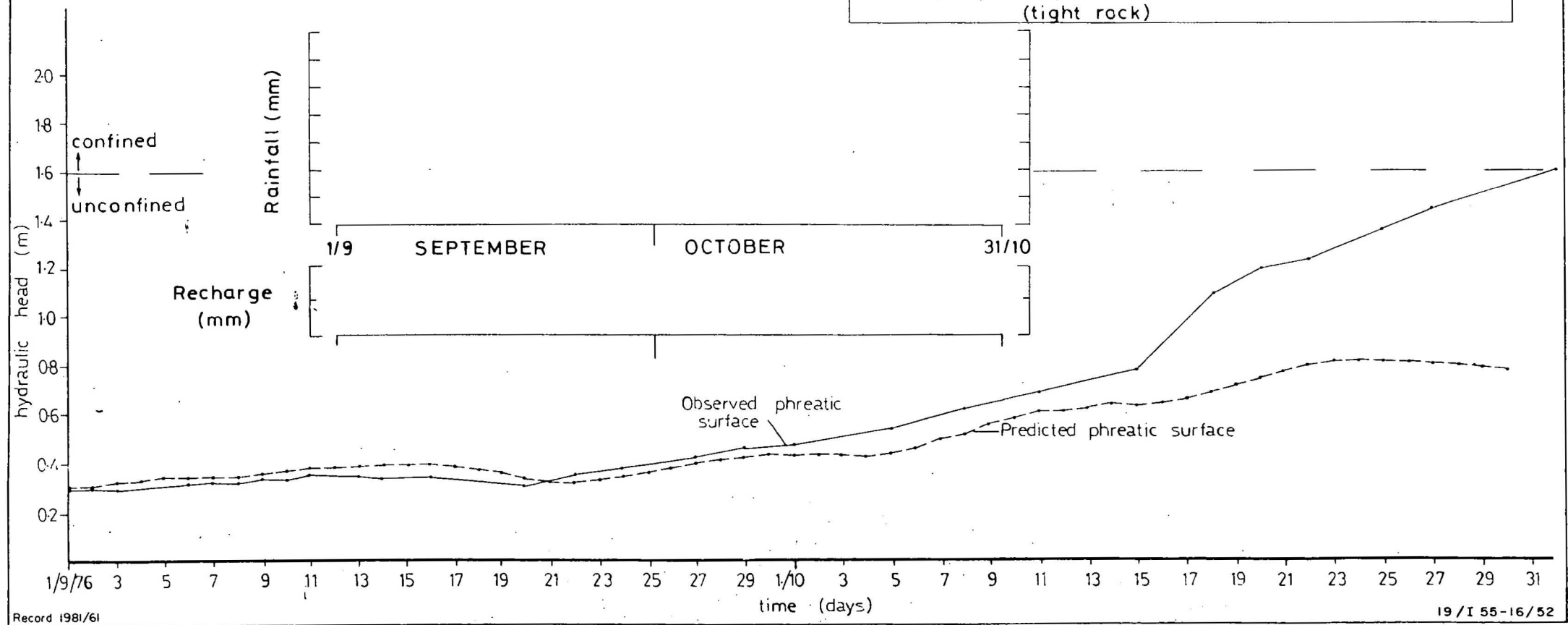
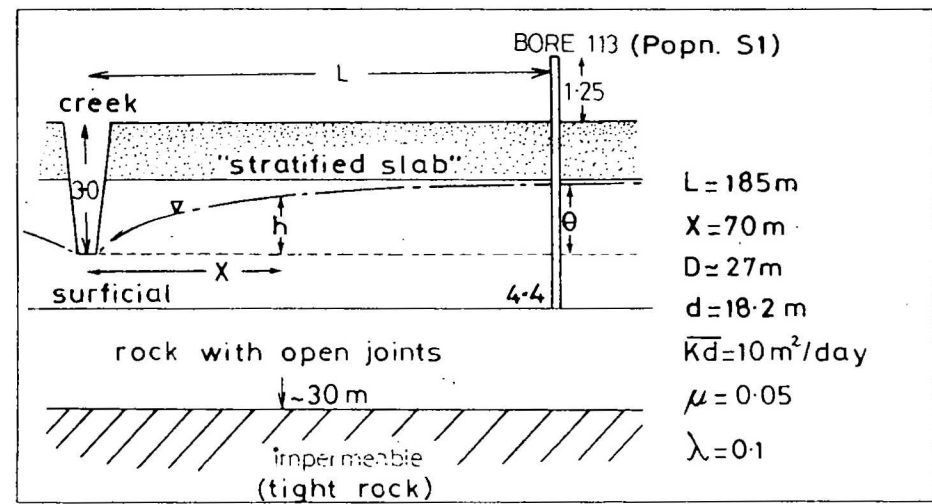


Fig. 64 COMPARISON BETWEEN PREDICTED AND
OBSERVED VALUES OF HYDRAULIC HEAD

NORTH BASIN – BORE 106

Observation period : 1/9/76 – 31/10/76

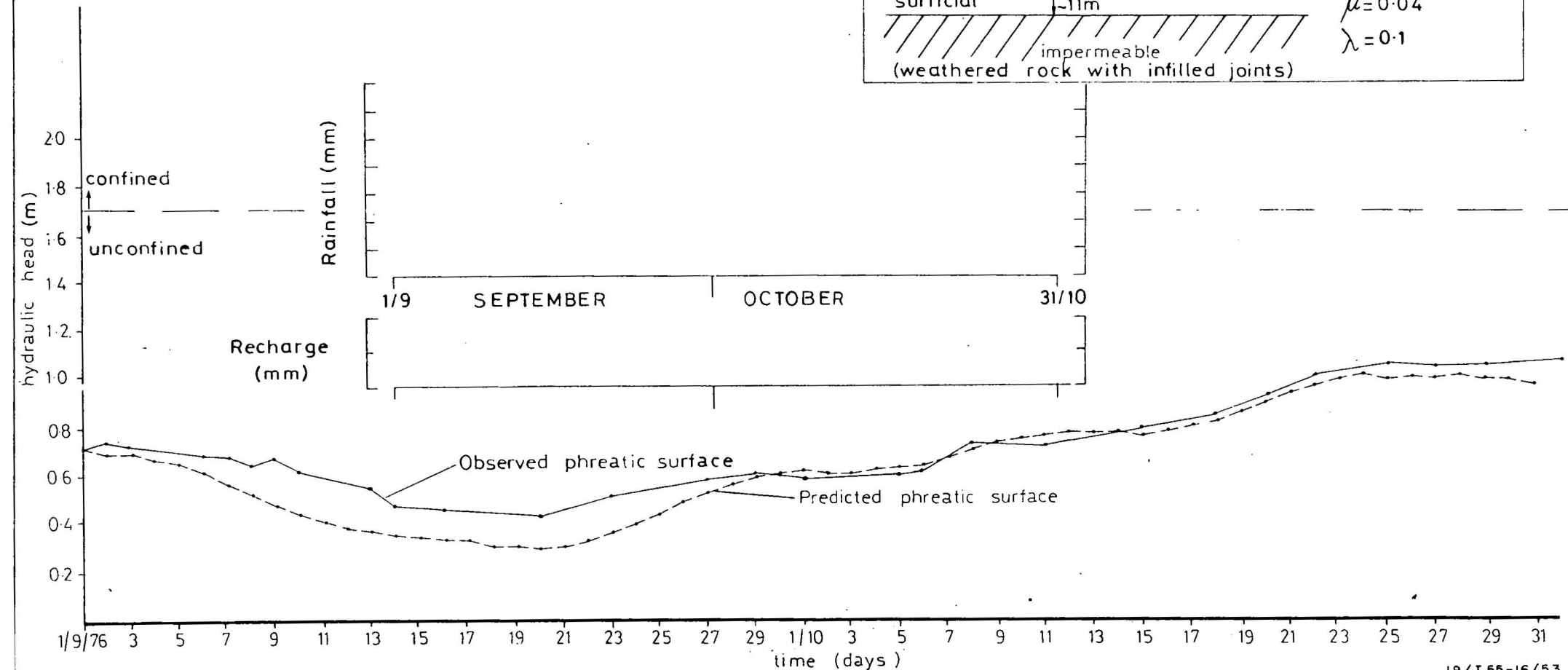
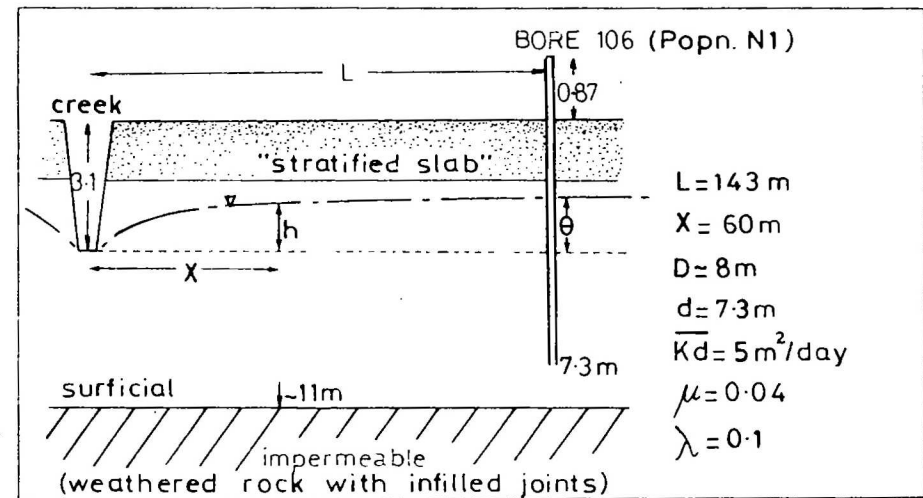
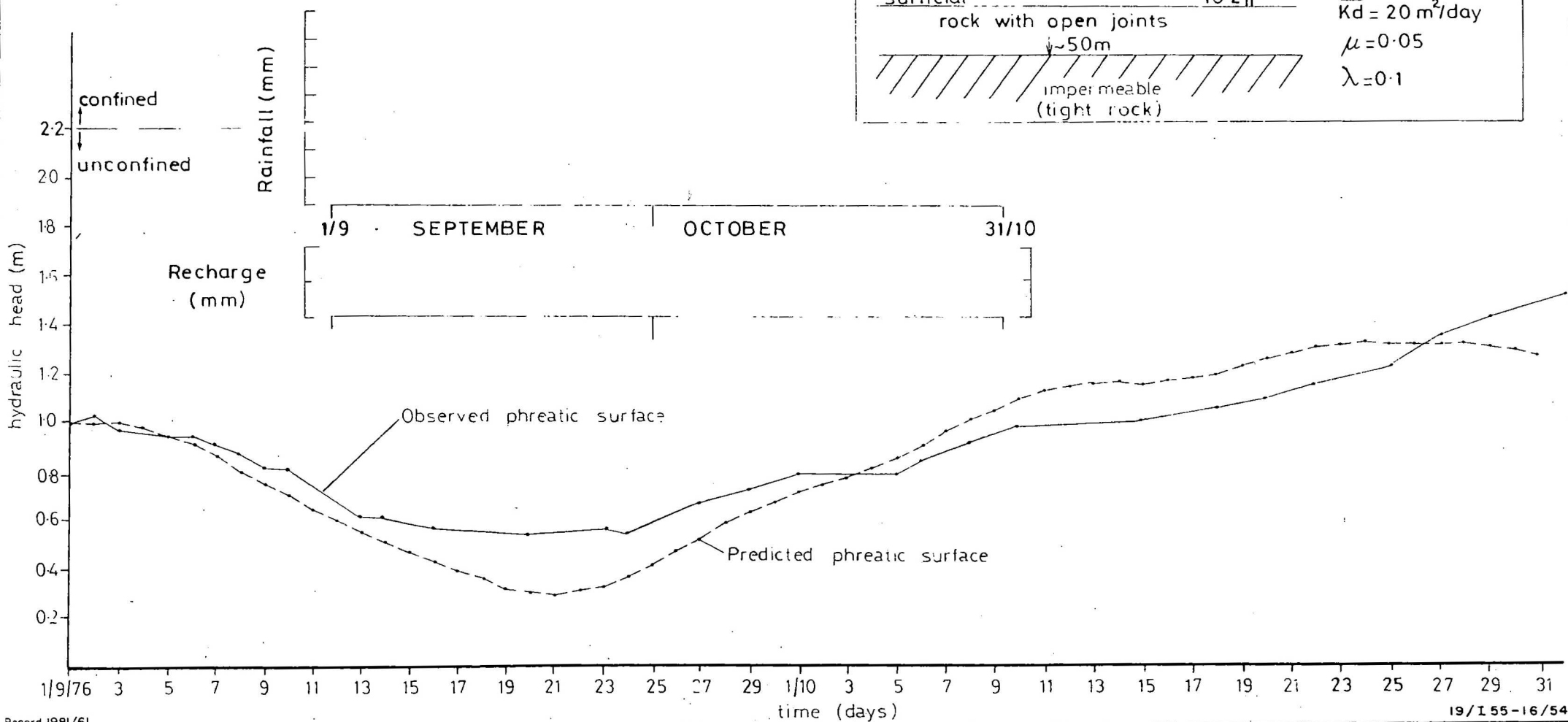
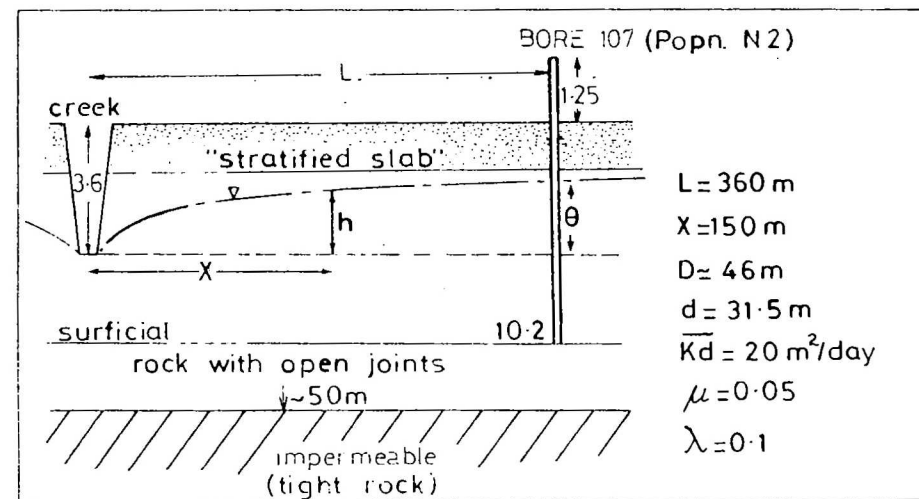


Fig.65 COMPARISON BETWEEN PREDICTED AND
OBSERVED VALUES OF HYDRAULIC HEAD
NORTH BASIN — BORE 107
Observation period : 1/9/76 — 31/10/76



Recommended drain spacings and locations

It has been shown that the model (7) gives satisfactory predictions of water-table fluctuations for $L < \sim 200\text{m}$ and, as a corollary, the stratified slab model which attenuates recharge from rainfall as an input to (7) is also verified. Furthermore, the model predictions for $200 < L < \sim 400\text{m}$ are accurate for small recharge events, but minimise groundwater potentials in times of high recharge for reasons discussed in the previous section.

The problem of optimising drain spacings in the Lanyon basins for any given rainfall event may be resolved by extending the (h,x) plane and placing an image drain at a distance L from the point $x = L$. Thus $\Theta(t)$ becomes the maximum value of $h(x,t)$ midway between two parallel drains spaced a distance $2L$ apart. One dimensional recharge to the system is calculated by the stratified slab model partitioning a rainfall of intensity 0.63 mm/hr. over 120 hours with a recurrence interval of 1 year (Fig. 66) selected from Bureau of Meteorology rainfall statistics for Canberra. Hydrogeological parameters are distributed according to groundwater populations depicted in Figures 44 and 45.

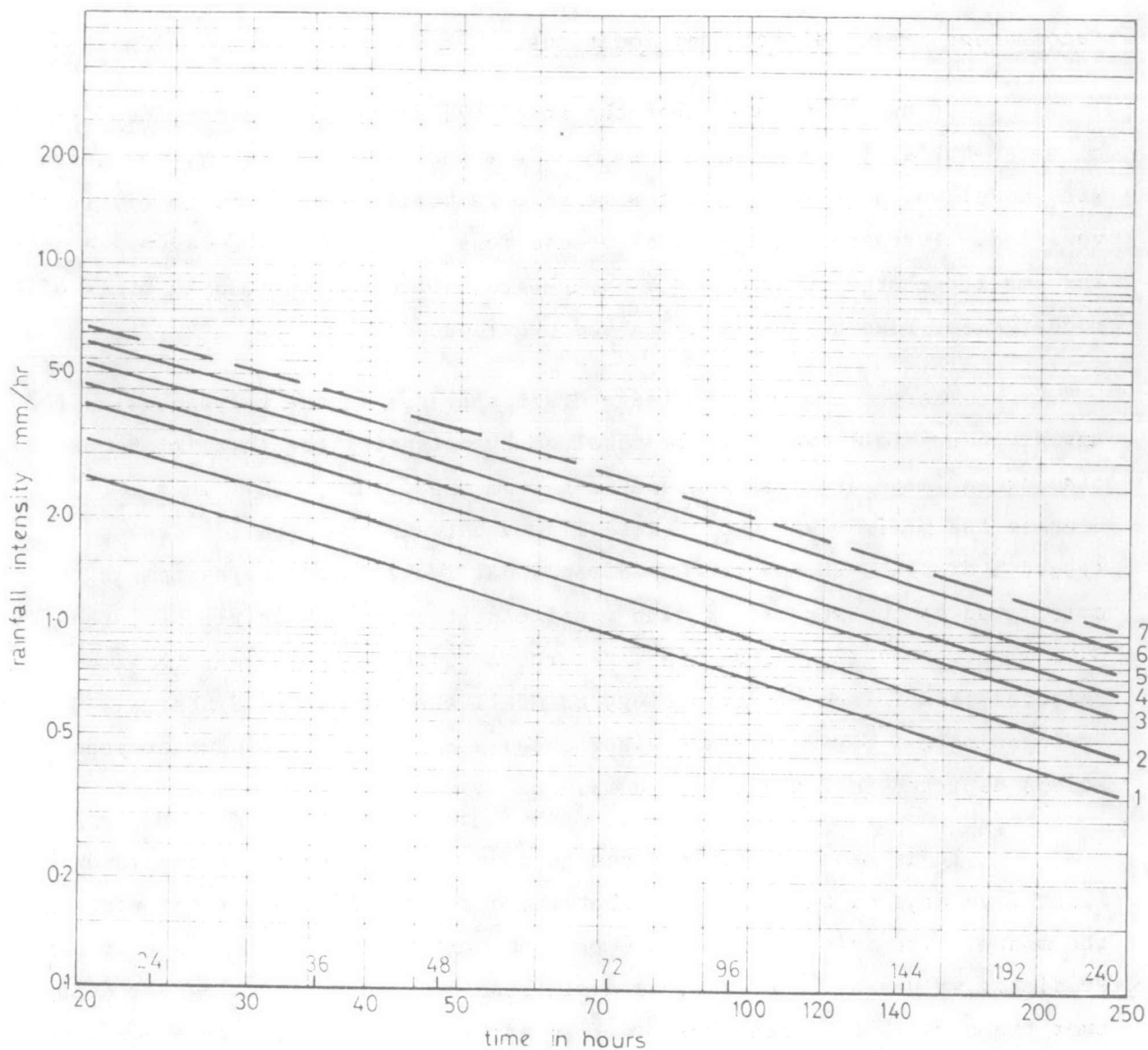
It is assumed that the design rainfall of 0.63 mm/hr occurs on the first five days of the month and that there is no addition for the rest of the month. The initial value of Θ at the start of the month is set at zero. Predicted values of Θ for various drain spacings and hydrogeological domains over the next 30 days are shown in Figures 67 to 69, and the data are synthesised in terms of periods of exceedance of height of the maximum point of the water-table above the drain axis in Figure 70.

It is apparent from Figure 70 that, should the design rainfall occur, drains 3 m deep spaced about $2L = 200\text{ m}$ apart or, for example, drains 4 m spaced 300 m apart, would be required to prevent the highest point of the water-table from rising above 1 metre below ground surface in populations N1 and S2. The same constraint requires drains 3 m deep spaced about 420 m apart or drains 4 m deep spaced about 480 m apart in population S1 (Fig. 68). For population N2 the requirements are drains 3 m deep spaced about 450 m apart or drains 4 m deep spaced about 600 m apart (Fig. 69).

The above results specify a required drain spacing in a particular groundwater population which is recharged by a hypothetical rainfall event.

Fig. 66

- 140 -



CURVE LEGEND
(top to bottom)

- 7 - ONCE IN 100 YEARS
- 6 - ONCE IN 50 YEARS
- 5 - ONCE IN 20 YEARS
- 4 - ONCE IN 10 YEARS
- 3 - ONCE IN 5 YEARS
- 2 - ONCE IN 2 YEARS
- 1 - ONCE IN 1 YEAR

**RAINFALL INTENSITY FREQUENCY
DURATION DIAGRAM**

24 - 240 hours

SOURCE: BUREAU OF METEOROLOGY

Fig. 67 PREDICTED MAXIMUM HEIGHTS OF THE PHREATIC SURFACE FOR VARIOUS DRAIN SPACINGS

Groundwater populations S2,N1.

($\bar{K}d = 5\text{m}^2/\text{day}$, $\bar{\mu} = 0.04$, $\theta_o = 0$)

Design rainfall 0.63 mm/hr. for 120 hrs.

Recurrence interval 1 year

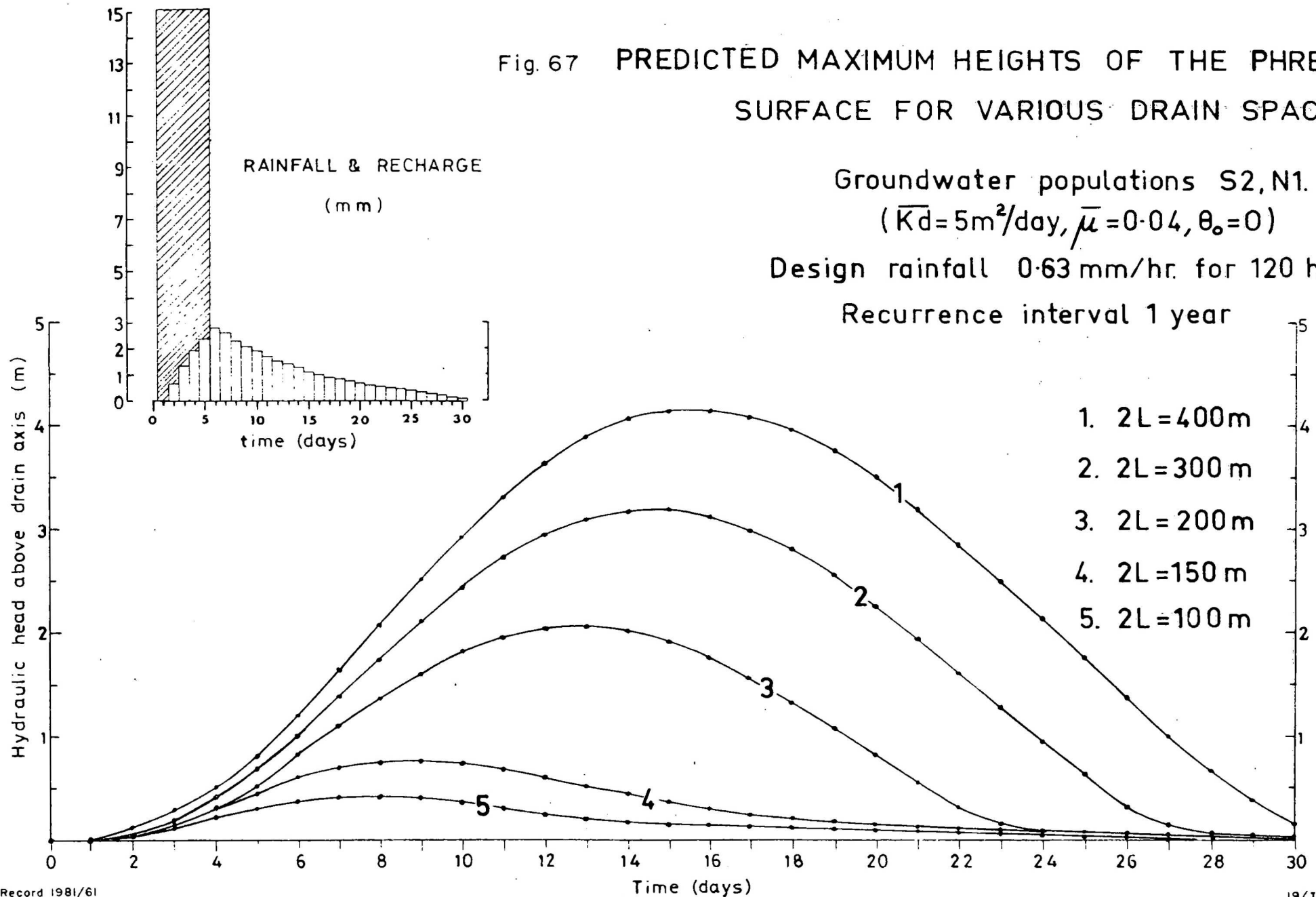


Fig.68 PREDICTED MAXIMUM HEIGHTS OF THE PHREATIC SURFACE FOR VARIOUS DRAIN SPACINGS

Groundwater population S1
 $(\bar{Kd}=15\text{m}^2/\text{day}, \bar{\mu}=0.05, \theta_0=0)$

Design rainfall 0.63 mm/hr. for 120 hrs.

Recurrence interval 1 year

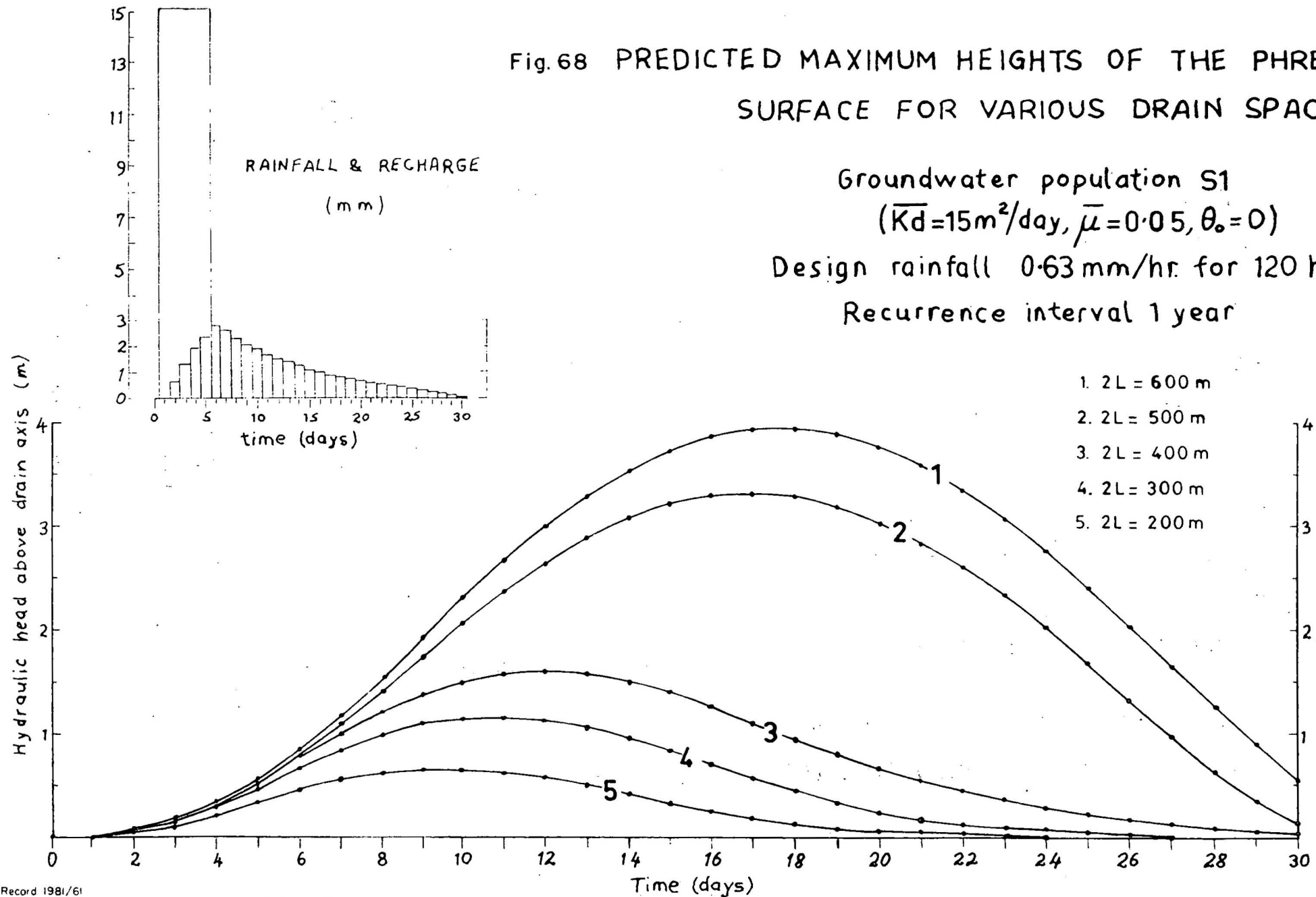


Fig. 69 PREDICTED MAXIMUM HEIGHTS OF THE PHREATIC SURFACE FOR VARIOUS DRAIN SPACINGS

Groundwater population N2
 $(\bar{Kd}=20\text{m}^2/\text{day}, \bar{\mu}=0.05, \theta_0=0)$

Design rainfall 0.63 mm/hr for 120 hrs.

Recurrence interval 1 year

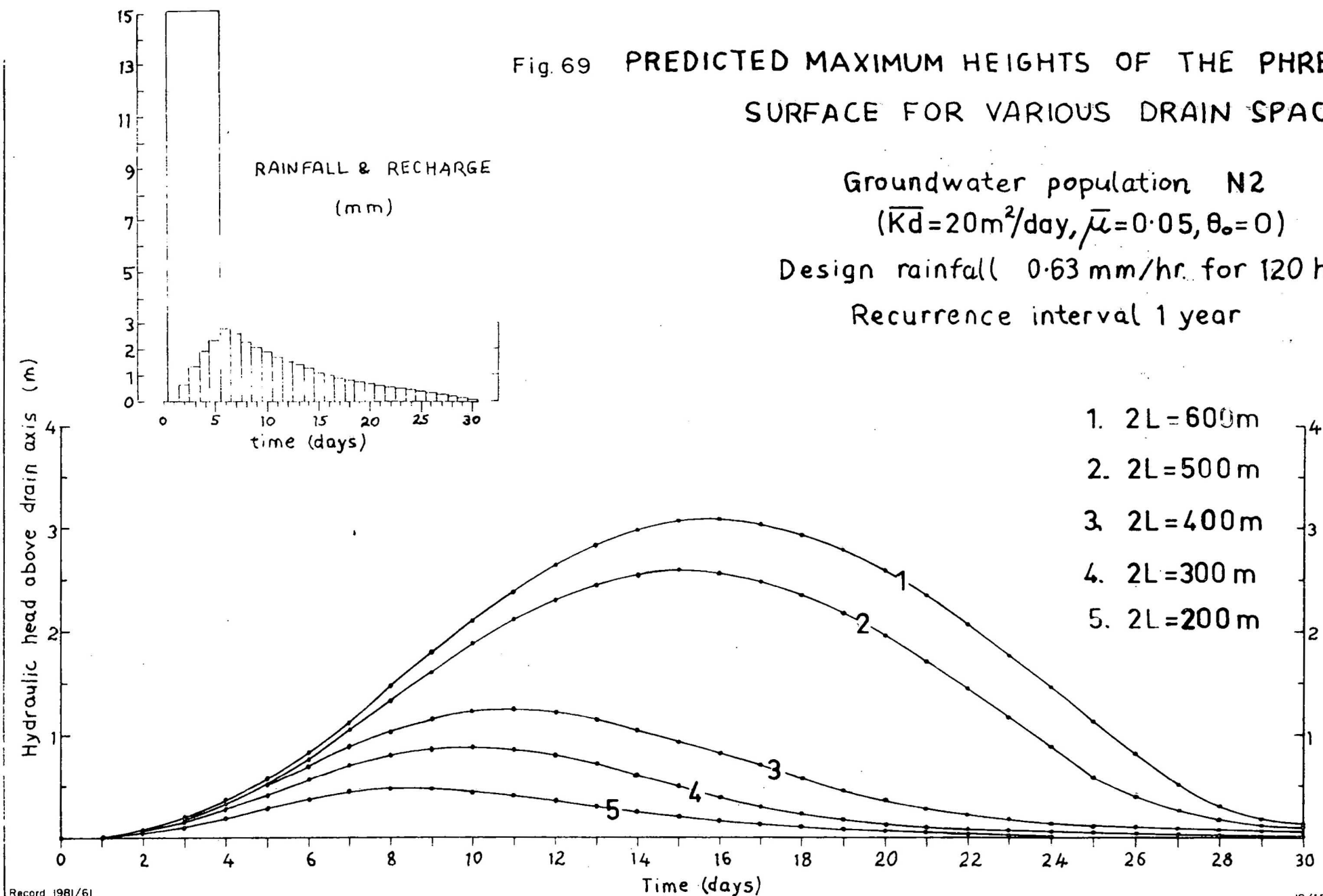
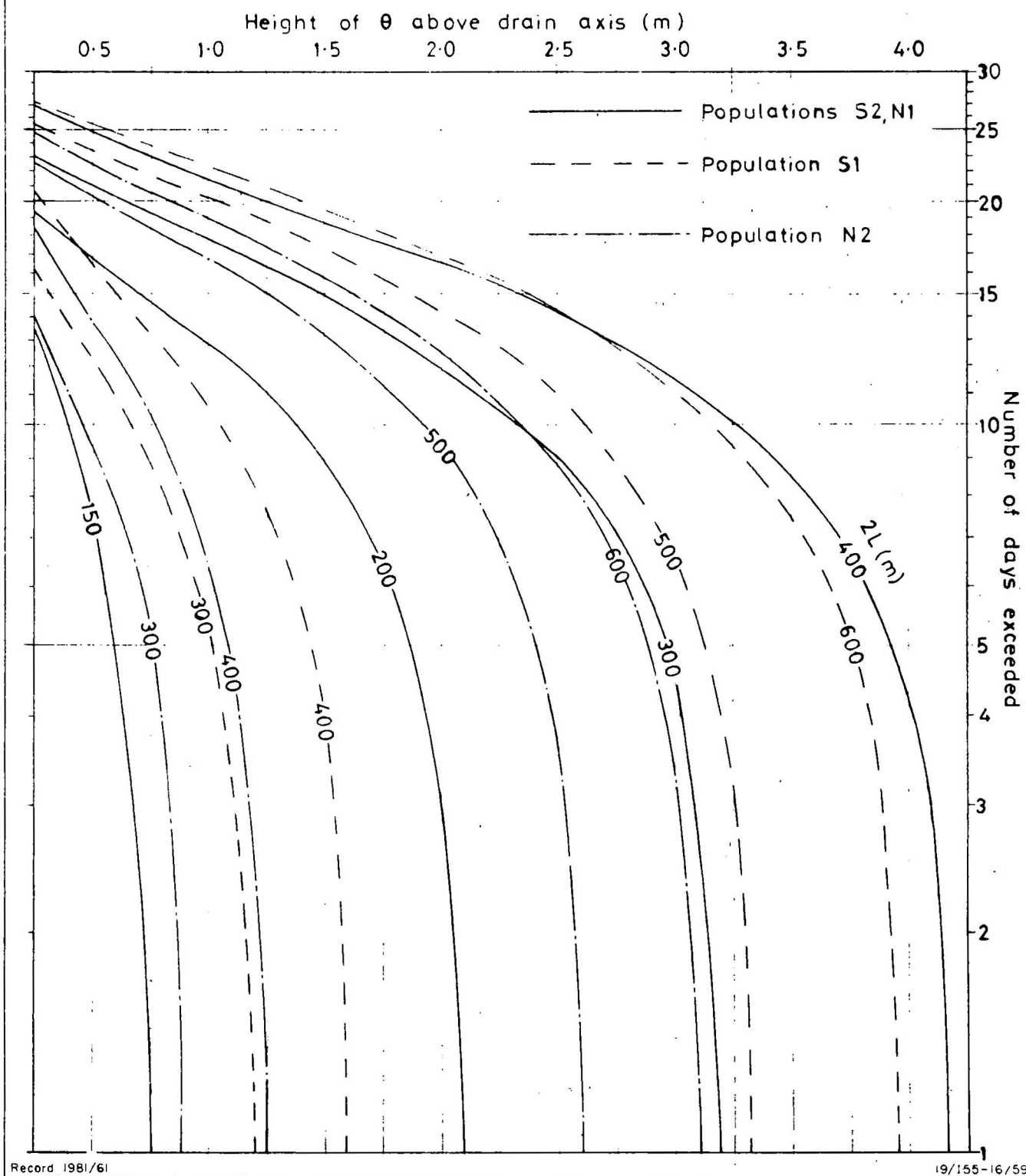


Fig. 70

Periods of exceedance of given maximum values of the phreatic surface over 30 days for a rainfall of 0.63 mm/hour over the first 120 hours of the month for various drain spacings.



The locations of drains within a population are constrained by the necessity to intersect groundwater mounds, caused either by upwards leakage in response to a potential difference or by surface recharge and piping where streams lose definition. In the south basin the drains must transect the neighbourhoods of bores 26, 117, 25, and 30 for maximum effectiveness; in the north basin drain locations are similarly fixed in the vicinities of bores 123, 12, and 5.

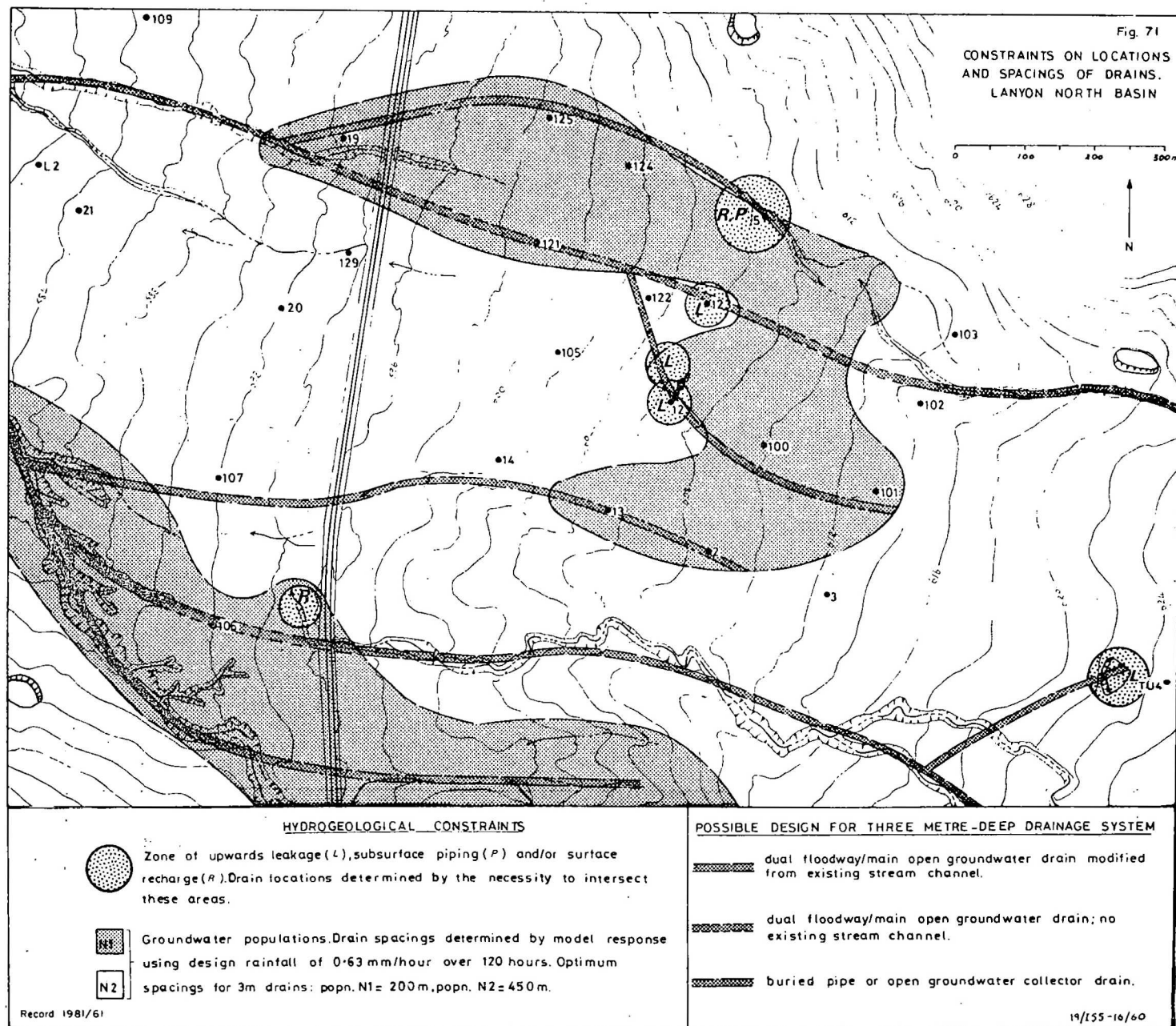
Hydrogeological constraints on drain locations and spacings for the north and south basins are shown in Figures 71 and 72 respectively; a tentative design for drains 3 m deep is also included. Obviously there are, in addition, urban planning constraints which would influence drain locations; these are not considered in this report. Therefore the final decisions of spacings, depths, and locations of groundwater drains can be made only by NCDC when considering the overall urban development strategy of Lanyon.

Note that the drain spacings discussed above are for conventional open ditches with a permeable base as constructed elsewhere in the Tuggeranong valley. The spacing varies slightly for buried pipe drains because of a small variation in the equivalent depth d , caused by a change in u , the wet perimeter of the drain.

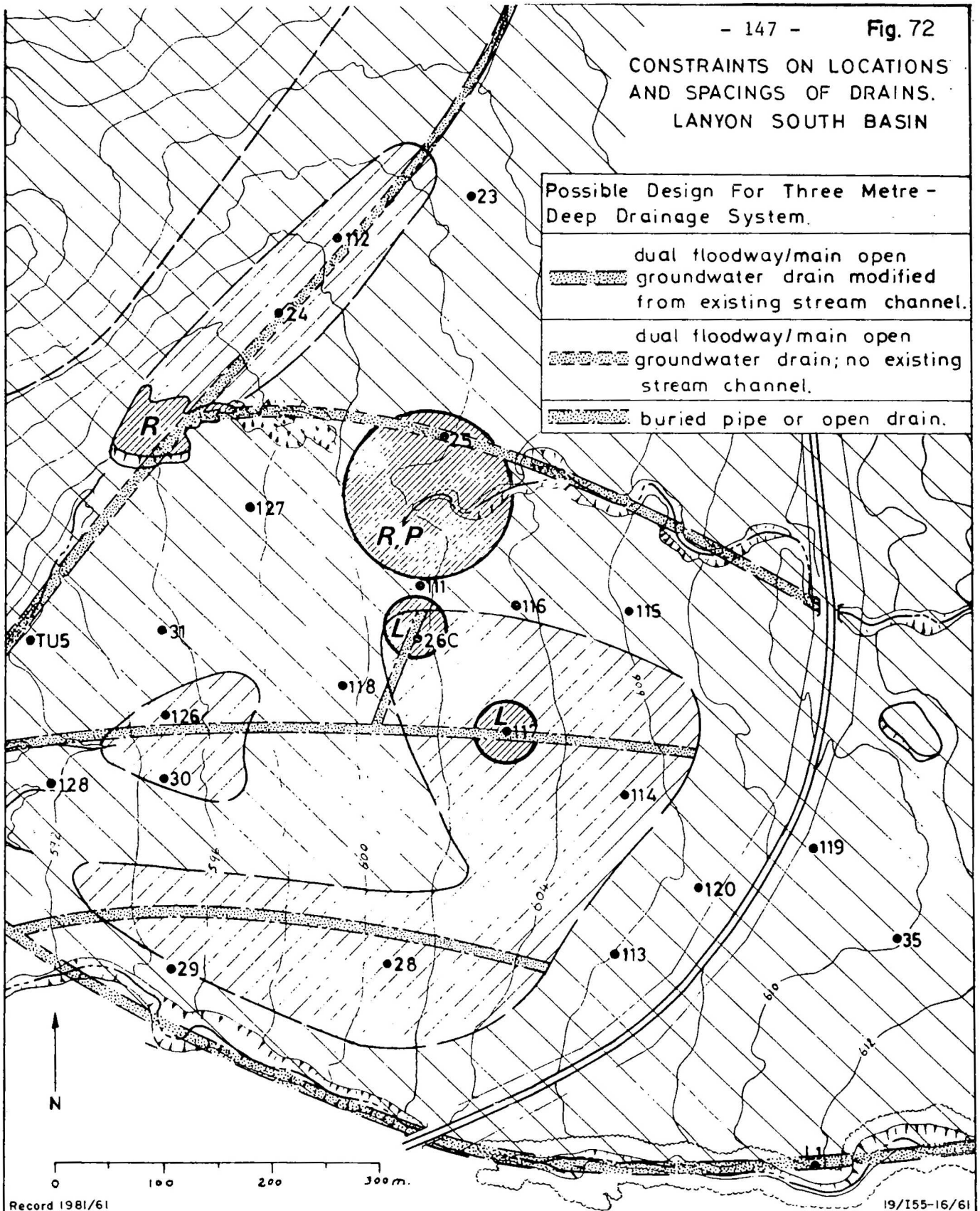
Groundwater monitoring after urban development

Little is known about changes to the groundwater regime following urban development of a rural catchment. The hydrogeological parameter most likely to be affected by urbanisation is recharge which would be increased in certain areas of the suburbs and parklands by lawn and garden watering supplementary to rainfall. Trenches for urban stormwater and sewage services will mostly be dug in the lower B horizon of the Lanyon clay or subsolum; these conduits will provide line sinks to increase the gross infiltration and storage capacity of the soil per unit area, but they will also serve to depress perched water-tables. On the other hand, the impermeable areas created by roadworks and buildings will substantially reduce available surface area for infiltration.

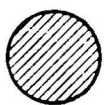
An important component of the hydrogeological system which provides one of the main driving forces to the basin hydrodynamics will remain largely unchanged by urban development. This is the recharge into the



CONSTRAINTS ON LOCATIONS
AND SPACINGS OF DRAINS.
LANYON SOUTH BASIN



HYDROGEOLOGICAL CONSTRAINTS



Zone of upwards leakage (L), subsurface piping (P) and/or surface recharge (R). Drain locations determined by the necessity to intersect these areas.



Groundwater populations. Drain spacings determined by model response using design rainfall of 0.63 mm/hour over 120 hours. Optimum



spacings for 3m drains: popn. S1 = 420 m, popn. S2 = 200 m.

fractured-rock aquifer in the perched basin and hills of the eastern part of the catchments which lie above the area affected by urbanisation.

A substantial pre-development data base exists for the Lanyon basins, and groundwater levels will continue to be recorded, but at a reduced frequency (about 3 to 4 times per year) up to the period of drain installation. In order to obtain the maximum benefit from the Lanyon investigation it is proposed that certain bores be preserved after urban development to assess changes to the hydrogeological system. Preservation of about five of the fractured-rock bores and a similar number of surficial piezometers in each basin would be desirable. It is to be hoped that the wholesale destruction of pre-development monitoring bores in the Tuggeranong valley urbanisation program can be avoided at Lanyon through close consultation between the civil engineer and hydrogeologist, especially during the initial land-clearing phase.

CONCLUSIONS

(1) Geology

The Lanyon basins are underlain by a gently warped sequence of Upper Silurian dacitic to rhyolitic welded ash-flow tuffs and interbedded sediments. The main structural features are the Murrumbidgee fault to the west and a subparallel high-angle north-trending fault which transects both of the basins. Minor block-faulting has occurred between parallel sets of southeast cross-faults on the upthrown eastern block.

Massive rhyolite dykes form the watershed between the north and south basins. These rocks probably represent vents for the cream rhyolite which forms the Lanyon Hills and much of the high country to the east around Mount Rob Roy.

(2) Jointing

- Four categories of joints exist in the Silurian volcanics;
- (i) open rough-faced extension fractures which store and transmit large quantities of groundwater,
 - (ii) shear joints and (iii) healed joints which do not yield groundwater,
 - and (iv) oblique shear joints which are poor but significant transmitters of groundwater.

. At least two major phases of fracture development are evident from observed age relationships of joints in outcrop and from geometrical considerations in stereographic plots of centroids of joint set concentrations.

. Reversals in directions of the principal stresses during successive stages of joint development occur in all lithological domains.

. Gross differences in successive principal stress directions are believed to define former regional compressive and tensile fields, whereas smaller-scale rotation of sets from one domain to the next is attributed to jostling on the major fault zones.

. The regional history of brittle deformation inferred from the analysis of joints is consistent with a model of epeirogenic uplift and erosional unloading in rocks which contain residual tectonic stresses.

. The most important joints in the hydrogeological sense are the youngest tensile fractures, which dip at less than 25° . It appears that significant recharge to these fractures occurs via intersecting older high-angle extension joints and oblique shear joints.

(3) Geomorphology

. The Lanyon north and south basins are developed on the lowest pediplains of an ancient stepped landsurface of parallel escarpments and planar surfaces extending from the Murrumbidgee River to Mount Rob Roy.

. Escarpments are formed in the densely welded zones of the ash-flow tuffs, and benches are developed in partially welded or non-welded zones.

. Remnants of planar surfaces at 900 m to 920 m elevation in the eastern part of the basins' catchments may be equivalent to the Monaro landsurface.

. A perched basin of mean elevation 850 m is preserved on the Molonglo landsurface above the south basin.

. A prominent break of slope at 650 m generally coincides with areas of deep chemical weathering and may be equivalent to the level of the Yass-Canberra tablelands which suffered almost complete reduction by subsequent pediplanation.

. The north and south basins are developed on a pediplain equivalent to the Yarralumla landsurface. Headward encroachment into the north basin by the northern pediment of the south basin has brought about the capture of several ancestral north basin streams.

. Five minor geomorphic surfaces (pediment, bajada, and three basin fill insets) are superimposed onto the Yass-Canberra and Yarralumla landsurfaces. Each geomorphic surface possesses a unique sequence of pedoderms, and is a surface expression of Cainozoic landscape modifications associated with intense periods of erosion and deposition of the surficial mantle.

(4) Surficial geology

. Seven pedoderms are recognised in the Lanyon basins.

. The Rob Roy pedoderm consists of prior braided stream deposits of lithic and feldspathic quartz arenites buried deep beneath Quaternary sediments in the north basin. Wood fragments have been identified in lenses of carbonaceous mud at the base of the sequence. The small elevation difference between the base of the pedoderm and the Murrumbidgee River suggests that a wedge of the north basin was downthrown during Cainozoic movement on the Murrumbidgee Fault and on some of the major cross-faults.

. The Murrumbidgee pedoderm is composed of a basal fanglomerate overlain by massive sheetwash sands. Relict complex cutans, multidirectional veining, joint planes, infilled channels, and a high degree of iron oxides segregation in the matrix are characteristic subsolum features. The Murrumbidgee pedoderm records an initial period of fan building with a dominant fluvial component passing into a mature stage of sheetflood deposition.

. The Tuggeranong pedoderm commenced with a period of renewed fan building and fluvial deposition of fanglomerates in the basins. The pedoderm extends upwards through fine sands to a dense plastic clay which may have been derived from an aeolian blanket. The Tuggeranong clay catena grades from a soloth in elevated positions to a solodic soil in the hydromorphic environment of the basins where it forms the highest (and oldest) terrace, or basin fill level. Subsolum features consist of distinctive mottling patterns and vertical clay veins. The initial pedogenetic environment was one of moderate aridity, but in many places there was substantial mineralogical modification to the solum

during subsequent moister climatic phases.

. The Lanyon pedoderm was deposited during a period of vigorous secondary planation of the Tuggeranong basin fill surface. Slopewash sheets on the footslopes grade into braided stream deposits of open gravels buried beneath a fining-upwards floodplain sequence. The Lanyon pedoderm defines the younger basin fill level. Pedogenesis was under humid conditions, probably with highly seasonal rainfalls, in which a catenary sequence of podzolics, lateritic podzolics, and latosols developed on the slopes. A strongly structured solodic soil, the Lanyon clay, developed under hydromorphic conditions in the basins.

. The Big Monk pedoderm, a yellow podzolic developed on slopewash sheets and colluvial fans, was deposited during a period of severe mass wastage of the regolith, apparently induced by the onset of periglacial conditions. A solodic soil is developed under hydromorphic conditions in the youngest basin fill inset. Subsolum patterns are sparse.

. The Gigerline pedoderm represents a return to periglacial conditions in which hillslope instability was most pronounced on southwesterly slopes. Brown earths developed on colluvial sheets on the hillslopes, and grey earths formed on a veneer of sand-size detritus uniformly distributed over all the basin fill surfaces. Red earths formed on aeolian sands blown up from the bed of the Murrumbidgee River.

. The Riverside pedoderm represents the last recognised period of landscape instability before European settlement. Prairie soils were developed on alluvial terraces in the eastern parts of the basins, but sedimentation rates in the western sectors were sufficiently slow and of such small magnitude that continuing pedogenesis was able to incorporate detritus into cumulic profiles of the older pedoderms.

(5) The perched basin

. The combination of a dominant southerly aspect and a mean increase in elevation of over 200 m has resulted in a greater susceptibility to mass wastage in the regolith of the perched basin during periglacial maxima. Surficial units older than the Big Monk pedoderm have been almost completely stripped.

/

. Soils of the perched basin are more gravelly than the equivalent units of the north and south basins, and their distribution appears to have been determined to a greater degree by slumping and solifluction processes.

. The valley section of the perched basin is characterised by a stepped rock-cut profile which resembles immature cryoplanation terraces and which appears to have developed contemporaneously with the Big Monk pedoderm.

(6) The hydrogeological system

. The Lanyon basins contain a complex system of leaky surficial aquifers hydraulically connected to the underlying fractured-rock aquifer.

. The most significant surficial aquifers in the basins are the Lanyon gravels; most of the major soaks of the lower basin surfaces occur where buried palaeochannels of Lanyon gravels lens out against much lower-permeability material.

. The aquitard which offers the greatest impedance to vertical transmission of groundwater is extremely weathered bedrock surfaces with clay-filled joints.

. There are five distinct hydrogeological domains in the basins.

Domain I is the discharge zone of the fractured-rock aquifer at the western ends of the basins, and its boundaries are relatively constant with time.

Domain II comprises the poorly drained areas of the lower basin surfaces where groundwater is transmitted upwards from confined surficial aquifers to phreatic aquifers. Its boundaries vary in accordance with antecedent precipitation, but dynamic equilibrium is attained at point sources.

Domain III defines areas of intensive mixing of groundwaters from surficial aquifers and the fractured rock, and is highly responsive to rainfall.

Domain IV represents areas where significant downwards leakage occurs from the surficial aquifers to the underlying fractured rock.

Domain V comprises the higher slopes and escarpments where the fractured rock receives direct recharge from rainfall. Much of this recharge is transmitted by deep circulation to domain I.

(7) Surface water-groundwater interaction

. Most of the streams which drain the north and south basins are unable to effectively conduct surface runoff through the basins without flooding

because of discontinuities in their channels. The streams are important line sources and sinks which greatly influence the hydrodynamics in both basins.

. Groundwater mounds are generated in the eastern part of the north basin where the northernmost stream loses definition and recharges surficial aquifers by surface outwash and subsurface piping from bed underflow.

. Streams which drain the western part of the north basin are natural groundwater drains with low radial resistance to drainage from the surficial aquifers. They flowed for most of the time between September 1974 and December 1976.

. The central east-west stream in the south basin discharges its flow over the ground surface near the centroid of the basin, and sustains a major swamp to the south of its terminus by piping of bed underflow water into the Lanyon gravels.

. The southern stream of the south basin is the only one in either basin which has a continuous channel from the head to the toe of the basin. It affords moderate radial resistance to groundwater drainage and its discharge was permanently sustained by baseflow from September 1974 to December 1976.

. The western stream channel of the south basin is a line sink for groundwaters in surficial aquifers of the northern pediment. It recharges the large farm dam on the western boundary by seepage down gradient from where its channel loses definition.

(8) Hydraulic continuity of the aquifers

. The distribution of correlation coefficients between water-level variations in fractured-rock aquifers and in surficial aquifers in the south basin implies four hydrogeological populations. Existence of populations has been verified by hypothesis testing using Fisher's Z transformation on the sample correlation coefficients to satisfy the condition of underlying normality.

. Piezometers whose groundwater potentials have a high correlation with corresponding potentials in the fractured rock of the discharge zone of the south basin comprise a population where there is direct hydraulic

connection between the surficial aquifers and the fractured rock. The common factor in this population is that the rock has open joints extending to the soil/rock interface to permit groundwater leakage.

. Piezometers with low to moderate correlation with the fractured rock define a population in which groundwater mixing is impeded by an ancient weathering surface of extremely weathered rock with clay-filled joints.

. The zone of surface recharge and bed underflow near the centroid of the south basin is delineated by a population whose surficial piezometer has a very low correlation with fractured-rock bores in the recharge and discharge zones of the basin.

. A fourth groundwater population in the south basin is defined by the radius of influence of the deeply incised southern stream, where the correlation coefficients decrease in proportion to distance away from the stream.

. Hypothesis testing in the north basin confirms a trimodal distribution of correlation coefficients, but a physical interpretation of the partitioning is difficult because the regressor variables are the groundwater potentials in the fractured-rock bore of the recharge zone.

(9) Infiltration

. Steady infiltration rates of the Riverside and Gigerline pedoderms range from 10 mm/hour to 15 mm/hour at field capacity. Replication in both basins produced consistent results for the Gigerline grey earth for all antecedent moistures, but infiltration rates for the Riverside prairie soil was highly dependent upon vegetation.

. One-dimensional infiltration capacities of the Lanyon clay are highly variable and depend considerably on the geometry and continuity of cracks. For low antecedent moisture, infiltration is dominated by rapid gravity flow down open cracks and along ped faces for about the first hour, until ped and plane cutans swell and partially close voids. Soaking of up to 2 to 3 weeks is required before moisture becomes uniformly distributed through peds.

. Infiltration rates in the Lanyon clay are maximised in the highly structured upper B horizon, and are minimised in the less organised lower B

horizon despite its much higher mean grainsize. The soil's structure is stable for alternating wetting and drying and there was no visible slaking of peds through the tests.

. Infiltration tests conducted in cylinders which were not removed from the ground were unreliable because of lateral potential gradients and delayed expulsion of entrapped air.

(10) Effective porosities

. Effective porosities for a rising water-table in a soil close to field capacity range from 1% in the lower B horizon of the Lanyon clay to 8% in the Riverside pedoderm.

(11) Recharge from rainfall

. Observed piezometer response to rainfall indicates that the simplest model describing leakage of infiltrated waters stored in a stratified modal sequence of pedoderms in the Lanyon basins is one in which the rate of leakage to the underlying aquifers is proportional to the head of water in storage.

. The recharge model partitions hourly rainfall into infiltration and interflow-surface runoff/storage. Estimates of the velocity of the wetting front are made using mean values of effective porosities and infiltration rates for each layer of the stratified slab.

. A threshold rainfall value of 5 mm is required before groundwater recharge occurs. Amounts less than this are wholly absorbed by interception and soil storage.

(12) Hydraulic conductivities

. Pump tests in the Lanyon gravels indicate that the cone of depression around the pumping well becomes elliptical in time with the long axis parallel to the trend of the palaeochannel containing the gravels before delayed yield is induced from the adjacent floodplain sediments.

. Hydraulic conductivities in the Lanyon gravels range from 0.9 m/day to 3.4 m/day (n=8) with a mean value of 2.2 m/day. The sands of the upper facies of the Lanyon pedoderm have a range of K-values from 0.1 m/day to 1.9 m/day (n=9) with a mean of 0.5 m/day.

. Two tests in the fractured-rock bores gave transmissivities of $6.5 \text{ m}^2/\text{day}$ and $9.8 \text{ m}^2/\text{day}$, and indicate a significant delay in yield from storage after several hours pumping. Mean hydraulic conductivity of the fractured rock is 0.5 m/day based on empirical relationships between joint spacings and apertures.

(13) Fluctuations in groundwater potentials

. Potentiometric surface contour maps show permanent groundwater mounds at four point sources in the surficial aquifers in the north basin and at two point sources in the south basin. Mounds are also generated around discontinuities in streams.

. In the north basin, groundwater fluctuations of less than 1 m were experienced around effluent streams, and around point and plane sources in the discharge zone during 1975 and 1976. Variations in head of up to 5 m occurred on the interfluves in the 'alternating' zone of the north basin.

. In the south basin, water-table fluctuations of up to 3 m occurred in the recharge zone on the eastern footslopes during 1975 and 1976. Groundwater potentials are progressively less responsive to changes in recharge from rainfall towards the western end of the basin. Steady-state conditions were attained in the soak around piezometer 26 and within the radius of influence of the westerly stream below the dam.

. The fluctuation map defines flow directions of bed underflow water from the central stream in the south basin. The dominant direction of flow is towards the southwest, where fluctuations are minimised.

(14) Groundwater balances

. The total groundwater recharge rate in the area of the north basin bounded by the northern and southern streams was $285 \text{ m}^3/\text{day}$ on 12 November 1976. Discharge was $220 \text{ m}^3/\text{day}$, of which over 90% was lost from the surficial aquifers.

. The total groundwater recharge rate through the arc of the south basin bounded by the western and southern streams was $360 \text{ m}^3/\text{day}$ on 12 November 1976. Discharge was $275 \text{ m}^3/\text{day}$, of which over 75% was lost from the surficial aquifers.

. Intrabasin deficits between groundwater inflow and outflow were experienced for all flow nets constructed between September 1974 and December 1976. The losses represent a continuing withdrawal from within the system by phreatophyte transpiration and evaporation from free-water surfaces which are charged by groundwater.

(15) Remedial drainage for urban development

. Sustained high groundwater potentials in certain areas of the north and south basins show that the existing natural drains are spaced too far apart and are not deeply enough incised to adequately drain the surficial aquifers for urban development.

. Comparisons between predicted and observed values of hydraulic head show that an analytical solution to the non-homogeneous diffusion equation in one spatial dimension is sufficient to simulate groundwater fluctuations in response to intermittent recharge for distances less than 200 m away from drainage channels.

. For large recharge events the analytical solution underestimates values of hydraulic head for distances greater than 200 m away from the drains, mainly because of an extraneous flow component parallel to the drain which the one-dimensional model does not take into account.

. The stratified slab model which partitions rainfall into interflow/storage and recharge is verified. The assignment of hydrogeological parameters according to distribution of populations supported by hypothesis testing of correlation coefficients is also shown to be valid.

. For a design rainfall of 0.63 mm/hour over 120 hours the following drain spacings are required to prevent the water-table midway between two parallel drains 3 m deep from rising above 1 m below ground surface:

populations N1, S2	-	spacing 200 m
populations S1	-	spacing 420 m
population N2	-	spacing 450 m

. Drain locations are constrained by the necessity to intersect the neighbourhoods of permanent groundwater mounds.

RECOMMENDATIONS

The following recommendations concerning remedial drainage of the Lanyon basins are made:

- (1) That the drain spacing model, including the stratified slab model for estimation of the recharge term, be used by the urban planning authorities for predictions of hydraulic head for all design rainfalls and proposed depth-spacing combinations.
- (2) That the neighbourhoods of all the permanent groundwater mounds identified in this report be intersected by drains. In particular, if the point sources of upwards groundwater flow in the surficial aquifers are not tapped by drains then waterlogging in these areas will persist for several weeks or months after significant groundwater recharge.
- (3) That a reasonable number of bores and piezometers be preserved after urban development to monitor changes to the groundwater regime.

ACKNOWLEDGEMENTS

Phil Jones and Geoff Baker provided solid field assistance under difficult conditions during the preliminary investigation in 1974. Marc Audibert (BRGM) was very helpful in the interpretation of pump tests during the preliminary investigation, and it was he who pointed out the necessity for a drain-spacings model. Many useful suggestions and constructive criticisms on hydrological aspects of the project from John Chappell (ANU) were very much appreciated. The author is indebted to Tjerd Talsma (CSIRO) for the loan of infiltration equipment and for his valuable advice on many aspects of unsaturated flow. Much worthwhile discussion occurred in the field with Dik van Dijk and Bruce Butler (CSIRO), and their interest and contribution towards an understanding of the surficial geology is gratefully acknowledged.

REFERENCES

- BLISSENBACH, E., 1954 - Geology of alluvial fans in semi-arid regions. Geological Society of America, Bulletin 65, 175-190.
- BREWER, R., CROOK, K.A.W., & SPEIGHT, J.G., 1970 - Proposal for soil-stratigraphic units in the Australian stratigraphic code. Journal of the Geological Society of Australia, 17. 103-9.
- BUTLER, B.E., 1959 - Periodic phenomena in landscapes as a basis for soil studies. CSIRO, Australia, Soil Publication 14.
- BUTLER, B.E., 1967 - Soil periodicity in relation to landform development in south-eastern Australia. In JENNINGS, J.N., & MABBUTT, J.A., (Editors) - LANDFORM STUDIES IN AUSTRALIA AND NEW GUINEA. Australian National University Press, Canberra, 231-55.
- CALVER, A., KIRKBY, M.J., & WEYMAN, D.R., 1972 - Modelling hillslope and channel flows. In CHORLEY, R.J., (Editor) - SPATIAL ANALYSIS IN GEOMORPHOLOGY. Methuen, London, 197-218.
- COSTIN, A.B., & POLACH, H.A., 1973 - Age and significance of slope deposits, Black Mountain, Canberra. Australian Journal of Soil Research 11., 13-26.
- CRAFT, F.A., 1931 - The physiography of the Shoalhaven River valley. iv. Nerriga. Proceedings of the Linnaean Society of New South Wales, 56, 412-30.
- CRAFT, F.A., 1932 - The physiography of the Shoalhaven River valley, vi. Conclusion. Proceedings of the Linnaean Society of New South Wales, 57, 245-60.
- CRAFT, F.A., 1933 - The surface history of Monaro, N.S.W. Proceedings of the Linnaean Society of New South Wales, 58, 229-44.

- DAVIS, W.M., 1938 - Sheetfloods and streamfloods. Geological Society of America, Bulletin 49, 1337-1416.
- DUNIN, F.X., 1976 - Infiltration: its simulation for field conditions. In RODDA, J.C., (Editor) - FACETS OF HYDROLOGY. Wiley, New York
- FRENCH, H.M., 1976 - THE PERIGLACIAL ENVIRONMENT. Longman, London.
- GOLDSMITH, R.C.M., 1975 - Lanyon trunk sewer, geological investigations, Tuggeranong, A.C.T. Bureau of Mineral Resources, Australia, Record 1975/173 (unpublished).
- GOLDSMITH, R.C.M., 1976 - Murrumbidgee Park Drive, Tuggeranong, A.C.T. Geological investigation. Bureau of Mineral Resources, Australia - Record 1976/106 (unpublished).
- GRAYBILL, F.A., 1961 - AN INTRODUCTION TO LINEAR STATISTICAL MODELS. McGraw-Hill, New York.
- GUTTERIDGE, HASKINS and DAVEY PTY. LTD., 1975 - Preliminary report on drainage of the Lanyon area. Development report prepared for the National Capital Development Commission, Canberra. (unpublished).
- HAAN, C.T., 1977 - STATISTICAL METHODS IN HYDROLOGY. Iowa State University Press.
- HOEK, E., & BRAY, J., 1974 - ROCK SLOPE ENGINEERING. Institute of Mining and Metallurgy, London.
- HOOKE, R. Le B., 1967 - Processes on arid-region alluvial fans. Journal of Geology 75, 438-460.
- IILRI (INTERNATIONAL INSTITUTE FOR LAND RECLAMATION AND IMPROVEMENT), 1972-74, - Drainage principles and applications. IILRI Publication 16, Vols. 1, 2 and 3, Wageningen.

- JACKSON, M.L., & SHERMAN, G.D., 1953 - Chemical weathering of minerals in soils. Advances in Agronomy 5, 219-318.
- KRUSEMAN, G.P., and DE RIDDER, N.A., 1970 - Analysis and evaluation of pumping test data. International Institute for Land Reclamation and Improvement, Wageningen, Bulletin 11.
- MAASLAND, M., 1959 - Watertable fluctuations induced by intermittent recharge. Journal of Geophysical Research, 60. 549-559.
- MAASLAND, M., & HASKEN, H.C., 1958 - The auger hole method of measuring the hydraulic conductivity of soil and its application to tile drainage problems. New South Wales Water Conservation and Irrigation Commission, Bulletin 2.
- MACIAS, T., (in prep.) - Slope stability of Tuggeranong Hill, Lanyon, A.C.T. Bureau of Mineral Resources, Australia - Record (unpublished).
- McDEVITT, W., 1975 - Lanyon subsurface investigations: installation of piezometers and associated soil testing. Department of Housing and Construction, Australia, Central Testing and Research Laboratories Report 144.
- MENDUM, J.R., 1975 - Geological investigation of Tuggeranong damsite, Murrumbidgee River, A.C.T., 1968 - Bureau of Mineral Resources, Australia, Record 1975/38 (unpublished).
- MILLER, D.E., & GARDNER, W.H., 1962 - Water infiltration into stratified soil. Proceedings of the Soil Science Society of America, 26, 115-19.
- OPIK, A.A., 1958 - The geology of the Canberra City district. Bureau of Mineral Resources, Australia, Bulletin 32.
- PIERREHUMBERT, C.L., 1974 - Point rainfall intensity-frequency-duration data. Bureau of Meteorology, Australia, Bulletin 49.

- PRICE, N.J., 1966 - FAULT AND JOINT DEVELOPMENT IN BRITTLE AND SEMI-BRITTLE ROCK. Pergamon Press, London.
- STACE, H.C.T., HUBBLE, G.D., BREWER, R., NORTHCOTE, K.H., SLEEMAN, J.R., MULCAHY, M.J., & HALLSWORTH, E.G., 1968 - A HANDBOOK OF AUSTRALIAN SOILS. Rellim, Glenside, South Australia.
- TALSMA, T., 1963 - Methods of measuring water-table depth and pressure levels. Fifth Congress, International Commission on Irrigation and Drainage, 17.1-17.11.
- TALSMA, T., 1974 - The effect of initial moisture content and infiltration quantity on redistribution of soil water. Australian Journal of Soil Research, 12, 15-26.
- VAN BEERS, W.F.J., 1958 - The auger hole method. International Institute for Land Reclamation and Improvement, Wageningen, Bulletin 1.
- VANDENBROEK, P.H., 1974 - Engineering geology of Tuggeranong town centre, A.C.T. Bureau of Mineral Resources, Australia, Record, 1974/184 (unpublished).
- VAN DIJK, D.C., 1959 - Soil features in relation to erosional history in the vicinity of Canberra. CSIRO, Australia, Soil Publication 13.
- VAN DIJK, D.C., 1969 - Pseudogley in Gundaroo subsola, southern tablelands, N.S.W. Australian Journal of Soil Research, 7, 143-61.
- VAN DIJK, D.C., RIDDLE, A.M.H., & ROWE, R.K., 1968 - Criteria and problems in groundsurface correlations in south-eastern Australia. Transactions of the Ninth International congress on Soil Science, 4, 131-8.

- VAN DIJK, D.C., & WOODYER, K.D., 1961 - The soils of the Yass River valley. CSIRO, Australia, Regional Research and Extension Study, Southern Tablelands, N.S.W., Report 6.
- VAN SCHILFGAARDE, J., 1970 - Theory of flow to drains. Advances in Hydro-science 6, 43-106.
- WELLMAN, P., & McDOUGALL, I., 1974 - Potassium-argon ages on the Cainozoic volcanic rocks of New South Wales. Journal of the Geological Society of Australia, 21, 247-72.

APPENDIX 1

PALYNOLOGICAL EXAMINATION OF DRILLCORE SPECIMENS

by

M.D. Muir

PROFESSIONAL OPINION

Carbonaceous fragments from a weathering profile near Lanyon, ACT

by M.D. Muir

A number of samples were examined from three drillholes, Lanyon 10, 12, and 13. Carbonaceous fragments observed in the petrographic thin section of micaceous sandstone were at first suspected to be megaspores. Palynological maceration failed to produce anything except small woody fragments which could not be identified in the light microscope. These woody fragments and other carbonaceous material, picked with a needle from the rock matrix under a dissecting microscope, were mounted and gold-coated for investigation under the scanning electron microscope (SEM).

Under the SEM, the carbonaceous material was confirmed as wood, but very badly preserved. Most of the specimens were heavily impregnated with iron minerals which obscured the structures. Figure A1 shows a typical example. The main elements in the longitudinal section are tracheids - hollow tubular structures, which in this specimen are loosely filled with flakes of iron minerals. On the right-hand side of the photograph (arrow) are horizontal elements known as ray cells. These too are mineral-impregnated. There is no indication anywhere that the wood contained vessels, and it is probably a soft wood of coniferous origin.

Figure A2 shows the surface of an unmineralised tracheid with a badly preserved bordered pit, which might well be coniferous.

The material is too heavily impregnated for more accurate identification. Softwoods with this type of structure are common from the Jurassic onwards and originated during the Permian. They can give us no more specific information as to the age of the profile.

However, further drilling might produce better material, especially if a site could be found where the overlying sediments are impervious (i.e., well-cemented sands, or clays) so that post-depositional leaching or precipitation of iron minerals could be minimised.

Wood alone can be useful stratigraphically but it is limited in stratigraphic accuracy. In better-preserved material, there would be a better chance of finding other, more precisely dateable plant microfossils such as spores or seeds.

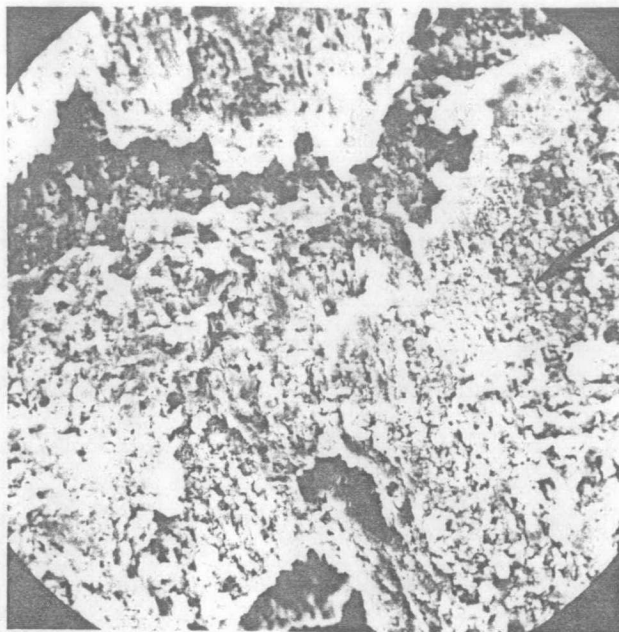


Fig. A1. Fossil wood from Lanyon 10. x300.
Arrow shows traces of ray cells.

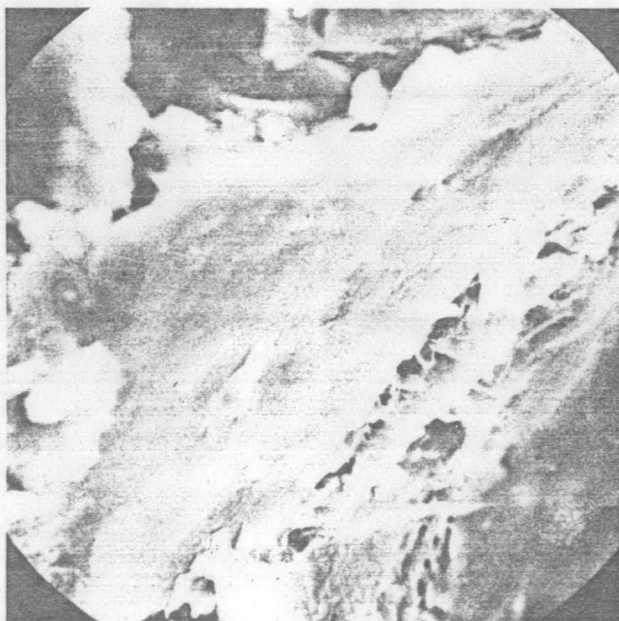


Fig. A2. Non-mineralised tracheid from
Lanyon 10. x1500. Poorly preserved
bordered pit in centre.

List of samples examined

Lanyon 10	22.70 m
Lanyon 12	7.75 m
Lanyon 13	28.70 m
	29.00 m
	29.25 m
	29.50 m
	34.95 m
	41.60 m

APPENDIX 2

POROSITY AND PERMEABILITY MEASUREMENTS ON DRILLCORE SPECIMENS

by

BMR Petroleum Technology Laboratory

Report on Testing Porosity and Flow Capacity to Gas and Liquid in
Sedimentary Strata Within the ACT (Lanyon Area)

Two 1 1/8-inch-diameter (28.8 mm) core plugs were drilled perpendicular and parallel to core axes from each of five samples. Because of the friable nature of the material, the samples were initially frozen and drilled with liquid nitrogen coolant.

The plugs were then dried in an oven for about 48 hours. Upon cooling, porosity and permeability tests with respect to air and dry nitrogen were carried out on each plug. Subsequently, the samples were saturated with filtered Canberra City water and subjected to water permeability tests; liquid porosity values were determined for each sample gravimetrically.

The results of the tests are shown in Tables A1 and A2. Table A1 shows the comparison of gas and water porosity and permeability values for each sample; Table A2 sequentially lists the liquid flow parameters for each sample (for determination of transmissivity to water). It should be noted that several flow tests were carried out on each sample to evaluate the effects of reduction in flow due to particle displacement in the pore channels.

Samples taken in the interval 5.5 to 6 m showed severe clay swelling on contact with fresh water, and additional outcrop material for this interval was supplied. The two sets of plugs from this zone are noted in the results as samples 1A and 1B.

Because of numerous joint planes, it was not possible to obtain a sample perpendicular to the core axis in the section from 17 to 18 m (sample 5).

(B.A. McKay)
Petroleum Technologist

Table A1
Porosity and permeability results - ACT sediments

Sample number and orientation	Sample depth interval (metres)	Air porosity (% bulk volume)	Permeability with respect to dry nitrogen (md.)	Liquid porosity (% bulk volume)	Liquid permeability (md.)	<u>Liquid porosity</u> Air porosity (percent)	Lithology
1AV	5.5 to 6.0	27.8	53	19.7	0.104	71.0	indurated oolluvium
1AH		29.3	379	Sample	disintegrated		(Lanyon)
1BV	3.6 to 4.1	31.2	228	21.8	11.0	70.0	indurated colluvium
1BH		32.5	740	20.0	3.3	61.6	(Lanyon)
2V	9 to 11	8.0	2.9	8.1	0.052	101	coarse sandstone
2H		8.9	11.7	9.1	0.090	102	(Rob Roy)
3V	12 to 13	10.4	13	9.9	0.76	95	coarse sandstone
3H		11.8	23	10.7	1.5	91	(Rob Roy)
4V	16 to 17	5.7	0.86	6.0	0.011	105	coarse sandstone
4H		5.7	56	6.7	0.006	113	(Rob Roy)
5V	17 to 18	6.6	1.9	6.5	0.16	99	coarse sandstone
5H	Unable to obtain sample due to joint planes						(Rob Roy)

V - Vertical to core axis or apparent bedding planes
H - Horizontal to core axis or apparent bedding planes

Samples 1A, 2, 3, 4, 5 from L10 drillcore (20731E 58389N)
Sample 1B from block of Lanyon subsolum material excavated from
creek bed at 20736E 58425N.

Table A2

Liquid flow parameters - ACT sediments

Sample number	Pressure (psi)	Volume (cc)	Time (secs)	Viscosity (op.)	Sample Length cms	Sample Cross-section area cm ²	Remarks
1AV	20	0.05	122.1	1.0	2.30	6.61	
			125.9				
			129.2				
			128.8				
			129.0				
			130.1				
			132.0				
			132.9				
1BV	10	2.0	85.0	1.0	2.55	7.85	
			102.3				
			103.6				
1BH	10	1.0	157.0	1.0	2.12	7.85	
			143.0				
			158.0				
			179.0				
			200.0				
			133.0				
2V	30	0.05	197.0	1.0	2.32	5.60	
			221.0				
			245.0				
2H	30	0.05	109.5	1.0	2.33	5.77	
			118.6				
			129.2				
3V	30	0.5	116.0	1.0	2.40	6.70	
			126.0				
			125.0				
3H	30	0.5	68.0	1.0	2.19	5.31	
			70.2				
			72.5				
4V	50	0.01	118	1.0	2.80	6.16	
			152				
			136.6				
4H	50	0.01	195.0	1.0	2.30	5.31	
			265.0				
			262.0				

Table A2 (Cont.)

Liquid flow parameters - ACT sediments

Sample number	Pressure (psi)	Volume (cc)	Time (secs)	Viscosity (cp.)	Sample Length cms	Sample Cross- section area cm ²	Remarks
5V	50	0.10	40.5	1.0	2.53	6.16	
			61.5				
			61.9				
			74.0				
			73.9				
5H			64.1				No sample

APPENDIX 3

GEOLOGICAL LOGS OF DIAMOND DRILLCORES

GEOLOGICAL LOG OF DRILL HOLE

CO-ORDINATES 106205 Canberra R.L. OF COLLAR 595m

SHEET 1 OF 3

[illegible]

Drill type Mayhew
Feed Hydraulic
Core Barrel type Treifus
.....
Driller BMR
Commenced 19.7.76
Completed 7.9.76
Logged by J. Kellett
Vertical Scale 1 cm = 1 m

NOTES

Fracture Log — Number of fractures per 25 cm of core. Zones of core loss blocked in.

Bedding and Joint Planes — Angles are measured relative to a plane normal to the core axis.

Defect Frequency — Number of natural defects (shears, joints, fractures) per 25 cm of core occurring at specified intercept angle range.

Water Level Measurements — ∇ Level when hole in progress at specified depth.
 ∇ Level in completed hole on specified date.

← Steady groundwater inflow; rate determined by airlifting.

← Liquid permeability (millidarcys) indicating direction of flow and liquid porosity (?) determined in BMR Pet. Tech. laboratory

GEOLOGICAL LOG OF DRILL HOLE

CO-ORDINATES 106205 (Canberra) - R.L. OF COLLAR 595 m -
1:50,000

SHEET 2 OF 3

Rock Type and Degree of Weathering	Discription Lithology, colour, strength.	Casing	Graphic Log	Lift and % core recovery	Depth and size of core	Fracture Log	Defect Frequency				Structures Joints, veins, seams, faults.	Formation Names	Water Level	Hydraulic Parameters
							0	30	60	80 90				
CORE NOT RECOVERED														
LITHIC FELDSARENITE Highly weathered	Yellow brown to grey. Contains abundant laminae of fine micaceous sandstone / mudstone.			95	22		4	2	2	1	Joints rough, Mn stained some clay lined. Partings parallel to bedding at 10°.			
				23		3	1	1	0					
				90		5	0	1	0					
				24		4	0	2	0					
ASHSTONE	Olive brown				24		5	2	2	2	No bedding apparent.			
					24		4	3	3	2				
CORE NOT RECOVERED														
Moderately Weathered	Grey, massive.			85	25		2	2	2	1	Schistosity 40° Open joints, rough and Fe stained faces. Fracture zone 15 cm			
ASHSTONE Fresh stained				26		4	1	1	1					
				87		3	0	1	0					
				27		3	1	1	0					
				28		4	0	2	0					
				100		2	0	1	0					
				92		2	1	1	0					
				30		2	0	2	0					
						2	1	1	0					
						1	0	1	0					
				3	2	1	0							
CORE NOT RECOVERED														
ASHSTONE Fresh	Grey, massive.			85	31		X	X	X	X	Fracture zone 1.2 m Joints rough, some lined with calcite. Fracture zone 40 cm Fracture zone 50 cm Rock fairly tight. Abundant healed fractures (calcite). Joints smooth.			
				32		3	2	1	0					
				60		4	3	2	3					
				33		4	3	2	2					
				100		X	X	X	X					
				34		X	X	X	X					
				100		X	X	X	X					
				35		X	X	X	X					
				100		X	X	X	X					
				36		4	4	3	3					
				83		4	2	2	1					
				37		3	2	1	0					
				100		3	1	1	0					
				40		7	3	2	0					
				X	X	X	X							
				X	X	X	X							
				1	1	0	0							
				2	0	0	0							
				1	0	0	0							
				0	1	0	0							
				1	0	0	0							
				2	1	1	0							
				1	1	1	0							
				1	1	2	0							

10.9
m³/day
(23.9-33.4)
(m)

← $10.9 \text{ m}^3/\text{day}$
 $(23.9 - 33.4)$
 (m)

Drill type Mayhew
Feed Hydraulic
Core Barrel type Treifus
Driller BMR
Commenced 19.7.76
Completed 7.9.76
Logged by J. Kelleff

NOTES

Fracture Log - Number of fractures per 25 cm of core. Zones of core loss blocked in.

Bedding and Joint Planes — Angles are measured relative to a plane normal to the core axis

Defect Frequency — Number of natural defects (shears, joints, fractures) per 25 cm of core occurring at specified intercept angle range.

Water Level Measurements — Level when hole in progress at specified depth.
 Level in completed hole on specified date.

← Noticeable seepage
(flow rate not recorded)

← Steady groundwater inflow; rate determined by airlifting:

GEOLOGICAL LOG OF DRILL HOLE

CO-ORDINATES 106205 Canberra R.L. OF COLLAR 595 m
1:50,000

SHEET 3 OF 3

Rock Type and Degree of Weathering	Discription Lithology,colour,strength.	Casing Graphic Log	Lift and % core recovery	Depth and size of core	Fracture Log	Defect Frequency Intercept Angle 0 30 60 80 90	Structures Joints,veins,seams,faults.	Formation Names	Water Level	Hydraulic Parameters
ASHSTONE Fresh	Blue grey massive		100	41		6 3 3 2	Rough open joints, minor precipitation of calcite on faces.			
				2 5 1 1						
				2 4 3 2						
				3 3 3 1						
				4 4 3 2						
				4 4 4 3						
				4 3 4 2						
				2 2 2 1						
				2 1 2 1						
				1 1 0 0						
2 1 0 0	Numerous healed fractures (not included in fracture log)									
3 1 1 0										
2 0 0 0										
1 0 0 0										
2 0 0 0										
2 0 0 0										
2 0 0 0										
1 0 0 0										
2 0 0 0										
2 0 0 0										
2 1 0 0	Smooth joints									
3 0 0 0										
1 1 0 1										
2 1 1 1										
3 0 1 0										
4 1 1 1										
3 1 1 1										
End of Hole 46.70m					47					(23.9 - 46.7m)

14.5 m³/day

(23.9 - 46.7m)

Drill type: Mayhew
Feed: Hydraulic
Core Barrel type: Treifus
Driller: BMR
Commenced: 19.7.76
Completed: 7.9.76
Logged by: J. Kellett
Vertical Scale 1cm = 1m
Record 1981/61

NOTES

Fracture Log — Number of fractures per 25 cm of core. Zones of core loss blacked in.

Bedding and Joint Planes — Angles are measured relative to a plane normal to the core axis.

Defect Frequency — Number of natural defects (shears, joints, fractures) per 25 cm of core occurring at specified intercept angle range.

Water Level Measurements — ∇ Level when hole in progress at specified depth.
 ∇ Level in completed hole on specified date.

← Noticeable seepage (flow rate not recorded)

← Steady groundwater inflow; rate determined by airlifting.

SHEET 1 OF 2

← Noticeable seepage
(flow rate not recorded)

← Steady groundwater
inflow; rate determined
by airlifting.

GEOLOGICAL LOG OF DRILL HOLE

CO-ORDINATES 104176 Canberra (1:50,000) R.L. OF COLLAR 606 m

SHEET 2 OF 2

Rock Type and Degree of Weathering	Discription Lithology, colour, strength.	Casing	Graphic Log	Lift and % core recovery	Depth and size of core	Fracture Log	Defect Frequency				Structures Joints, veins, seams, faults.	Formation Names	Water Level	Hydraulic Parameters		
							Intercept	Angle	0	30	60	80	90			
RHYODACITIC TUFF Fresh stained	Blue grey, porphyritic. Phenocrysts of plagioclase and quartz (2-5 mm). Rock very hard - slow drilling.				80		2	1	1	0					Joints rough and open, limonite stained. Hole making water. Rock becoming tighter below 23m. Joints smoother, calcite linings. Numerous fractures healed with calcite (Not recorded in defect frequency). Joints smooth, calcite and clay lined. Limonite stained. Fracture zone 7cm.	↔ 39.6 m ³ /day (12.6-22.15m)
					21	0	1	1	0							
					100	2	1	1	0							
					22	2	1	0	0							
					92	2	1	1	0							
					23	2	3	2	1							
					24	2	1	2	0							
					25	1	2	1	0							
					100	3	3	2	1							
					26	3	2	2	0							
					27	3	3	2	0							
					100	1	1	0	0							
					28	1	0	0	0							
					100	0	0	0	0							
					29	1	0	0	0							
					100	1	0	0	0							
					30	1	0	0	0							
					95	1	0	0	0							
					31	1	0	0	0							
					100	1	0	0	0							
					32	0	0	0	0							
					33	0	1	0	0							
							3	2	1	1						
							2	1	1	1						

Drill type Mayhew
Feed Hydraulic
Core Barrel type Treifus
Driller BMR
Commenced 8-9-76
Completed 29-9-76
Logged by J. Kelleff

NOTES

Fracture Log - Number of fractures per 25 cm of core. Zones of core loss
blocked in.

Bedding and Joint Planes — Angles are measured relative to a plane normal to the core axis.

Defect Frequency - Number of natural defects (shears, joints, fractures) per 25 cm of core occurring at specified intercept angle range.

Water Level Measurements - ∇ Level when hole in progress at specified depth.
 ∇ Level in completed hole on specified date.

← Noticeable seepage
(flow rate not recorded)

← Steady groundwater inflow; rate determined by airlifting.

[illegible]

SHEET 2 OF 2

Rock Type and Degree of Weathering	Discription Lithology, colour, strength.	Casing Graphic Log	Lift and % core recovery	Depth and size of core	Fracture Log	Defect Main Intercept Angle	Frequency 0 30 60 80 90	Structures Joints, veins, seams, faults.	Formation Names	Water Level	Hydraulic Parameters
Moderately Weathered	Brown , porphyritic.		100	21		2	1 1 0	Mainly smooth joints ; clay lined. Minor staining.			
RHYODACITIC TUFF	Brown - grey, porphyritic. Calcite, epidote and phyllosilicate veins discordant with low-angle joints.		100	22		3	2 0 0	Weathered joint 5 cm.			
			100	23		3	1 1 1	Extremely weathered zone (7cm).			
			100	24		2	3 2 1	Fracture zone 4 cm.			
			100	25		2	1 2 0	Fracture zone 7 cm.			
			100	26		3	4 2 2	Fracture zone 12 cm.			
			100	27		3	2 2 0	Fracture zones are generally clayey.			
			100	28		3	2 2 0	Fracture zone 10 cm.			
			100	29		3	1 1 0	Joints rougher, but generally clay filled or lined. Negligible staining.			
			100	30		2	1 0 0				
			100	31		3	1 1 0				
RHYODACITIC TUFF	Grey, porphyritic quartz (2-5 mm) and plagioclase (2-8 mm) phenocrysts.		100	32		2	1 0 0	Fracture zone 17 cm.			
			100	33		4	2 1 0	Fracture zone 21cm, clean, some staining.			
			100	34		2	1 0 0	Fract. zone 18cm. Limonite stain. Quartz veining associated with fractures.			
			100	35		3	2 2 1				
	End of Hole 35.10m										

5.1

m³/day.
(12.3 - 35.1 m,
mainly from
two fracture
zones below
33.5 m)

Drill type Mayhew
Feed Hydraulic
Core Barrel type Trefus
Driller BMR
Commenced 8.9.76
Completed 29.9.76
Logged by J. Kelleff
Vertical Scale 1 cm : 1 m

NOTES

Fracture Log — Number of fractures per 25 cm of core. Zones of core loss blacked in.

Bedding and Joint Planes — Angles are measured relative to a plane normal to the core axis.

Defect Frequency — Number of natural defects (shears, joints, fractures) per 25 cm of core occurring at specified intercept angle range.

Water Level Measurements — ∇ Level when hole in progress at specified depth.
— ∇ Level in completed hole on specified date.

← Noticeable seepage
(flow rate not recorded)

← Steady groundwater
inflow; rate determined
by airlifting.

19/155-16/70

BUREAU OF MINERAL RESOURCES,
GEOLOGY & GEOPHYSICSPROJECT LANYON DRAINAGE INVESTIGATION
LOCATION LANYON NORTH BASINHOLE NO. L 13
(CANBERRA 171)

GEOLOGICAL LOG OF DRILL HOLE

CO-ORDINATES 113205 (Canberra), R.L. OF COLLAR 606 m
1:50,000

SHEET 2 OF 3

Rock Type and Degree of Weathering	Description Lithology, colour, strength.	Casing Log	Graphical Log	Depth and size of core	Fracture Log	Defect Frequency Intercept Angle	Structures Joints, veins, seams, faults.	Formation Names	Water Level	Hydraulic Parameters
						0 30 60 80 90				
FELDSPATHIC QUARTZ ARENITE	Red with strong yellow mottling. Negligible variation in texture and mineralogy down to 26 m.			100		1 1 2	Joints smooth, Mn stained, about half of them clay lined, mostly tight. Bedding variable from 0 to 10°. Small scale, low angle, poorly preserved cross bedding			
Highly weathered	Friable			21		3 2 1 1				
	Clay Seam			22		1 1 1 1				
				23		3 2 1 1				
				24		2 2 1 2				
				25		1 1 1 1				
				26		2 1 1 1				
FELDSARENITE	Yellow-brown; 30% plag. and K feldspar - mostly altered. Sub-rounded Qtz. Abundant biotite.			95		1 1 1 1	Shear zone 20cm dip 65°			
Highly weathered				27		3 1 1 1				
				28		1 1 2 2				
Extr. weathered	Purple, laminated, 60% Qtz, 30% fsp, 10% rock fragments and micas.			29		1 1 1 1	Crushed zone 20cm. Slickensides on flat joints.			
Highly weathered	grading to			30		2 2 2 3	Contact 10°, sharp			
Mod. weathered	Yellow-brown			31		1 2 2 1	Bedding 0-10°, very small scale low angle cross stratification. Small convolute bedding, herringbone cross strat.			
	grading to			32		3 2 2 1	Joint faces Mn stained, fairly tight			
	Yellowish brown to grey, massive.			33		1 2 2 1	Fairly massive. Laminæ about 10°			
Slightly weath.				34		3 3 3 2	Joint open, some clay lined.			
ASHSTONE	Fine sandstone bed 3cm. Shear zone 10cm. Convolute bedding. Fracture zone 30cm.			35		1 2 1 0				
grading to				36		2 2 2 1	fracture zone			
	Grey, Massive.			37		3 3 2 1				
				38		1 3 2 0				
				39		2 4 2 1				
				40		X X X X				
						2 4 3 1				
						3 2 1 0				
						3 1 1 0				
						1 1 0 0	Open rough joints, Mn stained.			
						2 1 1 0				
						0 1 0 0				
						3 1 0 0				
						2 0 0 0				
						2 1 0 0				
						2 0 0 0				
						0 0 1 1				
						0 2 1 1				
						1 1 1 1				
						2 0 0 1				
						5 0 0 1				
						2 4 1 0				
						2 3 1 1				
						2 2 1 0				
						4 3 1 1				
						0 2 1 0				
						1 2 1 0				
						2 1 0 0				
						1 1 1 0				
						2 2 1 1				

Drill type Mayhew
Feed Hydraulic
Core Barrel type Treifus
Driller BMR
Commenced 19.10.76
Completed 9.11.76
Logged by J. Kelleff

Vertical Scale 1 cm = 1 m
Record 1981/61

NOTES

Fracture Log - Number of fractures per 25 cm of core. Zones of core loss blocked in.

Bedding and Joint Planes - Angles are measured relative to a plane normal to the core axis.

Defect Frequency - Number of natural defects (shears, joints, fractures) per 25 cm of core occurring at specified intercept angle range.

Water Level Measurements - ∇ Level when hole in progress at specified depth.
 ∇ Level in completed hole on specified date.

← Noticeable seepage (flow rate not recorded)

← Steady groundwater inflow; rate determined by airlifting.

BUREAU OF MINERAL RESOURCES,
GEOLOGY & GEOPHYSICS

PROJECT LANYON DRAINAGE INVESTIGATION

LOCATION LANYON NORTH BASIN

HOLE NO. L 13
(CANBERRA 171)

SHEET 3 OF 3

CO-ORDINATES 113205 (Canberra 1:50,000)

R.L. OF COLLAR 606 m

Geological Log of Drill Hole

Rock Type and Degree of Weathering

Discription Lithology, colour, strength.

Casing Log

Graphic Log

Lift and % core recovery

Depth and size of core

Fracture Log

Defect Frequency

Intercept Angle

Structures Joints, veins, seams, faults.

Formation Names

Water Level

Hydraulic Parameters

ASHSTONE	Grey, massive					<div>Abundant healed fractures (calcite).</div> <div>Joints reported are open, rough and Mn stained.</div>	<div>10.9 m³/day</div>
End of Hole 43.55 m							
<div> <div> <div>Drill type Mayhew</div> <div>Feed Hydraulic</div> <div>Core Barrel type Treifus</div> <div>Driller BMR</div> <div>Commenced 19.10.76</div> <div>Completed 9.11.76</div> <div>Logged by J. Kelleff</div> <div>Vertical Scale 1 cm = 1 m</div> </div> <div> <div> <div>NOTES</div> <div> <div>Fracture Log — Number of fractures per 25 cm of core. Zones of core loss blocked in.</div> <div>Bedding and Joint Planes — Angles are measured relative to a plane normal to the core axis.</div> <div>Defect Frequency — Number of natural defects (shears, joints, fractures) per 25 cm of core occurring at specified intercept angle range.</div> <div>Water Level Measurements — Level when hole in progress at specified depth.</div> <div> Level in completed hole on specified date.</div> </div> </div> <div> <div> <div>← Noticeable seepage (flow rate not recorded)</div> <div>← Steady groundwater inflow; rate determined by airlifting.</div> </div> </div> </div> </div>							

Record 1981/61

M(Pf) 230

19/155-16/7

GEOLOGICAL LOG OF DRILL HOLE

CO-ORDINATES 117206 (Canberra R.L. OF COLLAR 613. m
1:50,000)

SHEET 1 OF 3

Rock Type and Degree of Weathering	Description Lithology, colour, strength.	Casing Graphic Log	Lift and % core recovery	Depth and size of core	Fracture Log	Defect Frequency					Structures Joints, veins, seams, faults.	Formation Names	Water Level	Hydraulic Parameters
						Intercept	Angle	Frequency	Frequency	Frequency				
CLAYEY ALLUVIUM	Dark grey & black stratified clayey sands and silts.		50								Min. profile development	K2		
PRIOR STREAM DEPOSITS	Silty coarse rounded gravels. (grey) Cobbles		65	1							Fining downwards			
PRIOR STREAM DEPOSITS	Silty med grav; med sand		60	2								LANYON PEDODERM		
	Grey poorly sorted gravels		80								Gravel sub-angular to subrounded			
	Sed. sesquioxide nods.		NIL	3							Fining downwards	TUGG. PEDODERM		
OUTWASH FAN DEPOSITS	Brown silty gravels		70											
	Pale grey sandy silt; sesquioxidic		65	4							Massive	MURUMBIDGEE FANGLOMERATE		
FLOODPLAIN SEDIMENTS	Pale grey silty sand		60	5							Massive			
			30	6								TUGG. PEDODERM		
PRIOR STREAM DEPOSITS	Cobbles; rounded fresh acid volcanics		10	7							Open structure			
PALEOSOL SUB-SOLUM	Olive grey clayey sands & gravels		100	8							Argillans sinusoidal joint planes, tubules, general pedogenic organisation	MURUMBIDGEE FANGLOMERATE		
CLOSED FANGLOMERATE (GRAVELS)	Coarse pebbles in silt-sand matrix		75	9							Poorly sorted, rounded pebbles. Low porosity. Clayement-minor incipient cutans			
			30	10								TUGG. PEDODERM		
CLOSED FANGLOMERATE (COBBLES)	Subrounded fresh & weathered cobbles (10cm) and pebbles in coarse sand matrix. Cemented		100	11							Massive. Thick cutans of mainly white clay. All pores filled. Joints.			
			90	12								MURUMBIDGEE FANGLOMERATE		
LITHIC FELSARENITE	Purple; rounded qtz & fsp (fresh & weathered) Poorly-mod sorted. Some rock fragments up to 2 cm		100	13		1	2	0	0		Joints open (up to 1cm) but all clay filled.			
				14		2	1	1	0		Faint bedding variable from 0 to 10°	TUGG. PEDODERM		
Highly weathered				15		3	2	3	0					
			100	16		1	1	2	2		f-fracture zone 20cm	MURUMBIDGEE FANGLOMERATE		
			80	17		2	1	1	2					
MUDSTONE	Yellow brown. Massive.		100	18		2	3	2	1		Joints stained, clay lined. Closely jointed. Fracture zone 15cm. Rock very crumbly in places.	TUGG. PEDODERM		
	Very closely fractured, but rock strong between fractures. Qtz. & ep. veins		100	19		3	3	2	2		Numerous healed & closed fractures.			
			100	20		4	3	4	3		Joints mainly open & clay-free, a lot of staining.	MURUMBIDGEE FANGLOMERATE		
						2	3	3	2		Fracture zone 90 cm			

5.49m
at 9.12.76
(ground -
water
potential of
fractured
rock below
19.5m)

Drill type Mayhew

Feed Hydraulic

Core Barrel type Treifus

Driller BMR

Commenced 11.11.76

Completed 8.12.76

Logged by J. Kellert

Vertical Scale 1cm: 1m

Record 1981/61

NOTES

Fracture Log - Number of fractures per 25 cm of core. Zones of core loss blocked in.

Bedding and Joint Planes - Angles are measured relative to a plane normal to the core axis.

Defect Frequency - Number of natural defects (shears, joints, fractures) per 25 cm of core occurring at specified intercept angle range.

Water Level Measurements - ∇ Level when hole in progress at specified depth.
 ∇ Level in completed hole on specified date. \leftarrow Noticeable seepage (flow rate not recorded) \leftarrow Steady groundwater inflow; rate determined by airlifting.

BUREAU OF MINERAL RESOURCES, GEOLOGY & GEOPHYSICS		PROJECT LANYON DRAINAGE INVESTIGATION LOCATION LANYON NORTH BASIN		HOLE NO. L14 (CANBERRA 172)					
GEOLOGICAL LOG OF DRILL HOLE		CO-ORDINATES 117206 (Canberra) R.L. OF COLLAR 613 m 1:50,000		SHEET 2 OF 3					
Rock Type and Degree of Weathering	Description Lithology, colour, strength.	Casing Graphic Log	Depth and size of core recovery	Fracture Log	Defect Frequency Intercept Angle 0 30 60 80 90	Structures Joints, veins, seams, faults.	Formation Names	Water Level	Hydraulic Parameters
Moderately weathered between fractures MUDSTONE	Yellow brown, markedly Fe stained.		100			fracture zone 14 cm			
			70	21		fracture zone 70 cm			
	Massive.		100	22					
			85	23		Open smooth joints. All stained.			
	Very closely jointed.		100	24					
			100	25	f	fracture zone 95 cm			
			100	26	s	shear zone 20 cm, clayey			
	Grey Silicified		80	27	f	fracture zone			
			70	28	s	shear zone 18 cm			
			100	29	s	shear zone 10 cm			
Slightly weathered between fractures	Grey Silicified		100	30		Massive			
SILICIFIED ARENITE	ep veining		100	31		Joints open and stained.			
Slightly weath.	Grey brown; Qtz, k-spar & plag.		100	32					
PORPHYRITIC RHYOLITE	Pale grey, phenocrysts of Qtz, k-spar. Ep and Qtz veins		100	33		fracture zone 15 cm			
Fresh stained			100	34		fracture zone 20 cm			
(or shallow intrusive?)	Rock extremely hard. Some shale fragments		100	35		Rough joints, open and stained.			
FELDSARENITE	Yellow brown with original sedimentary fabric well preserved. Mod. sorted sub-rounded Qtz & f-spar. sill 2 cm		100	36		fracture zone 15 cm			
Highly weathered			100	37		Joints open, clay lined. Bedding 50° (well developed)			
SILICIFIED ARENITE	Grey-brown; Qtz, k-spar & plag. A lot of Qtz & ep. veining.		95	38		fracture zone 20 cm			
Slightly weath.			100	39		Joints open, stained			
PORPHYRITIC RHYOLITE	Pale pink; phenocrysts of Qtz & k-spar. Lot of veining.		100	40		Massive			
Fresh stained			100			(shear zone 10 m fracture zone 15 cm)			
SILICIFIED MUDSTONE	Grey with prominent red & black staining around fractures		100			Joints rough, open and stained			
Moderately to highly weathered between fractures	Chamosite?		100			fracture zone 18 cm			
			100			Rock very closely fractured. Schistosity 40°			
			100			Low grade metamorphosed down to 39.5 cm			

Drill type	Feed	Core Barrel type	Driller	Commenced	Completed	Logged by	Vertical Scale	Record
Mayhew	Hydraulic	Treibus	B.M.R.	11/12/76	8/12/76	J. Kellett	1 cm = 1 m	1981/61

NOTES
Fracture Log — Number of fractures per 25 cm of core. Zones of core loss blacked in.
Bedding and Joint Planes — Angles are measured relative to a plane normal to the core axis.
Defect Frequency — Number of natural defects (shears, joints, fractures) per 25 cm of core occurring at specified intercept angle range.
Water Level Measurements — ∇ Level when hole in progress at specified depth. ∇ Level in completed hole on specified date.

Noticeable seepage (flow rate not recorded)	Steady groundwater inflow; rate determined by airlifting.
←	←

BUREAU OF MINERAL RESOURCES, GEOLOGY & GEOPHYSICS			PROJECT LANYON DRAINAGE INVESTIGATION LOCATION LANYON NORTH BASIN					HOLE NO. 114 (CANBERRA 172)																						
GEOLOGICAL LOG OF DRILL HOLE			CO-ORDINATES 117206 (Canberra R.L. OF COLLAR 612 m 1:50,000)					SHEET 3 OF 3																						
Rock Type and Degree of Weathering	Discription Lithology, colour, strength.	Casing Graphic Log	Lift and % core recovery	Depth and size of core	Fracture Log	Defect Frequency Intercept Angle 0 30 60 80 90	Structures Joints, veins, seams, faults.	Formation Names	Water Level	Hydraulic Parameters																				
SILICIFIED MUDSTONE Slightly weathered between fractures	Grey		100	41		<table border="1" style="width:100%; text-align: center;"> <tr><td>x</td><td>x</td><td>x</td><td>x</td><td>x</td></tr> <tr><td>x</td><td>x</td><td>x</td><td>x</td><td>x</td></tr> <tr><td>x</td><td>x</td><td>x</td><td>x</td><td>x</td></tr> <tr><td>x</td><td>x</td><td>x</td><td>x</td><td>x</td></tr> </table>	x	x	x	x	x	x	x	x	x	x	x	x	x	x	x	x	x	x	x	x	Very closely fractured, Blocky.			58.2 m ³ /day (19-25-41-15)
x	x	x	x	x																										
x	x	x	x	x																										
x	x	x	x	x																										
x	x	x	x	x																										
<div style="display: flex; justify-content: space-between;"> <div style="width: 15%;">END OF HOLE 41.15m</div> <div style="width: 85%;"></div> </div>																														

Drill type Mayhew

Feed Hydraulic

Core Barrel type Treifus

Driller BMR

Commenced 11.11.76

Completed 8.12.76

Logged by J. Kelleff

Vertical Scale 1 cm = 1 m

NOTES

Fracture Log — Number of fractures per 25 cm of core. Zones of core loss blocked in.

Bedding and Joint Planes — Angles are measured relative to a plane normal to the core axis.

Defect Frequency — Number of natural defects (shears, joints, fractures) per 25 cm of core occurring at specified intercept angle range.

Water Level Measurements — Level when hole in progress at specified depth.
 Level in completed hole on specified date.

Noticeable seepage (flow rate not recorded)

Steady groundwater inflow; rate determined by airlifting.

APPENDIX 4

LOGS OF AUGER HOLES DRILLED DURING PRELIMINARY INVESTIGATION, 1974

UNDISTURBED SOIL SAMPLING: LANYON NORTH BASIN

(Rapid unedited field logs only; subject to modification and amendment).

HOLE 1

27.6.74

<u>Depth (cm)</u>	<u>Description</u>
0 - 5	Dark grey organic sandy silt (moist)
5 - 23	Brown clayey silt (moist)
23 - 41	Reddish brown heavy clay (moist)
41 - 86	Olive brown massive heavy clay (moist)
86 - 135	Mottled grey and reddish brown indurated clayey medium gravel (moist)
135 - 158	Weakly cemented clayey fine gravel (wet)
158	Indurated sand-gravel? - core not recovered
End of hole	158 cm
Standing water level	156 cm

HOLE 2

5.6.74

0 - 8	Peat	
8 - 46	Black massive peaty clay (moist)	
46 - 61	Dark grey massive clayey coarse sand (moist)	
61 - 76	Grey silty fine gravel (moist)	
76 - 102	Massive silty coarse sand (wet))
102 - 137	Brown cohesionless medium to coarse sand (saturated))
137 - 152	Pale grey silty coarse sand (wet))
152 - 160	Pale grey fine gravel (saturated))
160 - 170	Mottled grey and brown silty medium sand (wet))
170 - 178	Pale grey fine gravel (saturated))
178 - 206	Mottled grey and brown weakly cemented silty medium sand (wet))
206 - 211	Pale grey fine sand (saturated))
211 - 218	Grey weakly cemented silty coarse sand (wet))
218 - 259	Cohesionless coarse sand grading to medium gravel (saturated))
259 - 274	Indurated gravels? - core not recovered	
End of hole	274 cm	
Static head	> 0	

HOLE 3

27.6.74

0 - 3	Peat
3 - 15	Dark grey organic sandy silt (moist)
15 - 41	Pale grey silty fine sand (moist)
41 - 81	Pale grey massive clayey fine gravel (moist)
81 - 117	Brownish grey weakly cemented clayey coarse sand (moist)
117 - 122	Pale grey massive silty fine gravel (moist)
122 - 168	Cohesionless sandy fine gravel (moist)
168 - 188	Indurated silty sand; massive but porous (moist)
188 - 218	Indurated sands?)
218 - 234	Sand aquifer?)
234 - 355	Indurated sands?) From auger cuttings only
355 - 366	Gravel aquifer?)
366 - 371	Indurated gravels?)
End of hole 371 cm	
Standing water level 196 cm	

HOLE 5

4.6.74

0 - 10	Dark brown peaty silty sand (moist)
10 - 23	Mottled brown and grey silty sand (moist)
23 - 31	Dark brown peaty medium sand (wet)
31 - 38	Dark grey peaty silt (wet)
38 - 66	Black peaty clayey fine gravel (saturated) AQUIFER
66 - 76	Mottled yellowish brown and grey massive clayey sand (moist)
76 - 91	Mottled olive grey and brown massive heavy sandy clay (moist)
91 - 99	Mottled brown and grey massive clayey coarse sand (moist)
99 - 127	Mottled olive grey and yellow massive heavy sandy clay (moist)
127 - 145	Mottled brown and grey indurated sands (moist)
145 - 274	Indurated sands? (core not recovered)
End of hole 274 cm	
Standing water level 0 cm	

HOLE 7

1.3.74

0 - 8	Black organic silt (moist)	
8 - 38	Black massive peaty clay (moist)	
38 - 56	Grey clayey coarse sand (moist)	
56 - 76	Dark grey silty caly (moist)	
76 - 112	Grey clayey fine gravel (saturated))
112 - 183	Pale grey weakly cemented silty fine gravel (wet)) AQUIFER
183 - 224	Cohesionless sand? (core not recovered))
224 - 254	Mottled dark grey and brown massive dandy clay (moist)	
254 - 274	Pale grey slightly clayey coarse sand (saturated)	AQUIFER
274 - 732	Indurated sands? - core not recovered	
End of hole	732 cm	
Standing water level	0 cm	

HOLE 12

29.5.74

0 - 23	Blocky organic silty clay (wet)	
23 - 107	Dark grey organic massive clayey sand (moist)	
107 - 152	Grey clayey coarse sand with rock fragments up to 1½ cm (moist)	
152 - 183	Light grey silty coarse sand (wet))
183 - 229	Cohesionless coarse sand (saturated)) AQUIFER
229 - 259	Mottled grey and brown massive heavy clay (moist)	
259 - 290	Light grey slightly clayey fine gravel (saturated)	AQUIFER
290 - 305	Mottled dark grey and brown massive sandy clay (moist)	
305 - 467	Indurated sands? - core not recovered	
End of hole	457 cm	
Static head	> 0	

HOLE 13

29.5.74

0 - 6	Peat	
6 - 10	Black peaty clay (moist)	
10 - 15	Dark grey peaty silty clay (moist)	
15 - 48	Black massive peaty clay (moist)	
48 - 69	Dark grey massive heavy sandy clay (moist)	
69 - 86	Mottled black and dark brown massive heavy clay (moist)	
86 - 132	Mottled light grey and yellowish brown clayey coarse sand; massive but porous (moist)	
132 - 218	Mottled grey and brown massive silty fine gravel (moist)	
218 - 239	Cohesionless medium gravel (saturated))
239 - 249	Light grey silty fine sand (saturated))
249 - 274	Cohesionless fine gravel (saturated))
274 - 295	Yellowish brown medium sand (saturated))
295 - 312	Pale grey silty fine sand (wet))
312 - 325	Cohesionless medium gravel (saturated))
325 - 335	Pale brown medium sand (saturated))
335 - 356	Brown silty coarse gravel (saturated))
	(Gravel size grains are sub-angular, rhyodacitic))
356 - 366	Indurated sands?	
End of hole	366 cm	
Standing water level	52 cm	

)AQUIFER

HOLE 14

30.5.74

0 - 6	Peat	
6 - 13	Dark grey sandy silt (moist)	
13 - 28	Pale grey sandy silt (moist)	
28 - 46	Mottled brown and black massive heavy sandy clay (moist)	
46 - 71	Mottled grey and brown clayey coarse sand (moist)	
71 - 79	Cohesionless fine gravel (wet)	
49 - 97	Mottled pale grey and yellowish brown silty clay (moist)	
97 - 122	Grey silty fine gravel (wet))
122 - 127	Reddish brown fine sand (wet))

)AQUIFER

127 - 160	Mottled pale grey and yellowish brown weakly cemented clayey coarse sand; massive but prours (moist)
160 - 175	Olive brown massive heavy sandy clay (moist)
175 - 193	Indurated clayey coarse sand
End of hole	193 cm
Standing water level	122 cm

HOLE 17

27.6.74

0 - 13	Dark grey peaty clayey silt (wet)
13 - 25	Black peaty silty clay (moist)
25 - 46	Grey massive sandy silt (moist)
46 - 56	Pale grey silty coarse sand (saturated) AQUIFER
56 - 109	Mottled grey and brown massive heavy sandy clay (moist)
109 - 137	Grey indurated silty sand (moist)
137 - 175	Grey weakly cemented silty fine gravel (saturated) AQUIFER
175 -	Indurated sand-gravel? - core not recovered
End of hole	175 cm
Static head	70

HOLE 19

1.3.74

0 - 20	Grey sandy organic silt (moist)
20 - 61	Dark grey massive heavy sandy clay (moist)
61 - 91	Grey massive heavy gravelly clay (moist)
91 - 183	Brown indurated silty fine gravel (moist); massive but porous.
183 - 213	Pale grey indurated medium gravel (moist)
213 - 244	Pale yellow silty fine sand (moist)
244 - 279	Yellowish brown cemented coarse sand (moist)
279 - 305	Brown cohesionless fine gravel (moist)
305 - 366	Brown cohesionless coarse sand (saturated))
366 - 427	Greyish brown silty fine gravel (saturated)) AQUIFER
427 - 457	Mottled yellowish brown and grey cemented clayey fine gravel (moist)
457 - 762	Indurated sand gravel? core not recovered
End of hole	762 cm
Standing water level	305 cm

HOLE 20	27.5.74
0 - 31	Dark brown sandy silt (moist)
31 - 46	Light grey massive clayey silt (moist)
46 - 69	Light grey and brown mottled clayey silt (moist)
69 - 76	Light grey sandy silt (wet)
76 - 107	Massive olive grey fat clay (moist)
107 - 122	Transition zone - sandy clay (moist)
122 - 145	Mottled grey and brown heavy blocky clay (moist)
145 - 152	Transition zone
152 - 163	Weakly cemented clayey medium sand (moist)
163 - 183	Grey cohesionless medium sand (moist)
183 - 351	Cohesionless medium sand (wet))
351 - 381	Mottled light brown and grey silty medium sand (wet))
381 - 427	Statified medium sands and silts (wet))
427 -	Indurated sands?)
End of hole	427 cm
Standing water level	366 cm

AQUIFER

HOLE 21	28.5.74
0 - 6	Peat
6 - 15	Dark grey sandy silt (wet)
15 - 33	Pale grey massive silty coarse sand (moist)
33 - 61	Mottled dark grey and brown massive heavy clay with carbonate nodules at base (moist)
61 - 125	Mottled grey and brown massive clayey medium and coarse sand (moist)
125 - 135	Pale grey silty clay (moist)
135 - 152	Indurated silty sand (moist)
152 - 201	Brown massive sandy heavy clay (moist)
201 - 305	Grey and brown weakly cemented silty coarse sand of fine gravel; several thin (2 cm) cohesionless lenses. (moist, wet in lenses)
305 - 328	Pale grey massive clayey silt (moist)
328 - 338	Brown clayey fine gravel (wet))
338 - 353	Pale grey silty fine sand (wet))
353 - 366	Yellowish brown clayey fine gravel (wet))
366 - 381	Pale grey silty coarse sand (wet))

AQUIFER

381 - 396	Brown silty medium gravel (saturated))
396 - 414	Reddish brown fine sand with cobbles (sat- urated)))AQUIFER
414 - 457	Mottled brown and grey clayey medium gravel) - weakly cemented (wet))
457 - 465	Pale grey massive clayey medium sand (moist)	
465 - 549	Indurated sands? - core not recovered	
End of hole	549 cm	
Standing water level	398 cm	

LANYON SOUTH BASIN

Date: 27-6-74

HOLE 23

<u>Depth cm</u>	<u>Description</u>
0-3	Peat
3-28	Dark grey organic silty clay (moist)
28-36	Black massive organic clay (moist)
36-79	Massive olive grey fat clay (moist)
79-107	Mottled yellowish brown and grey massive heavy sandy clay (moist)
107-122	Mottled yellowish brown and grey massive clayey coarse sand (moist)
122-188	Mottled yellowish brown and olive grey massive heavy sandy clay (moist)
188-213	Mottled brown and olive grey fat clay (moist)
213-218	Transition zone
218-254	Reddish brown silty coarse sand (saturated) AQUIFER
254-272	Reddish brown weakly cemented clayey medium sand (wet) AQUIFER
272-295	Brown silty fine gravel; coarse gravel fragments (saturated) AQUIFER
295-335	Massive indurated sands? - core not recovered; may contain cohesivless saturated layers
335-366	Cemented gravels? - core not recovered; possible aquifer
366-556	Indurated sands? - core not recovered; possible cohesionless saturated layers

End of hole 556 cm

Standing water level 5 cm

Date: 5-6-74

HOLE 25

0-3	Peat
3-15	Dark grey peaty silt (moist)
15-20	Black peaty fine sand (moist)
20-38	Black organic silty coarse sand (moist)
38-56	Grey massive clayey medium sand (moist)
56-89	Mottled grey and brown weakly cemented silty medium to coarse sand, massive but porous (moist)
89-119	Mottled yellowish brown and grey clayey coarse sand; massive but porous (moist)

119-130	Brown weakly cemented clayey medium gravel (moist)
130-137	Olive grey massive heavy sandy clay (moist)
137-152	Brown cemented silty coarse sand, massive but porous (moist)
152-168	Brown weakly cemented medium sand; massive but porous (wet) AQUIFER
168-183	Greyish brown weakly cemented fine gravel (saturated) AQUIFER
183-208	Yellowish brown weakly cemented red sand grading to coarse sand (wet); feeble clay binder AQUIFER
208-245	Grey massive indurated clayey fine gravel (wet) AQUIFER
245-297	Cohesionless coarse sand (saturated) AQUIFER
297-366	Weakly cemented massive sandy clays - core not recovered; may contain high permeability layers
366-368	Hard indurated gravels? - core not recovered

End of hole 368 cm

Static head 70 cm

Date: 6-6-74

HOLE 26

0-10	Peat
10-56	Black massive peaty clay (moist)
56-66	Dark grey clayey coarse sand (wet)
66-137	Grey clayey fine gravel (wet)
137-165	Black massive peaty clay (moist)
165-183	Mottled grey and brown clayey coarse gravel; massive but porous (moist)
183-290	Cohesionless sands - core not recovered AQUIFER
290-320	Coarse gravels & cobbles - core not recovered AQUIFER
320-396	Cohesionless medium sand (saturated) AQUIFER
396-417	Hard cemented gravels - core not recovered

End of hole 417 cm

Static head > 0 cm

DATE: 13-6-74

HOLE 28

0-10	Peat
10-127	Black massive peaty clay (moist); sandy clay lenses at 20 - 25 cm 30 - 33 cm 91 - 99 cm 114 - 117 cm
127-198	Mottled grey and brown massive heavy gravelly clay (moist)
198-229	Mottled grey and brown massive heavy gravelly clay with disseminated sub-angular to sub-rounded cobbles (moist grading to wet)
229-249	Greyish brown clayey coarse sand (saturated) AQUIFER
249-285	Mottled yellowish brown and grey weakly cemented clayey fine gravel (wet) AQUIFER
285-330	Mottled yellowish brown and grey silty medium sand (saturated) AQUIFER
330-351	Mottled brown and grey silty coarse sand - fine gravel (saturated) AQUIFER
351-381	Mottled yellowish brown and grey weakly cemented, massive clayey coarse sand (wet)
381-711	Cemented clayey sands and gravels with saturated layers of cohesionless material; silt and clay lenses - core not recovered.

End of hole 711 cm

Standing water level 152 cm

Date: 12-6-74

HOLE 29

0-5	Peat
5-71	Black massive peaty clay (moist)
71-94	Black massive heavy sandy peaty clay (moist)
94-155	Mottled grey and brown massive heavy sandy clay (moist)
155-241	Mottled grey and brown cemented massive clayey fine gravel (moist)
241-269	Mottled grey and yellowish brown weakly cemented clayey medium gravel (wet) AQUIFER
269-307	Brown silty fine gravel (saturated) AQUIFER

307-315	Brown clayey fine gravel (saturated)AQUIFER
315-320	Cohesionless coarse sand (saturated) AQUIFER
320-356	Cohesionless coarse gravel (saturated) AQUIFER
356-366	Stratified siltsand clayey sands (moist-wet)
366-589	Indurated sands and gravels - core not recovered; may contain thin saturated layers

End of hole 589 cm

Standing water level 191 cm

Date: 7-6-74

HOLE 30

0-5	Peat
5-20	Black peaty silty clay (moist)
20-28	Black massive peaty clay (moist)
28-36	Black massive heavy sandy clay (moist)
36-107	Black massive peaty clay (moist)
107-145	Mottled grey and brown massive heavy sandy clay (moist)
145-160	Mottled grey and brown massive clayey coarse sand (moist-wet)
160	Indurated clayey sands? - core not recovered

End of hole 160 cm

Standing water level 160 cm

Date: 10-6-74

HOLE 31

0-3	Peat
3-23	Dark grey peaty clayey silt (moist)
23-41	Pale grey gravelly silt (saturated) AQUIFER
41-122	Mottled grey and brown massive heavy fine gravelly clay with disseminated coarse gravel fragments (moist)
122-175	Mottled yellowish brown and pale grey massive heavy sandy clay (moist)
175-229	Mottled yellowish brown and grey massive weakly cemented clayey medium sand (moist)
229-246	Brown weakly cemented clayey coarse sand of low plasticity (wet) AQUIFER

246-267	Brown silty fine gravel with some coarse gravel fragments (saturated) AQUIFER
267-305	Cemented gravels with occasional cobbles in places - core not recovered
305-348	Massive indurated sands? - core not recovered

End of hole 348 cm

Standing water level 76 cm

Date: 14-4-74

HOLE 35

0-3	Peat
3-56	Dark grey organic clayey fine gravel (moist)
56-122	Brown silty fine gravel (dry)
122-229	Cohesionless coarse sands - fine gravels? - core not recovered
229-366	Cohesionless coarse sands - fine gravels? - core not recovered saturated AQUIFER
366-427	Cemented clayey fine gravel? - core not recovered
427	Massive indurated outwash?

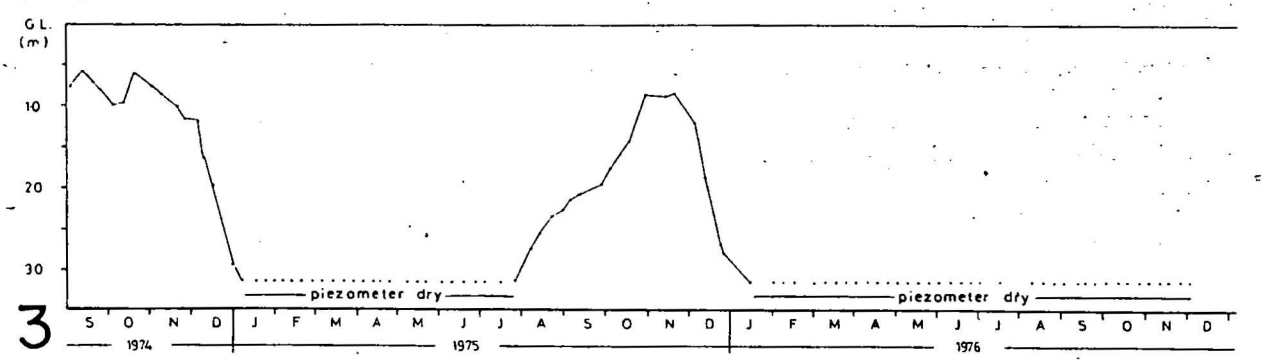
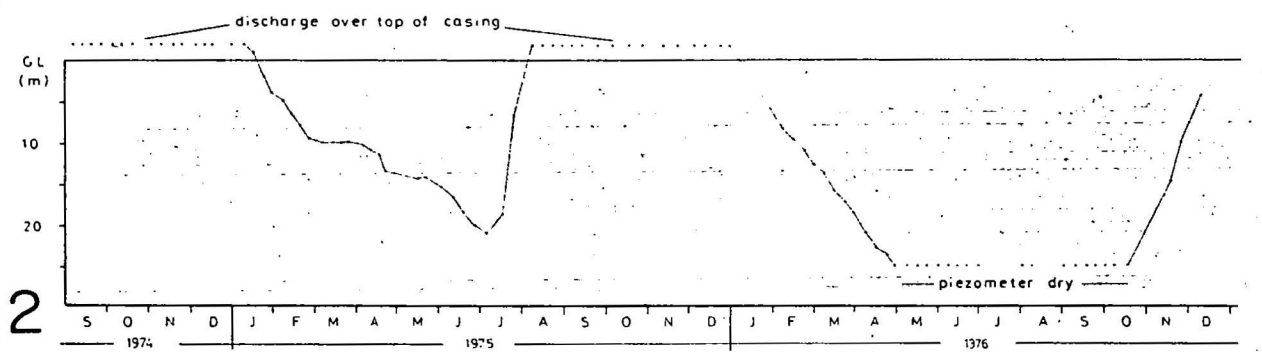
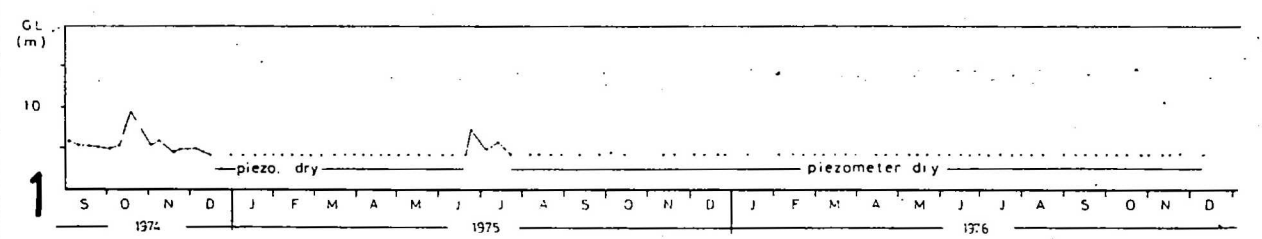
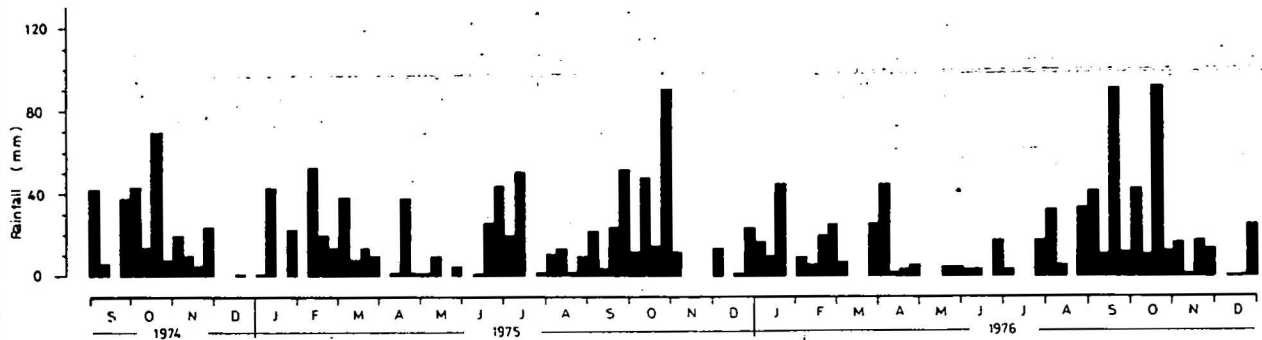
End of hole 427 cm

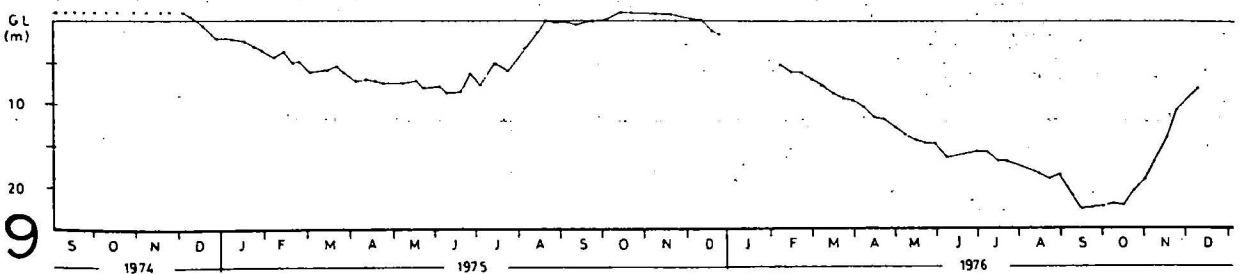
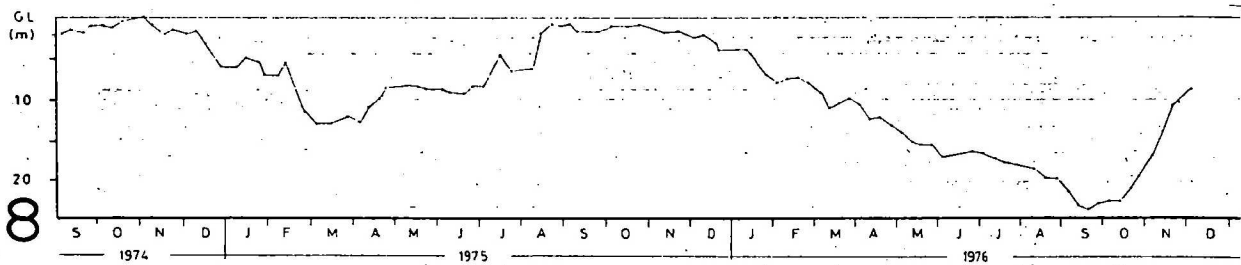
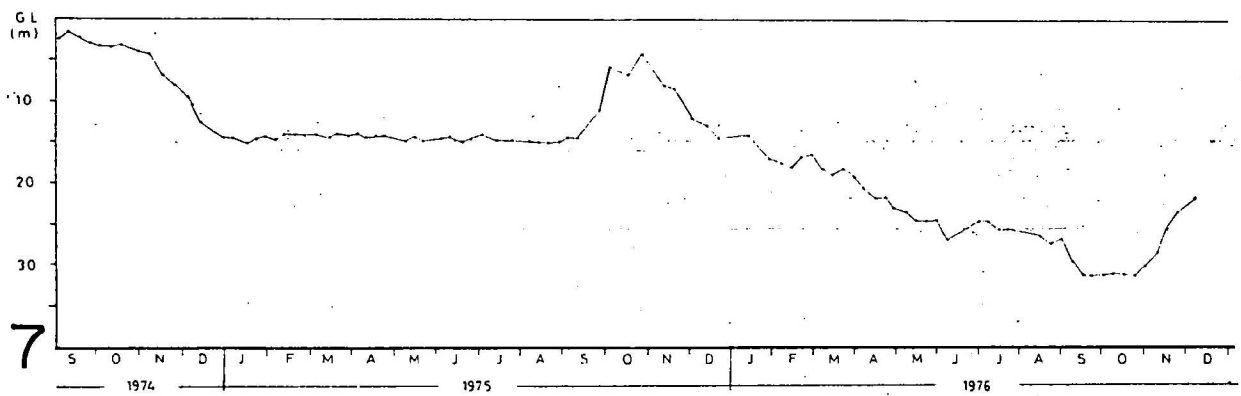
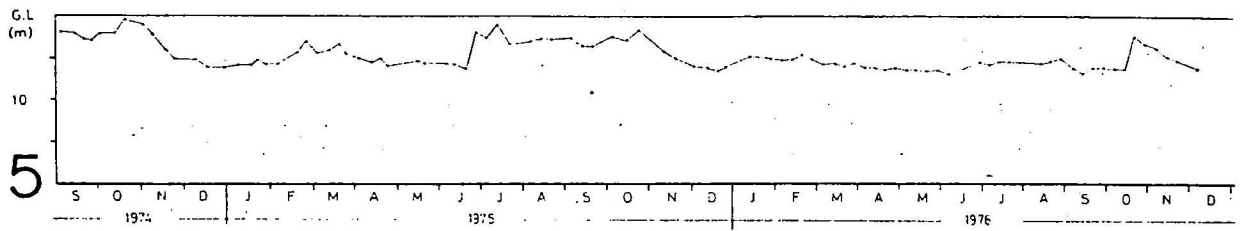
Standing water level 229 cm

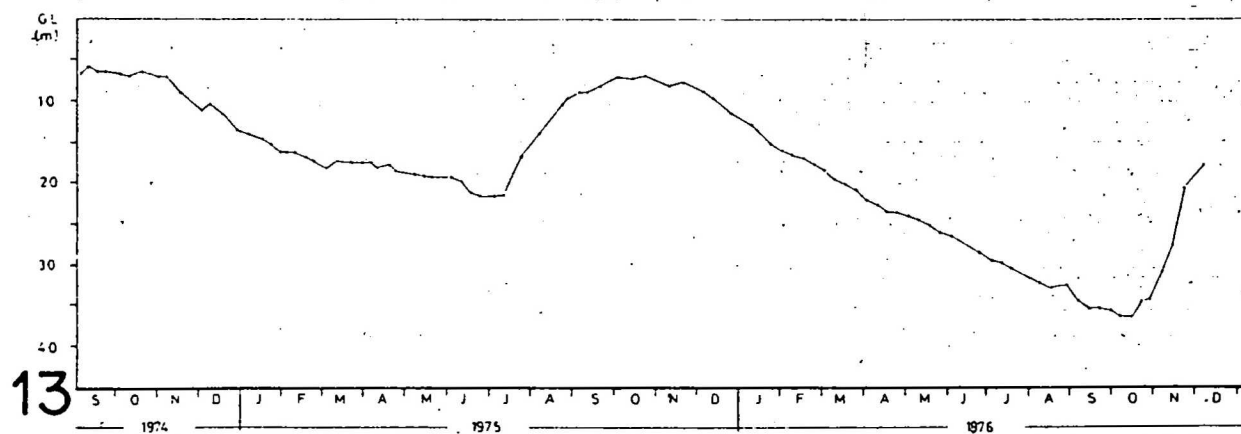
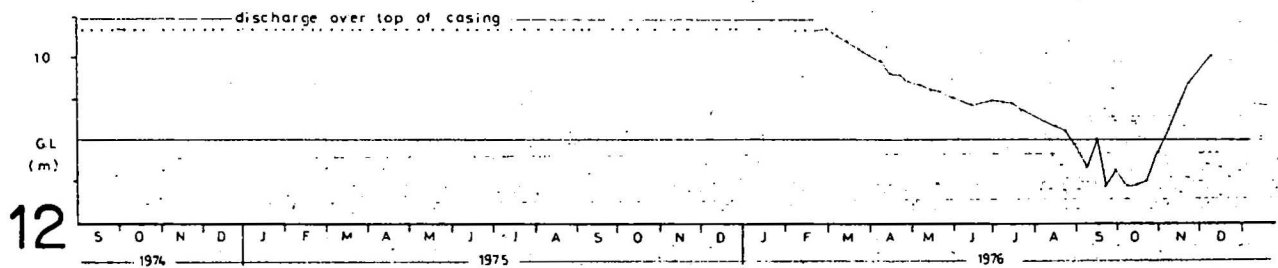
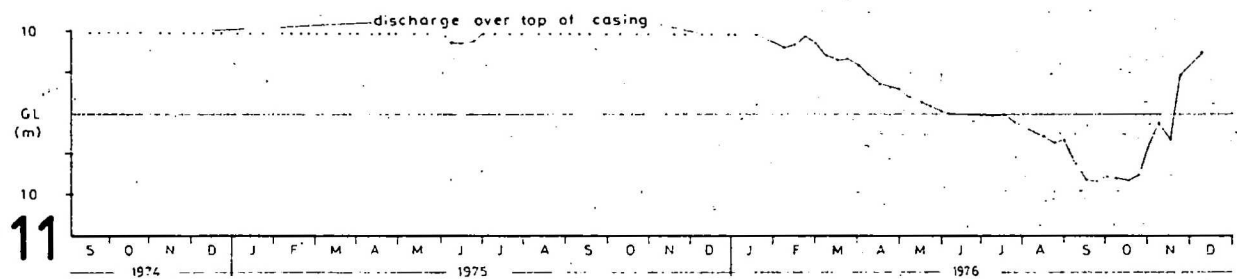
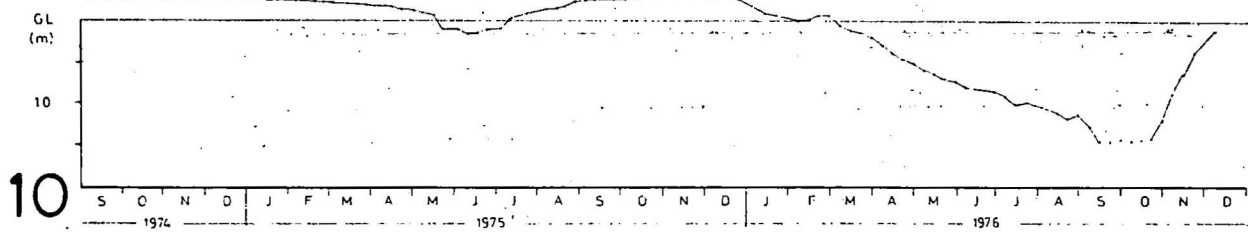
APPENDIX 5

BORE HYDROGRAPHS

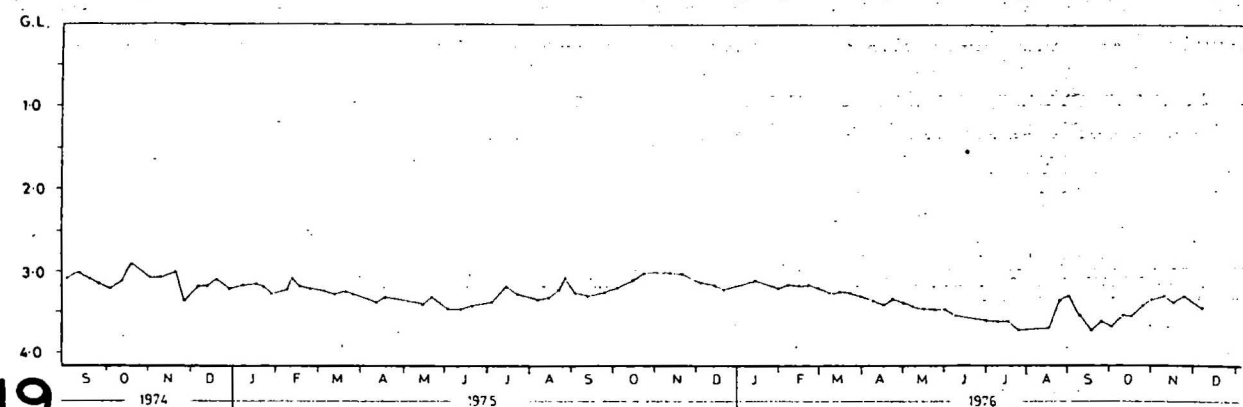
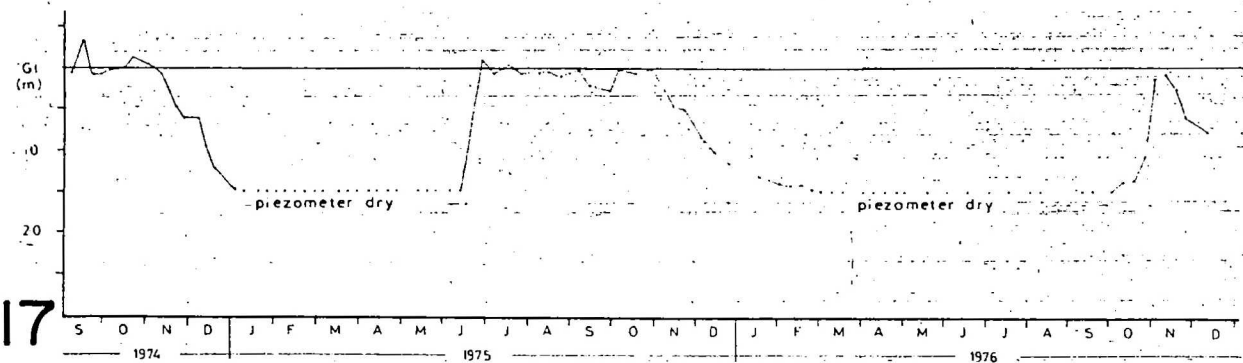
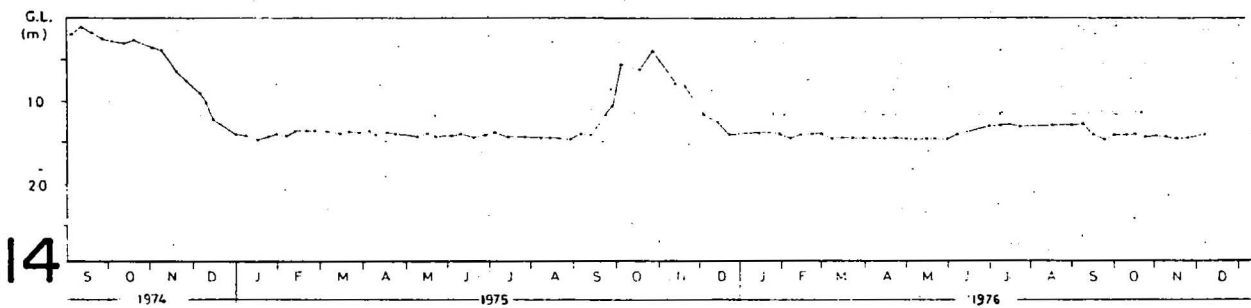
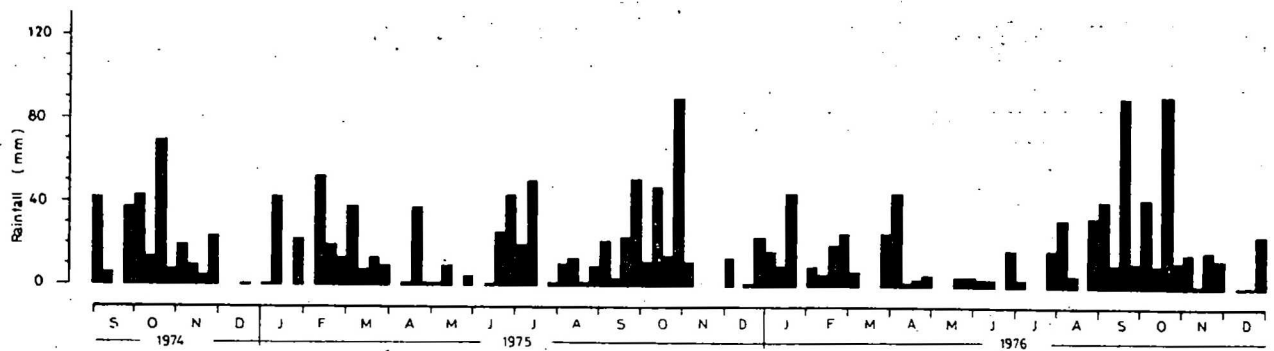
Appendix 5 Bore Hydrographs — North Basin

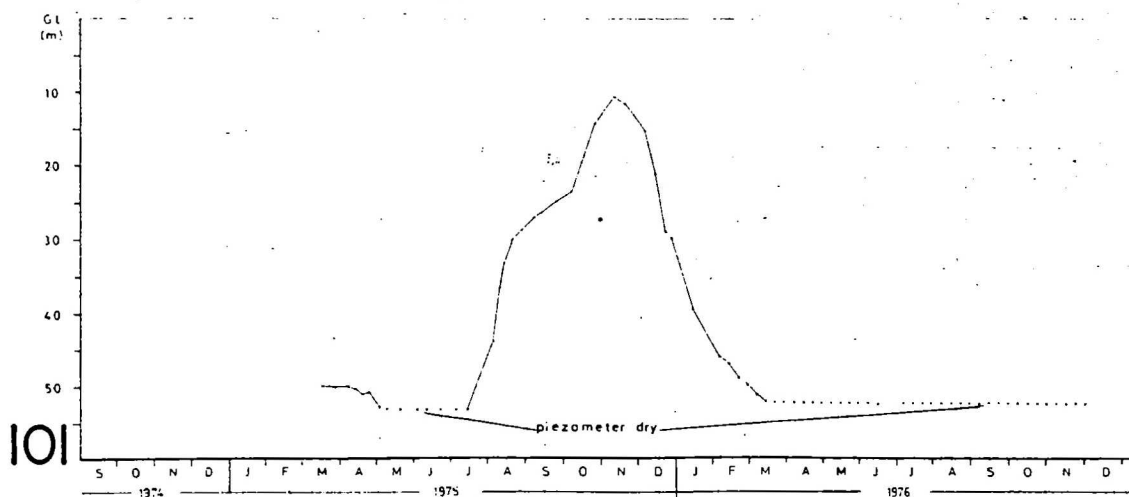
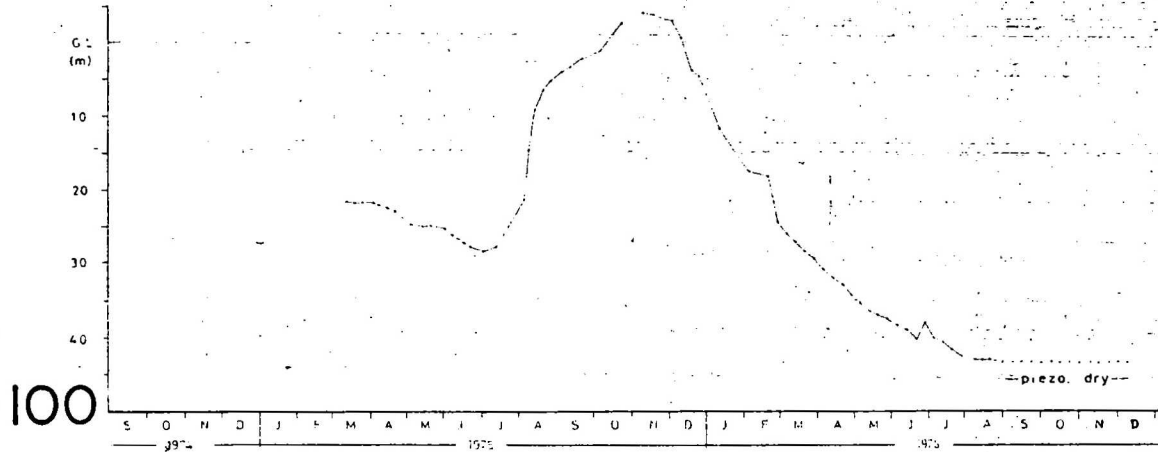
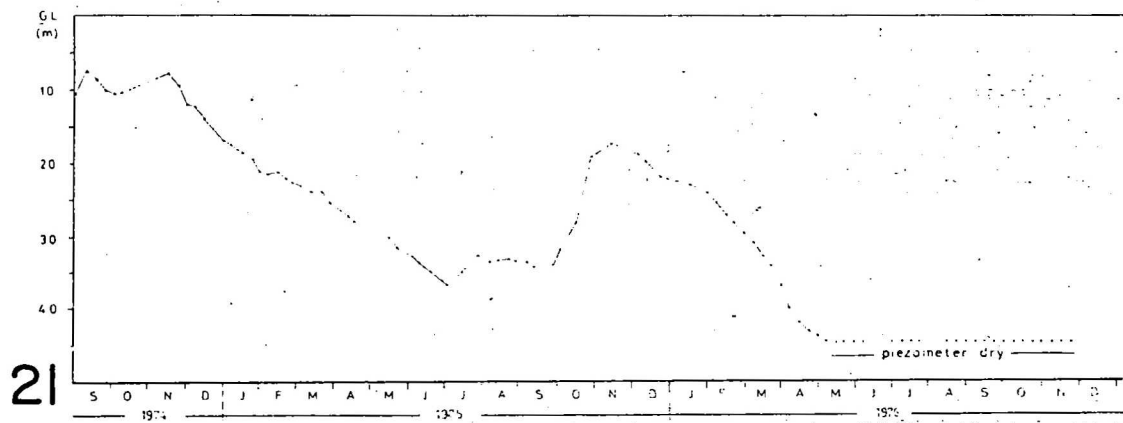
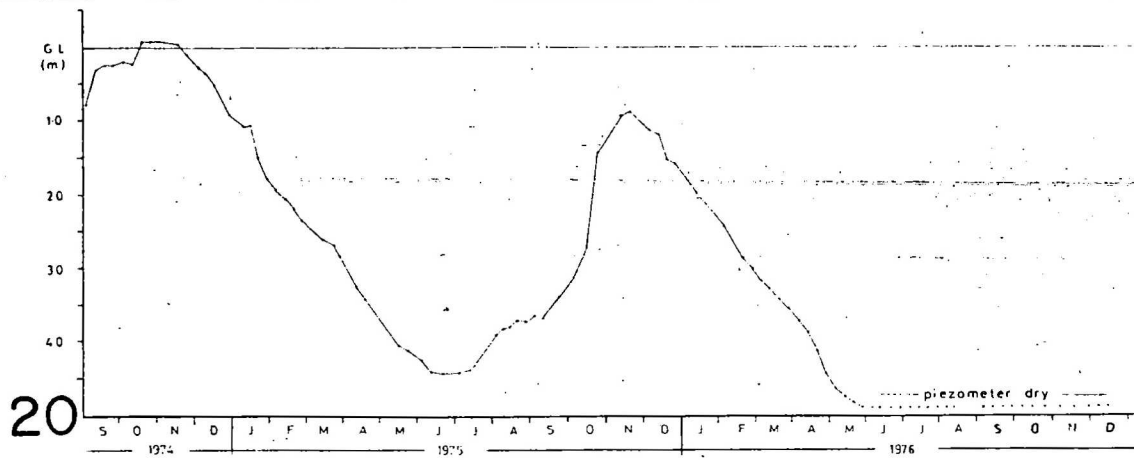




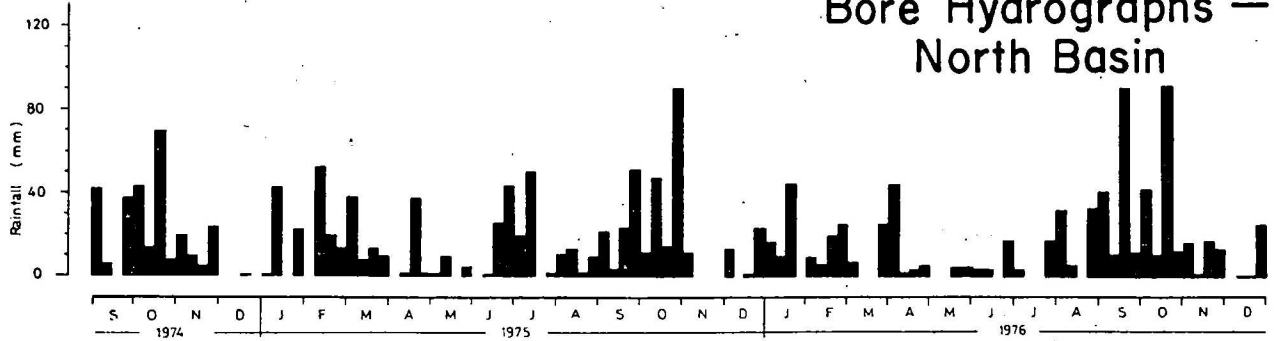


Bore Hydrographs — North Basin

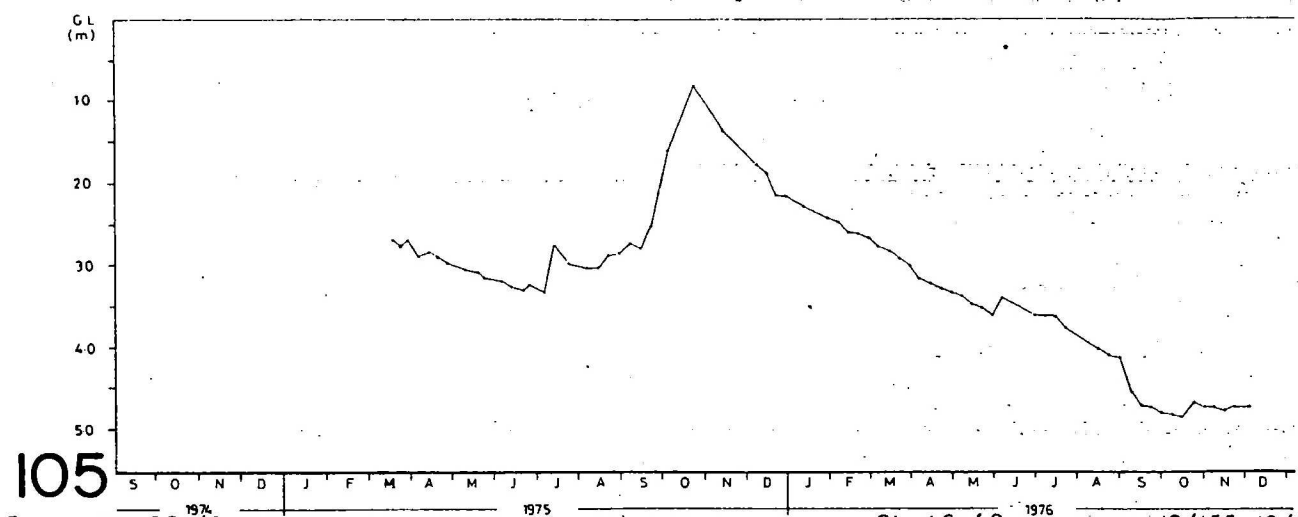
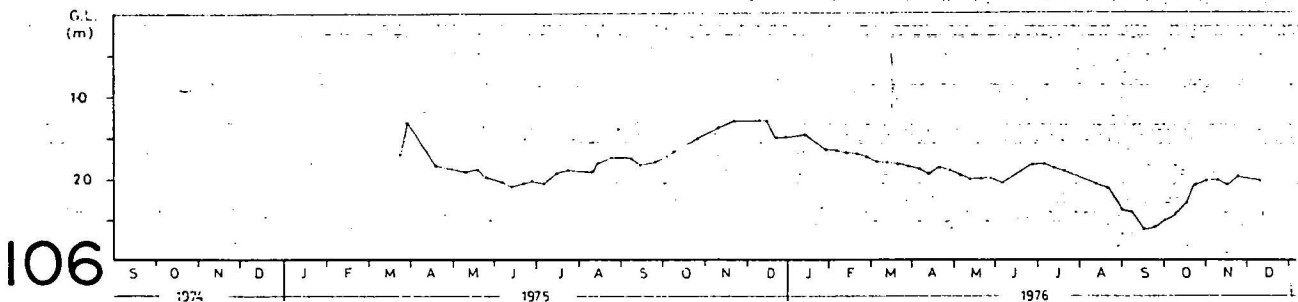
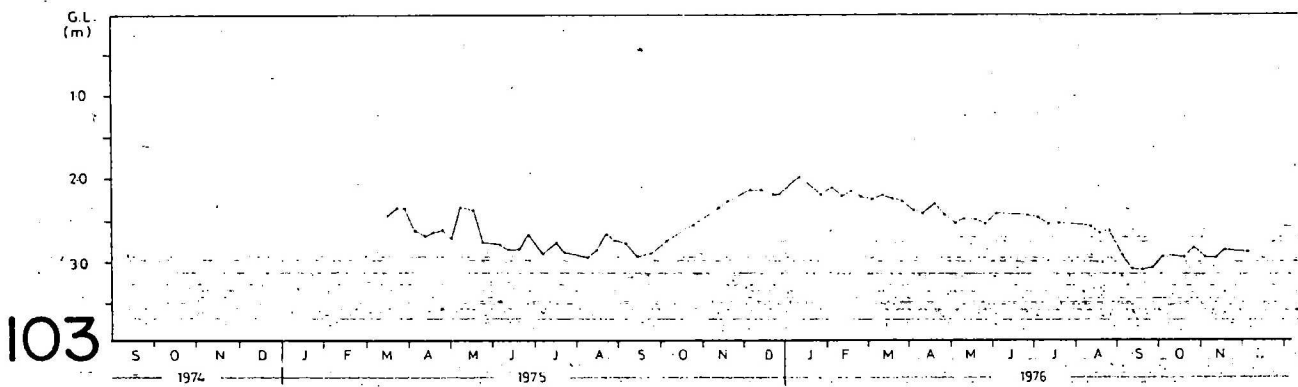
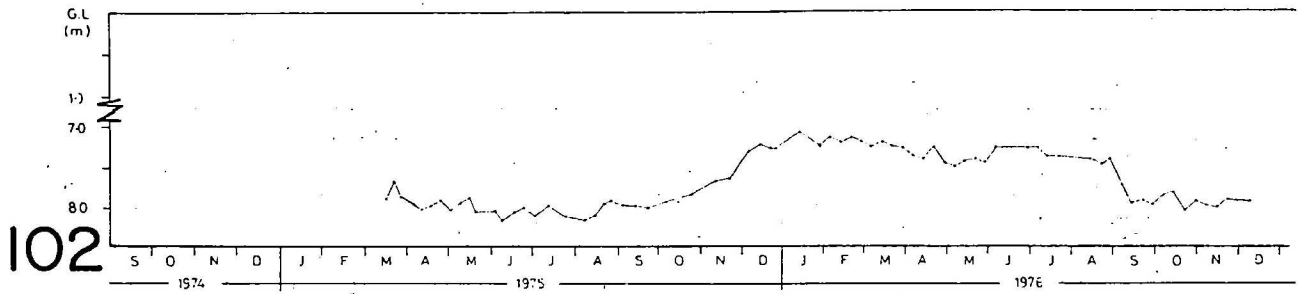


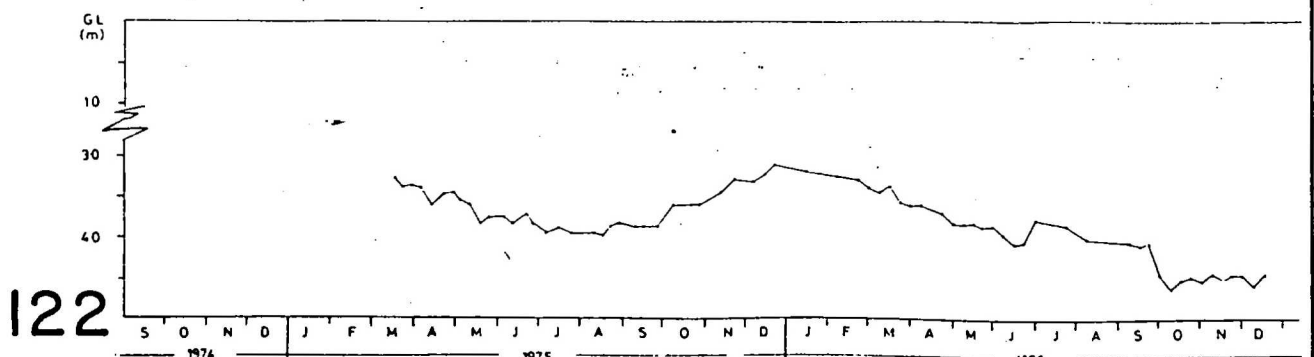
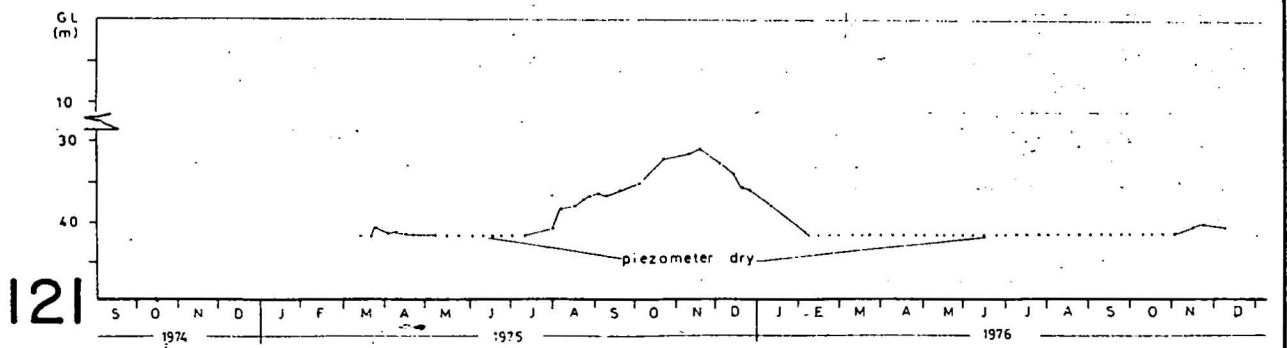
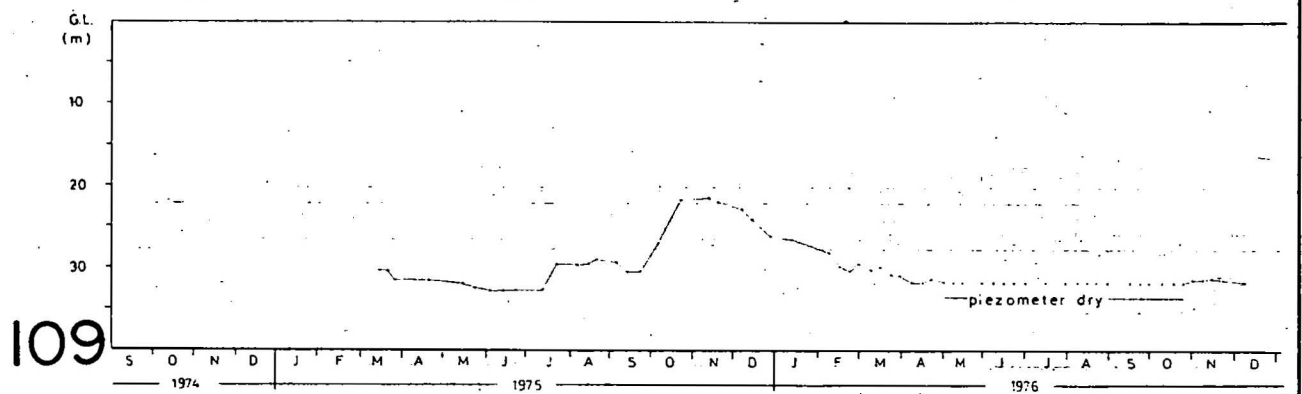
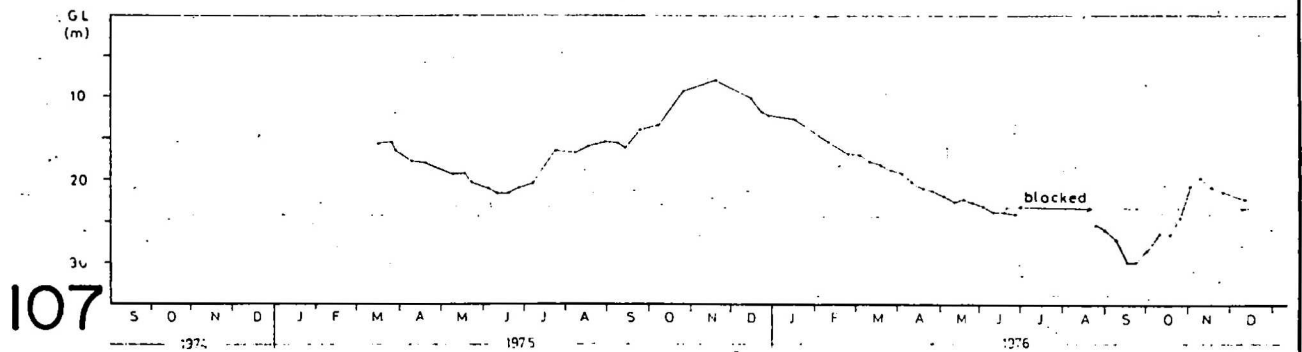
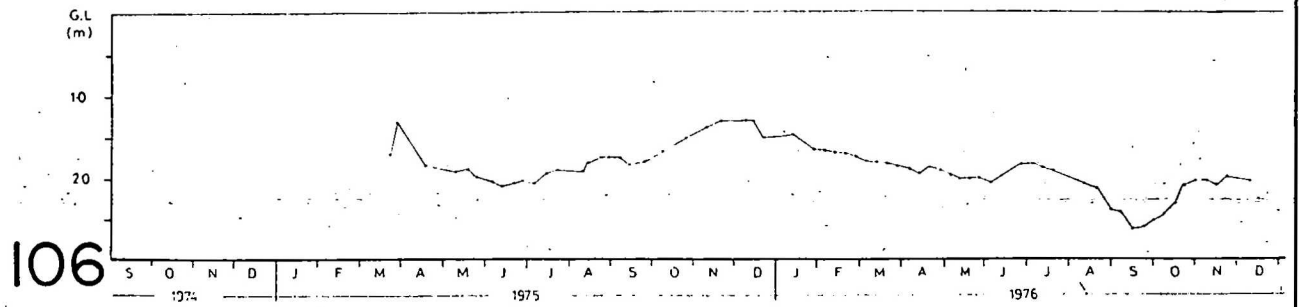


Bore Hydrographs — North Basin

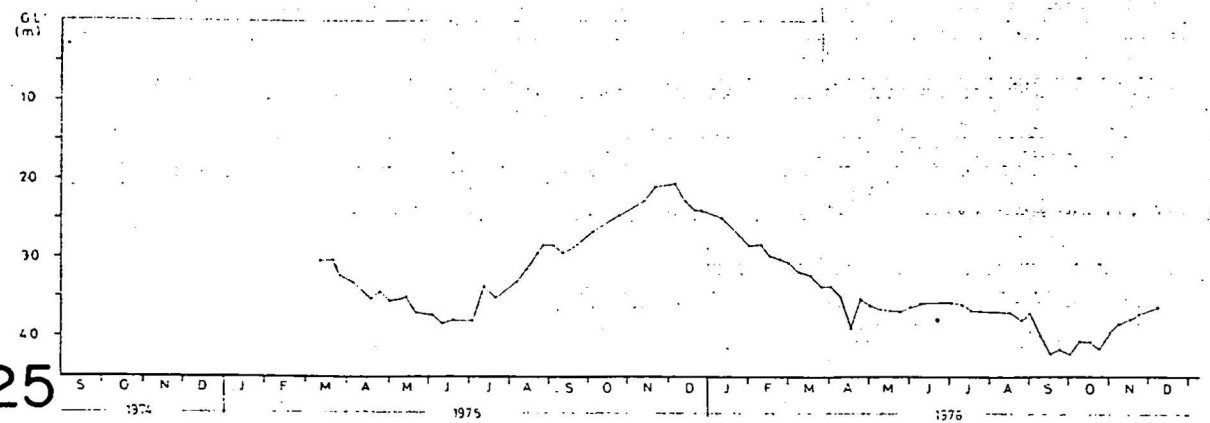
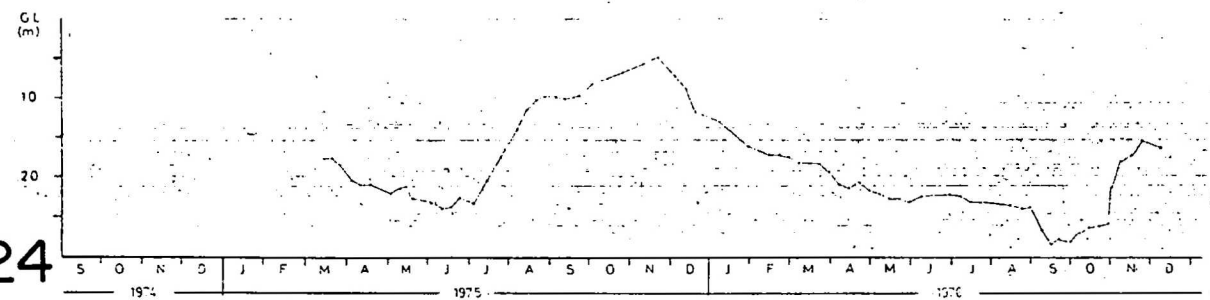
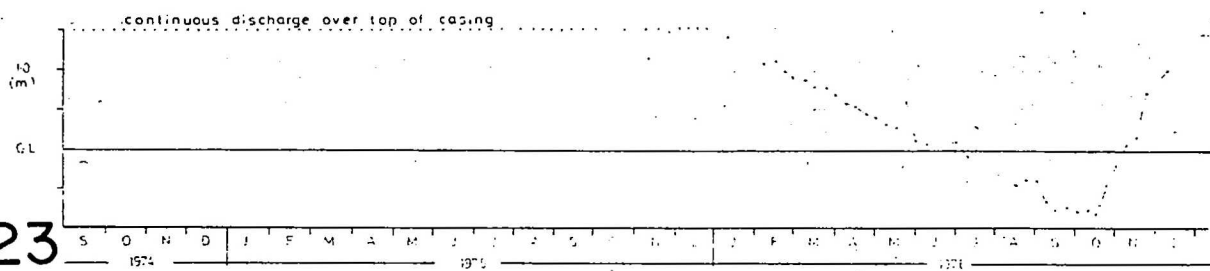
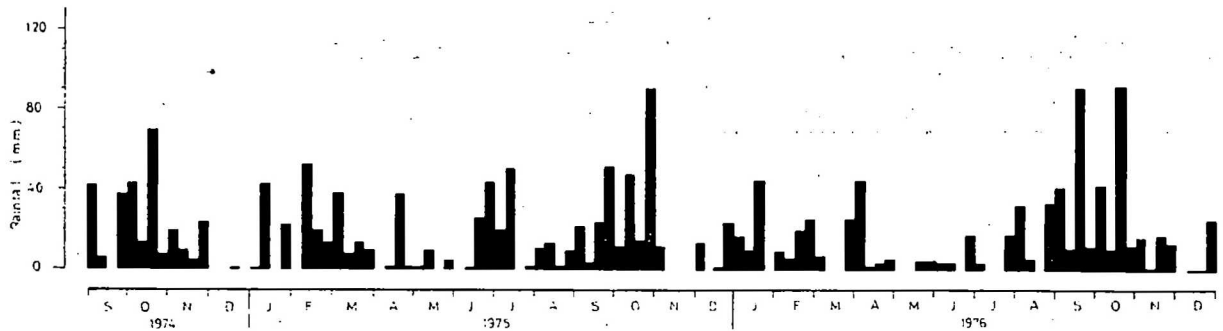


RAINFALL FIGURES - YARRALUMLA ACT

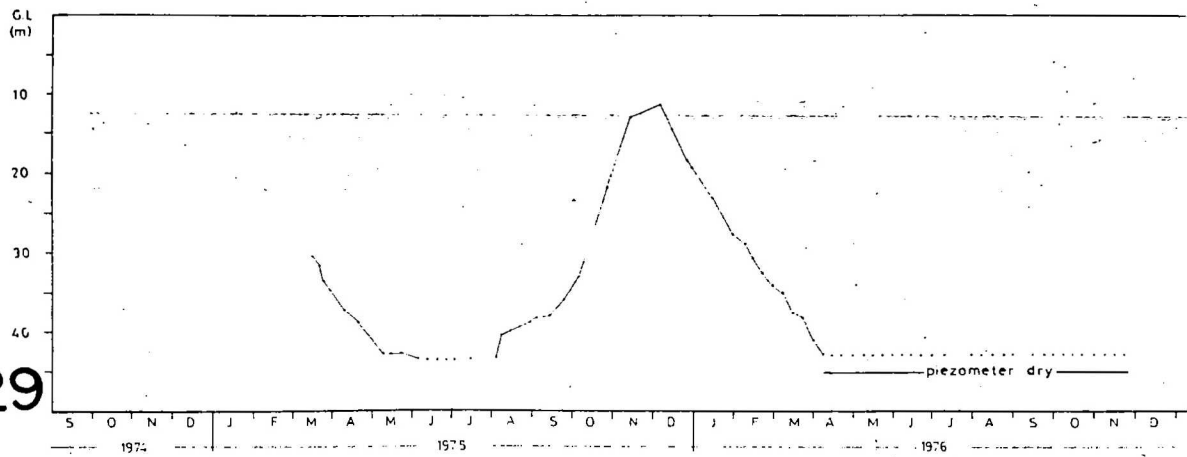




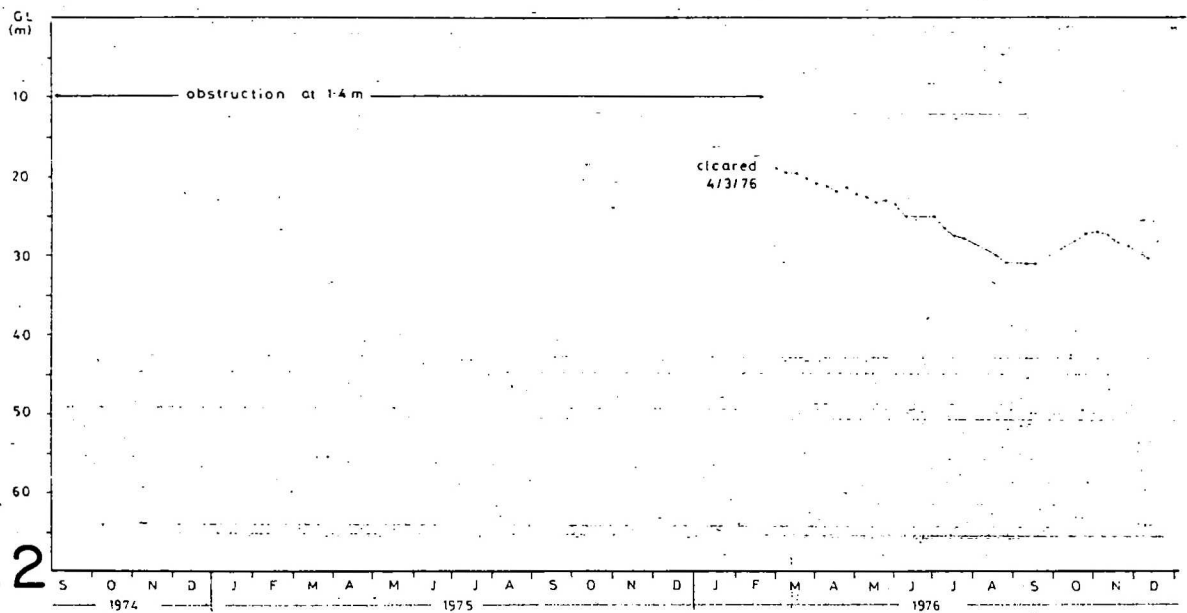
Bore Hydrographs — North Basin



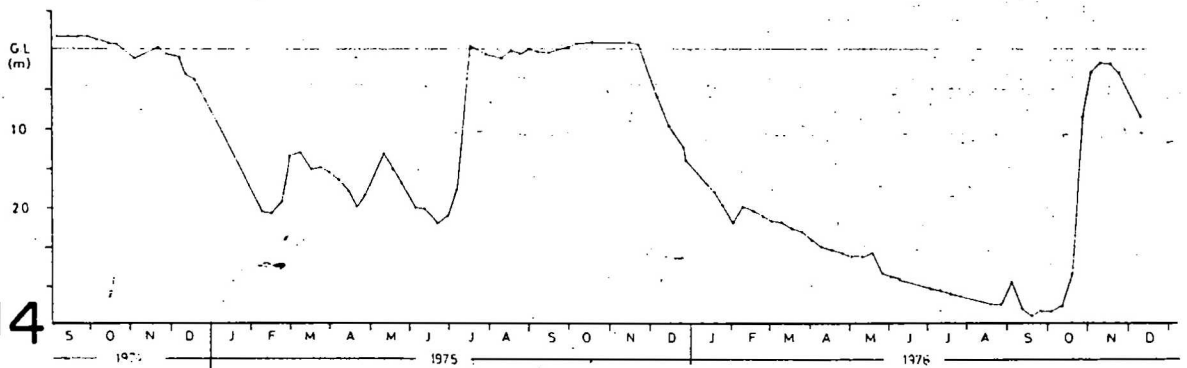
I29



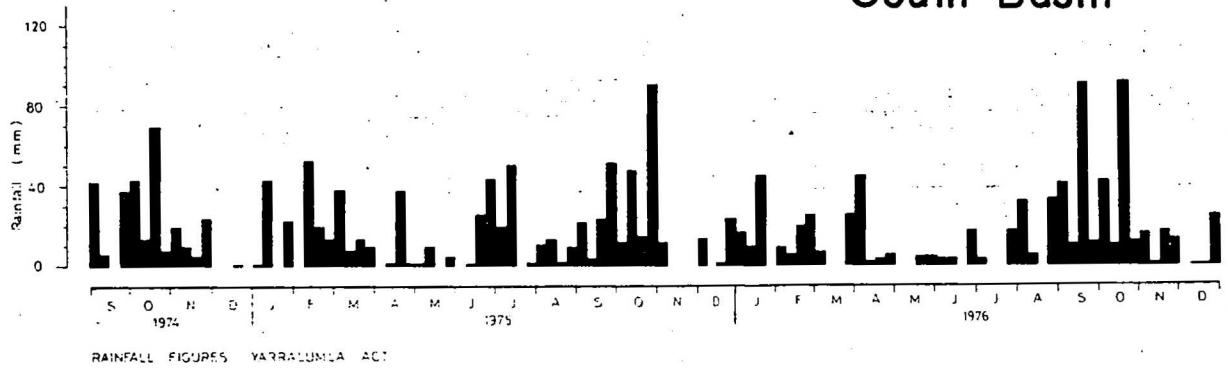
L2



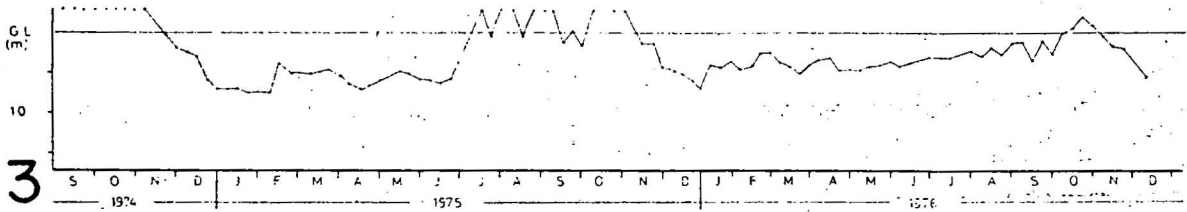
TU4



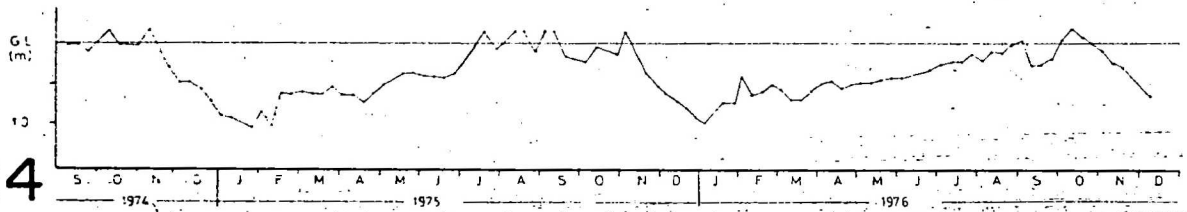
Appendix 5 Bore Hydrographs - South Basin



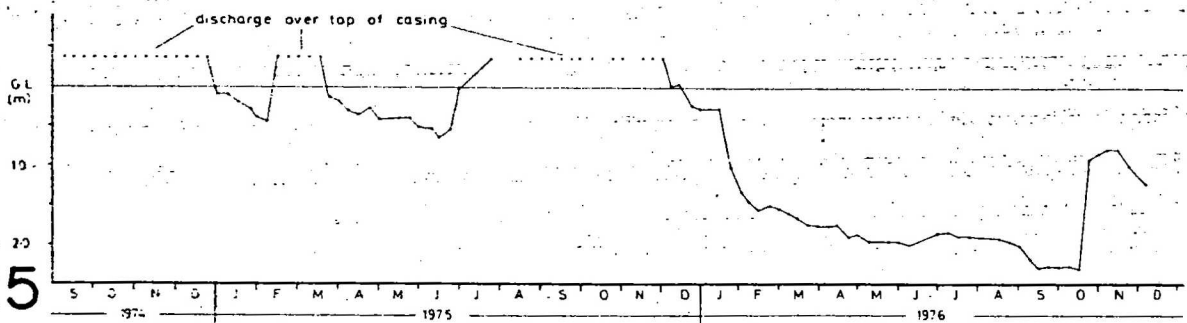
23



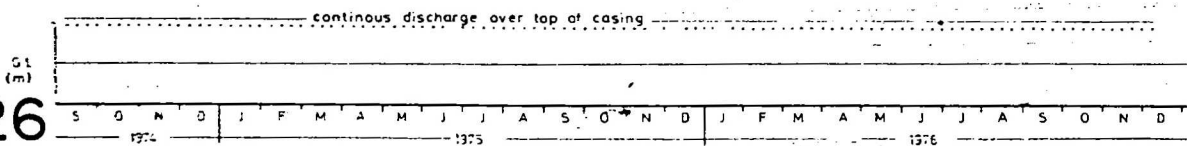
24

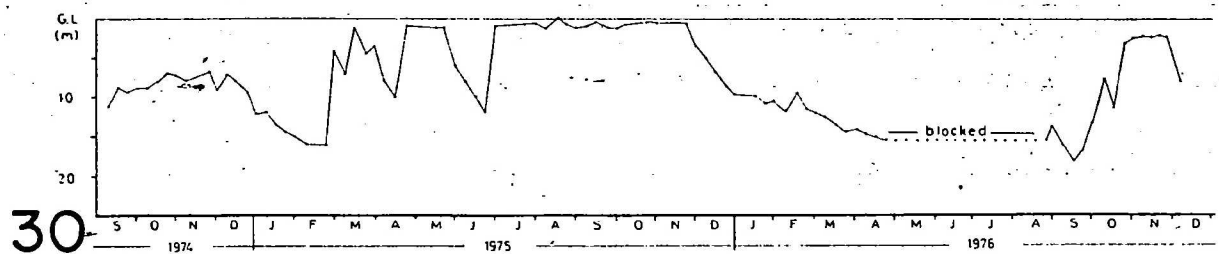
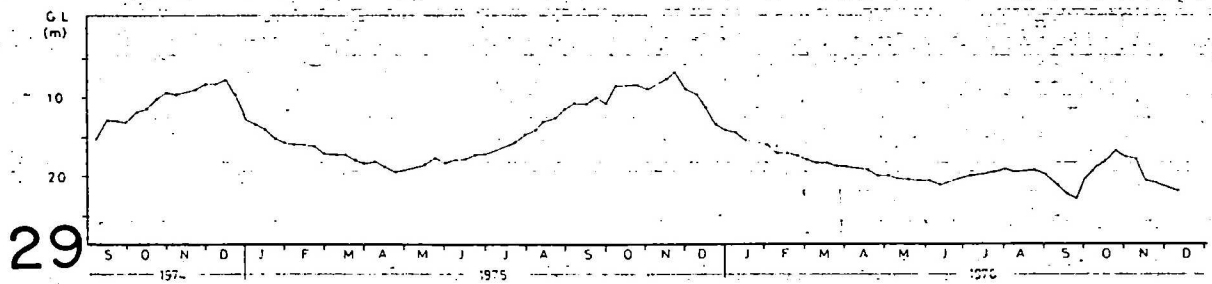
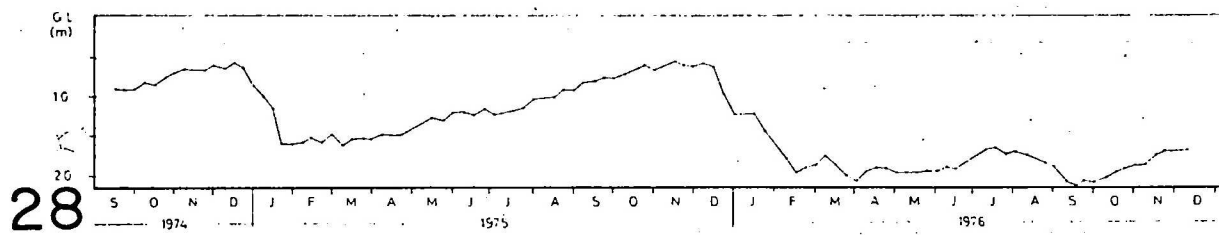
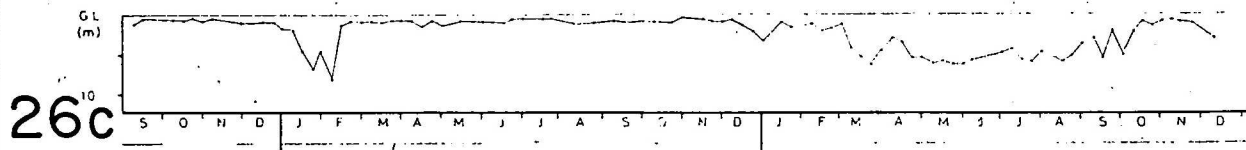
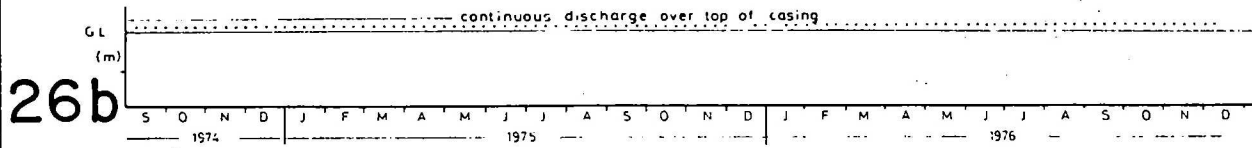


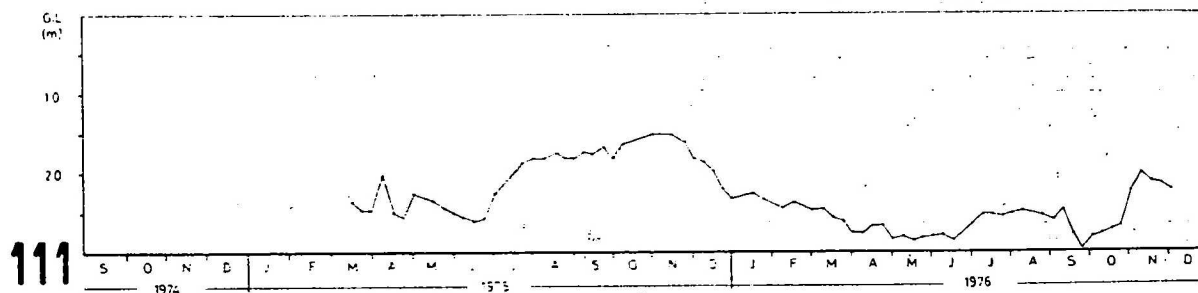
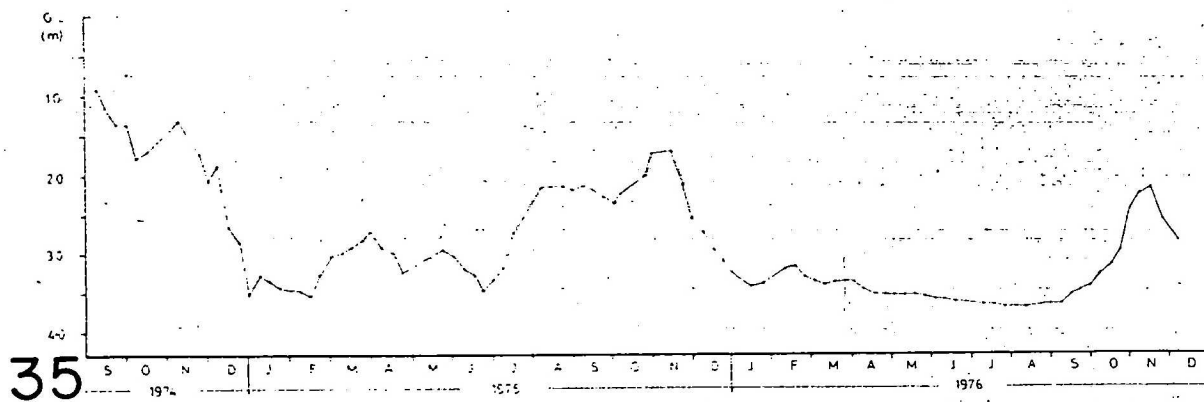
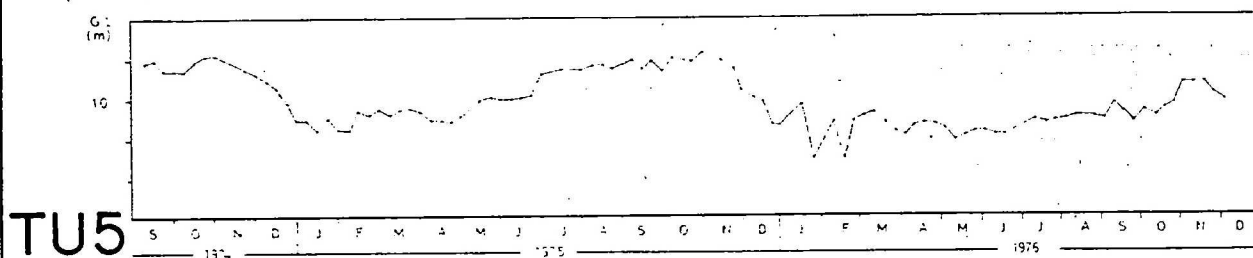
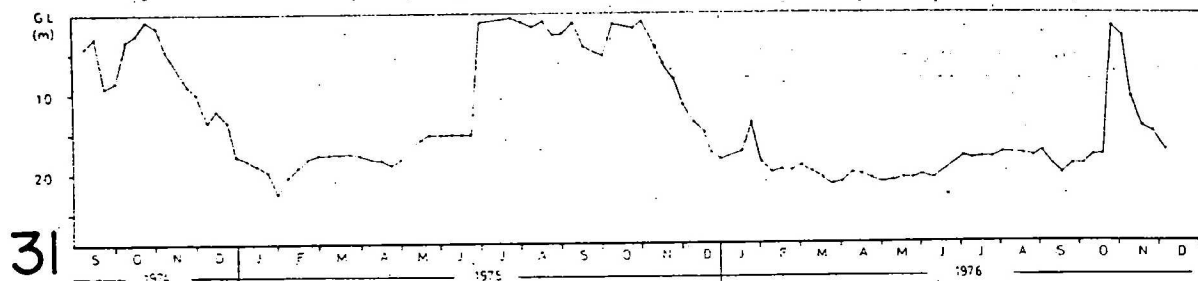
25



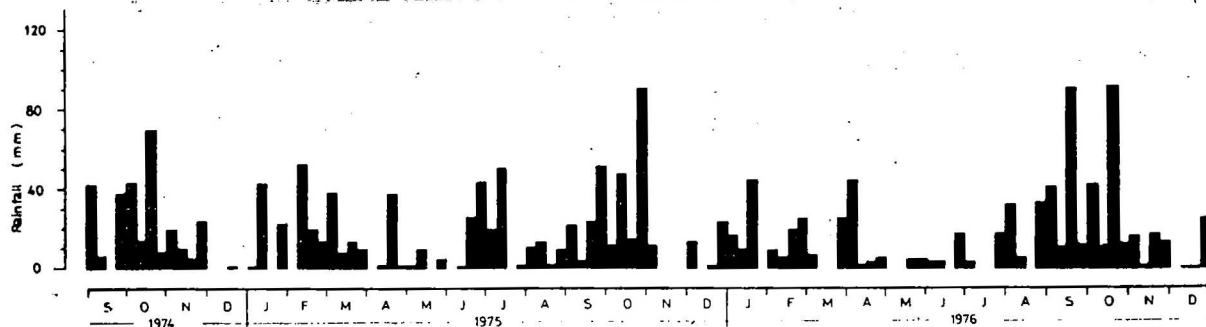
26



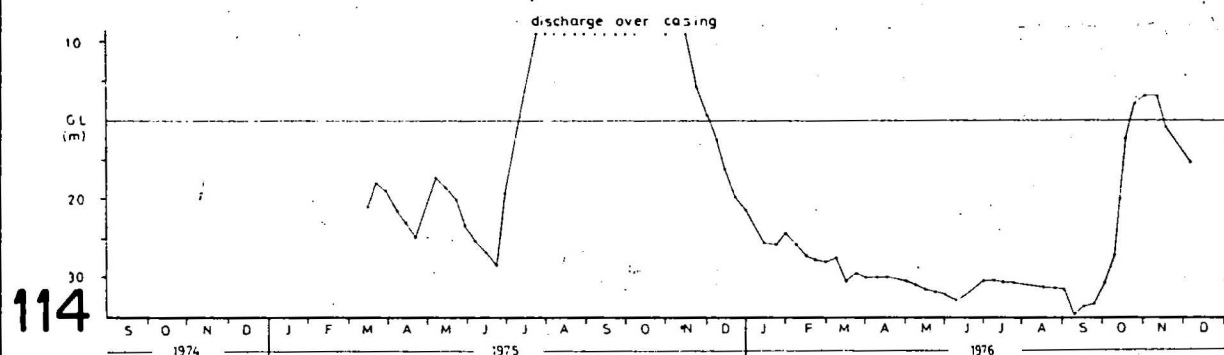
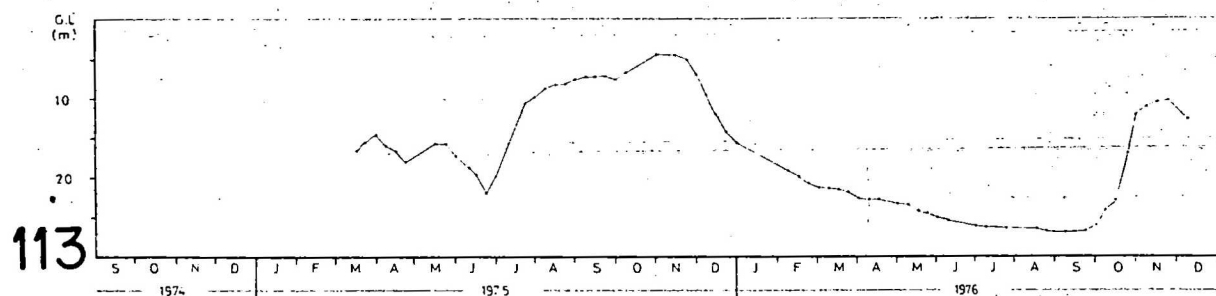
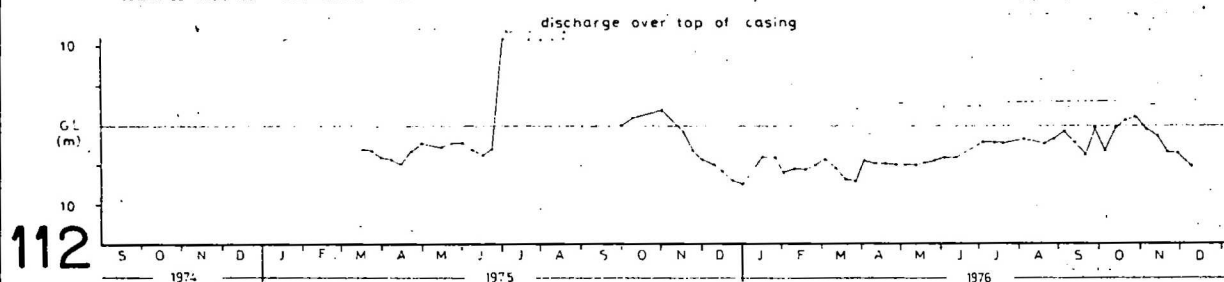


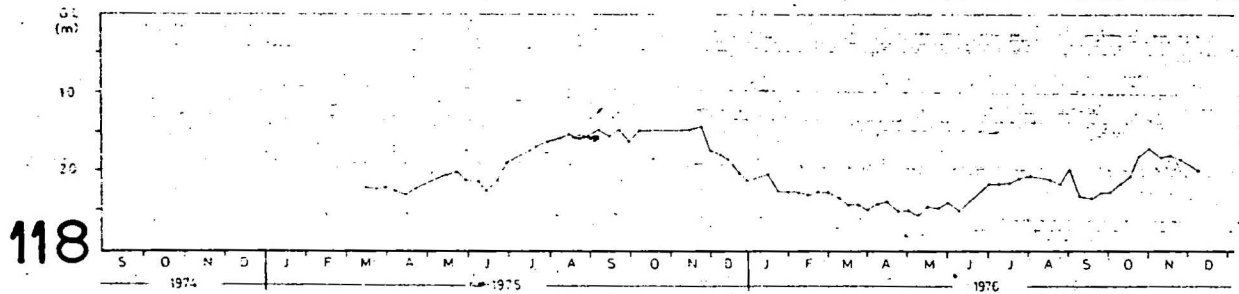
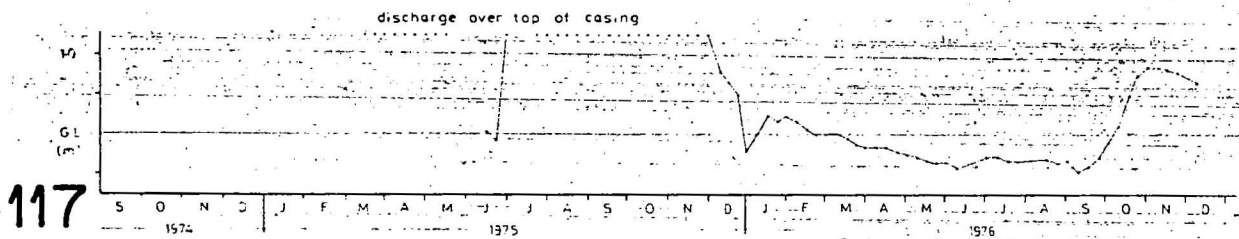
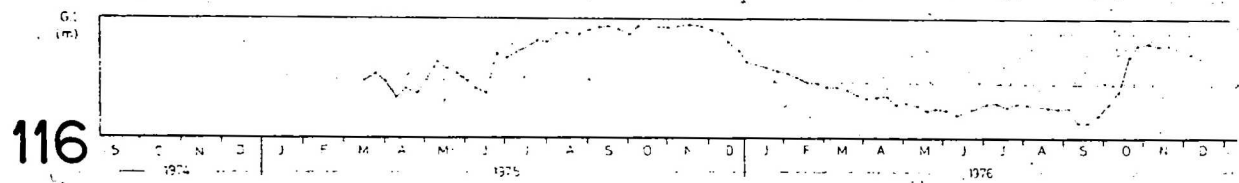
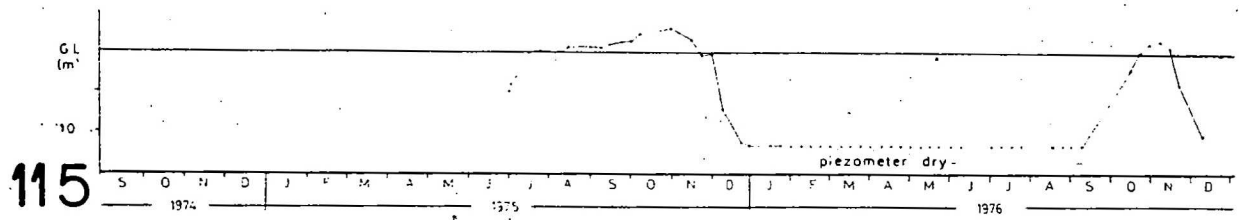


Bore Hydrographs - South Basin

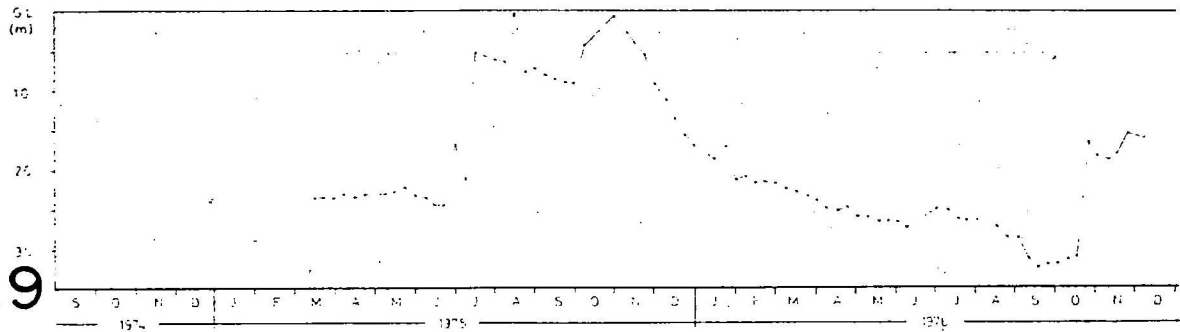


RAINFALL FIGURES - YARRALUMLA ACT

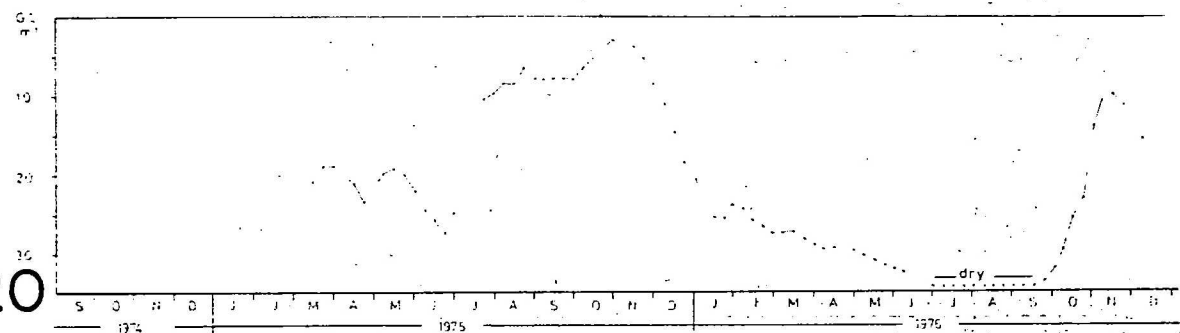




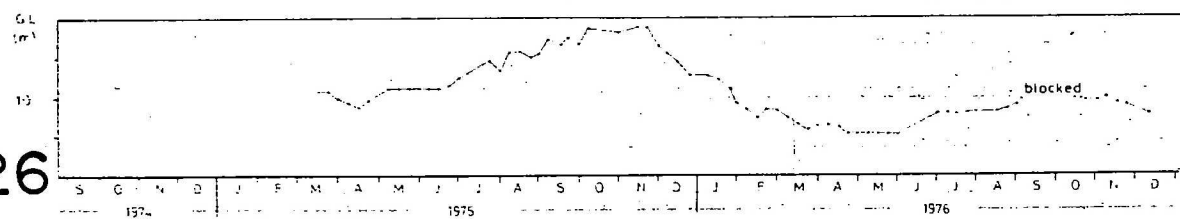
119



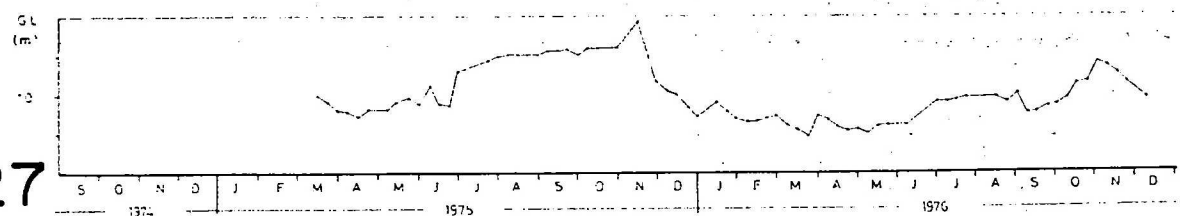
120

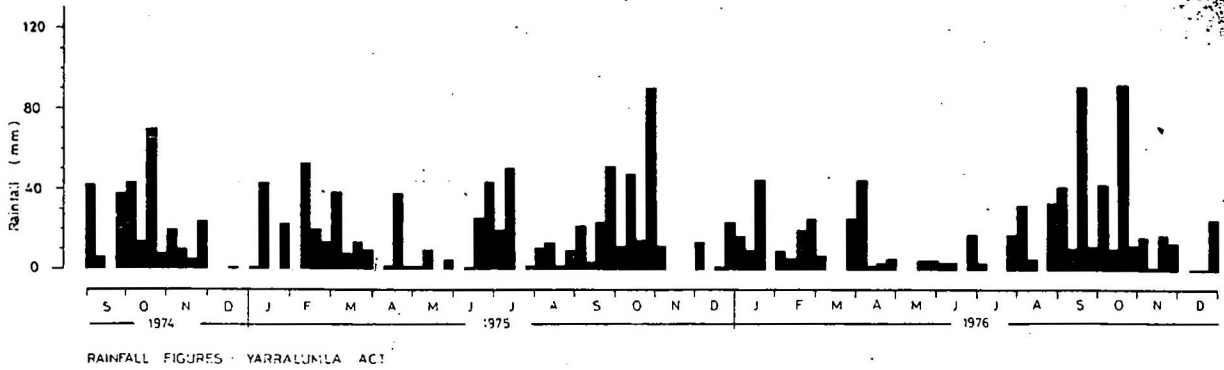


126

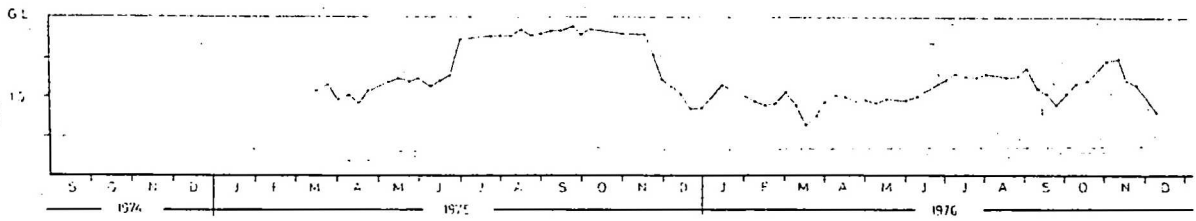


127

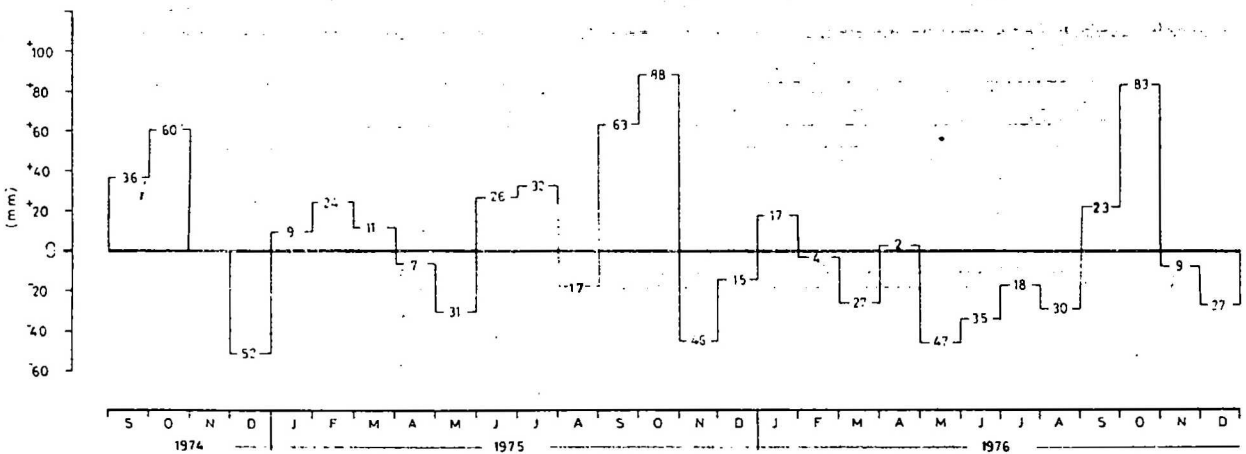
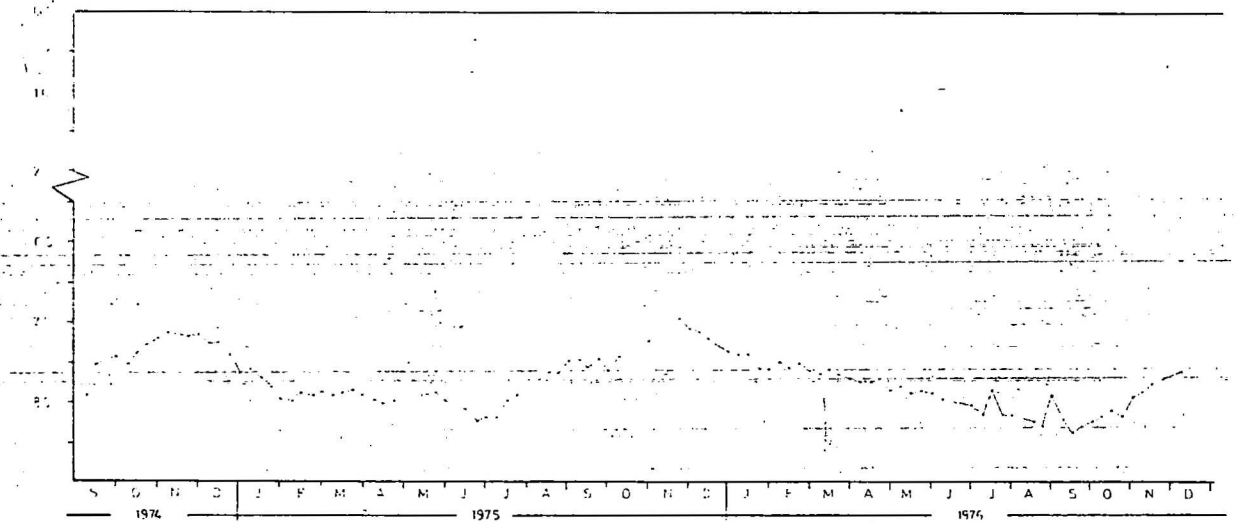




128



L1



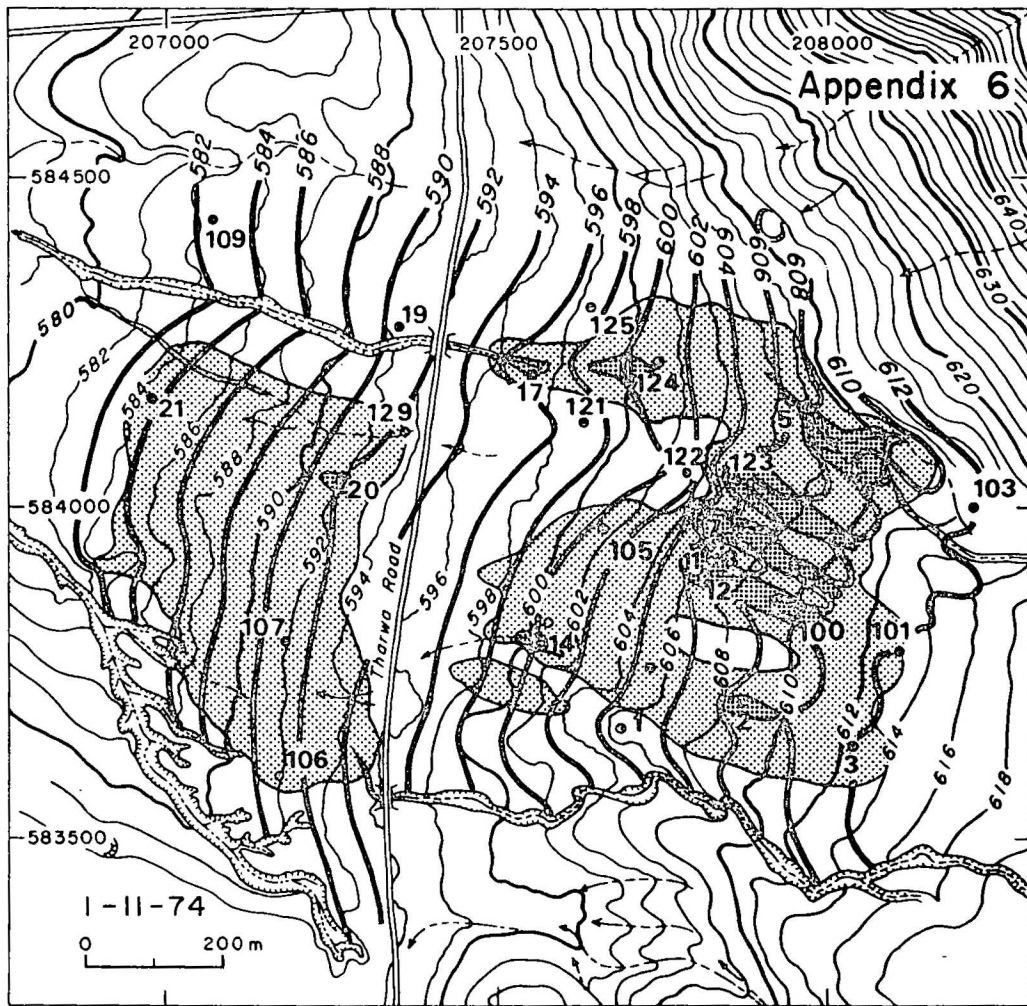
DIFFERENCE BETWEEN MONTHLY RAINFALL FOR
PERIOD SEPT. 74 - DEC. 76 AND AVERAGE
MONTHLY RAINFALL (YARRALUMLA 1928-1976)

MONTH	J	F	M	A	M	J	J	A	S	O	N	D
AVERAGE RAINFALL	58	60	59	54	48	43	43	53	50	78	59	54
1974									86	138	59	2
1975	67	84	70	47	17	69	75	36	113	166	13	39
1976	75	56	32	56	1	8	25	23	73	161	50	27

ALL MEASUREMENTS IN (mm)

APPENDIX 6

FLUCTUATIONS OF POTENTIOMETRIC SURFACE IN
SURFICIAL AQUIFERS, LANYON NORTH AND SOUTH BASINS

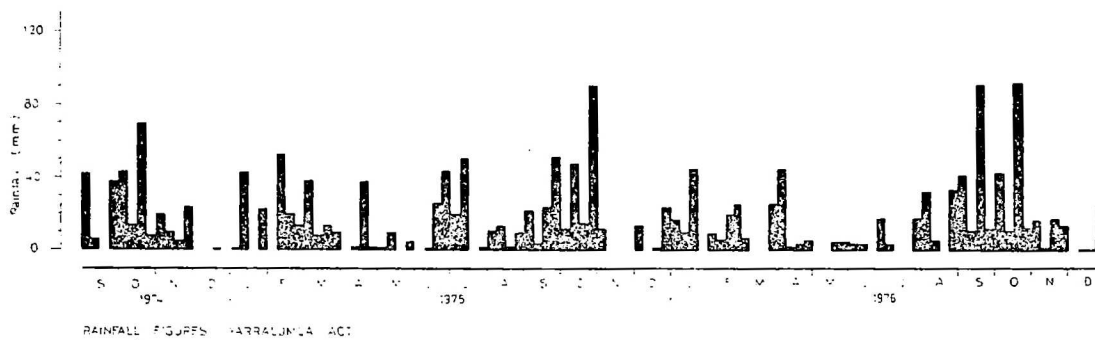


Record No. 1981/61

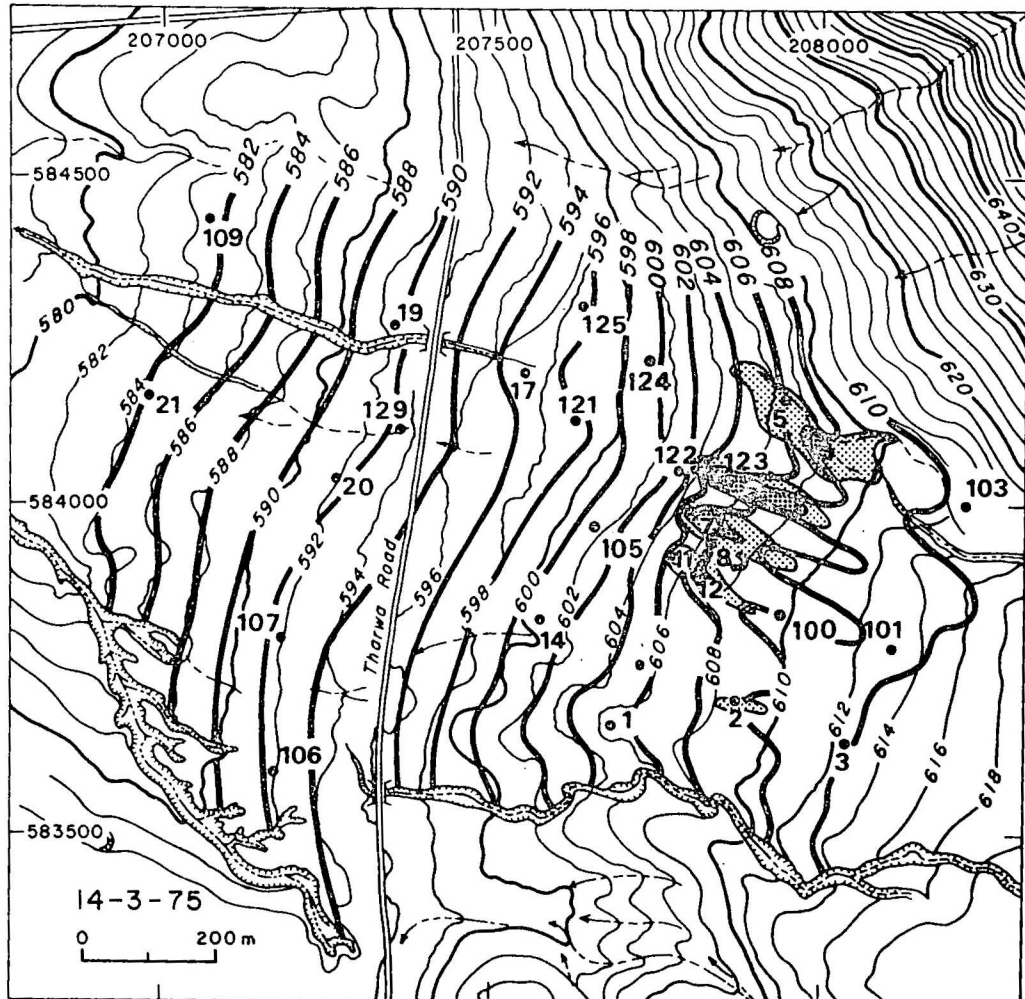
Sheet 1 of 12

19/155-16/85

- Contour in metres of the potentiometric surface in the surficial aquifers
- ▨ Areas where potentiometric surface was at or above ground level
- ▤ Areas where potentiometric surface was within one metre of ground level
- Piezometer



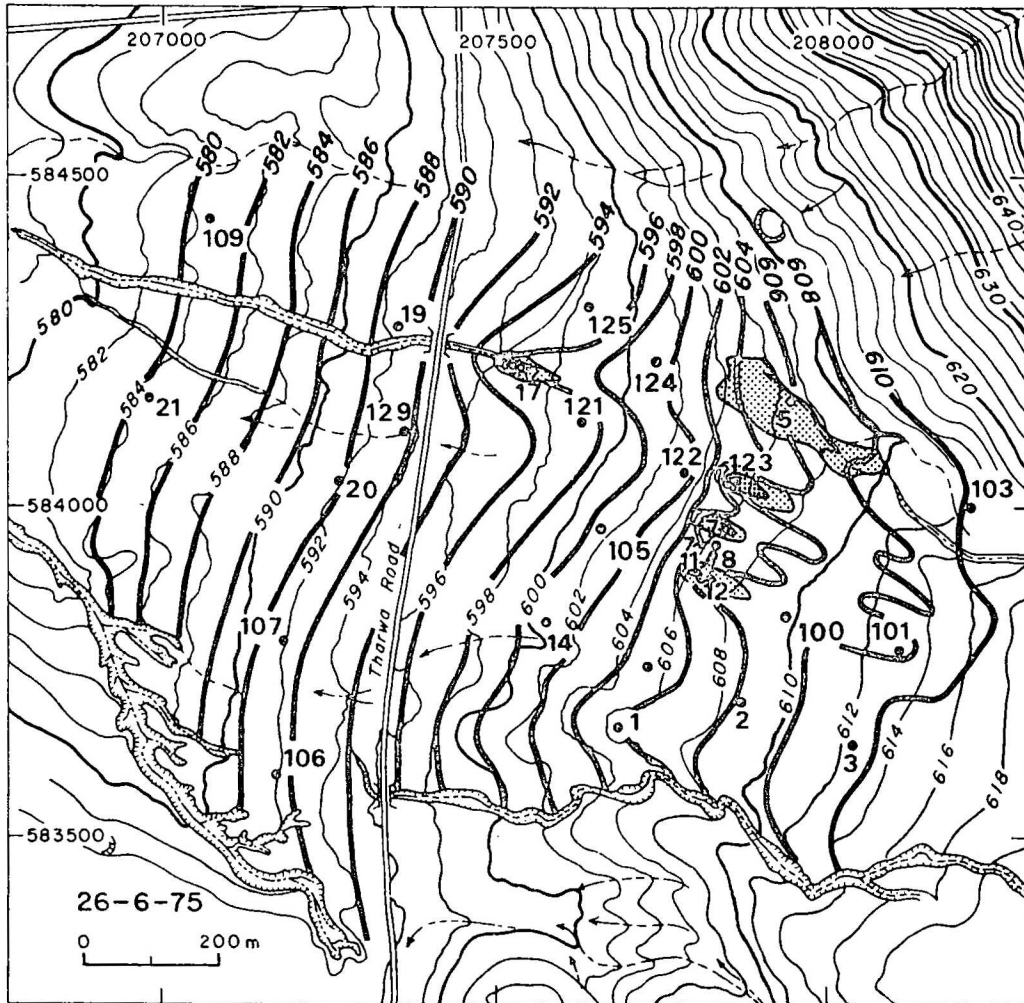
Fluctuation in potentiometric surfaces, Nov. 1974 to Dec. 1976
North Basin



Record No. 1981/61

Sheet 2 of 12

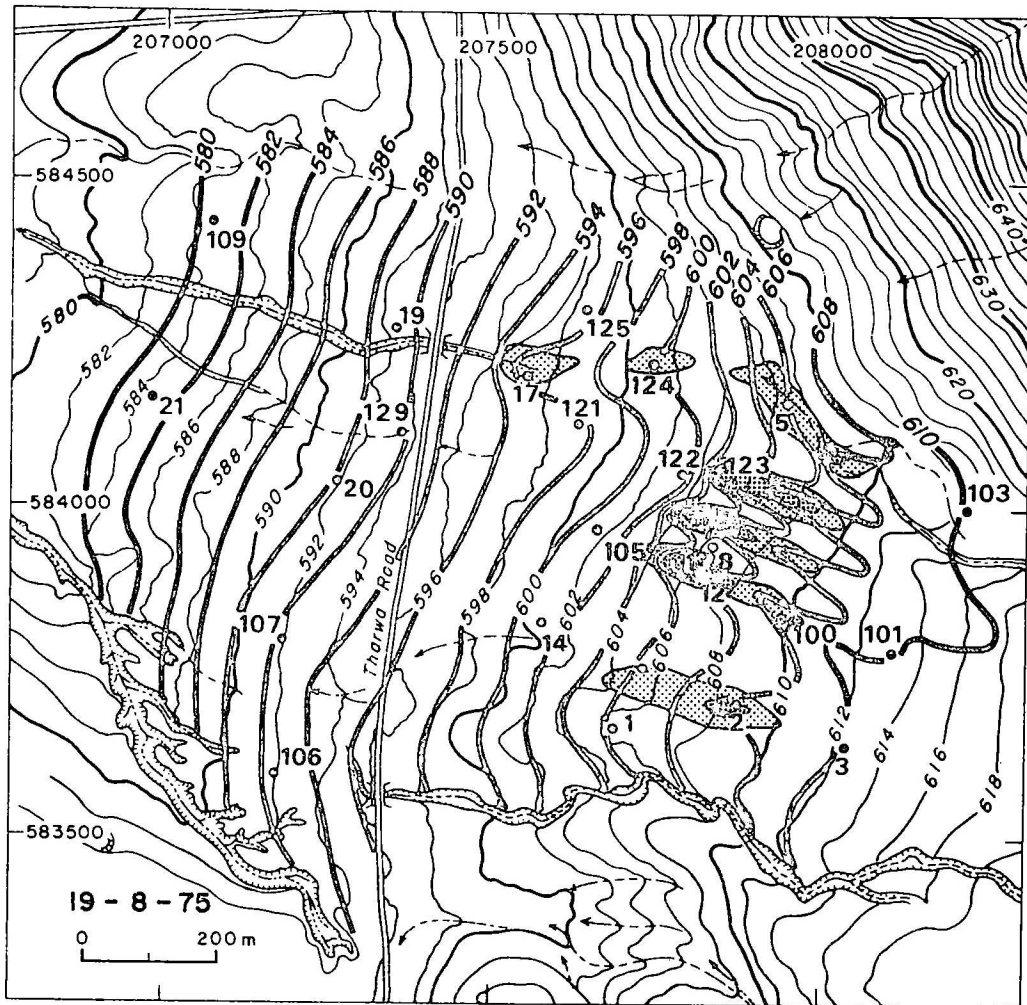
19/155-16/85



Record No. 1981/61

Sheet 3 of 12

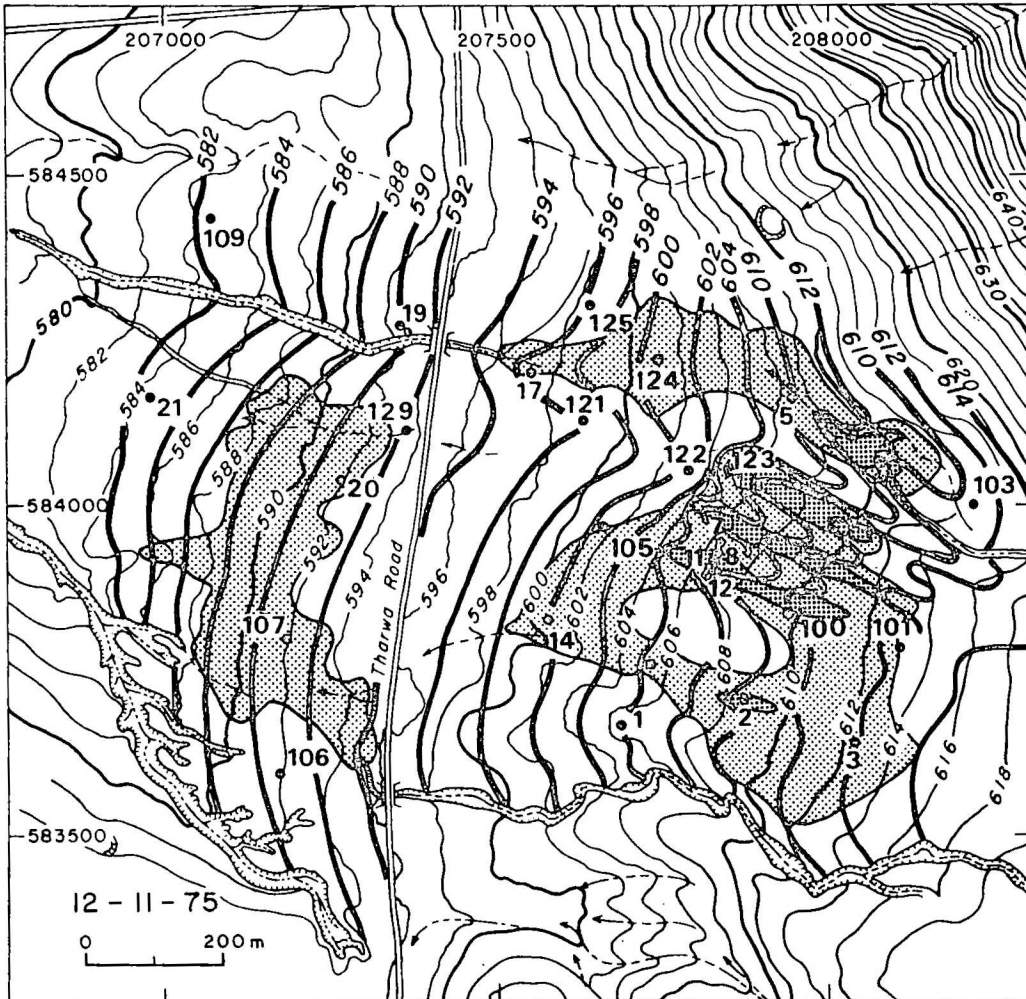
19/155-16/85



Record No. 1981/61

Sheet 4 of 12

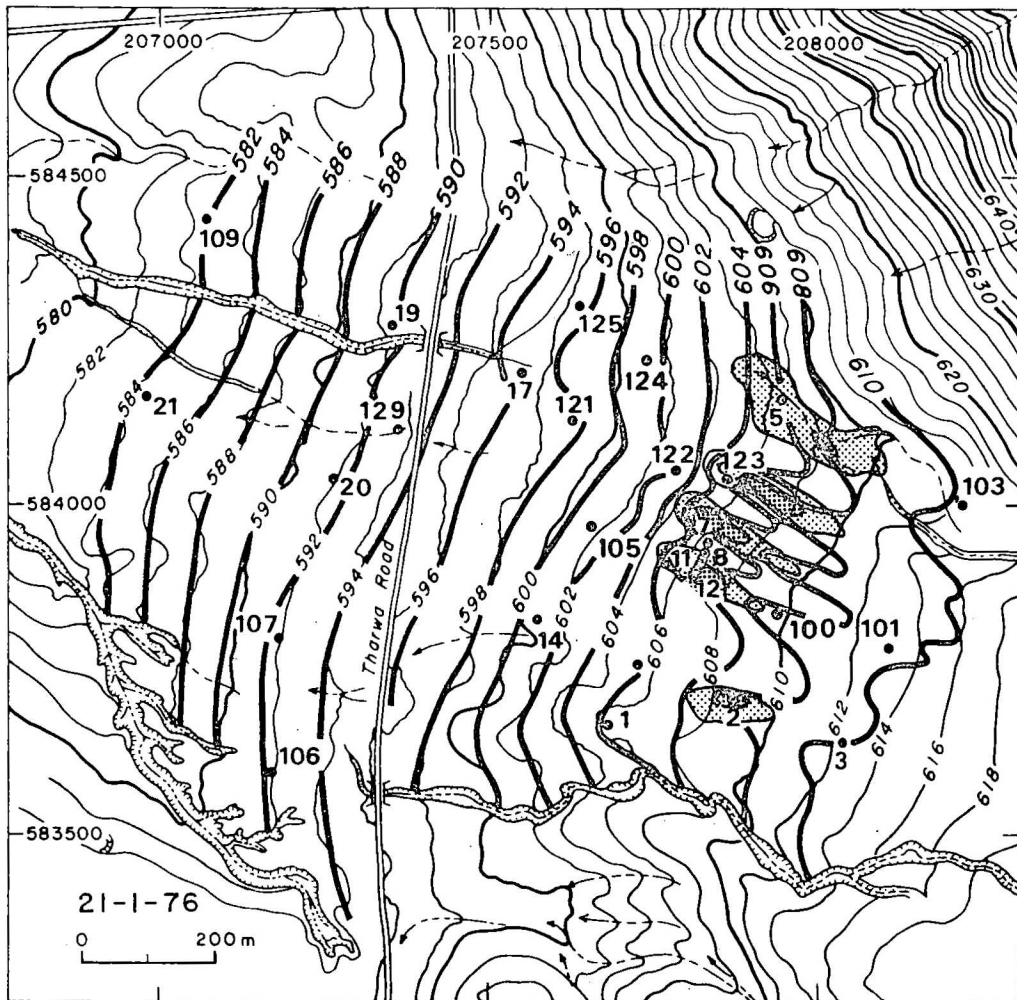
19/155-16/85



Record No. 1981/61

Sheet 5 of 12

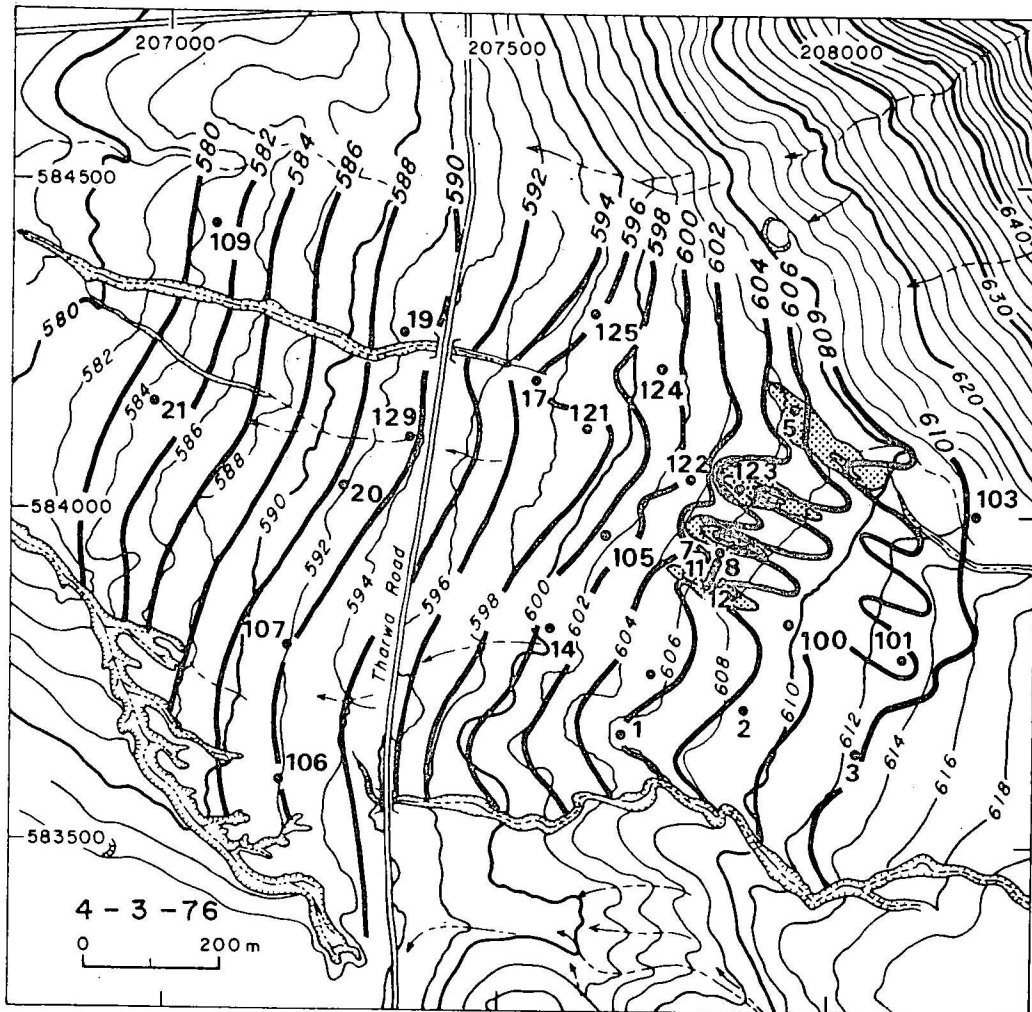
19/155 - 16/85



Record No 1981/61

Sheet 6 of 12

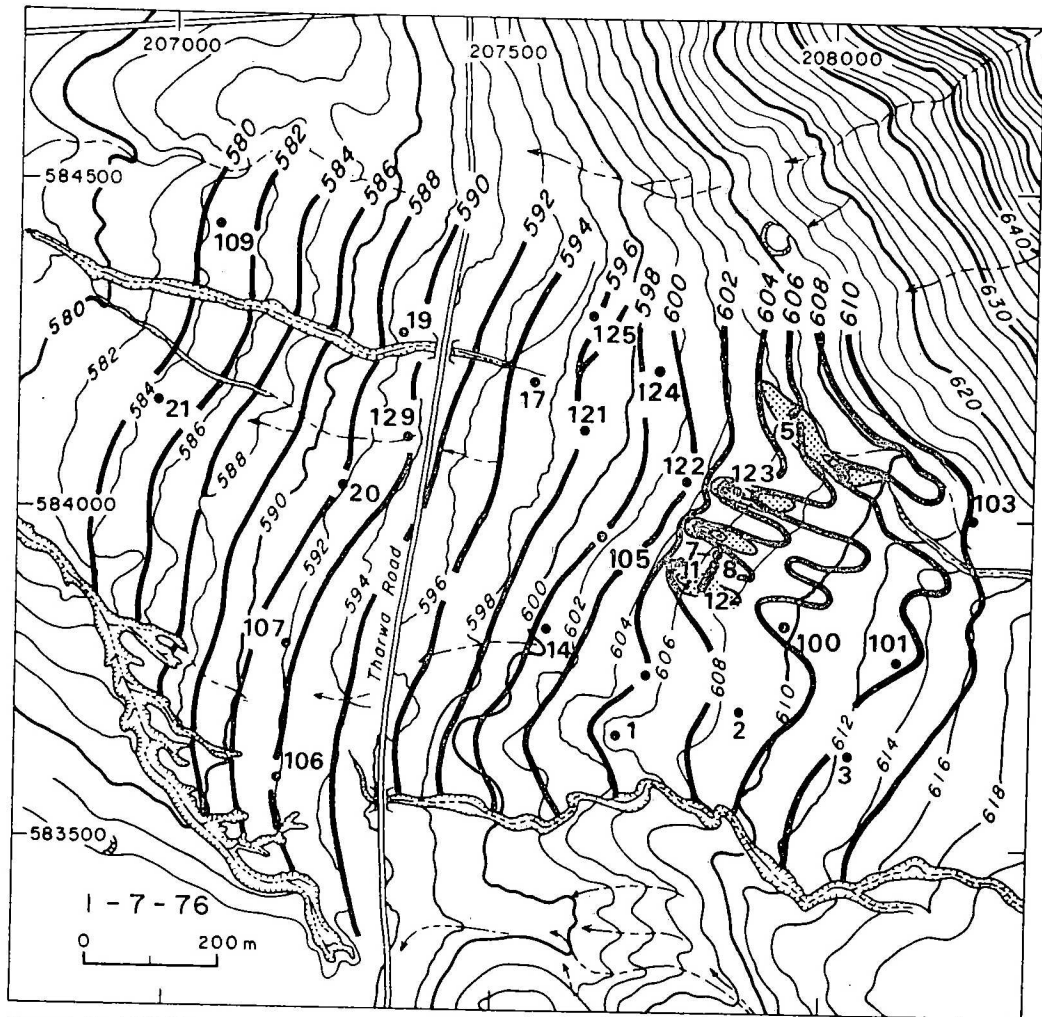
19/155 - 16/85



Record No. 1981/61

Sheet 7 of 12

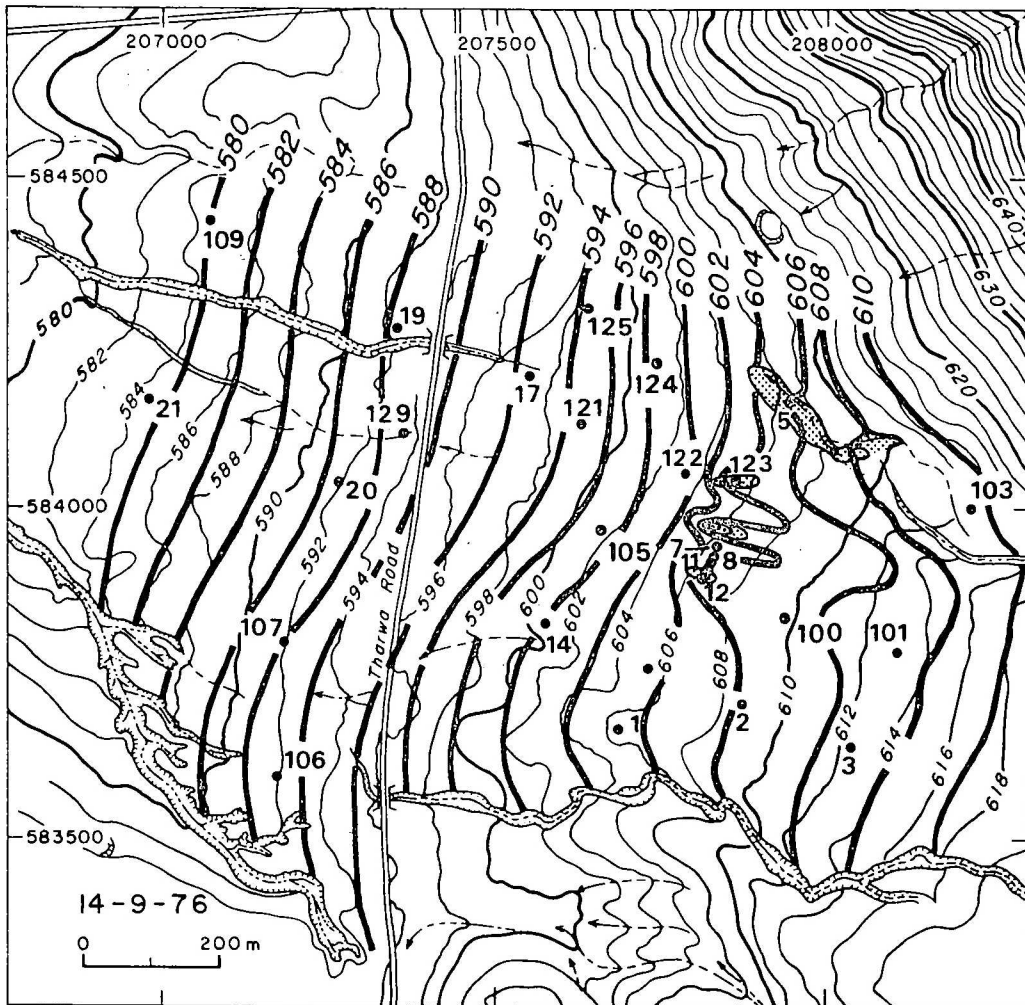
19/155 - 16/85



Record No. 1981/61

Sheet 8 of 12

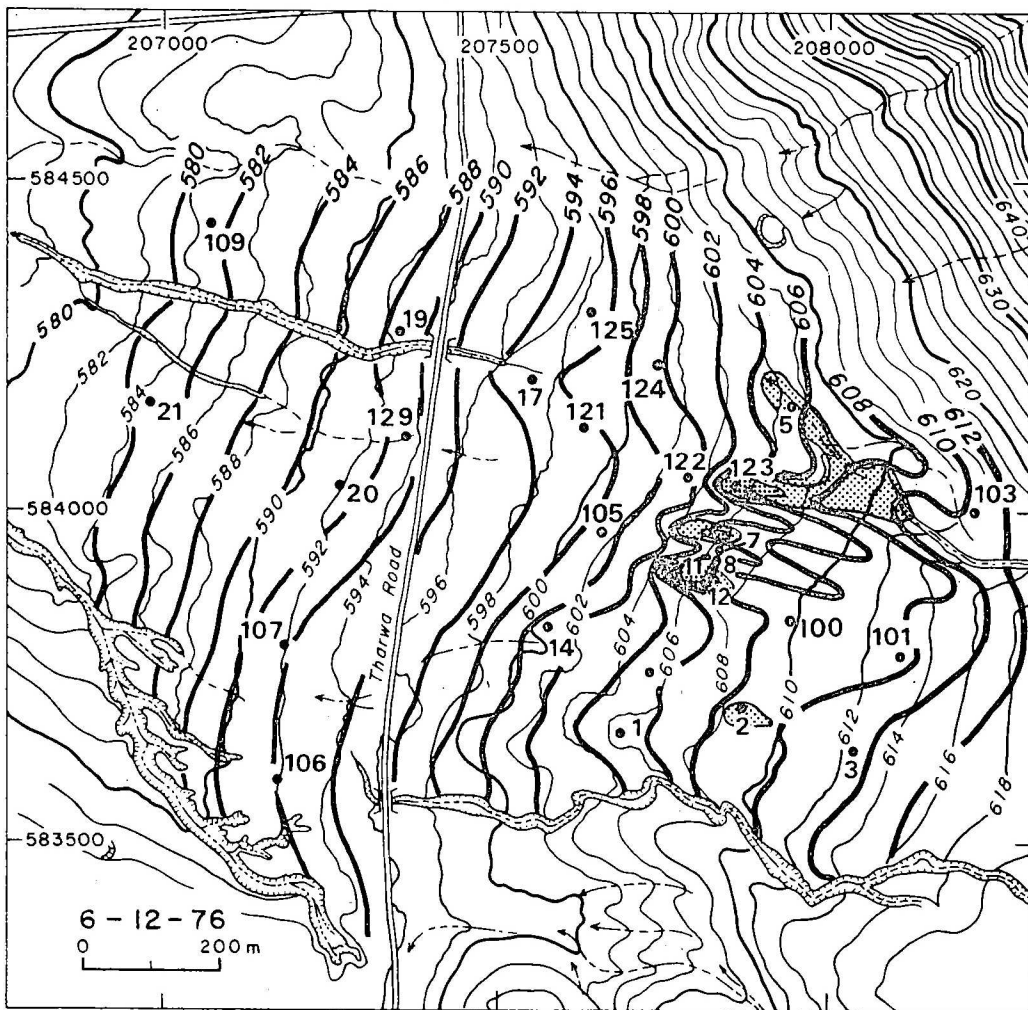
19/155 - 16/85



Record No. 1981/61

Sheet 9 of 12

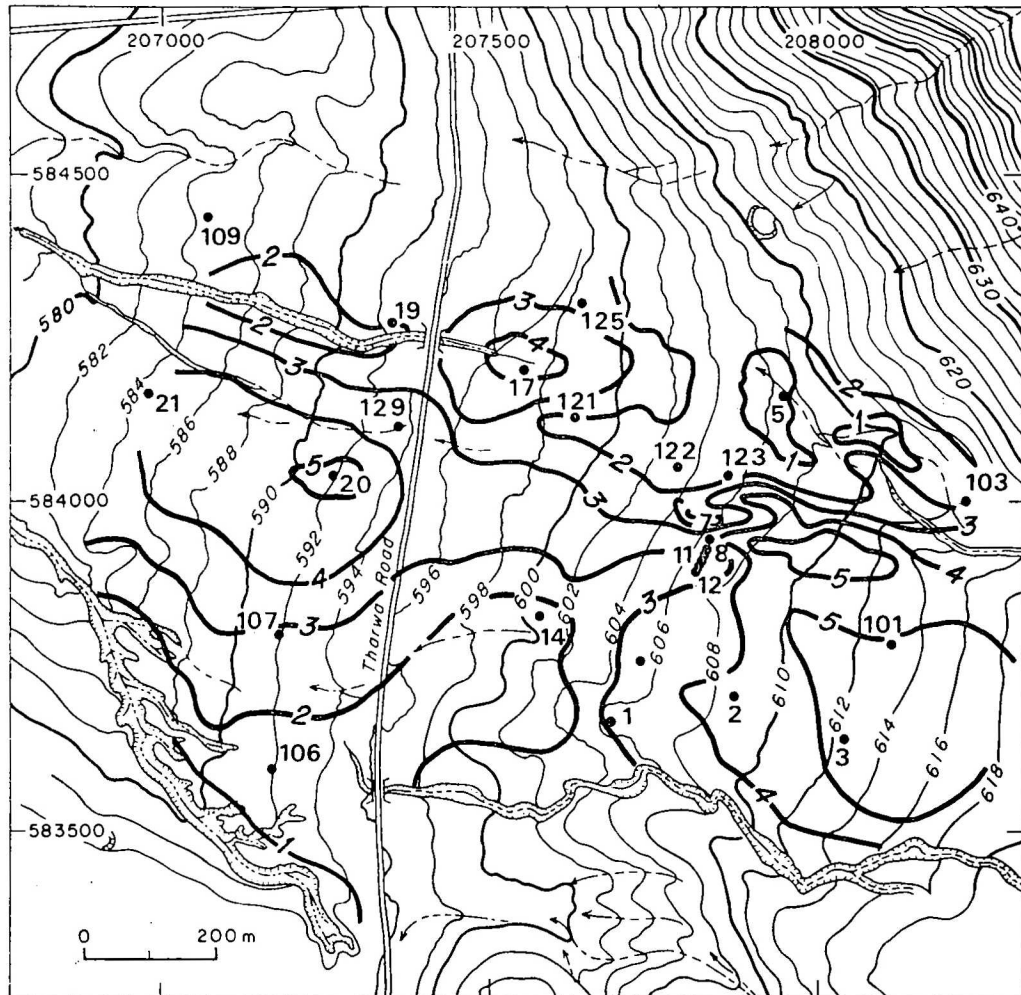
19/155-16/85



Record No. 1981/61

Sheet 11 of 12

19/155-16/85

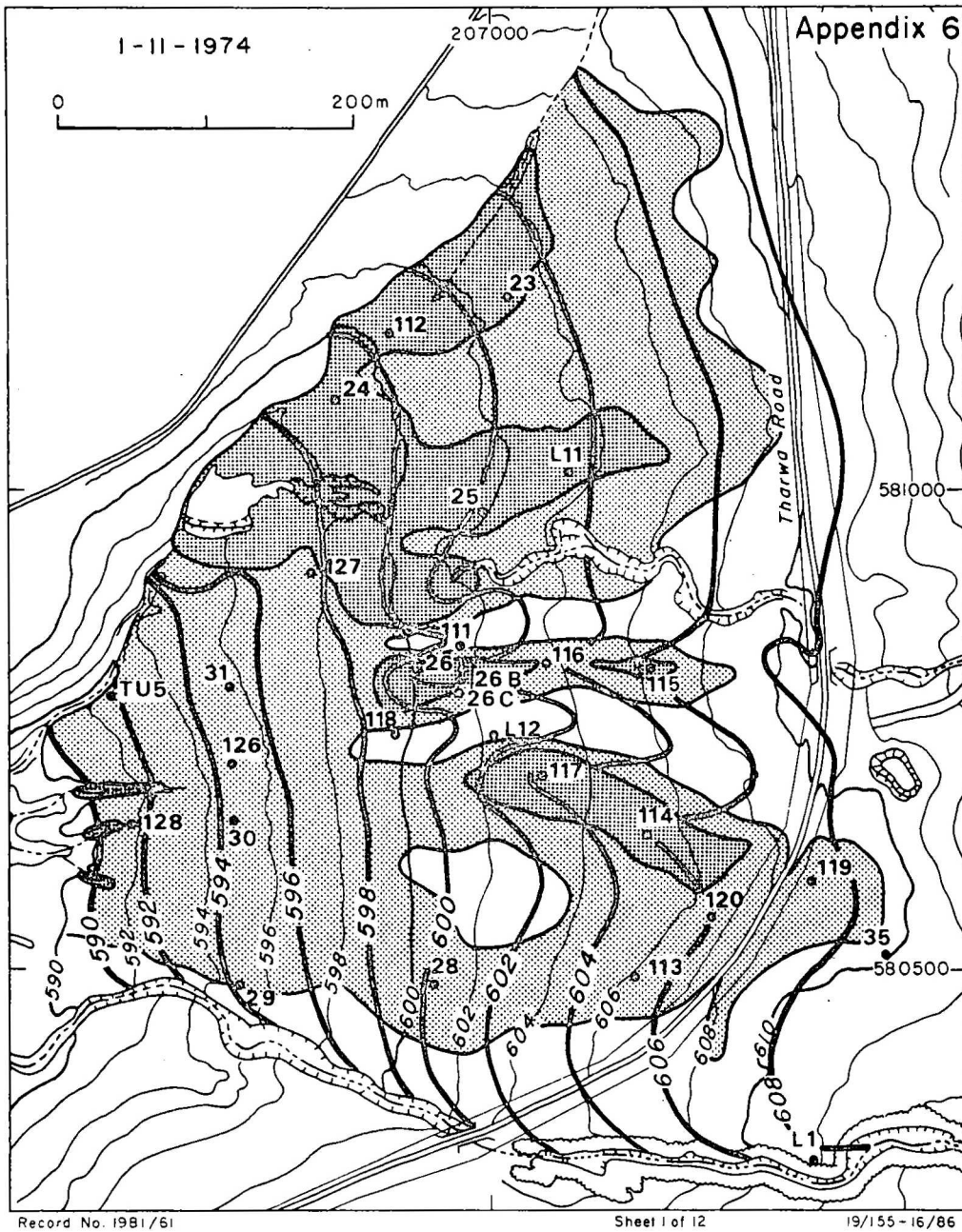


Record No. 1981/61

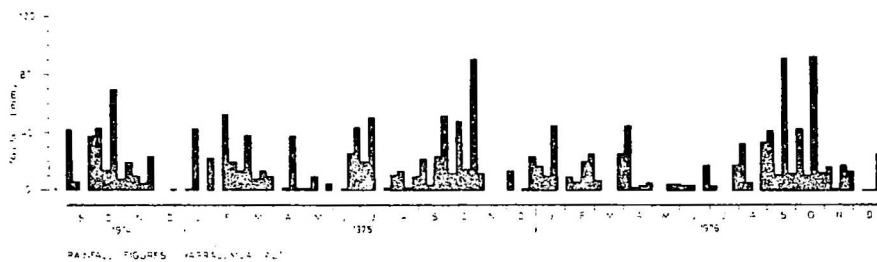
Sheet 12 of 12

19/155 - 16/85

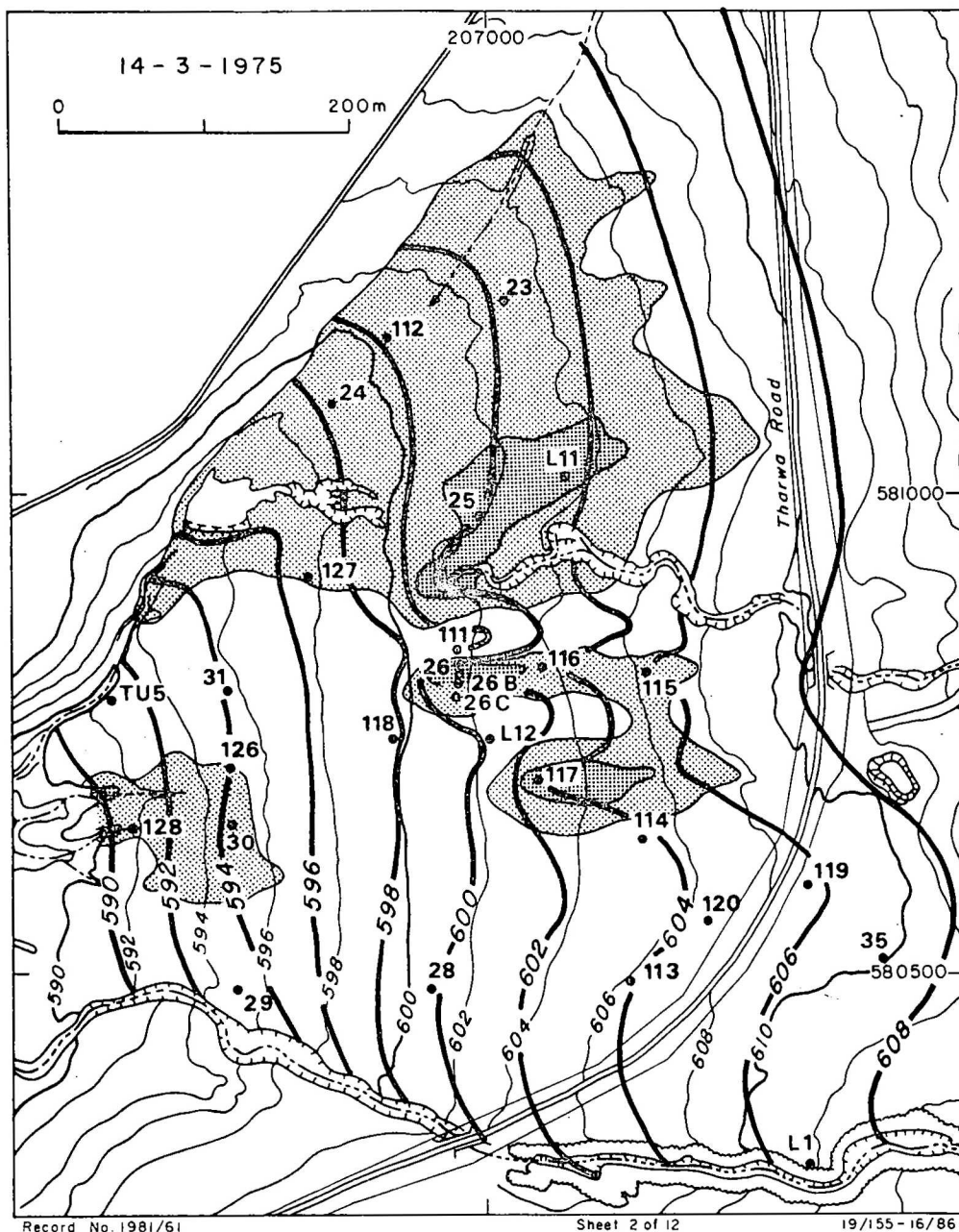
— Contour in metres of maximum fluctuation of potentiometric surface
in surficial aquifers over the period 3.9.74 to 6.12.76



- Contour in metres of the potentiometric surface in the surficial aquifers
- ▨ Areas where potentiometric surface was at or above ground level
- ▤ Areas where potentiometric surface was within one metre of ground level
- Piezometer



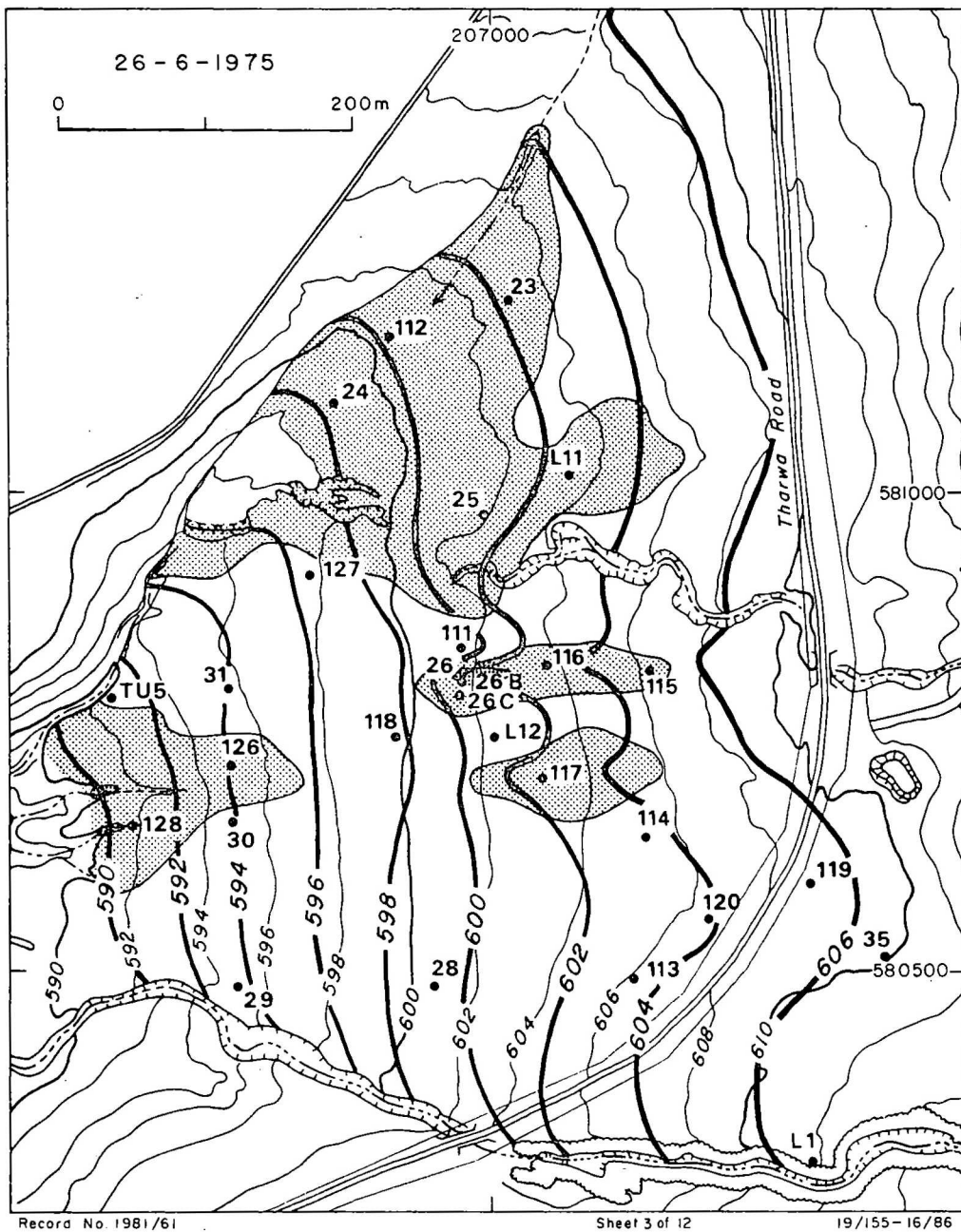
Fluctuation in potentiometric surfaces, Nov. 1974 to Dec. 1976
South Basin



Record No. 1981/61

Sheet 2 of 12

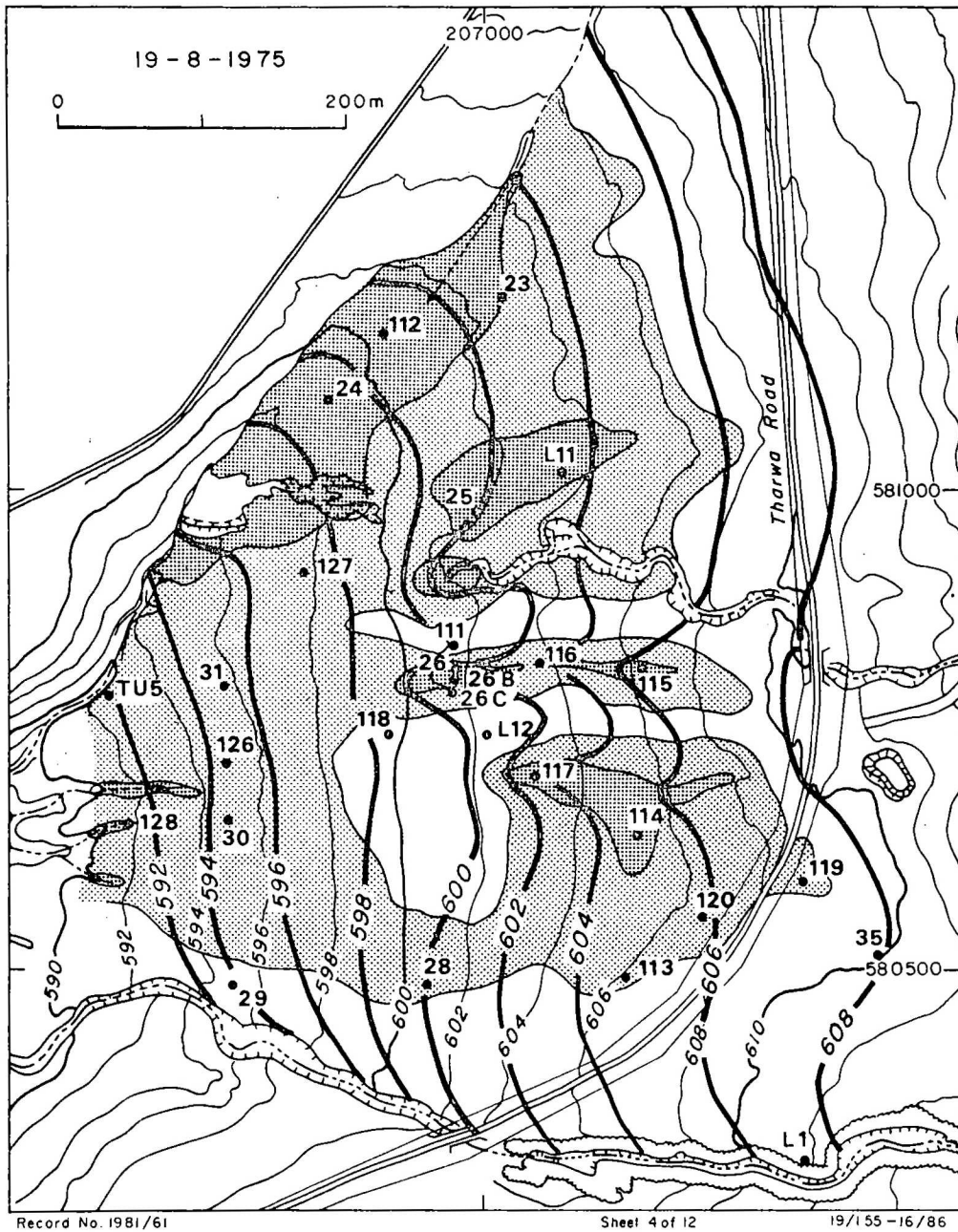
19/155-16/86



Record No. 1981/61

Sheet 3 of 12

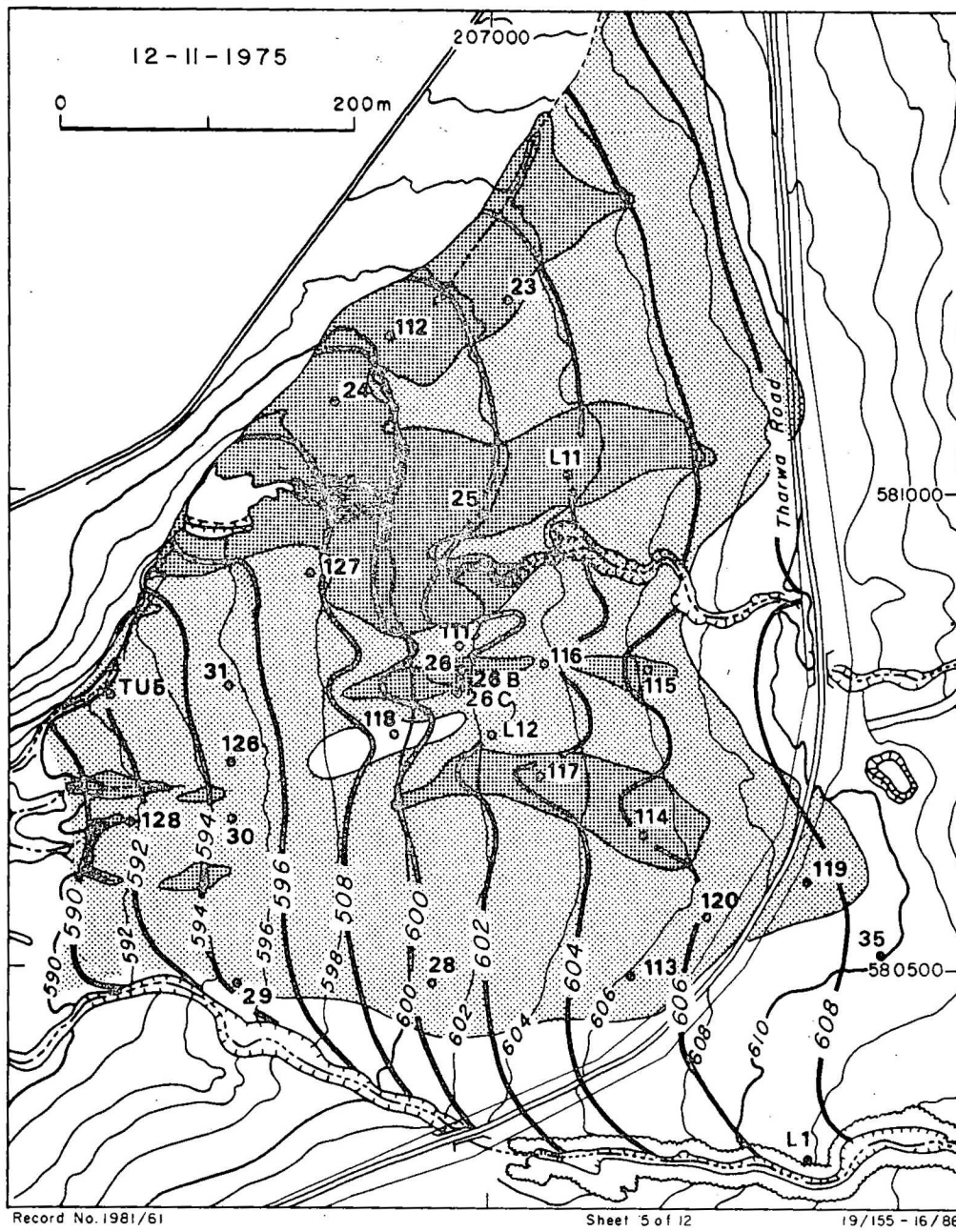
19/155-16/86

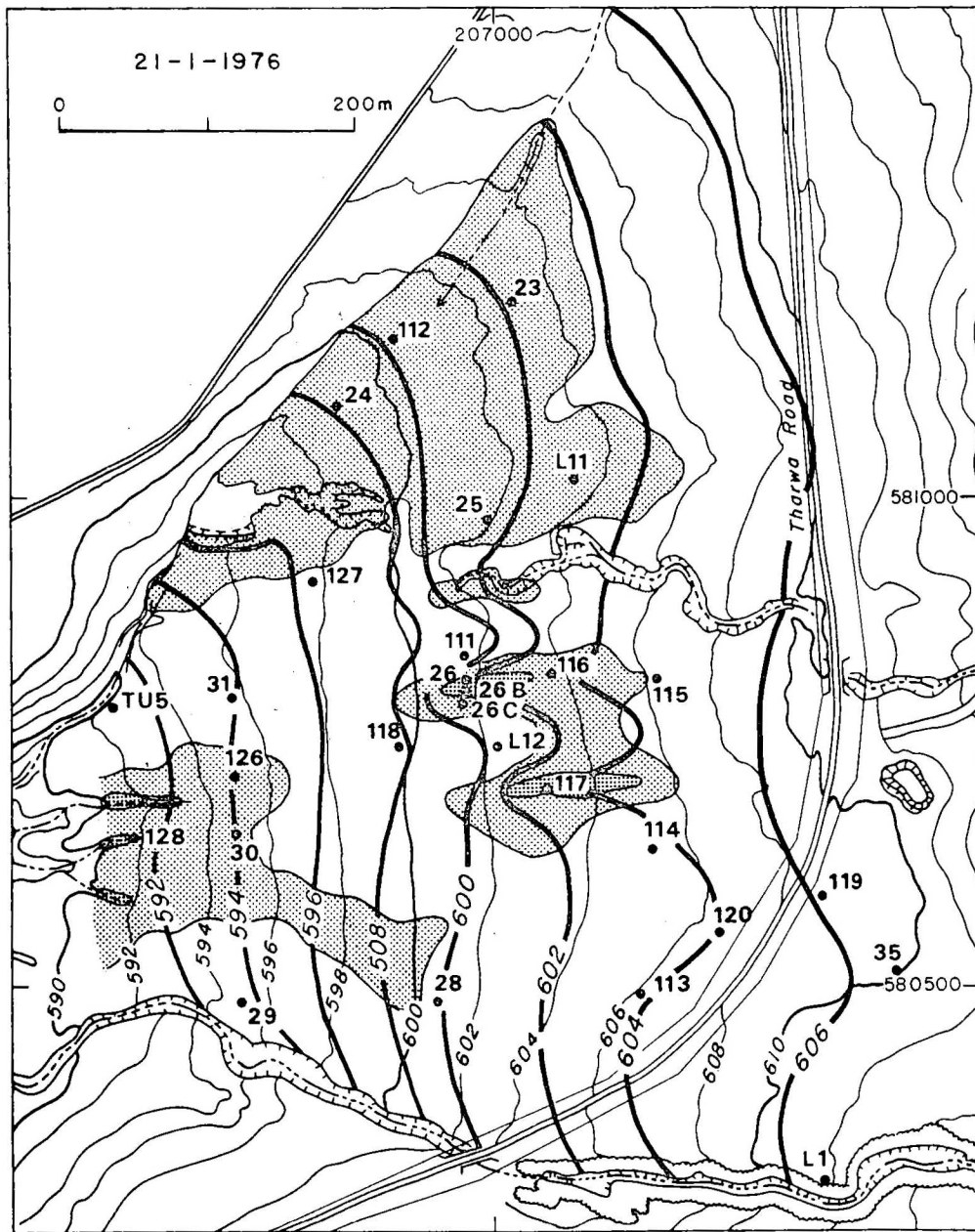


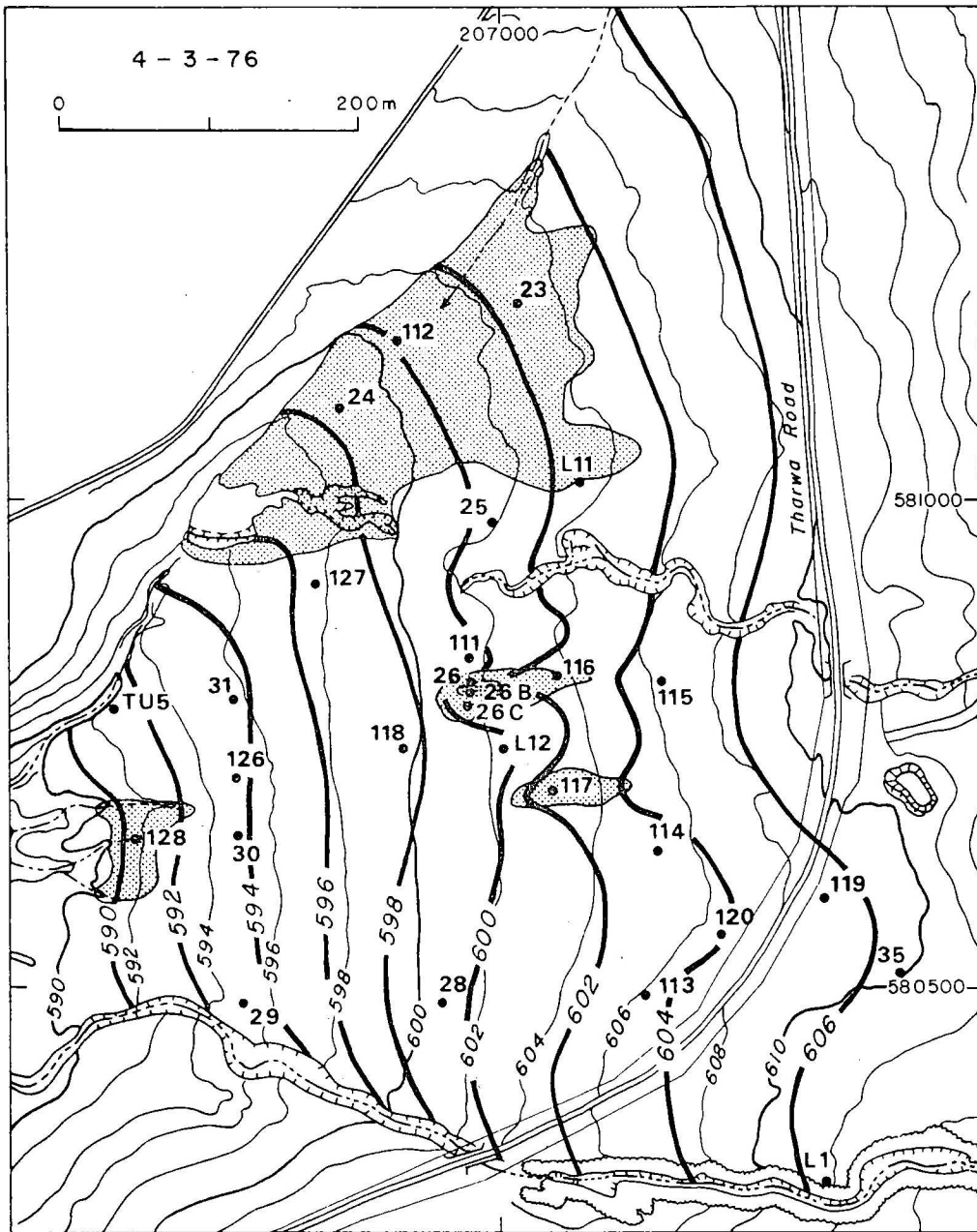
Record No. 1981/61

Sheet 4 of 12

19/155-16/86



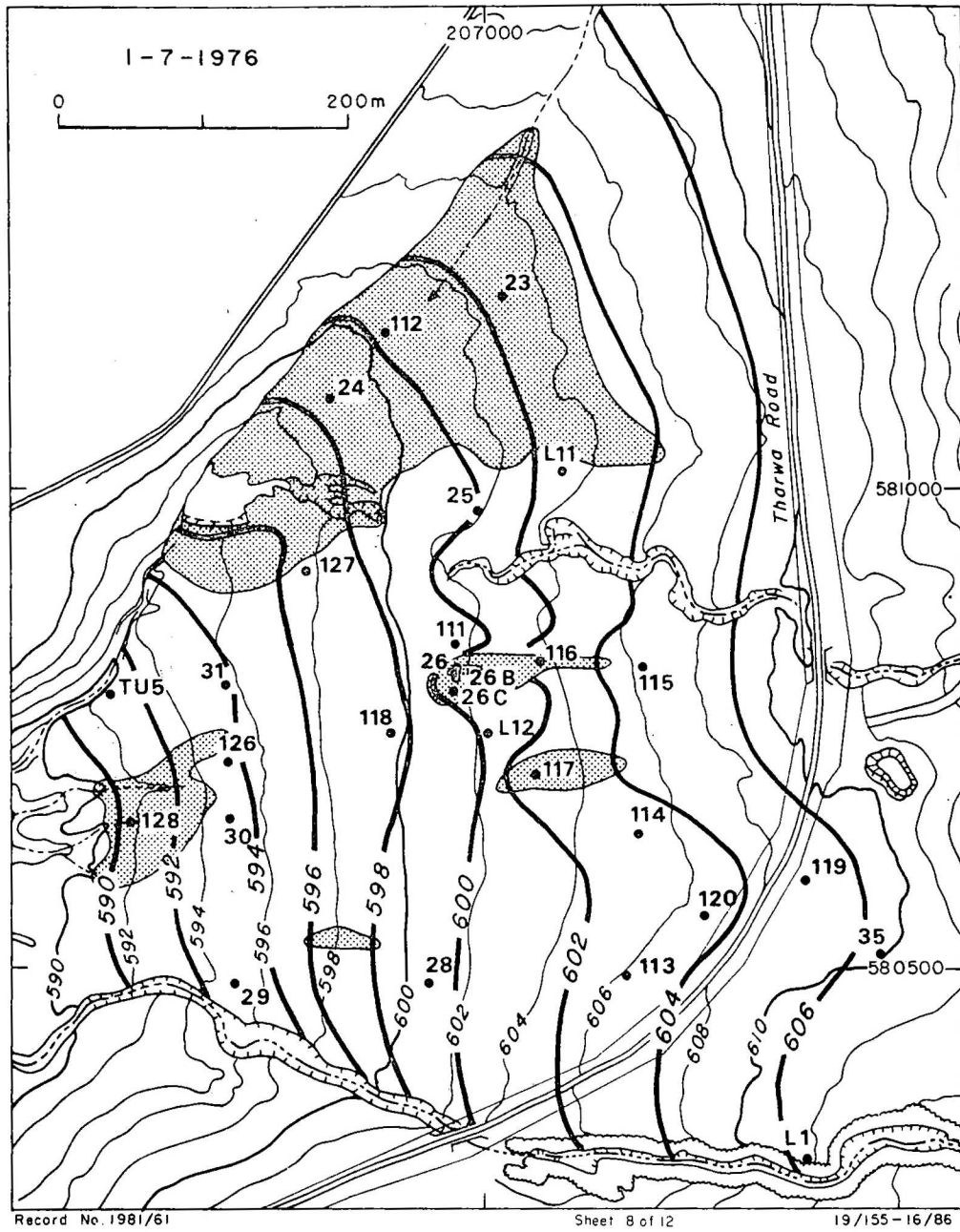




Record No. 1981/61

Sheet 7 of 12

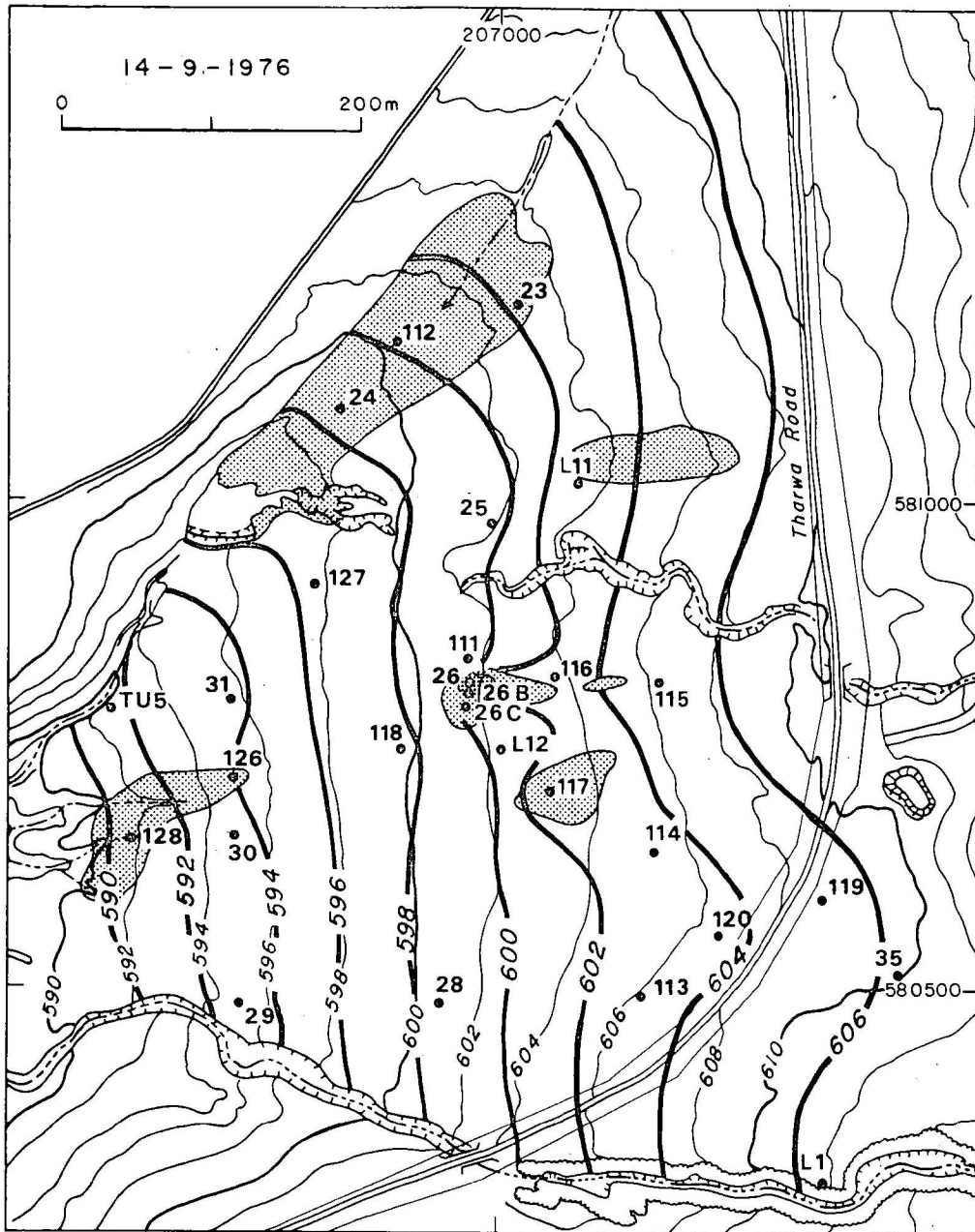
19/155-16/86



Record No. 1981/61

Sheet 8 of 12

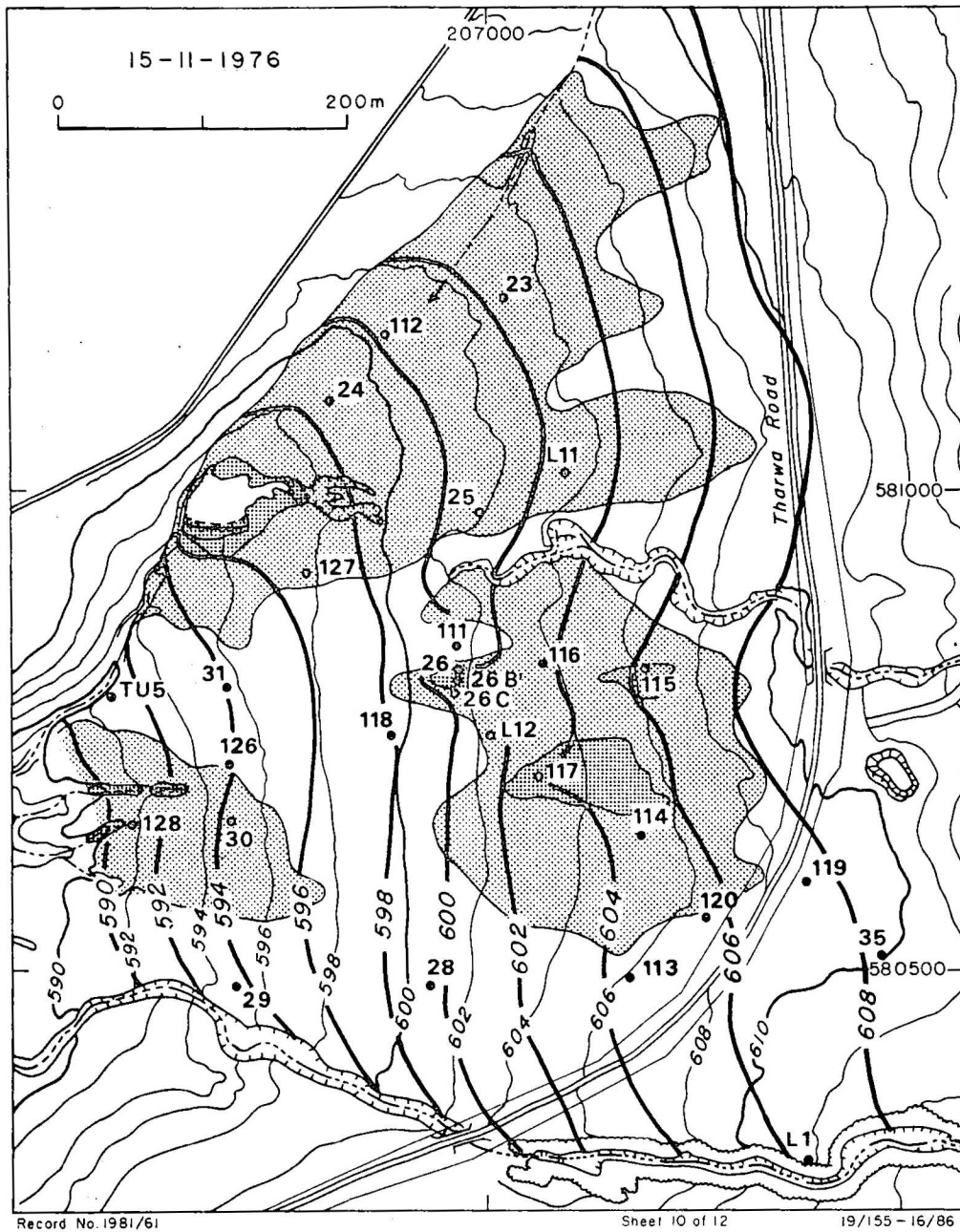
19/155-16/86



Record No 1981/61

Sheet 9 of 12

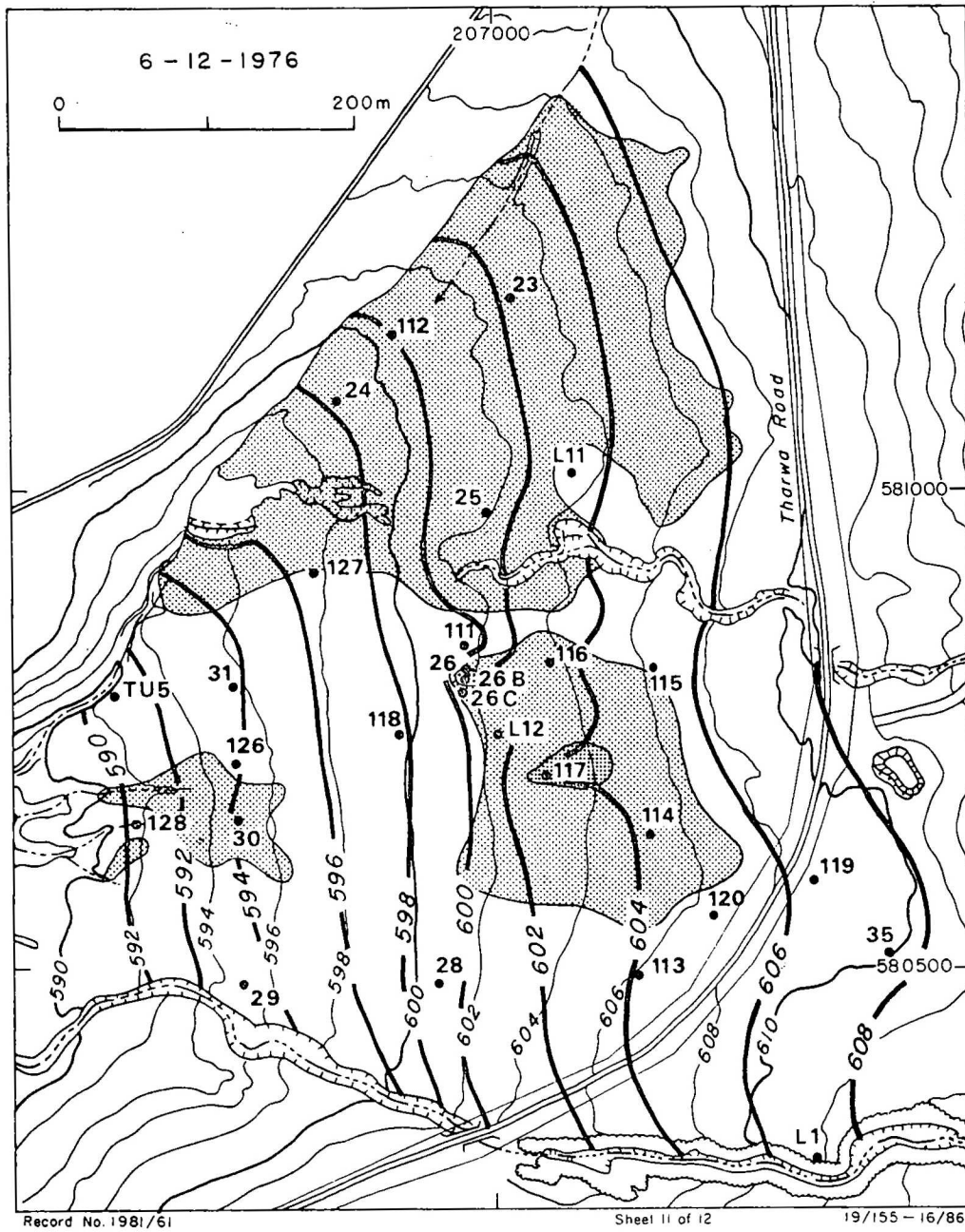
19/155-16/86



Record No. 1981/61

Sheet 10 of 12

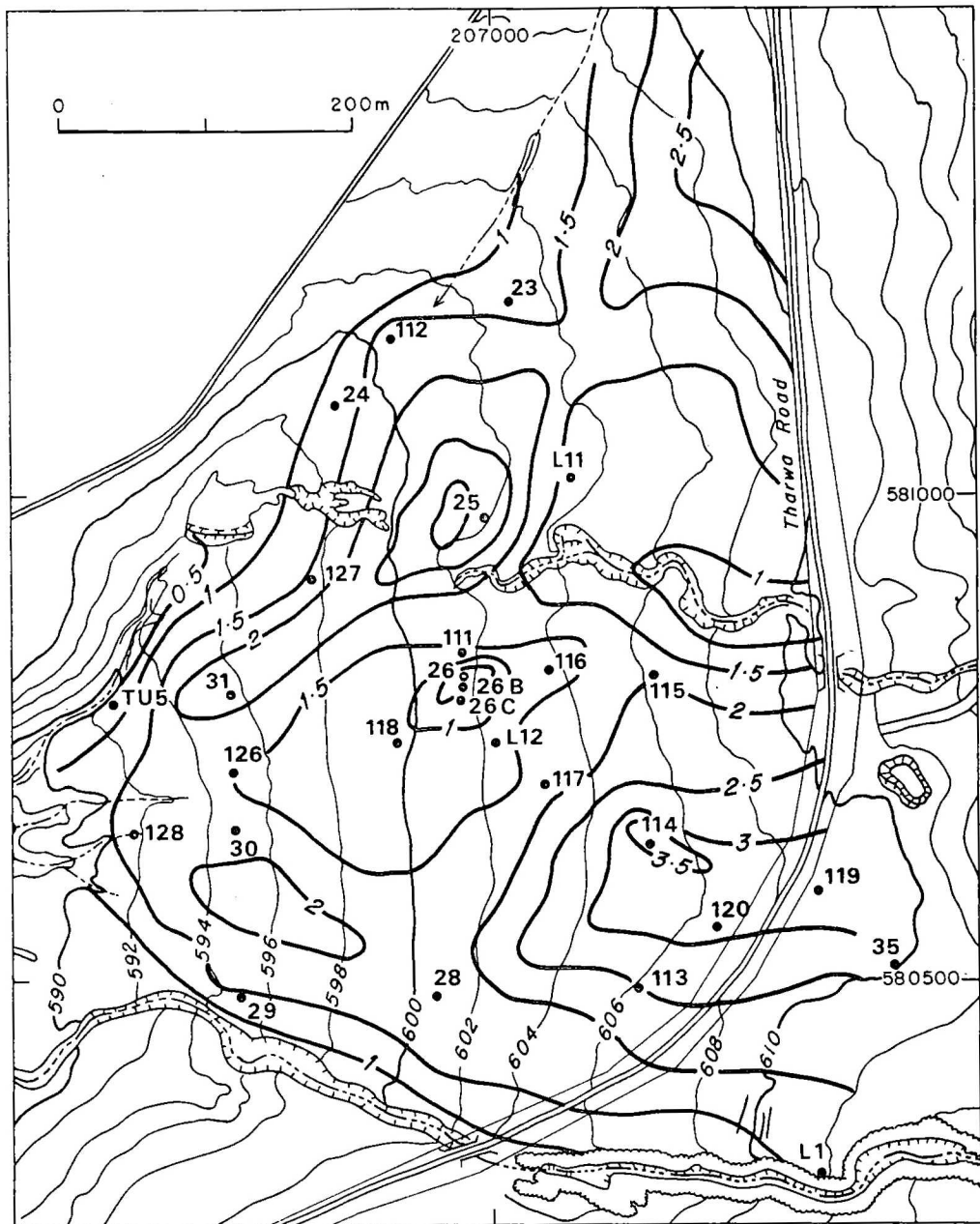
19/155 - 16/86



Record No. 1981/61

Sheet 11 of 12

19/155 - 16/86



Record No 1381/61

Sheet 12 of 12

19/155-16/86

— Contour in metres of maximum fluctuation of potentiometric surface
in surficial aquifers over the period 3.9.74 to 6.12.76

GEOLOGICAL MAP OF CENTRAL LANYON A.C.T.

0 1km

N

Reference

CAINOZOIC

- Alluvium
- Colluvium, conglomerates

UPPER MESOZOIC?

- Purple-red lithic and feldspathic quartz arenites

UPPER SILURIAN

- Blue-grey porphyritic rhyodacite, dacite
- Purple-blue porphyritic rhyodacite
- Cream to pale purple porphyritic rhyolite thin red terrestrial sandstone
- Massive green-grey to pink rhyolite dykes
- Purple porphyritic rhyodacite
- Brown ash-fall tuff and fine blue rhyolite
- Purple-blue porphyritic rhyodacite
- Blue-grey fine to medium densely welded rhyolite
- Black shale
- Quartz sandstone
- Green-grey porphyritic rhyodacite
- Shale
- Tuffaceous sandstone, ash-fall tuff
- Agglomerate
- Green-grey tuff
- Tuffaceous sandstone, ashstone
- Blue-grey, green-grey and purple porphyritic Sandstone rhyodacite
- Mudstone, shale, chert, sandstone

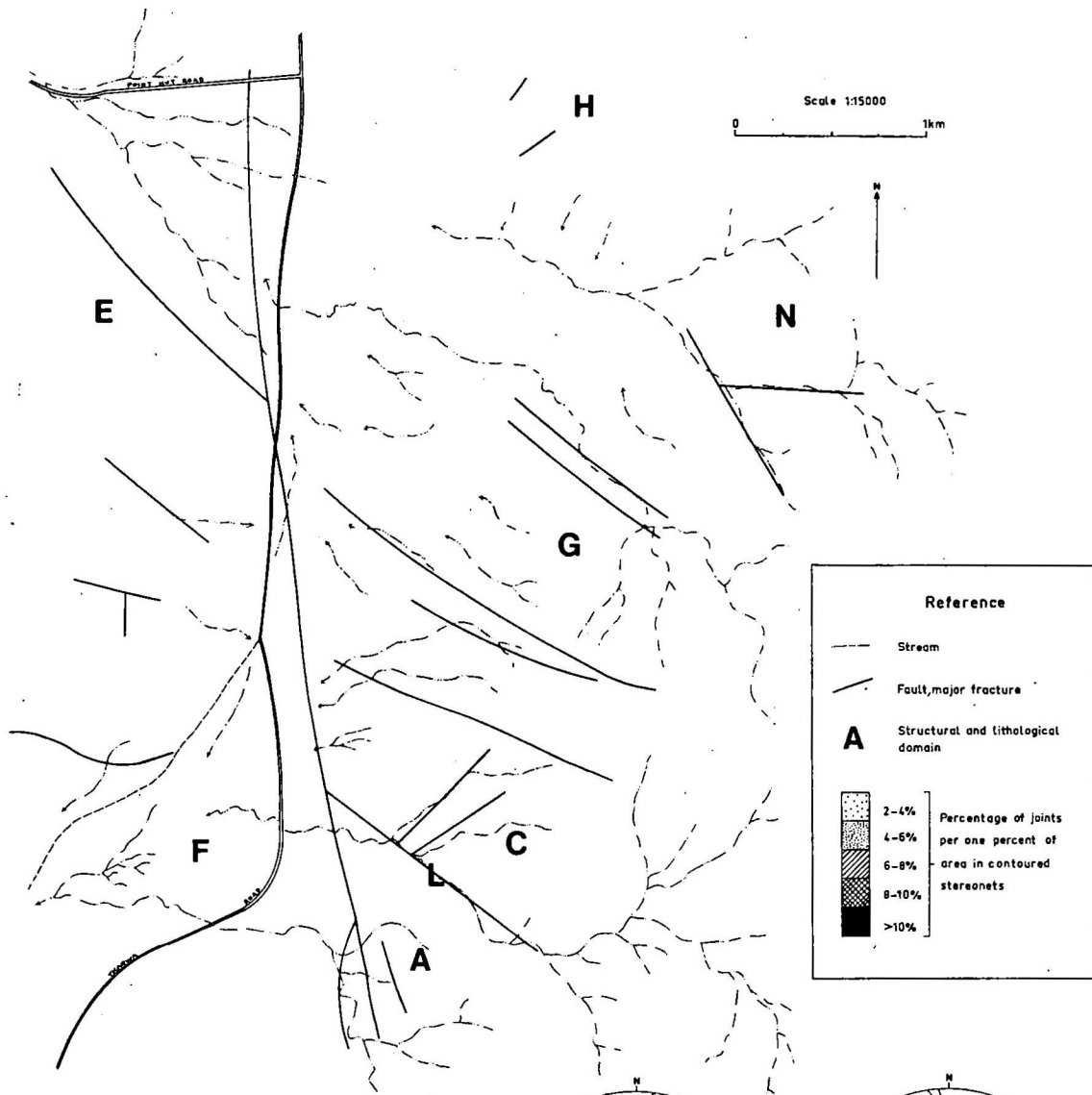
- Rock outcrop
- Geological boundary, accurate
- Geological boundary, approximate
- Geological boundary, concealed
- Approximate zonal boundary in ash-flow tuff units
- Fault, accurate
- Fault, approximate
- Fault, inferred (generally concealed)
- Shear-zone
- Quartz
- Rhyolite dyke
- Dip and strike of bedding
- Dip and strike of foliation
- Plunge of minor fold axis
- Drill hole

Sections
V/H = 2

PLATE 1

SCALE		COMMONWEALTH OF AUSTRALIA	
BUREAU OF MINERAL RESOURCES		COMMONWEALTH OF AUSTRALIA	
A.C.T. 1:10,000 Planning Series (prelim.)		Geological map of central Lanyon	
J. R. Kellatt		Hydrogeological Investigations of Two Basins at Lanyon A.C.T. 1974-1976	
COMPILED AND CHECKED BY J. R. K.	CHECKED AND APPROVED BY J. R. K.	TO ACCOMPANY RECORD 1981/61	DRAWN BY J. R. K.
SUPERVISOR J. LOOSE		DRAWING NUMBER 19/155-16/62	

JOINT ANALYSIS, CENTRAL LANYON, A.C.T.



Contours of poles to joints,
lower hemisphere, equal area
projection

Stereographic plot of centroids
of significant joint set
concentrations

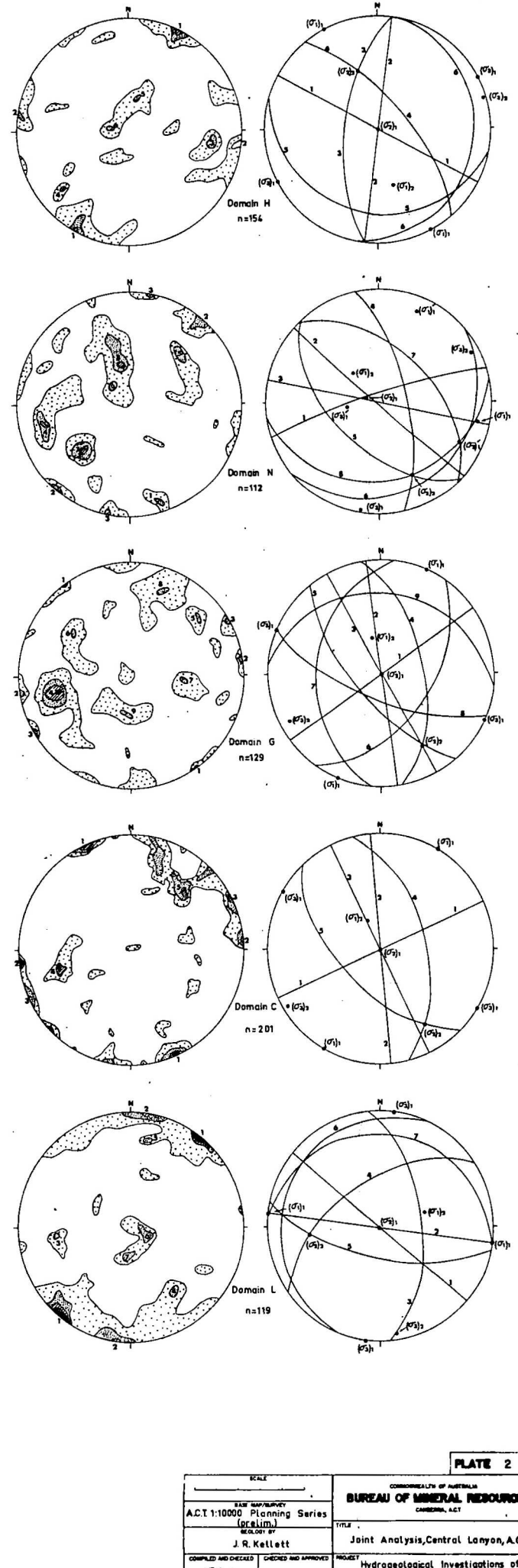
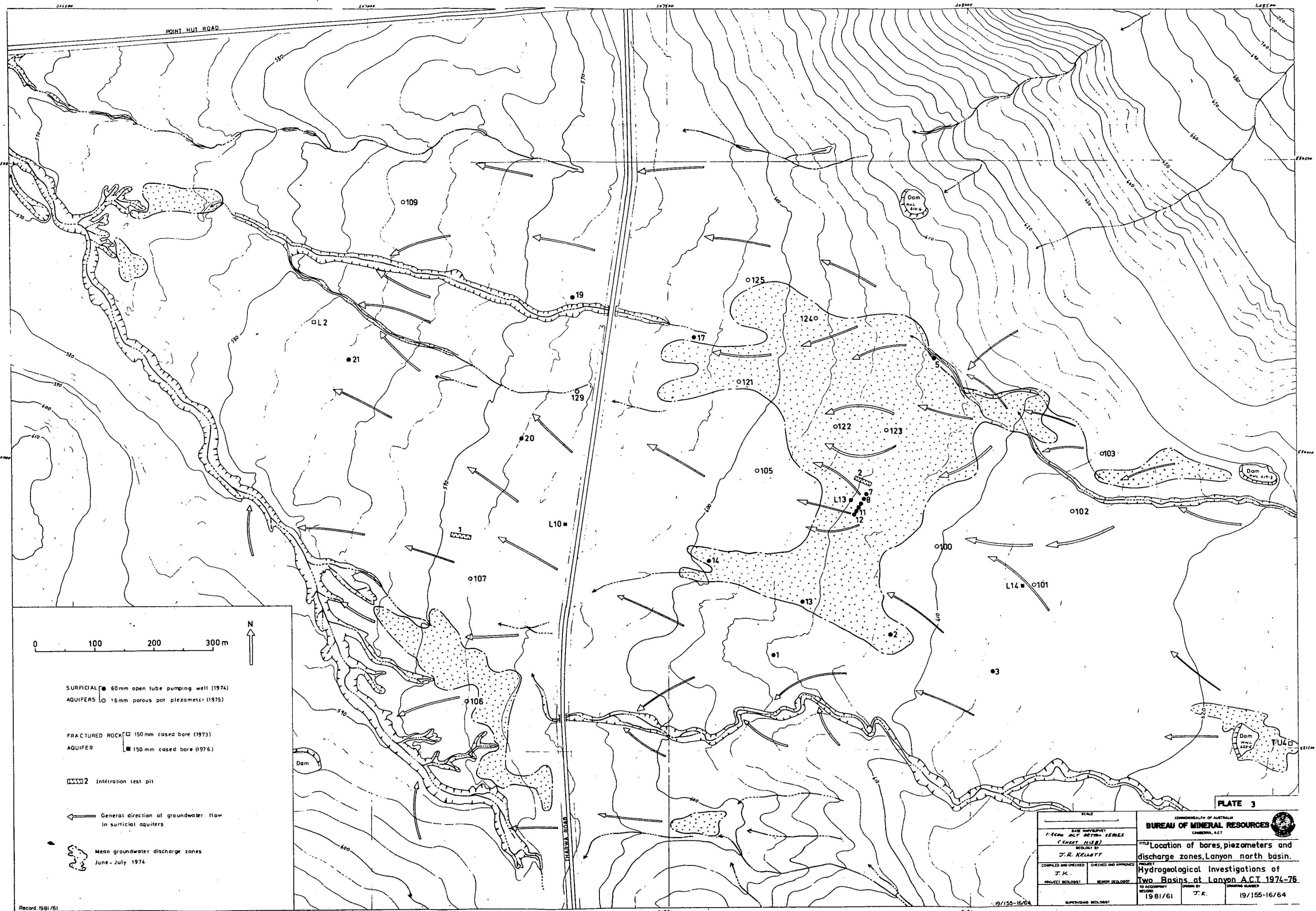
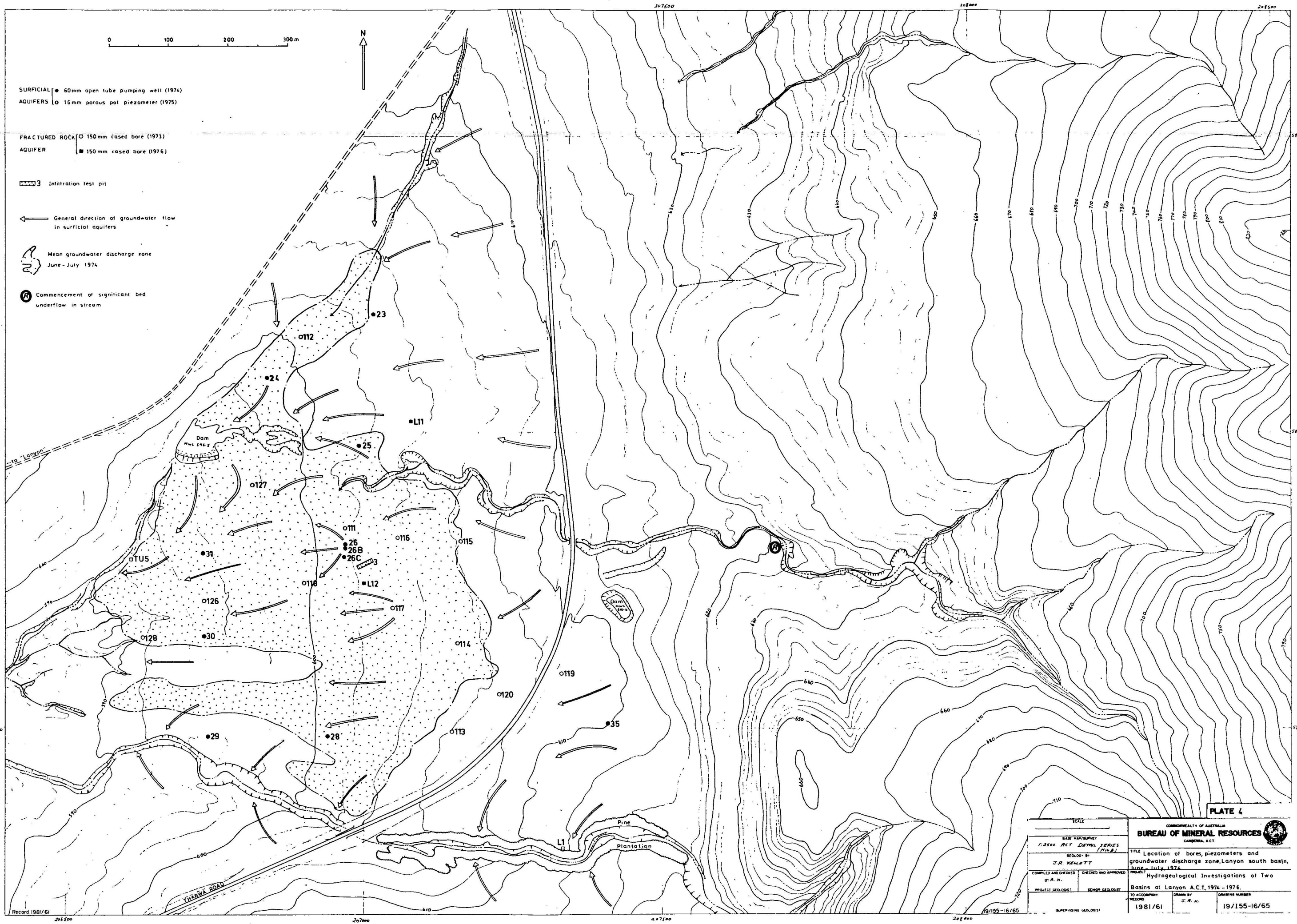


PLATE 2

SCALE		BUREAU OF MINERAL RESOURCES CANBERRA, A.C.T.	
ACT 1:10000 Planning Series (Scale 1:10000)		TITLE Joint Analysis, Central Lanyon, A.C.T.	
COMPILED AND CHECKED J.R.K.		PROJECT Hydrogeological Investigations of Two Basins at Lanyon A.C.T., 1974-1976	
PROJECT: 825/1971		TO ACCOMPANY RECORD 1981/61	
SUPERVISING GEOLOGIST		DRAWN BY J.R.K. DRAWING NUMBER 19/155-16/63	





0 100 200 300 m

N

SURFICIAL • 60mm open tube pumping well (1974)
AQUIFERS ○ 15mm porous pot piezometer (1975)

FRACTURED ROCK □ 150mm cased bore (1973)
AQUIFER ■ 150mm cased bore (1976)

3 Infiltration test pit

General direction of groundwater flow
in surficial aquifers

Mean groundwater discharge zone
June-July 1974

Commencement of significant bed
underflow in stream

Record 1981/61

SCALE		1:2500 ACT DETAIL SERIES (H10.1)	
BASIC MAP/SURVEY		GEOLOGY BY J.R. KELLY	
COMPILED AND CHECKED BY A.M.		CHECKED AND APPROVED BY A.M.	
PROJECT GEOLOGIST		SENIOR GEOLOGIST	
TO ACCOMPANY RECORD		DRAWN BY J.R. KELLY	
SUPERVISING GEOLOGIST		DRAWING NUMBER	
19/155-16/65		19/155-16/65	

PLATE 4

COMMONWEALTH OF AUSTRALIA
BUREAU OF MINERAL RESOURCES
CANBERRA, ACT

TITLE Location of bores, piezometers and
groundwater discharge zone, Lanyon south basin,
June-July 1974

PROJECT Hydrogeological Investigations of Two
Basins at Lanyon A.C.T., 1974-1976